

**KINETICS OF HYDROGEN EVOLUTION REACTION
ON Ni-Me-P ELECTRODES**

by

Reza Karimi Shervedani

A thesis presented to the Département de Chimie in fulfillment
of the requirements for the degree of Ph. D.

FACULTÉ DES SCIENCES
UNIVERSITÉ DE SHERBROOKE

Sherbrooke, Québec, Canada, August 1997



National Library
of Canada

Acquisitions and
Bibliographic Services

395 Wellington Street
Ottawa ON K1A 0N4
Canada

Bibliothèque nationale
du Canada

Acquisitions et
services bibliographiques

395, rue Wellington
Ottawa ON K1A 0N4
Canada

Your file *Votre référence*

Our file *Notre référence*

The author has granted a non-exclusive licence allowing the National Library of Canada to reproduce, loan, distribute or sell copies of this thesis in microform, paper or electronic formats.

The author retains ownership of the copyright in this thesis. Neither the thesis nor substantial extracts from it may be printed or otherwise reproduced without the author's permission.

L'auteur a accordé une licence non exclusive permettant à la Bibliothèque nationale du Canada de reproduire, prêter, distribuer ou vendre des copies de cette thèse sous la forme de microfiche/film, de reproduction sur papier ou sur format électronique.

L'auteur conserve la propriété du droit d'auteur qui protège cette thèse. Ni la thèse ni des extraits substantiels de celle-ci ne doivent être imprimés ou autrement reproduits sans son autorisation.

0-612-26382-7

Le 29 Août 1997, le jury suivant a accepté cette thèse, dans sa version finale.

MEMBERS

SIGNATURES

M. Oumarou Savadogo
Ecole Polytechnique de Montreal

M. Hugues Ménard
Département de chimie

Mme Gessie Brissard
Département de chimie

M. Andrzej Lasia
Département de chimie

ABSTRACT

Hydrogen is a wholly non-polluting and renewable fuel. It may be obtained in a clean way by the electrocatalytic hydrogen evolution reaction (HER). Fossil fuels which are polluting and non-renewable, can be potentially replaced by hydrogen. Electrocatalytic hydrogen production calls for efficient and durable electrodes. A knowledge of the mechanism and kinetics of the electrode reactions is necessary in order to find the origin of the electrocatalytic activity, and improve the properties of the electrode to obtain desirable properties.

The first chapter of this study is an introduction on the concepts and techniques which should be considered for evaluation of the electrode activity, factors affecting the electrode activity and specific materials for electrodes. Fundamental theories and equations are presented in the second chapter.

The candidate materials for cathodes are limited. Those that have high surface area suffer from low physical stability and deterioration in long-term operation, *e.g.*, Ni-Zn or Ni-Mo. If physical stability is improved the activity is decreased, *e.g.*, Ni-Zn electrodes with low Zn content. When both properties are improved the production expense is increased, *e.g.*, Ni-Al plasma sprayed electrodes. The main propose of this study is to prepare new electrode materials and study their activity and reaction mechanism for the HER. Three categories of the electrodes of nickel phosphorous family were studied, Ni-P, Ni-Mo-P, and Ni-Zn-P. The experimental part containing preparation and treatments of the electrodes, techniques and methods used for electrochemical measurements, data acquisition, modeling, and determination of the kinetics is presented in the third chapter.

Ni-P materials are very stable in alkaline solutions. Their stability is better than Ni. Phosphorous is not removed by means of leaching the electrodes in HF, alkaline solutions,

heating, and/or oxidation to produce a rough surface. The activity of these electrode materials depends on the method of their preparation. Electrodes prepared at low current densities and temperature were active for the HER. The increase in electrode activity is due to increase in the surface roughness. The most active Ni-P electrode prepared in this study had a surface roughness of 10^3 . XRD patterns of Ni-P electrodes show that as deposited samples, in all the cases, have amorphous structure. After heating at 400°C the structure of electrodes changed to crystalline with domination of Ni_3P phase (for high phosphorous content electrodes) or Ni_3P and Ni (for low phosphorous content electrodes). In the fourth chapter the results related to the electrode preparation and treatments, modeling and approximation of the kinetics obtained on Ni-P electrodes are presented and discussed.

Ni-Mo-P electrodes were prepared by “multi-step” electrodeposition. Under special conditions, stable and active electrodes were prepared. The activity of the electrodes was increased through increase in surface roughness as well as intrinsic activity. Cycling of the electrodes between the HER and oxygen evolution reaction (OER) deactivated them. Mo was mostly dissolved during electrooxidation of these materials. In the fifth chapter the results obtained on preparation, treatments, modeling and kinetics of Ni-Mo-P electrodes are presented and discussed.

Ni-Zn-P electrodes were prepared by subsequent electrodeposition of Ni, Ni-P, and Ni-Zn-P. The top-most layer was obtained by gradual addition of zinc to the plating bath. After leaching the electrodes in 30% KOH, about 80 % of Zn was removed leading to a porous surface with a large area. Excellent stability was observed for three-step deposited electrodes. Among three-step deposited electrodes, those prepared at high current densities are the most active ones. They are chemically and physically very stable, and electrochemically showed very good activity and stability. They are characterized by low Tafel slopes and large surface area with roughness factor of 10^4 . Ni-Zn-P electrodes are attractive candidates for alkaline water electrolysis. In the sixth chapter the results related to electrode preparation, activities for the

HER, modeling, and criteria for model selection of Ni-Zn-P electrodes are presented and discussed.

Electrochemical impedance spectroscopy (EIS) and steady-state polarization are mainly used to explain their behavior. In order to explain the activity of the electrodes the real surface area must be known. A new technique for the surface roughness determination *i.e.*, “CO molecular probe” was developed in this thesis. Ni-Zn-P porous electrodes which showed excellent stability and high electrocatalytic activity were used and their surface roughness was measured by the EIS and compared with the values obtained by other techniques such as surface oxidation, cyclic voltammetry (cv), ratio of the polarization current densities, and CO molecular probe. The results are in a very good agreement with those obtained by the EIS, implying that the information obtained by EIS technique are basically correct. Besides, the results show that dissolved CO in NaOH can be oxidized on Ni and Ni-Zn-P electrodes. This is a new observation of CO behavior on nickel based electrodes. In chapter seven the results obtained by different techniques for surface roughness of Ni-Zn-P electrodes are presented and compared.

SOMMAIRE

L'hydrogène constitue une source d'énergie à la fois renouvelable et non polluante. Il peut être obtenu d'une façon propre pour l'environnement via la réaction de dégagement d'hydrogène (RDH). Les combustibles fossiles, polluants et non renouvelables peuvent être remplacés par l'hydrogène. La production d'hydrogène par voie électrochimique fait appel à des électrodes efficaces et durables. Une connaissance détaillée du mécanisme et de la cinétique des réactions aux électrodes est nécessaire afin de déterminer l'origine de l'activité électrocatalytique et améliorer les performances des électrodes.

Dans le premier chapitre de cette étude, les concepts et les techniques à prendre en considération pour évaluer l'activité des électrodes (cathodes pour la RDH) ainsi que les différents facteurs influençant cette activité électrocatalytique sont introduits. Une revue des nombreux matériaux d'électrodes à base de nickel préparés pour la production électrochimique d'hydrogène termine le premier chapitre. Les aspects fondamentaux et les équations utilisées sont présentées au cours du second chapitre.

Les matériaux candidats pour la préparation de nouvelles électrodes présentent une faible stabilité mécanique et se détériorent à long terme (par exemple Ni-Zn, Ni-Mo). Lorsque la stabilité mécanique est améliorée, l'activité électrocatalytique diminue (électrodes Ni-Zn à faible teneur en Zn). Lorsque la stabilité mécanique et l'activité sont simultanément augmentés, le coût de production des électrodes s'accroît considérablement (électrodes Ni-Al obtenues par projection au plasma). Le but principal de cette étude est de préparer de nouveaux matériaux d'électrodes, d'étudier leur activité vis-à-vis de la RDH et de déterminer le mécanisme des réactions impliquées. Trois types d'électrodes à base de nickel et de phosphore (Ni-P, Ni-Mo-P et Ni-Zn-P) ont ainsi été étudiées. La partie expérimentale contenant la préparation, la caractérisation et l'activation des électrodes, les techniques et

méthodes utilisées pour les mesures électrochimiques, la modélisation et la détermination de la cinétique des réactions sont présentées dans le troisième chapitre.

Les matériaux d'électrodes Ni-P sont très stables en solution alcaline. Leur stabilité est meilleure que celle du Ni. Le phosphore n'est pas éliminé par lixiviation des électrodes dans HF, dans une solution alcaline par chauffage et/ou par oxydation, les procédés utilisés pour obtenir des surfaces rugueuses. L'activité électrocatalytique de ces électrodes dépend du mode de préparation utilisé. Les électrodes préparées à faible densité de courant et basse température sont actives pour la RDH. L'augmentation de l'activité de l'électrode est liée à l'augmentation de la rugosité de surface. L'électrode de Ni-P la plus active préparée dans cette étude a une rugosité surface de 10^3 . L'utilisation de la diffraction des rayons X montre le caractère amorphe de tous les matériaux préparés. Après chauffage à 400°C , la structure des électrodes change pour devenir cristalline avec prédominance de la phase Ni_3P (pour les électrodes à forte teneur en P) ou Ni_3P et Ni (pour les électrodes à faible teneur en P). Dans le quatrième chapitre, les résultats concernant la préparation, l'activation et la caractérisation des électrodes, la modélisation et l'approximation de la cinétique des réactions obtenues avec les électrodes Ni-P sont présentés et discutés.

Les électrodes Ni-Mo-P sont préparées par électrodépositions successives. Dans des conditions spéciales, des électrodes stables et actives ont été obtenues. L'activité des électrodes augmentait par augmentation de la rugosité de surface comme de l'activité intrinsèque. Le balayage de potentiel entre le domaine de la RDH et celui de la réaction de dégagement d'oxygène (RDO) conduit à la désactivation des électrodes. Le Mo est dissous en grande partie durant l'électro-oxydation des matériaux. Dans le cinquième chapitre, les résultats concernant la préparation, l'activation et la cinétique des réactions obtenues avec les électrodes Ni-Mo-P sont présentés et discutés.

Les électrodes Ni-Zn-P ont été préparées par électrodéposition successives de Ni, Ni-P et Ni-Zn-P. La couche extérieure a été obtenue par addition graduelle de Zn dans le bain de plaquage. Après lixiviation dans une solution KOH 30%, environ 80 % du Zn est éliminé conduisant ainsi à une électrode poreuse de grande surface. Les électrodes préparées en trois étapes présentent une excellente stabilité mécanique. Parmi ces électrodes, celles préparées à densité de courant élevée sont les plus actives. Elles sont chimiquement et mécaniquement très stables et d'un point de vue électrochimique présentent une bonne activité et une bonne stabilité. Elles se caractérisent par une faible pente de Tafel et une surface active élevée avec un facteur de rugosité de l'ordre de 10^4 . Les électrodes Ni-Zn-P constituent d'excellents candidats pour l'électrolyse de l'eau en milieu alcalin. Dans le sixième chapitre, les résultats concernant la préparation, l'activité électrocatalytique, la modélisation et les critères pour la sélection d'un modèle pour les électrodes Ni-Zn-P sont présentés et discutés.

La spectroscopie d'impédance électrochimique (SIE) et la polarisation stationnaire sont principalement utilisées pour déterminer leur comportement. Afin d'expliquer l'activité des électrodes, la surface active réelle doit être connue. Une nouvelle technique pour la détermination du coefficient de rugosité utilisant le monoxyde de carbone (CO molecular probe) a été développée. Les électrodes Ni-Zn-P qui présentent une excellente stabilité mécanique et une activité électrocatalytique élevée ont été utilisées dans cette étude. La valeur de la rugosité de surface a été mesurée par spectroscopie d'impédance électrochimique (SIE) et comparée à la valeur obtenue par d'autres techniques telles que l'oxydation de surface, la voltamétrie cyclique (vc), le rapport des densités de courant de polarisation et par "CO molecular probe". Quelle que soit la technique utilisée, les résultats sont cohérents et nous permettent de conclure que la spectroscopie d'impédance électrochimique est une technique fiable. Les résultats montrent également qu'en milieu basique (NaOH) le CO dissous peut être oxydé sur Ni et sur Ni-Zn-P. Cette observation concernant le comportement du CO sur des électrodes à base de Ni s'avère originale. Dans le septième chapitre, les résultats des mesures

du facteur de rugosité des électrodes Ni-Zn-P obtenues par différentes techniques sont présentés et comparés.

ACKNOWLEDGMENTS

I wish to present my deep appreciation to professor Andrzej Lasia for his direction, guidance, and consultation during the course of this thesis work. The many stimulating and sincere discussions that I had with professor Lasia during the course of this project, as well as theoretical courses, preparation of the educational seminar lectures, and scientific meeting presentations are invaluable to author. Professor Lasia is always helpful and kindly. Each time that difficulties appeared, he has been able and willing to provide excellent suggestions and instructions.

I would like to thank my colleagues for their enlightening discussions, suggestions, and collaborations. Thanks are also due to Dr. Yigeng Li and Dr. Danielle Miousse for their help in the initial stages of this work, Dr. Jean-Marc Chapuzet for his help in translation of the abstract, Mr. Pierre Mangy for SEM-EDX, Miss. Anita Lemieux for ICP, and Mr. Yanick Gregoire for XRD analysis. I wish to thank Professor Hugues Menard and Jean Lessard for shearing the facilities in their laboratories.

Great thanks to my parents and all of my family. Their encouragement, endless love and kindness made this work easy to me.

I should acknowledge Ministry of Culture and Higher Education of IRAN (MCHE) for my scholarship and, Natural Science and Engineering Research Council of Canada (NSERC) for the financial support of this project.

TABLE OF CONTENTS

ABSTRACT	ii
SOMMAIRE	v
ACKNOWLEDGMENTS	ix
TABLE OF CONTENTS	x
LIST OF TABLES	xviii
LIST OF FIGURES	xxi
LIST OF SYMBOLS	xxviii
INTRODUCTION	1
CHAPTER 1 REVIEW	5
1.1 Electrocatalysis.....	5
1.2 Hydrogen production by electrolysis.....	7
1.3 Major aspects in evaluation of the performance of cathodes.....	8
1.3.1 Surface characterization.....	9
1.3.2 Stability.....	10
1.3.3 Methods of electrode preparation.....	12
1.3.4 Poisoning.....	13
1.3.5 Effect of temperature.....	14
1.4 Factors affecting the activity.....	15

1.4.1 Surface state.....	15
1.4.2 Single crystals.....	17
1.4.3 Ion implantation.....	17
1.4.4 Adatoms.....	18
1.4.5 Modified electrodes.....	19
1.5 Specific materials for electrodes.....	20
1.5.1 Smooth nickel.....	20
1.5.2 Raney nickel.....	22
1.5.3 Nickel boride.....	23
1.5.4 Nickel sulfide.....	24
1.5.5 Nickel phosphorous.....	24
1.5.6 Nickel oxide.....	25
1.5.7 Nickel alloys.....	26
1.5.8 Intermetallic compounds.....	28
1.5.9 Amorphous materials.....	29
CHAPTER 2 THEORY.....	31
2.1 General approach for simple reactions.....	31
2.2 Hydrogen evolution reaction (HER).....	35
2.2.1 Elementary reactions.....	35
2.2.2 Adsorption isotherms.....	35
2.2.3 Reaction rates.....	37

2.2.4	Steady-state.....	39
2.2.5	Equilibrium conditions.....	40
2.2.6	Mechanism of the HER.....	41
2.2.6.1	Volmer–Heyrovský mechanism.....	41
2.2.6.2	Volmer–Tafel mechanism.....	43
2.2.6.3	Volmer–Heyrovský–Tafel mechanism.....	44
2.3	Evaluation of surface covered by adsorbed hydrogen and kinetic parameters.....	45
2.3.1	Steady-state polarization curves (Tafel plots).....	46
2.3.2	Open circuit potential decay.....	48
2.3.3	Electrochemical impedance spectroscopy.....	49
2.3.3.1	Fundamental concepts.....	50
2.3.3.2	Ideally polarized electrode.....	51
2.3.3.3	Faradaic reaction without mass transfer limitation....	51
2.3.3.4	Impedance of faradaic reaction in the presence of adsorption of reacting species.....	54
2.3.3.5	Impedance of solid electrodes.....	58
2.3.3.5.1	Constant phase element, CPE, model.....	58
2.3.3.5.2	Porous electrode model.....	59
2.3.3.5.3	Two–CPE model.....	62
2.4	Approximation of rate constants and symmetry coefficients.....	63

CHAPTER 3	EXPERIMENTAL.....	65
3.1	Introduction.....	65
3.2	Electrodes.....	65
3.2.1	Reference electrode (preparation and potential calibration)...	65
3.2.2	Auxiliary electrode.....	66
3.2.3	Working electrode.....	67
3.2.3.1	Preparation of nickel phosphorous, Ni-P, electrodes.	67
3.2.3.2	Preparation of nickel molybdenum phosphorous, Ni-Mo-P, electrodes.....	68
3.2.3.3	Preparation of nickel zinc phosphorous, Ni-Zn-P, electrodes.....	70
3.2.3.4	Preparation of polycrystalline nickel, Ni, electrode.	71
3.2.3.5	Composition, structure, and surface morphology of the working electrodes.....	72
3.2.3.6	Electrode treatment.....	73
3.3	Cell, solutions, and instruments for kinetic measurements of the HER.....	74
3.3.1	Cell.....	74
3.3.2	Solutions.....	74
3.3.3	Instruments and data acquisition.....	75
3.4	Studies of the hydrogen evolution reaction.....	75
3.4.1	Steady-state polarization curves (Tafel plots).....	75

3.4.2 Electrochemical impedance spectroscopy.....	76
3.5 Surface behavior of Ni-Zn-P electrodes in alkaline solutions.....	76
3.5.1 Steady-state and equilibrium time (shift in equilibrium potential).....	76
3.5.2 Evaluation of the surface roughness of Ni-Zn-P electrodes by <i>in situ</i> methods.....	77
3.5.2.1 Coulometric oxidation of the electrode surface.....	77
3.5.2.2 Cyclic voltammetry.....	77
3.5.2.3 Adsorption and electrooxidation of carbon monoxide, CO molecular probe.....	78
3.5.2.3.1 Adsorption of CO on polycrystalline Ni electrode.....	78
3.5.2.3.2 Adsorption of CO on Ni-Zn-P electrode.....	79
3.6 Data analysis.....	80

CHAPTER 4 STUDIES OF THE HYDROGEN EVOLUTION REACTION ON Ni-P ELECTRODES.....	82
4.1 Introduction.....	82
4.2 Results and discussion.....	83
4.2.1 Composition, structure and surface morphology of Ni-P electrodes.....	83
4.2.2 HER on Ni-P electrodes obtained from bath A.....	89

4.2.3	Activation by anodic oxidation and potential cycling.....	97
4.2.4	Heating of Ni-P at 550°C.....	101
4.2.5	HER on Ni-P electrodes obtained from baths B and C.....	102
4.3	Summary.....	109
CHAPTER 5	KINETICS OF THE HYDROGEN EVOLUTION REACTION ON Ni-Mo-P ELECTRODES IN ALKALINE SOLUTIONS.....	110
5.1	Introduction.....	110
5.2	Results and discussion.....	111
5.2.1	Composition and surface morphology of electrodes.....	111
5.2.2	HER on Ni-Mo-P electrodes.....	115
5.2.2.1	Steady-state polarization.....	115
5.2.2.2	Activation by anodic oxidation and potential cycling.....	117
5.2.2.3	Electrochemical impedance spectroscopy.....	121
5.3	Summary.....	139
CHAPTER 6	KINETICS OF THE HYDROGEN EVOLUTION REACTION ON Ni-Zn-P ELECTRODES IN ALKALINE SOLUTIONS.....	140
6.1	Introduction.....	140
6.2	Results and discussion.....	140
6.2.1	Electrode composition and surface morphology.....	140
6.2.2	Steady-state polarization.....	146

6.2.3 Electrochemical impedance spectroscopy.....	146
6.2.4 Model selection (criteria).....	155
6.2.5 Electrode oxidation.....	166
6.3 Summary.....	172

CHAPTER 7 SURFACE BEHAVIOR OF Ni-Zn-P ELECTRODES IN ALKALINE SOLUTIONS AND EVALUATION OF THE SURFACE ROUGHNESS BY *IN SITU* METHODS.....

7.1 Introduction.....	174
7.2 Results and discussion.....	176
7.2.1 Electrode composition and surface morphology.....	176
7.2.2 Evaluation of the surface roughness of Ni-Zn-P electrodes by <i>in situ</i> methods.....	176
7.2.2.1 Ratio of the steady-state polarization current densities.....	178
7.2.2.2 Electrochemical impedance spectroscopy.....	181
7.2.2.3 Coulometric oxidation of the electrode surface.....	184
7.2.2.4 Cyclic voltammetry.....	186
7.2.2.5 Adsorption of carbon monoxide, CO.....	191
7.2.2.5.1 Adsorption of CO on polycrystalline Ni electrode.....	191
7.2.2.5.2 Adsorption of CO on Ni-Zn-P electrodes..	195
7.3 Summary.....	199

FINAL CONCLUSIONS AND CONTRIBUTIONS TO ORIGINAL RESEARCH	200
BIBLIOGRAPHY.....	205

LIST OF TABLES

1	Influence of pretreatment on the composition of Ni ₇₀ P ₃₀ electrode deposited at $j = 200 \text{ mA cm}^{-2}$ from bath A.....	88
2	Kinetic parameters of HER obtained on Ni ₇₀ P ₃₀ electrodes from the steady-state polarization curves in 1 M NaOH at 70°C.....	91
3	Kinetic parameters of the HER obtained on Ni ₇₀ P ₃₀ electrode from the steady-state polarization curves and the EIS measurements in 1 M NaOH at 70°C before and after various treatments ^a	95
4	Comparison of the roughness factors, R, and the real exchange current densities, j_0 / R , obtained on Ni ₇₀ P ₃₀ electrodes at 70°C in 1 M NaOH.....	96
5	Kinetic parameters of the HER obtained in 1 M NaOH at 70°C from steady-state polarization experiments on untreated and heated (3h at 400°C in air) Ni-P electrodes before and after electrochemical treatment by cycling (between -1.2 and +0.6 V vs. HgO/Hg) and constant potential oxidation (one hour at +0.75 V vs. HgO/Hg).....	99
6	Kinetic parameters of the HER obtained on amorphous Ni-P electrodes from steady-state polarization curves in 1 M NaOH at 70°C.....	102
7	Kinetic parameters of the HER obtained on amorphous Ni-P electrodes from steady-state polarization curves and the EIS measurements in 1 M NaOH at 70°C.....	107
8	Comparison of the roughness factors, R, and real exchange current densities, j_0 / R , obtained on Ni ₇₃ P ₂₇ and Ni ₉₂ P ₈ electrodes in 1 M NaOH at 70°C.....	108
9	Kinetics of the HER from steady-state polarization curves obtained on Ni-Mo-P electrodes in 1 M NaOH without any special treatment.....	118

10	Kinetics of the HER obtained on Ni-Mo-P electrodes from steady-state polarization curves in 1 M NaOH after electrochemical pretreatments.....	119
11	Kinetic parameters of the HER obtained on Ni-Mo-P electrodes from steady-state polarization curves and the EIS measurements in 1 M NaOH, using NLS program.....	136
12	Roughness factors and intrinsic activities of the HER obtained on Ni-Mo-P electrodes in 1 M NaOH.....	138
13	Kinetic parameters of the HER obtained on nickel based electrodes from the steady-state polarization curves.....	147
14	Parameters values and their standard deviations obtained using the CPE model to approximate experimental the EIS data obtained on Ni ₅₄ Zn ₂₀ P ₂₆ electrode in 1 M NaOH at 70°C.....	156
15	Parameters values and their standard deviations obtained using the two-CPE model to approximate the EIS data obtained on Ni ₅₄ Zn ₂₀ P ₂₆ electrode in 1 M NaOH at 70°C.....	158
16	Parameters values and their standard deviations obtained using porous model to approximate the EIS data obtained on Ni ₅₄ Zn ₂₀ P ₂₆ electrode in 1 M NaOH at 70°C.....	159
17	Kinetic parameters obtained using porous model data in Table 16.....	163
18	Kinetic parameters for the HER obtained from the steady-state polarization and the EIS measurements on Ni-Zn-P electrodes, using porous model.....	166
19	Average of the double layer capacitances, \bar{C}_{dl}^* , and roughness factors, R, obtained on Ni ₆₆ Zn ₁₄ P ₂₀ electrode in 1 M NaOH at 70°C using different techniques.....	190
20	Electrooxidation charges of CO and corresponding surface roughness obtained	

	on Ni electrode in 1 M NaOH at 25 ⁰ C, $Q_{Ni,theory.} = 0.463 \text{ mC cm}^{-2}$	197
21	Electrooxidation charges of CO and corresponding surface roughness obtained on Ni ₆₆ Zn ₁₄ P ₂₀ electrode in 1 M NaOH at 25 ⁰ C.....	197

LIST OF FIGURES

1	Series connection of R_s and C (a), corresponding complex plane (b), Bode (c) and (d) plots; $R = 100 \Omega$, $C = 20 \mu\text{F}$ (375).....	51
2	Parallel connection of R_{ct} and C in series with R_s (a), corresponding complex plane (b), and Bode (c and d) plots; $R = 100 \Omega$, $C = 20 \mu\text{F}$ (375).....	52
3	Equivalent circuit in the case of one adsorbed species: (a) $B < 0$, (b) $B >$ (375)....	55
4	Complex plane plots in the case of one adsorbed species and $B < 0$; total impedance (continuous line), faradaic impedance (dash line), parameter used $R_{ct} = 100 \Omega$, $R_a = 40 \Omega$, $L = 0.2 \text{ H}$, $C_{dl} = 2 \times 10^{-5} \text{ F}$, $R_s = 10 \Omega$ (375).....	55
5	Complex plane plots in the case of one adsorbed species and $B > 0$; total impedance (continuous line), faradaic impedance (dash line), parameter used: $R_{ct} = 100 \Omega$, $R_o = 40 \Omega$, $L = 0.2 \text{ H}$, $C_{dl} = 2 \times 10^{-5} \text{ F}$, $R_s = 10 \Omega$ (375).....	56
6	Complex plane plots for porous electrode according to de Levi's modified model: (a) general case, eqn. [2.93], (b) limiting case for shallow pores, eqn. [2.96], (c) limiting case for very deep pores, eqn. [2.97] (375).....	61
7	Scanning electron micrographs of the cross-section of $\text{Ni}_{70}\text{P}_{30}$ electrode, deposit thickness 16-17 μm : (A) before heating; (B) after 3h heating at 400°C in air.....	84
8	Scanning electron micrographs of $\text{Ni}_{70}\text{P}_{30}$ electrode : (A) no pretreatment, (B) after leaching in 1 M HF at 25°C for 40 min, (C) after 3h heating at 400°C in air, and oxidation in 1 M NaOH at 30°C for 3h at +0.200 V vs. Hg/HgO, (D) as deposited Ni_{92}P_8 (from bath B).....	86
9	X-Ray diffraction patterns of $\text{Ni}_{70}\text{P}_{30}$ electrodes, (A) as deposited and (B) after 3h heating at 400°C in air (similar patterns were observed for $\text{Ni}_{73}\text{P}_{27}$ electrodes),	

	and of Ni ₉₂ P ₈ electrodes, (C) as deposited and (D) after 3h heating at 400°C in air	
	The lines indicate Ni ₃ P phase.....	87
10	Steady-state polarization curves obtained on Ni ₇₀ P ₃₀ in 1 M NaOH at 70°C; (Δ) no pretreatment, (□) after 3h heating at 400°C in air, (O) after 3h oxidizing at +0.200 V vs. Hg/HgO in 1 M NaOH at 70°C, and (●) after 40 min treating with 1 M HF at 25°C. The continuous lines were obtained using data in Table 3.....	90
11	Complex plane plots obtained on untreated Ni ₇₀ P ₃₀ electrodes in 1 M NaOH at 70°C. The continued lines indicate the fitted data using the CNLS method and CPE model.....	92
12	Dependence of the average of double layer capacitance, \bar{C}_{dl} , and parameter ϕ on overvoltage obtained for the HER on Ni ₇₀ P ₃₀ electrode in 1 M NaOH at 70°C : (Δ) untreated electrode, (□) heated at 400°C for 3h in air, (O) oxidized at +0.200 V vs. Hg/HgO, 1 M NaOH 70°C for 6h (●) kept in 1 M HF, 40 min under N ₂ at 25°C. See table 1.....	93
13	Dependence of the charge transfer resistance, R _{ct} , on overvoltage obtained for the HER on Ni ₇₀ P ₃₀ electrodes in 1 M NaOH at 70°C : (Δ) untreated, (□) after 3h heating at 400°C in air, (O) after 6h oxidizing at +0.200 V vs. Hg/HgO in 1 M NaOH at 70°C, and (●) after 40 min treatment with 1 M HF at 25°C. The continuous lines were obtained using data in table 3.....	94
14	Cyclic voltammograms obtained on Ni ₇₀ P ₃₀ electrodes in 1 M NaOH at a sweep rate of 50 mV s ⁻¹ at 70°C ; continuous line 1 : 180th cycle for untreated electrode, dashed line 2 : electrode heated at 400°C for 3h in air.....	100
15	Steady-state polarization curves obtained on untreated (O) Ni ₉₂ P ₈ and (●) Ni ₇₃ P ₂₇ electrodes in 1 M NaOH at 70°C. The continued lines were obtained using data in table 7.....	103

16	Complex plane plots obtained on untreated Ni ₉₂ P ₈ electrodes in 1 M NaOH at 70°C. The continuous lines indicate fitted results using the CNLS method and porous model.....	105
17	Dependence of the charge transfer resistance, R _{ct} , on overvoltage for the HER obtained on untreated (O) Ni ₉₂ P ₈ and (●) Ni ₇₃ P ₂₇ electrodes in 1 M NaOH at 70°C. The continuous lines were obtained using data in Table 7.....	106
18	Scanning electron micrographs prepared from the surface of Ni-Mo-P electrodes, letters indicate the electrodes in Table 1. Fig. 1F presents the cross section of the electrode D. The thickness of the Ni, Ni-P, and Ni-Mo-P layers are respectively 20, 20, and 7 μm.....	114
19	Steady-state polarization curves obtained for the HER in 1 M NaOH on “one-step” deposited Ni ₇₄ Mo ₁₆ P ₁₀ (Δ) at 25°C, (□) at 70°C, “three-step” deposited (●) Ni ₈₆ Mo ₁₂ P ₂ , (O) Ni ₇₁ Mo ₂₇ P ₂ , (▲) Ni ₅₀ Mo ₄₅ P ₅ , and “two-step deposited” (■) Ni ₇₃ P ₂₇ , (the substrate of electrode C and D) at 70°C. The continued lines are obtained from fitted data using NLS.....	116
20	A typical cyclic voltammogram obtained on Ni ₇₄ Mo ₁₆ P ₁₀ electrode in 1 M NaOH at 25°C with 50 mV s ⁻¹ scan rate. The same pattern was observed at 70°C.....	120
21	Complex plane and phase angle plots obtained for the HER in 1 M NaOH on “one-step” deposited Ni ₇₄ Mo ₁₆ P ₁₀ (A,F) at 25°C, (B,G) at 70°C, “three-step” deposited (C,H) Ni ₈₆ Mo ₁₂ P ₂ , (D,I) Ni ₇₁ Mo ₂₇ P ₂ , and “two-step deposited” (E,J) Ni ₇₃ P ₂₇ (the substrate of electrode C and D) at 70°C. The behavior of electrode Ni ₅₀ Mo ₄₅ P ₅ (<i>i.e.</i> , electrode F, Table 9) was similar to Ni ₇₁ Mo ₂₇ P ₂ (<i>i.e.</i> , electrode D, Table 9) with smaller R _{ct} . The continuous lines indicate fitted results using the CNLS method, see section 5.2.2.3 for models. The first letters in the parentheses indicate the complex plane plots as well as the electrode <i>name</i> , the second letters indicate only the complex plane plots.....	132

- 22 (A) Dependence of the average of double layer capacitance, \bar{C}_{dl} , and (B) parameter ϕ on overpotential for the HER in 1 M NaOH on "one-step" deposited $Ni_{74}Mo_{16}P_{10}$ (Δ) at 25°C, (\square) at 70°C, "three-step" deposited (\bullet) $Ni_{86}Mo_{12}P_2$, (O) $Ni_{71}Mo_{27}P_2$, (\blacktriangle) $Ni_{50}Mo_{45}P_5$, and "two-step deposited" (\blacksquare) $Ni_{73}P_{27}$ (the substrate of electrode C and D), at 70°C..... 134
- 23 Dependence of charge transfer resistance, R_{ct} , on overpotential for the HER in 1 M NaOH on "one-step" deposited $Ni_{74}Mo_{16}P_{10}$ (Δ) at 25°C, (\square) at 70°C, "three-step" deposited (\bullet) $Ni_{86}Mo_{12}P_2$, (O) $Ni_{71}Mo_{27}P_2$, (\blacktriangle) $Ni_{50}Mo_{45}P_5$, and "two-step deposited" (\blacksquare) $Ni_{73}P_{27}$ (the substrate of electrode C and D), at 70°C. The continued lines are obtained from fitted data using NLS method..... 135
- 24 Scanning electron micrographs prepared from the surface of Ni-Zn-P electrode, (A) as deposited in "one-step", (B) as deposited in "three-step", (C) electrode "B" but after leaching at 70°C in 30% KOH for 24h, (D) electrode "C" after 8 days the HER at constant current, $j = 500 \text{ mA cm}^{-2}$, and 70°C in 30% KOH..... 143
- 25 Scanning electron micrographs prepared from the cross-section of "three-step" deposited Ni-Zn-P electrodes, (A) as-deposited, and (B) after 24h leaching at 70°C in 30% KOH. The bright regions show the alloy which is indicated on the picture..... 145
- 26 Steady-state polarization curves obtained for the HER on "three-step" deposited $Ni_{54}Zn_{20}P_{26}$, (after leaching in 30% KOH at 70°C for 24h): (\blacktriangle) in 1 M NaOH at 25°C, (\square) in 1 M NaOH at 70°C, (O) after 8 days activation in 30% KOH at 70°C, (Δ) in 1 M NaOH at 25°C on "one-step" deposited $Ni_{56}Zn_{27}P_{17}$. The continued lines are obtained using linear regression method..... 148
- 27 Complex plane plots, $-Z''$ vs. Z' , and Bode plots, phase angle vs. $\log\omega$ ($\omega = 2\pi f$) for the HER obtained on "three-step" deposited $Ni_{54}Zn_{20}P_{26}$ electrode, in 1 M NaOH at 70°C, CPE (A,D), two-CPE (B,E), and porous (C,F) models. The

	continued lines are obtained from fitted data using the CNLS method.....	154
28	Complex plane plots obtained on $\text{Ni}_{54}\text{Zn}_{20}\text{P}_{26}$ electrode at $\eta = -0.125$ V, in 1 M NaOH at 70°C, fitted to different models: continuous line - porous model, dashed line - "two-CPE" model, dashed-dotted line - "one CPE" model; (A) in high frequencies range and (B) in the whole range of frequencies.....	161
29	Dependence of the average of double layer capacitance, \bar{C}_{dl} , and parameter ϕ on overpotential obtained for the HER on "three-step" deposited $\text{Ni}_{54}\text{Zn}_{20}\text{P}_{26}$, (\blacktriangle) in 1 M NaOH at 25°C, (\square) in 1 M NaOH at 70°C, (O) after 8 days activation in 30% KOH at 70°C, (Δ) on "one-step" deposited $\text{Ni}_{56}\text{Zn}_{27}\text{P}_{17}$ in 1 M NaOH at 25°C (porous model was used in all these cases).....	165
30	Steady-state polarization curves obtained for the HER on "three-step" deposited $\text{Ni}_{54}\text{Zn}_{20}\text{P}_{26}$ electrode, (\blacktriangle) in 1 M NaOH at 25°C, (\square) in 1 M NaOH at 70°C, (O) after 8 days activation in 30% KOH at 70°C, (Δ) in 1 M NaOH at 25°C on "one-step" deposited $\text{Ni}_{56}\text{Zn}_{27}\text{P}_{17}$. The continued lines are obtained from fitted data using NLS method.....	167
31	Dependence of charge transfer resistance, R_{ct} , on overpotential for the HER obtained on "three-step" deposited $\text{Ni}_{54}\text{Zn}_{20}\text{P}_{26}$ electrode, (\blacktriangle) in 1 M NaOH at 25°C, (\square) in 1 M NaOH at 70°C, (O) after 8 days activation in 30% KOH at 70°C, (Δ) in 1 M NaOH at 25°C for "one-step" deposited $\text{Ni}_{56}\text{Zn}_{27}\text{P}_{17}$. The continued lines are obtained from fitted data using NLS (R_{ct} from porous model was used in all these cases).....	168
32	A typical cyclic voltammogram obtained on $\text{Ni}_{54}\text{Zn}_{20}\text{P}_{26}$ electrode at 70°C, in 1 M NaOH, with 20 mV s^{-1} scan rate. The same pattern was observed at 25°C.....	169
33	Variation of peak charge, Q_p , roughness factor, $R = Q_p / 0.1$, and the peak current (at 0.450 V /Hg/HgO, see Fig. 32), j_p , as functions of scan rate, obtained from cathodic peak between 0.400 to 0.500V vs. Hg/HgO, at 70°C, in	

	1 M NaOH.....	171
34	Scanning electron micrographs prepared from the surface of Ni ₆₆ Zn ₁₄ P ₂₀ electrode, (A) as deposited and (B) after leaching in 30% KOH at 70°C for 24h.....	177
35	Steady-state polarization curves obtained for the HER on Ni ₆₆ Zn ₁₄ P ₂₀ electrode in 1 M NaOH at 70°C in N ₂ atmosphere with different polarization time. A negative shift in E _{eq} for 1 and 5 seconds per point polarization time, and a positive shift for longer times is observed.....	179
36	Steady-state polarization curves obtained for the HER on Ni ₆₆ Zn ₁₄ P ₂₀ electrode in 1 M NaOH at 70°C in H ₂ atmosphere with different polarization time. While a negative shift in E _{eq} is observed for 1 and 5 seconds per point polarization time, no shift is observed for longer times.....	180
37	(A) Complex plane and (B) phase angle plots obtained on Ni ₆₆ Zn ₁₄ P ₂₀ in 1 M NaOH at 70°C. The continued lines are obtained from fitted data in porous model using the CNLS method.....	183
38	Chronopotentiogram obtained on Ni ₆₆ Zn ₁₄ P ₂₀ electrodes in 1 M NaOH at 70°C under 2 mA cm ⁻² anodic current-stepThe expected reactions are presented on the figure.....	185
39	Cyclic voltammograms obtained on Ni ₆₆ Zn ₁₄ P ₂₀ electrode at 70°C in 1 M NaOH in the range of -0.810 to -1.000 V vs. Hg/HgO with different scan rates: (A) (1) 5, (2) 10, (3) 20, (4) 50, (5) 100, (6) 200, (7) 500, and (8) 1000 mV s ⁻¹ . (B) Comparison one of the cyclic voltammograms obtained at 500 mV s ⁻¹ for different data acquisition modes (AM x/4, x varies from 1 to 4) using M270 software as well as for analogue method, see the text.....	188
40	Dependence of capacitive current density on scan-rate at 70°C in 1 M NaOH extracted from cyclic voltammograms obtained on Ni ₆₆ Zn ₁₄ P ₂₀ electrode from	

	average of the current densities, $(j_c + j_a) / 2$ at -0.910; analogue (●), and digital with different acquisition mode, AM, in EG&G M270 software; (O) 1/4, (□) 2/4, (▲) 3/4, and (◆) 4/4.....	189
41	Cyclic voltammograms obtained on polycrystalline nickel electrode at 25°C in 1 M NaOH and 20 mV s ⁻¹ scan rate; the first cycle (1) in the absence of CO, (2) in the solution saturated with CO, (3) after 25 min bubbling with CO followed by 25 min bubbling with N ₂ , (4) after one 25 min bubbling with CO followed by 100 min bubbling with N ₂ or replacing the solution by a new and deoxygenated pure 1 M NaOH, and (5) the second cycles for all the cases.....	193
42	A typical cyclic voltammogram selected from Fig. 41 (curve 3) to show our method for extraction of data, only peak (abc area), and up to middle line area (a'b'c area).....	194
43	Cyclic voltammograms obtained on Ni ₆₆ Zn ₁₄ P ₂₀ at 25°C in 1 M NaOH and 20 mV s ⁻¹ scan rate; the first cycle, (1) in the absence of CO, (2) after 2.3h bubbling with CO, and (3) after 2.3h bubbling with CO followed by replacing the solution with a new and deoxygenated pure 1 M NaOH solution, and (4) the second cycles in all the cases.....	196

LIST OF SYMBOLS

A, B, C	Parameters describing impedance of the electrodes according to the eqn. [2.82], $A = 1 / R_{ct}$
b	Tafel slope, slope of linear part of steady-state polarization curve
\bar{C}_{dl}	Average double layer capacitance in a whole frequency range, at a given constant potential
C_O, C_R	Redox concentrations
CPE	Constant phase element
E	Potential
E_{eq}	Equilibrium potential
E^0	Formal potential, standard potential at a given concentration
F	Faraday constant
f	Constant at a given temperature and equal F / RT , or frequency in EIS technique
g	Interaction parameter for adsorbed species
\tilde{i}	Phasor of the current of perturbed system in EIS
j	Current density
j_{dl}	Double layer capacitive current density
j_0	Exchange current density
k^0	Standard rate constant
k_i	Forward reaction rate constant for i^{th} step of the reaction

k_i	Backward reaction rate constant for i^{th} step of the reaction
\tilde{r}	Phasor of the reaction rate of perturbed system in EIS
R_{ct}	Charge transfer resistance
RHE	Reversible hydrogen electrode
R_s	Solution resistance
T	Temperature in Kelvin, and also capacitance parameter in CPE model
R	Gas constant
$Z(j\omega)$	Total impedance
Z'	Real component of impedance
Z''	Imaginary component of impedance
\hat{Z}_f	Faradaic impedance
\hat{Y}_f	Faradaic admittance
β	Symmetry coefficient for charge transfer process
ΔG_{abs}^0	standard free energy of adsorption in the absence of external electrical potential
η	Overpotential (or overvoltage)
η_{250}	Overvoltage at $j = 250 \text{ mA cm}^{-2}$
$\tilde{\eta}$	Phasor of the overpotential of perturbed system in EIS
θ	Surface coverage by adsorbed hydrogen
$\tilde{\theta}$	Phasor of the surface coverage of perturbed system in EIS
θ_0	Surface coverage by hydrogen at equilibrium potential.
ρ	Specific resistance of the solution, $\Omega \text{ cm}^3$

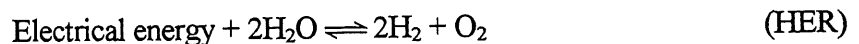
v	Scan rate dE / dt in cyclic voltammetry
v_b	Backward reaction rate
v_f	Forward reaction rate
v_i	i^{th} step reaction rate
v_{net}	Net reaction rate
σ_1	Total charge required for one monolayer surface coverage by adsorbed H
ϕ	Dimensionless parameter related to the dispersion of double layer capacitance
ω	Angular frequency

INTRODUCTION

In the last three decades a great interest has been devoted to the research of electrolytic hydrogen production from aqueous solutions (1-4). The main reasons for this interest are: (i) the environmental problems arising from pollution of fossil fuels combustion and necessities to replace them by a clean fuel, (ii) great interest in using hydrogen as a storable energy carrier, and (iii) hydrogen itself as a source of energy.

Fossil fuels (oil, coal, natural gas) suffer from two shortcomings; they are polluting and non-renewable. The fossil fuels are pollutants even when conceivably converted to the electricity far from the cities. Among the several alternatives to fossil fuels (5), hydrogen is the cleanest one both in production and combustion. The only possibility is to resort to renewable energy sources (5) as solar, ocean-thermal, wind, geothermal and nuclear. Hydrogen is not only the cleanest energy carrier, but also the cleanest fuel in nuclear energy (fusion). Therefore, in order to overcome the environmental problems and storage the natural unstable energies (solar, wind, thermal, etc.) hydrogen production is imperative.

Hydrogen has not yet obtained, generally, sound validity as an integrating fuel. The reasons are safety and cost of production. While the former is an engineering problem, the latter calls for fundamental research. The most wide spread technique for hydrogen production is based on the following reaction (2):



The electrical energy may be taken from different sources as were mentioned above. Hydrogen produced by this method is usually recombined with O_2 , hydrogen oxidation reaction, HOR, in suitable burners, where the product is water and energy as:



The main part for the HER (or HOR) is the electrochemical cell, which contains electrodes and solution (1). One of the most important problems is design and preparation of the electrodes to be physically and chemically stable, and electrochemically active (and preferably resist to the poisoning effects). Practically, it means the need of electrodes with large surface area and long lifetime without losing the activity. This task needs basic methods to study the new materials, design the catalyst, find the origin of activity, improve it, and get the desired properties.

The first chapter of this thesis is a review of the concepts of electrocatalysis, activity, and electrode materials, particularly nickel based electrodes, for the HER. The methods of the electrode preparation as well as the techniques of the kinetic studies are verified, the basic points are highlighted, and the goal of the thesis, *i.e.*, development of new electrode materials for the HER, is presented. The second chapter is concerned with fundamental theories and equations which are used for evaluation of the electrodes behavior. In chapter three the experiment outlines containing electrode preparation, and electrochemical measurements are presented. In chapters four, five, and six the results obtained for preparation and activities of Ni-P, Ni-Mo-P, and Ni-Zn-P electrodes are presented and discussed, respectively.

Chapter seven deals with the results obtained on determination of the surface roughness of Ni-Zn-P electrode by *in situ* methods, specially with a new technique, CO molecular probe, for surface roughness determination which was developed in this thesis. Also a new behavior was found for dissolved CO, oxidation on nickel based electrodes.

Ni-Me-P is selected as the title of the thesis in which "Me" is the symbol of a metal to cover the titles of all the electrodes studied, *i.e.*, Ni-P, Ni-Mo-P and Ni-Zn-P.

Publications

Some parts of the work which is described in this thesis have been already published or submitted for publication, and other parts are in preparation as follows:

1. R. Karimi-Shervedani and A. Lasia, "Studies of the Hydrogen Evolution Reaction on Ni-P Electrodes," *J. Electrochem. Soc.*, **144**, 511 (1997).
2. R. Karimi-Shervedani and A. Lasia, "Kinetics of the Hydrogen Evolution Reaction on Ni-Zn-P Electrodes in Alkaline Solutions," *J. Electrochem. Soc.*, **144**, 2652 (1997).
3. R. Karimi-Shervedani and A. Lasia, "Kinetics of the Hydrogen Evolution Reaction on Ni-Mo-P Electrodes in Alkaline solutions," *J. Electrochem. Soc.*, *in preparation*, (1997).
4. R. Karimi-Shervedani and A. Lasia, "Surface behavior of Ni-Zn-P Electrodes, Evaluation of the Surface Roughness by *in situ* Methods" *J. Electrochem. Soc.*, *in preparation*, (1997).

Oral presentations

During the course of this thesis, parts of it were presented at scientific conferences as:

1. R. Karimi-Shervedani and A. Lasia, "Mechanism of the Hydrogen Evolution Reaction on Ni-Zn-P Electrodes in Alkaline solutions," *189th Meeting of The Electrochemical Society*, Los Angeles, California, USA, May 5-10, 1996, Abstract No. 900.

2. R. Karimi-Shervedani and A. Lasia, "Mechanism of the Hydrogen Evolution Reaction on Ni-Mo-P Electrodes in Alkaline solutions," *190th Meeting of The Electrochemical Society*, San Antonio, Texas, USA, October 6-11, 1996, Abstract No. 802.

3. R. Karimi-Shervedani and A. Lasia, "Surface behavior of Ni-Zn-P Electrodes," *191st Meeting of The Electrochemical Society*, Montreal, Quebec, CANADA, May 4-9, 1997, Abstract No. 1702.

CHAPTER 1

REVIEW

In this chapter a short review on the concept of electrocatalysis will be presented. Then, the electrocatalytic activity and electrode materials for electrocatalytic hydrogen evolution reaction, particularly nickel based electrodes, will be reviewed.

1.1 Electrocatalysis

Electrocatalysis is a catalysis of the electrode reactions. It can be accomplished by the action of the electrode material (heterogeneous) (6) or alternatively the action of species in solution (homogenous) or both. Heterogeneous electrocatalysis deals with the effects of electrode materials on the mechanism and the rate of electrode reactions (7,8). In other words, the scope of electrocatalysis as a science is to establish a predictive basis for design and the optimization of electrocatalysts (1).

The voltage applied to an electrolytic cell, ΔV , contains several contributions as:

$$\Delta V = \Delta E + \Sigma\eta + \Delta V_{\Omega} + \Delta V_t \quad [1.1]$$

where ΔE is thermodynamic decomposition potential difference determined by nature of the electrode reactions, it is independent of electrode material and the reaction rate; $\Sigma\eta$ is the sum of the overpotentials, *i.e.*, the extra voltage required to drive the electrode reactions at a practical rate, and is related to the rate of electrochemical reaction; ΔV_t is what usually called instability, *i.e.*, the voltage increases due to electrochemical deactivation of the electrode that usually arises from degradation of the electrode material with the time; ΔV_{Ω} includes all ohmic drops in the electrode structure and the electrolyte. The latter includes: (i) any ohmic drop due to an eventual poor conduction of electrode materials, (ii) barrier at the support-overlayer boundary of the activated

electrodes, and (iii) resistance of electrolyte. The first two parameters are related to the fundamental research while the third one is an engineering problem (9). ΔV_t is very often either neglected or not sufficiently well studied in fundamental research. From the practical point of view, this is a very important parameter. Many very-good electrocatalysts have not yet found their application due to their poor stability (1). Fundamental research is usually focused on the evaluation of the term $\Sigma\eta$, the target being the study of the structure-activity relationships of materials. In fact this is the total value of ΔV in eqn. [1.1] which bears upon the energy efficiency of the electrocatalytic cell.

There are several ways to improve the electrolytic efficiency. Some aspects as cell design, temperature optimization, separator structure, etc. remain as a matter of engineering task (10,11). As a fundamental science, electrocatalysis can be regarded as a research in the area of *new operating conditions* or *new materials* in order to (i) improve activity, efficiency and selectivity of electrodes, (ii) increase the electrode life time, (iii) reduce investment and operation costs, and (iv) avoid pollution (1). In a general sense, reduction of ΔV is obtained either by increasing the real surface area, or by reducing the overpotential. In other words, the evaluation of electrode materials is accomplished by comparing the apparent current density at a given electrode potential, or more commonly, by comparing the overpotential at a given apparent current density. It is evident that an increase in real surface area will produce a more favorable electrode performance as much as a reduction in overpotential. In fact, one of the procedures adopted in practice to increase the activity of the cathodes is to increase their real surface area.

While the reduction of ΔV related to an increased surface area has a decisive practical impact, it cannot be strictly considered as an electrocatalytic effect, unless the variation of the electrode surface area also involves a modification of the nature of surface active sites. Therefore, in evaluating a new material two factors have to be considered: geometrical and electronic.

The question is: “What parameters should be used for the evaluation of the electrocatalytic activities.” It is well known that in the absence of mass transfer effects and ohmic drop, and at high overpotentials a linear relation exists between the overpotential, η , and the logarithm of current density, j , which is known as Tafel plot, eqn. [1.2].

$$\log j = \log j_0 - \frac{1}{b} \eta \quad [1.2]$$

where b is the Tafel slope and j_0 the exchange current density. The exchange current density is used in some cases as a comparison of the activity of the electrodes (13,14,15). However, since the aim of new materials is to increase the practical current density at a given current density, the comparison of the exchange current densities may be often misleading. At low overpotentials, electrodes with high j_0 and large Tafel slopes may be more active than electrodes with low j_0 and low Tafel slopes, but this rule may not be applicable at high overpotentials. Further, the Tafel slope may increase as the current density increases due to the changes of reaction mechanism or surface conditions of the electrode (16). On the other hand while the j_0 depends on the real surface area, the Tafel slope is not influenced by the surface area. Thus, if the procedure of electrode activation results in a change of the Tafel slope, electronic factors are certainly responsible for that, *i.e.*, intrinsic electrocatalytic activity improvement has been achieved. A more reasonable way for comparing the electrocatalytic activities is comparing their overpotentials at a specific and practically high current density, *e.g.*, 250 mA cm⁻², 500 mA cm⁻² etc. This will be discussed later in this chapter.

1.2 Hydrogen production by electrolysis

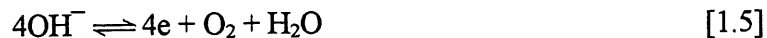
Hydrogen can be produced by electrolytic hydrogen evolution reaction in aqueous solutions as a desired product (17,18) or by-product in chlor-alkali process (19) and in chlorate production (20), which are among the most popular electrochemical processes. The hydrogen evolution reaction (HER) is one of the simplest electrode reaction (6), and the only reaction for which a complete

theory of electrocatalysis has been developed (21). The reason is that the reaction proceeds through a limited number of steps with possibly only one intermediate.

The total reaction of water electrolysis can be expressed as:



This reaction has to be considered for two aspects: electrolytic production of (i) hydrogen, and (ii) heavy water. It should be mentioned that while most of the fundamental studies on the HER are based on data in acid solutions, strongly alkaline solutions are technologically more common. However, recently, a great number of papers have been devoted to studies in alkaline solutions. The hydrogen and oxygen production reactions at cathode and anode in alkaline solutions can be presented as:



The relative inefficiency of cathodes and anodes has remained one of the most outstanding factors of energy dissipation. It orients the research in the direction of improving hydrogen electrocatalysis (22).

1.3 Major aspects in evaluation of the performance of cathodes

Although hydrogen can be produced from both acidic and basic solutions, alkaline solutions are preferred for electrolytic hydrogen production because of corrosion problem. Nickel electrodes have benefits as low price and stability in alkaline solutions. Below, review of nickel based electrodes is presented.

1.3.1. Surface characterization

In the case of solid electrodes, knowledge of the real surface area is a prerequisite for proper evaluation of the activity with respect to other samples. It is very difficult to determine the real surface area because there are no unique techniques applicable to all materials. When the surface area determination cannot be accomplished, evaluation of synergetic effects (increase in the number of active sites per unit of the surface area) can only be ambiguous. Although many of the experimental results in literature are still insufficiently characterized from this point of view, in general, the need for a surface area determination requires more studies. Sometimes BET (Brunauer-Emmett-Teller, a method in which surface area of the electrode and the shape of the pores may be evaluated by gas adsorption, *e.g.*, N₂) values are given, but the BET area may not correspond to the electrochemically active one, especially if supported catalysts are used or inert components are parts of composite material (22). Although in determination of the surface area from capacitance measurements there is no absolute reference for many materials and there is no potential at which the capacitance is the same even among different metal crystal faces (22), relative measurements for different samples of the same materials are acceptable.

The best approach is usually an *in situ* determination based on voltammetry or charging curves, usually within the hydrogen adsorption region (22) which is known as hydrogen under-potential deposition (UPD-H). It is of course necessary to know the actual value of θ_H for absolute determinations, but the method is practicable on relative basis. Only in a few cases, *e.g.*, for Pt, the method becomes absolute (22), σ_1 or total surface coverage can be estimated.

Whenever composite materials are used, the surface composition becomes an essential parameter to assess the actual electrocatalytic activity. The dominating role of surface composition in electrocatalysis was stressed by Frumkin *et al.* long time ago (23). This task is difficult since the equipment for surface analysis is not an ordinary tool in electrochemical laboratories. As a matter of fact, the surface of electrodes remains insufficiently characterized in most instances, so that no

more than a phenomenological observation can be made. In the cases where surface analysis has been carried out, it has usually opened new horizons to the understanding of the electrocatalytic behavior of the materials (22,24). In some instances surface analysis has been essential to show that synergetic effects were only apparent (25). Surface characterization includes also the study of its modification under cathodic load or after pretreatment. *In situ* activation usually results in the case of composite structures which are difficult to identify by X-Ray diffraction, and may contain metallic and non-metallic components. Particularly crucial is the case of the surface structure of glassy metals or amorphous alloys.

The field of cathode or anode activation requires use of complementary physical techniques to evaluate systems otherwise difficult to understand. Electrochemical techniques are sufficient to evaluate the kinetic parameters and state intermediates, especially if a digital acquisition of the open-circuit potential-decay transients, or the Electrochemical Impedance Spectroscopy (EIS) coupled with computer data processing, are used together with steady-state polarization data (26-41). However, the chemical and physical characterization of the surface remains essential.

1.3.2 Stability

In a technological perspective, electrocatalytic activity is not the only requirement for a good cathode. The electrode must be stable under the working conditions, *i.e.*, ΔV should not drift with time. In practice, the choice of a material is based on a balance between activity, overall efficiency and stability. The test of cathode stability is thus an essential step in applied research (42-50). The most outstanding source of instability is corrosion that can arise at open circuit when a cell is shut-down for maintenance or other reasons (51,52). The cathode can be simply corroded or oxidized. In the later case, the residual oxide can be deleterious for the catalytic activity since it may remain unreduced even under cathodic load. Therefore, cathode materials usually contain additives whose function is to reduce the consequences of shut-downs (53). Moreover, a use of complexing agents may be useful (Rowland's effect) to remove the surface oxides (54). Therefore,

this type of tests should be considered in experiments (30,51,53,55). If the cathode is corroded during the shut-down, addition a cathodic protection agent may be necessary (20,55).

Hydrogen penetration into the cathode and hydride formation during the HER is a general phenomenon (56-66). In the case of metals, the process of hydrogen dissolution into the cathode depends on the crystal structure, atomic size and electronic structure of the metal (67). Hydrides are the cathodic analogues of oxides. While metals are always covered by oxides during oxygen evolution, during the HER many of them form hydrides. These phenomena may increase or decrease the activity of the electrode for the oxygen and/or hydrogen evolution reactions (7,68,69). Hydrogen absorption may be deleterious, for example in the case of Ni and Co it is believed that increase in the overpotential at the beginning of electrolysis is due to the hydrogen absorption (36, 70).

While anodic oxides may be precursors to anodic dissolution (71), that is metal atom becomes surrounded by a water-like environment which reduces the energy required to leave the lattice, the formation of hydrides can result in the phenomenon of hydrogen embrittlement (72). Hydrogen usually penetrates through the lattice interstices (73) thus causing an expansion of the crystal. Internal bursts or blisters may result if large amount of hydrogen is collected in a localized area (74). The metal may become mechanically fragile and, in some cases, such as LaNi_5 , the structure of the material may collapse to a powder (75). It has been pointed out that the "explosion" of the cathodes can be prevented by working at relatively high temperatures and moderate current densities (instead of high current density and ambient temperature) so that the internal fugacity of H_2 gas (depending on the overpotential) is maintained relatively low (76). Additives are usually introduced into the cathode material to reduce the effect of hydrogen embrittlement (77-80). Raney metals, in particular Raney nickel (nickel alloy with Al or Zn), can be pyroforic in air because of the large amount of dissolved hydrogen (81) and the presence of very small crystallites. There are some solutions proposed for this problem. For instance, Raney nickel can be incorporated into a nickel matrix so that the heat of $\text{H}_2\text{-O}_2$ recombination is dissipated through the metal (82-84).

Phosphorous and nickel can be alloyed with different atomic percents and produce alloys that show very good resistivity for corrosion in alkaline solution, better than nickel (85-99). A typical material for alkaline water electrolysis is nickel. It is often prepared in a Raney form and the active metal (Al, Zn) is leached out to leave a very high real surface area. Raney nickel does not resist well to intermittent electrolysis (46-48) and, occasionally, its overpotential increases with time (22). However, this area still calls for more research to achieve active and stable electrode materials.

1.3.3 Methods of electrode preparation

The method of preparation is the most crucial and usually the least controllable variable. The method of preparation remains the most open aspect in this part regarding the originality and inventiveness. It is hard to list all the methods, because in many cases details have been left purposely obscure. However, cathodes can be coated with an active layer by (i) electrodeposition (100), (ii) thermal decomposition (101-103), (iii) flame and plasma spraying (104-109), (iv) *in situ* activation (109-113) (v), electroless deposition (85,86,87,114-119), (vi) pressing powders with a suitable binder (42-44,102,103,120-123), and (vii) electrodeposition of suspended powder with Ni, Co, etc. (84,124-128).

Different methods of preparation usually result in cathodes with different activity (46). However, the same procedure may produce different results in different laboratories. Only by identifying the factors responsible for electrocatalytic activity, and finding suitable conditions to control them during the electrodeposition, it will be possible to standardize procedures and perhaps to establish some reference standards.

In some cases, as prepared electrodes may be inactive or insufficiently active, etching (activation) may be needed to achieve the expected activity. The activation usually involves the removal of a passivating layer formed during the preparation. This is the case of Ni-Zr and Ni-Ti alloys (89,129-131) because their surface is initially passivated by TiO_2 or ZrO_2 . These layers can be

removed by HF. The duration and conditions of treatment may affect on final activity. This kind of activation may not be generalized and remains as a matter of research for new electrode materials (132).

When thermal decomposition is used to prepare the catalyst layer, generally it is followed by activation either at high temperature in the hydrogen atmosphere or by *in situ* reduction under cathodic current. However, this method may not be always satisfactory (22). The temperature and duration of this process are crucial parameters. Another parameter is the nature of the support (substrate). In some cases no effect has been observed, however the effect of the substrate is evident in other cases, or even essential, as in the case of catalysts dispersion.

1.3.4 Poisoning

Poisoning effect may come from the adsorption of organic compounds or deposition of metallic species that may exist as impurities in the electrolytic solution, in the cell hardware or other components of the electrical reactor. The impurities which have been considered are Pb, Fe, Cr, Hg, Ni, and Cu (34,133). In other cases impurities as S-compounds, *e.g.*, thiourea, (28,33,134-136), CO (137,138), and ions as CN^- (28) have also been considered as poisons for electrodes. The poisoning effect depends on the nature of chemical interactions between the impurity and the cathode. For example, Fe as an impurity in the alkaline solutions has shown a negligible effect on the activity of mild steel for the HER while it has decreased the activity of Pt and sometimes increased the activity of Ni and Ti in the same conditions (133,139). It is said that poisoning effect depends on the porosity of the electrode and decreases as the porosity increases (139-141).

From a fundamental point of view the efficiency of poisoning depends on physical structure of the deposited impurity, *i.e.*, the nature of the chemical interaction between the impurity and the electrode surface. In other words, a different mechanism of deposition may result in a structure of

the deposit which does not inhibit the active surface substantially. In the case of Pt electrodes, Brossard and Huot (142) have reported that if Fe content is around 14 ppm, the cathode may even be activated. Poisoned cathodes can be recovered by *in situ* dissolution of Fe and activation of the cathode in the presence molybdate (110-113,142,143) which increases the electrode activity through Fe-Mo interaction on the electrode surface.

Gas bubbles can also deactivate the electrode by forming a physical barrier (70,144-147). While bubble movement may enhance mass transfer resulting in an increase of the current density (148-152), the bubbles blocking effect may increase ohmic drop (153-157). Effect of bubbles calls primarily for an engineering solution, such as adequate electrolyte flow rate and optimization of cell design, but they can also be related to the electrocatalysis since the wetting of the surface depends on the electrode material.

1.3.5 Effect of temperature

Since the rate of the HER is kinetically limited, increase in temperature can be beneficial for this process. However, in many cases, the Tafel slope has been observed not to increase linearly with T, $b = -2.303RT/\alpha F$, but to increase at a lower rate or even to remain constant (158-160). This has stimulated discussions (161-166) about the fundamental significance of such an “anomalous” behavior which has been interpreted in terms of a partial potential dependent entropy of activation as opposed to the classical theory of constancy of ΔS^\ddagger (167-168). This is not always the case, and in the contrary to claims that the classical Tafel slope is probably an exception than a rule (169), the correct increase in Tafel slope has often been observed (170-173). On the other hand, the Tafel slope has been observed even to decrease with temperature (174).

It seems obvious that in such extreme cases a change in the mechanism and or in the electrode surface is probably responsible for the decrease in b. In other words, the temperature not only raises the reaction rate on account of the activation energy, but it can also catalyze some

modification in the nature of the surface active sites. It is essential to consider that an increase in temperature accelerates not only the hydrogen reaction, but also all other reactions which can proceed in parallel, including surface segregation in alloys and oxide reduction on passive surfaces. It has been shown in few cases that if all the interfering factors are considered, the anomalous temperature effect does not appear (175). It has been pointed out that in most cases the temperature dependence was obtained as a side-product of mechanistic study, and the accuracy of measurements was not high enough to confirm anomalous behavior. The transfer coefficient, α , for the HER, the reduction of hydroxylamine, and bromate on the mercury electrode is strictly independent of temperature while for reduction of iodate ion this parameter is clearly temperature dependent (176). Therefore, the behavior of the Tafel slope with respect to T does not seem to be a result of transfer coefficient dependency on T. However, the anomalous effect of temperature on Tafel slope remains as a matter which has not been understood well yet.

1.4 Factors affecting the activity

1.4.1 Surface state

The theory predicts that the electrocatalytic activity depends on the heat of adsorption of the intermediate on the electrode surface in a way giving rise to the well known "volcano" curve. The prediction has been verified experimentally (177) and the volcano curve remains the main predictive basis on which the catalytic activity is discussed (178,179), and it seems to be valid for simple metals. The electrocatalytic activity is a periodic function of the position of metals in the Mendeleev Table (180-182), although the quality of data is not sufficiently good for comparison yet.

The aim of the cathode activation is; (i) to replace the active but expensive materials by cheaper ones, and (ii) to increase the activity of cheaper materials so as to approach or even surpass that of the more expensive catalysts. One way is to increase the real surface area of the promising metals as Ni (increase in apparent activity), and the second one is alloying or combining two or more

components to obtain catalysts whose electrocatalytic activity exceeds the activity of the pure components. The latter phenomenon is named synergetic effect as it was suggested earlier in this chapter. The synergism theory is still in its infancy in electrochemistry. There is no theory to be able to predict interactions between sites and be a guide for choice of the way to combine the elements and rise in activity.

However, combination of Ni or Co with Mo resulted in an enhancement of the activity for the HER (183-184). This approach is based on Brewer-Engel's theory (185,186) for bonding in metals and intermetallic phases. Although it may be a basis for some predictions which can guide in the selection of components for composite materials, all discussions go back to the heat of hydrogen adsorption (187-189). Therefore, a theory is needed to describe the dependence of the adsorption strength of hydrogen on electronic properties of composite materials. However, before a sound theory can be proposed, it is necessary that experimental picture be free from the any obscurities, ambiguities and irreproducibility due to characterization of the surface of various materials, and to the insufficient identification of various factors which can influence kinetics of the HER.

A morphological modification of the surface state without addition of foreign materials can result in an enhancement of the apparent activity of cathodes. This includes the mere increase in real surface area which is normally achieved in practice by sand blasting the electrodes (83,190) This is as a rule the first operation, both for activated cathodes and for activated anodes, it is done before proceeding to the coating step. The effect of roughening is usually an increase in real surface area and cleaning the surface. The reaction mechanism will not change by changing the number of sites if the nature of the active sites does not change (191). Choquette *et al.* (126), Lasia and Rami (192), and Diard *et al.* (193) reported that oxidation of nickel increased its activity towards the HER. Lian *et al.* (194) reported that oxidation or cycling the nickel cobalt, electrodes between anodic and cathodic potential increased their activity for the OER alkaline water solutions. Korovin *et al.* (195) suggested that anodic Ni oxides catalyze the HER if they are not formed at too high potentials, otherwise they may depress the HER (22).

One of the most often used forms of Ni is Raney Ni which is obtained from Ni-Al or Ni-Zn alloys by leaching Al or Zn in alkaline solution. However, the properties of the resulting electrocatalyst appear to be depended on the nature of the new surface composition (48,81,147). Raney Ni may be prepared by low pressure plasma spray (104-107), or electrodeposition methods (28,42,43,48,196-198). The leached electrodes have shown a high real surface area and low Tafel slope. On such surfaces the activity of the sites at the edges and peaks of crystallites may be different (191,199,200). The effect of temperature on the Tafel slope is more anomalous (105). This may suggest the temperature-induced surface modification, also gas bubbles in the pores may escape more easily at higher temperatures. The roughness factor of Raney electrodes exceeds of 10^3 leading to a considerable decrease in overpotential at a specified current density as compared with the activity of a smooth Ni (28,42,43,48,83,133, 196-198).

1.4.2 Single crystals

The crystallographic orientations have minor differences on the electrocatalysis of hydrogen at low overpotential, the differences vanish at higher overpotentials and surface coverage (201). High coverage with adsorbed hydrogen far from equilibrium smoothes down the differences in the energy of the sites from face to face (202-204). In other words the experimental error in overpotential measurements is more than Φ [where Φ is changes in the overpotential from one surface orientation, *e.g.*, Pt(111) to another one, *e.g.*, Pt(110)] at high overpotentials.

1.4.3 Ion implantation

Ion implantation is often recommended as an efficient tool to enhance electrocatalysis either by disrupting the surface structure of the catalyst or by placing active atoms on an inactive or less active matrix. In order to investigate the effect of surface damages, self-implantation or ion beam bombardment is the most appropriate method. Implantation of Ni on Ni has led to a modest

enhancement of the surface area, but not to changes in electrocatalytic activity (*i.e.*, increase in the number of active sites per unit of surface area) (22, 205). Ion implantation of an active metal on an inactive or less active support is obviously expected to lead to electrocatalytic effects. This is the case of various catalytic metals implanted on glassy carbon.

1.4.4 Adatoms

Adatoms can be deposited *in situ* on the cathode surface by the under-potential process. The mechanism of adsorption, its potential dependence and the state of adsorbed atoms has been widely studied and discussed in literature (206-208). The choice of metals to be deposited is limited to the elements which can be deposited in the under-potential region. It is reported that adatoms of Pb, Tl, Se, Sn, etc. on Au, Pt, Ir, and Ag always cause deactivation of the surface for the H₂ evolution (209-211), through blocking the active sites (212).

Studies of adatoms activation of Raney Ni can have a greater practical impact. It is interesting that the adsorption of Cd or Pb normally results in a sizable enhancement of catalytic activity of Raney Ni (213-215). It was reported that the Tafel slope of Raney Ni was decreased to 30 mV as the catalyst was first soaked in a nitrate solution of the Cd or Pb (213,215). The electrocatalytic activity was observed to increase slowly with the time of adsorption as well as time of polarization.

However, experimental results in the literature do not come to an unique conclusion. For example, it has been reported that the nature of the anion is also important. While maximum effect has been observed with Cd(NO₃)₂ and Pb(NO₃)₂, using CdSO₄ no effect has been observed on smooth Ni (22). It has been suggested that mechanism involves reduction of NO₃⁻ is responsible for electrode activation (215). Also, adatoms do not usually show very good stability on the surface. Therefore, activation of electrodes by means of adatoms does not seem to be very hopeful, if designed electrodes has to work under high cathodic currents densities, 250 mA cm⁻² 500 mA cm⁻², 1000 mA cm⁻² etc.

1.4.5 Modified electrodes

The term "modified electrodes" is a general name used for the electrodes obtained by attaching a monomolecular layer of a specific compound on the surface of the conducting substrate (22). Of course this definition has not been followed by various authors. It is used sometimes for electrodes modified by more than one monolayer deposit as it will be implicitly shown later in this chapter. In electrocatalysis, modified electrodes are common in the field of oxygen reduction.

For the HER or OER, where current densities are very high, modified electrodes are uncommon. However, few investigations have been carried out with modified electrodes for the HER. Although it has been suggested that cobalt porphyrins are active materials for the OER (216) and HER (217-219), the catalyst has not shown good physical stability. Based on our literature review, no more studies have been reported until now.

Another kind of modification may be obtained by deposition of "heteropolyacids" as $H_4MN_{12}O_{14}$, where M can be P or Si and N can be W or Mo (220-227). In all the cases the increase in the electrode activity has been suggested (228,229). The mechanism of the HER has been investigated in acidic and alkaline solutions by Keita *et al.* (220-231). The exchange current densities have been reported are quite high ($\sim 0.01 \text{ A cm}^{-2}$) (221). However, the electrocatalytic activity which that have been assessed on the basis of the exchange current densities (221) may not explain electrode activities at high current densities. In the other words an electrode with a large exchange current density does not necessarily show a high activity at high current densities. High stability has also been suggested for these electrodes. It is interesting that no deactivation has been observed in the presence of metallic impurities in the solution (231). Similar studies have been performed by Savadogo *et al.* (232-236). The activity of nickel electrodeposited from baths containing $H_3PW_{12}O_{40}$ (234,236) or $H_4SiW_{12}O_{40}$ (235) has been studied. An improvement in overpotential and remarkable increase in exchange current density was reported in 1 M H_2SO_4 . Moreover the HER in 3 M KOH was studied on nickel electrodes modified by galvanostatic deposition of

$\text{H}_3\text{PW}_{12}\text{O}_{40}$, $\text{H}_3\text{PMo}_{12}\text{O}_{40}$ or $\text{H}_4\text{SiW}_{12}\text{O}_{40}$. The best electrocatalytic activity was reported for nickel electrodes modified by $\text{H}_3\text{PMo}_{12}\text{O}_{40}$ (4 g per L) (233). Good activity for nickel electrodes modified by electrodeposition of nickel in the presence of heteropolyacides and Cu(II) on stainless steel has also been reported by Savadogo *et al.* (232). The mechanism of the HER was studied in both acid and alkaline solutions. The increase in the activity has been attributed to improvement in overpotential and significant increase in exchange current density. However, no changes in Tafel slopes has been reported (232). Exchange current densities of 12 and 1.1 mA cm^{-2} were reported in acidic and alkaline solutions, respectively.

1.5 Specific materials for electrodes

In this part we will review the cathodic materials, in particularly nickel, its alloy and other nickel based compounds (as metalloids, sulfides, oxides, etc.). Cathodic hydrogen evolution reaction is catalyzed by platinum metals (Pt and Ru in particular) and to a lesser extent by iron, cobalt and nickel. Among the transition metals only nickel is stable in concentrated alkaline solution at hydrogen equilibrium potential. However, different procedures have been suggested to modify the electrode surface and its morphology with the aim to increase the real surface area or intrinsic activity, compensate the low catalytic activity of nickel, and take advantage of its low price (11,47,81,83,109,120-123,147,190,237-246). We start with smooth nickel electrodes and then review some other important nickel based electrode materials.

1.5.1 Smooth nickel

Theory of the mechanism and kinetics of the HER was studied and will be discussed in next chapter. The activity of Ni electrodes decreases under long time the hydrogen evolution reaction (144,247,248). Although there are different reasons for different electrode materials (247), deactivation of Ni is studied by different authors and attributed to the hydrogen absorption (28,70,75,144,249-250). Some authors have reported that mechanism may not change (248) while

others have reported changes in mechanism so that the hydrogen desorption will become rate controlling (247).

It is difficult to obtain a clean nickel surface free of oxides. Oxides are always present on the surface of transition metals in alkaline solutions. At the open circuit they are intermediates in the mechanism of corrosion. The resistance of Ni towards corrosion in alkaline solutions is much better than that of Fe (22). Nickel oxides with different structure and oxidation degree can be formed on nickel electrodes (251,252). They may have different structure in the same oxidation state. The stability, degree of oxidation, and reducibility of the oxides depend on the conditions of their formation (250,253-256). If the temperature (and also anodic current) is high enough, more than 70°C, α -Ni(OH)₂, which is formed in anodic region, will convert to the β -Ni(OH)₂. β -Ni(OH)₂ remains stable even in the cathodic potential regions (251,252,256-259). By repeating oxidation-reduction of Ni in alkaline solution a thick layer of nickel oxides can be produced on the electrode surface (252). The thickness of the oxide layer may be determined from the total charge in the oxidation process. Depending on the anodic potential, Ni may be oxidized to Ni(II), Ni(III), or even Ni(IV) (260) which on reversing the potential will be reduced to Ni or Ni(II). Hall has reported activation of Ni surface for the HER by anodic oxidation (109) due to Ni(OH)₂ formation. This was confirmed by Lasia and Rami (192), Choquette *et al.* (126), and Diard *et al.* (193). They reported that oxidation of nickel increased the activity of this electrode for the HER. Deactivation of cathodes occurs during the cell shut-down (51-53). A method to cure this problem is to increase the hydrogen absorption ability, *i.e.*, metal hydride formation during the HER. Therefore, the cathode can be charged at cathodic potential and discharged during shut-down leading to the protection of the cathodes (53,127). The adsorbed hydrogen on Ni electrodes can be estimated by charging curves, potentiodynamic curves, impedance measurements, and simple discharging (OPD-H desorption) following galvanostatic charging (OPD-H adsorption) experiments (26,27,31,34, 35,61,64,135,192,260-263). The amount of adsorbed hydrogen decreases in the presence of halide ions (264). This is due to a decrease in the M-H adsorption energy induced by ion-specific adsorption with partial charge transfer. The effect is lower for Cl⁻ and higher for I⁻.

The theories related to the effect of anions on electrode behavior, particularly for cathodes in the HER, will be reviewed in next chapter.

1.5.2 Raney nickel

To improve the electrode matrix and increase the electrode activity, sintered, Teflon bonded, phosphate-bonded Ni electrodes, and Raney metal as Raney Ni, Raney cobalt (Co-Al or Co-Zn) and Raney copper (Cu-Al or Cu-Zn), have been proposed (26,109,125,126,147,238,239,266-268) and a good improvement in electrode activities, both in Tafel slope and overpotential, was observed in the most cases. A decisive modification in electrode kinetics is obtained using Raney nickel materials (42-44,48,106,121-123,147,196,245,268-273), *i.e.*, alloying of Ni with another component (usually Al or Zn) which is then leached out away in caustic solution. The dissolution of the soluble component leaves a porous structure with a very high real surface area and particularly active sites. Therefore, Raney Ni coatings are used to compensate the low catalytic activity and simultaneously to take advantages of Ni low price and stability in alkaline solutions. As an electrocatalyst, Raney Ni was first proposed by Justi *et al.* (269).

Various method of preparation of Raney nickel electrodes have been proposed: (i) plasma spraying of the granulated Raney nickel precursor alloy on to the nickel support (106,121,147), (ii) annealing of Al or Zn coated electrodes which leads to formation of smooth layers of Ni-Al or Ni-Zn alloys of variable composition by interdiffusion of Ni and Al or Zn (121-123,147), (iii) sheradizing that is exposing the nickel surface to zinc vapors at 300 to 400°C in the inert atmosphere which allows preparation of Ni-Zn alloys with defined composition and thickness (147), (iv) cold rolling (105), and (v) galvanostatic deposition of Ni-Zn from aqueous bath (26,49,123,196,268,273).

Different attempts have been made to increase the physical and electrochemical stability of Raney nickel electrodes (81,124, 274). The composition of the precursor has an important influence on

the adsorption properties of the Raney nickel, hence on its electrocatalytic activity (275). It has been reported that sintering (237) or electrocodeposition (24,84,124,183,276) can improve the properties of Raney nickel electrodes and stabilize their structure and electrochemical behavior. In this regard Ni is deposited together with some other metals as V, Cr, Zr, Co, Mo, Fe, Cu etc. (48,183,197,277). The electrochemical activity and physical stability have been improved, yet the expense of electrode preparation is high (106). A new method, multi-step electrodeposition, has been recently described to solve the problem of low physical stability of Raney nickel catalysts. This method was presented by Machado *et al.* for preparation of Ni-Zn and Ni-Zn-Co (197). Poor adhesion has been observed for one-step galvanostatic deposition Raney nickel (273). However, the reproducibility, adhesion and physical stability for multi-step have been desirable. Besides, it is possible to control the composition and the structure of the electrode (273,278). The surface behavior, Tafel slope, and kinetics of the Raney nickel electrodes will be discussed in next chapters (16,42-44,103,106,121-126,149,243,278).

1.5.3 Nickel boride

The borides of transition metals have been quoted as one of the most promising materials for the HER in alkaline solutions (102,103). Among them, amorphous nickel boride which has been obtained by reaction between borohydride and aqueous nickel salt is the best known of this group (133,280-282). The size of particles of this product has been 10 to 50 nm (282). The HER has been studied on this material and a low Tafel slope and overpotential has been obtained. A systematic study on nickel boride was performed, and a good activity was reported for these electrodes (103). Borodzinski and Lasia modified the method and prepared nickel boride doped with Ru, Rh, Cr, Pt, Mo, and Zn and studied their kinetics towards the HER by the EIS and polarization techniques (102). High activity of these materials has been attributed to their large surface area, and in some cases surface roughness has been more than 10^4 .

1.5.4 Nickel sulfide

Study of hydrogen evolution reaction on nickel sulfide electrodes dates back to 1970's (282,283). Recently, Ni-S electrodes were prepared by simple electrodeposition method from aqueous baths (100,284-286). The composition of the electrodes depends on the reagents concentration, especially thiourea, and bath conditions. These materials are known to be amorphous. Paseka has shown that these electrodes have a good activity for HER, and they can absorb relatively large amount of hydrogen, more than pure nickel (286). High activity of these materials has been attributed to their ability of hydrogen absorption. These properties are different from the well known fact that sulfur deposited on the nickel surface reduces both the rate of the HER and the amount of adsorbed hydrogen (287,288). It is interesting that dissolution of sulfur does not decrease the activity. The kinetic behavior of leached electrodes is similar to Raney electrodes. However, using co-deposition of nickel sulfide with small amount of Mo may slow down the weight loss and stabilize the surface (128).

1.5.5 Nickel phosphorous

Ni-P materials may be obtained by electro- or electroless deposition. Their composition depends on the bath composition, temperature, pH, and current density (284,289-299). The structure of the electrodeposited Ni-P alloys depends on the method of preparation and P content. The relation between the amount of P and crystallinity is not clear (86,300,301). It has been suggested that electrodeposited alloys containing 0 to 10 at. % of P are crystalline, between 10 to 15 at. % of P are either crystalline or amorphous, and alloys containing more P are amorphous (299). Others reported that the alloys containing less than 14 at. % of P were crystalline (301). However, amorphous samples containing low amount of phosphorus obtained by electrodeposition were also reported (52,302). A microcrystalline structure has been attributed to the electroless deposition of Ni-P alloys containing less than 7 at. % of P (in some cases less than 11.3 at. % of P) (114,86). The deposited Ni-P alloys form usually metastable phases. Ni-P alloys with less than 22.7 at. % of P

upon heating change to Ni_3P and Ni while the alloys with more than 24.6 at. % of P change to a uniform Ni_3P phase and their surface may be covered with phosphorous compounds (297).

Phosphorus may be partially leached out from these alloys, *e.g.*, by an electrochemical oxidation. Crystalline samples show active oxidation while amorphous alloys exhibit passivation (298,299). Hoffmann and Well (295) and Diegle and Sorensen (296) proposed a mechanism for this behavior in acidic and alkaline solutions in which the electrode surface is blocked by hypophosphite groups that are formed by chemical or electrochemical oxidation of phosphorous.

Conflicting reports on the activity of Ni-P electrodes towards the hydrogen evolution reaction (HER) in alkaline solutions have been published in the literature (52,114,268,303,304,305). Podesta *et al.* (303) reported large increase in activity towards the HER of nickel-phosphorus electrodes containing 25.9 at. % of P after heating them in air and a decrease in activity of those containing 12.5 at. % of P. Paseka (52) found high activities of Ni-P electrodes containing low amount of P (3 wt. %), prepared at low current densities and at low temperatures. The latter author reported that the activity of these electrodes decreased after heating or storing them at the open circuit potential. On the other hand Gonzalez *et al.* (268) reported low activity of $\text{Ni}_{70}\text{P}_{30}$ electrodes.

1.5.6 Nickel oxide

Surface oxides sometimes catalyze and sometimes inhibit the hydrogen evolution reaction (1,193). Nickel oxides may be produced chemically or by anodic oxidation (258,306). They may also be produced under low or high anodic potentials in non-buffered (307), buffered (308), or alkaline (193,244,251,253,254,256,279,309-312) solutions.

Nickel oxides exist in different forms, $\alpha\text{-Ni}(\text{OH})_2$, $\beta\text{-Ni}(\text{OH})_2$, $\beta\text{-NiOOH}$, and $\gamma\text{-NiOOH}$ (215). Their occurrence depends on anodic applied potentials (193,253,254,258,311,312). As the anodic

potential increases higher oxidation states and more stable oxides may be formed ($\alpha, \gamma \rightarrow \beta, \beta$). At very high anodic potentials higher degrees of oxidation of nickel has also been suggested, *e.g.*, NiO_4^{2-} , (253). It should be mentioned that aging may also cause $\alpha \rightarrow \beta$ conversion (254). $\beta\text{-Ni(OH)}_2$ and $\beta\text{-NiOOH}$ are stable in normal conditions. These oxides have been chemically produced, characterized by X-Ray diffraction, and used as standards for XPS analysis (306). Recently, the effect of temperature was studied by Divisek *et al.* (256). They have reported some effects showing that at high temperature ($> 70^\circ\text{C}$) $\alpha\text{-Ni(OH)}_2$ (less stable) can be converted to $\beta\text{-Ni(OH)}_2$ (more stable). Any type of nickel oxides (α, γ) or (β), which exist on the nickel surface, will be reduced to (Ni) or $\beta\text{-Ni(OH)}_2$, respectively (313), in cathodic potential range. $\beta\text{-Ni(OH)}_2$ can not be reduced at cathodic potential (258). This may produce a negative error in coulometric determination of the surface area (279). The activity of preoxidized nickel electrodes was investigated for the HER in alkaline solution at ambient temperature by Choquette *et al.* (126), Lasia and Rami (192), and Diard *et al.* (193). They found an increase in electrode activity for the HER. Such an observation has also been reported by others (125,126). Recently, Barral *et al.* (314) studied properties of passive layers formed in KOH and Ni(OH)_2 layers deposited under different conditions in $\text{Ni(NO}_3)_2$ neutral solutions by the EIS in 1 M KOH. They have found that thick deposits are constituted of highly hydrated layers $\alpha\text{-Ni(OH)}_2$ and passive layers corresponded to a less hydrated $\beta\text{-Ni(OH)}_2$. However, all the authors who have studied nickel oxides, directly or implicitly, believe that $\beta\text{-Ni(OH)}_2$ which is formed at higher anodic current densities is the only stable oxide that remains on the surface at cathodic potentials.

1.5.7 Nickel alloys

The most straightforward way to achieve electrocatalysts is alloying two or more metals. This method has been used for long time. Various methods have been suggested to deposit a thin and active layer of alloying material on a support. The most commonly employed are: (i) electroplating, (ii) thermal decomposition, and (iii) *in situ* formation. The electrochemical and mechanical stability and electrochemical activity vary for different methods (106,315-320). In the case of *in situ*

activation with molybdates no changes in Tafel slope was observed (111,112). It means that the synergetic effects have been ruled out and the source of activity has been increase in the real surface area. As Ni-Mo layers were prepared by thermal decomposition of suitable materials, clear synergetic effects were observed (321). While part of activity is related to the large surface area, synergetic effects were manifested by the change in the reaction mechanism, *i.e.*, change in Tafel slope (316,322).

Investigations of several co-deposits on mild steel have shown (277,318) the electrocatalytic sequence: Ni-Mo > Raney Ni > Ni-Co > Ni-Fe > Ni-Cr > Ni. It seems well established that the thermal procedure gives rise to oxides as precursors of the active alloys (323,324). This has been demonstrated in the case of La-Mo coatings (101). The precursors can then be reduced *in situ* or pre-reduced in H₂ atmosphere before use (324). Various methods of preparation have been compared by Divisek *et al.* (46). They have shown that the thermal method is superior to electroplating, but not for Ni-Mo-Cd coating which seems to possess special properties. The source of the activity of Ni-Mo-Cd coatings have been investigated using potential decay technique by Conway *et al.* (29,325). Using X-Ray analysis they found that the coating was very likely amorphous (326). However, I did not find experimental X-Ray diffraction data for this alloy in the literature. It was reported that the cathodic behavior can be explained in terms of hydride phase formation at low overpotentials (327).

The specific role of Mo in various alloys has been investigated (46,106). It has been found that Mo is not stable in alkaline solutions and tends to be leached out, which would be the origin of the deactivation observed in cathodic polarization (46). The deactivation results in a progressive increase in Tafel slope with the time. Such results have been reported by Fan *et al.* (315) and Divisek *et al.* (46). However, this seems to be in contradiction with the Brown's claim of long term stability and resistance to cell shut-downs for the thermally prepared Ni-Mo coating (322). Deactivation was not reported for Ni-Mo-Al by Lasia *et al.* (106). The structure of the layer may differ depending on the details of the preparation procedure. Despite the large amount of data

collected in the molybdenum alloys field, the options for the HER seem to be restricted to Ni-Mo, Ni-Co-Mo, or Co-Mo. However, the desired conditions have not been achieved. It seems that what has been concluded about activity of the electrodes, based on exchange current density for the HER, is valid usually near the equilibrium potential. Therefore, Raney Ni still stands out as a possible catalyst (28,49,55,147,197) for the HER. The role of Zn or Al does not seem to be simply that of sacrificial components, *i.e.*, insertion followed by leaching and leaving a large surface area. Residual Zn or Al presents in the structure probably plays a role in activity of the electrode. Finally, I have to point out that Raney electrodes as Ni-Al-Mo (46,106), Ni-Co-Zn (196,197,244,246), Ni-Mo-Zn (277), and Ni-Zn-P (278) seem to be highly promising.

1.5.8 Intermetallic compounds

The intermetallic compounds are somehow different from metallic alloys. They are obtained by combining two or more metals in well defined proportions corresponding to the appearance of a new phase. The modification of the surface properties of intermetallics has been usually related to their capability of absorbing hydrogen with formation of hydride phases (328). However, the formation of a hydride is not necessarily a reason for better activity (75,329). In some cases large amount of hydrogen dissolved in the bulk of intermetallic phase is a reason for mechanical instability. For example, LaNi_5 powder has been Teflon-bonded, pressed and sintered, or pressed as a coating on a support (25,28,75,140,329) often it was doped with Al, Co, or Cu to improve its properties. These cathodes were operated under long term (7000h) the HER. They have been defined as stabilized high surface area electrodes. However, it has been reported that some erosion of the surface occurs probably due to hydride formation (329). It has also been suggested that the activity of CeNi_3 is two orders of magnitude higher than LaNi_5 (330). Since intermetallics show a great capacity of hydrogen dissolution, they are also used as hydrogen storing materials (28,76,328,331-333).

1.5.9 Amorphous materials

Amorphous materials have first been used in catalysis (334-336) where some evidence for higher activity was obtained (337-339). There is no clear evidence that the amorphous state is really the origin of enhanced catalytic activity (338). Recently, Paseka (52,284,286) studied the HER on amorphous Ni alloys and found good electrocatalytic activities of these materials. He has attributed high activity of these materials to hydrogen absorption and even bulk hydride formation (52,284,286). Paseka has also presented X-Ray diffraction data suggesting an amorphous structure of these electrodeposited materials. Hydride formation in amorphous materials has also been reported by Conway *et al.* (340-343). This matter that increase in activity is achieved by "increase in real surface area" (26,344) or by "increase in the ability of hydrogen absorption" (52,284,286,302) has remained as a subject of challenge. It will be discussed in chapter seven of this thesis.

However, there are some limitations in technological applications of amorphous materials: (i) their tendency to crystallize with time, especially at higher temperatures or high current densities, (ii) relatively low surface roughness (52,344), as compared with Raney nickel (196,197,244,246,278), (iii) the presence of inactive oxides on the surface, and (iv) high price.

However, Paseka prepared active electrodes by electrodeposition which had amorphous structure (52). Although the method is low expense, but the crystallization of the electrode may occurs by heating. This process deactivate the electrodes (52).

The surface of amorphous alloys containing Ti, Zr, or Mo is covered by oxides (337,345,346). These oxides may be removed by HF. This process also partially increases the porosity and, consequently, the activity of the electrodes.

It is necessary to stress again that for technological applications the electrocatalytic activity (increase in the number of active sites per unit of surface area) is not the only property that has to be optimized. Stability can be by far more crucial. Raney metal structures need to be strengthened without losing their activity aspect.

Development of new electrode materials for the HER remains as a matter and the main aim of this research.

CHAPTER 2

THEORY

The HER as an essential reaction in electrocatalysis has a great fundamental as well as technological interest. The studies of kinetics and mechanism of the HER are necessary to evaluate the electrode materials for technological applications (347). In this chapter theories and techniques used in this thesis will be discussed.

2.1 General approach for simple reactions

In general, for an electrode reaction which has a discharge reaction as a rate controlling step without adsorption intermediate, one may write (348)



where Ox and Red are oxidized and reduced species, and n is number of the electrons transferred in the redox reaction, the forward and backward reaction rates, v_f and v_b , can be given as:

$$v_f = k_f C_O(0, t) = \frac{i_c}{nFA} \quad [2.2]$$

$$v_b = k_b C_R(0, t) = \frac{i_a}{nFA} \quad [2.3]$$

in which k_f and k_b are forward and backward reaction rate constants, $C_O(0, t)$ and $C_R(0, t)$ are the concentrations of Ox and Red at the electrode surface at time t , i_c and i_a are cathodic and anodic currents, A is the surface area of the electrode, F is the Faraday constant, and k_f and k_b are *potential dependent rate constant*. k^0 is called *standard rate constant* which is the value of k_f and k_b at E^0 . Thus

$$k_f = k^0 \exp[-\alpha n f (E - E^{0'})] \quad [2.4]$$

$$k_b = k^0 \exp[(1 - \alpha) n f (E - E^{0'})] \quad [2.5]$$

where $E^{0'}$ is formal potential, α is transfer coefficient and its value is $0 < \alpha < 1$. Using eqns. [2.2] and [2.3] the net reaction rate relation can be written as:

$$v_{\text{net}} = v_f - v_b = k_f C_O(0, t) - k_b C_R(0, t) = \frac{i}{nFA} \quad [2.6]$$

and the current as:

$$i = i_c - i_a = nFA[(k_f C_O(0, t) - k_b C_R(0, t))] \quad [2.7]$$

Combination of eqns. [2.4], [2.5], and [2.7] produces

$$i = nFAk^0 [C_O(0, t) \exp[-\alpha n f (E - E^{0'})] - C_R(0, t) \exp[(1 - \alpha) n f (E - E^{0'})]] \quad [2.8]$$

Eqn. [2.8] is called *current-potential* equation. At the equilibrium $E = E_{\text{eq}}$, the net current, i , is zero, and the bulk and surface concentrations of redox species are the same. In these conditions the cathodic and anodic currents are identical and could be expressed in terms of the *exchanged current*, i_0 , as:

$$i_0 = nFAk^0 [C_O^* \exp[-\alpha n f (E_{\text{eq}} - E^{0'})]] = nFAk^0 \{C_R^* \exp[(1 - \alpha) n f (E_{\text{eq}} - E^{0'})]\} \quad [2.9]$$

or

$$i_0 = nFAk^0 C_O^{*(1-\alpha)} C_R^{*(\alpha)} \quad [2.10]$$

Often the current and exchange current are normalized to unit area to provide *current and exchange current densities*, $j = i / A$ and $j_0 = i_0 / A$.

Dividing the eqn. [2.8] by [2.10] and replacing the $\exp[(-\alpha n f)(E_{\text{eq}} - E^{0'})] = (C_{\text{O}}^* / C_{\text{R}}^*)^{-\alpha}$ obtained from eqn. [2.9], will give:

$$j = j_0 \left\{ \frac{C_{\text{O}}(0, t)}{C_{\text{O}}^*} \exp(-\alpha n f \eta) - \frac{C_{\text{R}}(0, t)}{C_{\text{R}}^*} \exp[(1 - \alpha) n f \eta] \right\} \quad [2.11]$$

where $\eta = E - E_{\text{eq}}$ is named *overpotential*. This equation is known as the *current-overpotential equation*. The approximate forms of this equation are given below:

(i) if the solution is well stirred or current density is kept low (j less than 10% of limiting current) that is the surface concentrations do not differ appreciably from the bulk values, then eqn. [2.11] becomes

$$j = j_0 \{ \exp(-\alpha n f \eta) - \exp[(1 - \alpha) n f \eta] \} \quad [2.12]$$

which is known as the *Butler-Volmer equation*.

Since mass transfer effects are not included here, the overpotential associated with any given current serves solely as an activation energy. The more sluggish reaction kinetics, the larger is the *activation overpotential* for any particular net current. If the reaction is very fast, any overpotential is due to *mass transfer effect*.

(ii) for sufficiently small η , eqn. [2.12] can be written as:

$$j = j_0 (-\alpha f \eta) \quad [2.13]$$

which shows that the net current is linearly related to the overpotential in a narrow overpotential range near E_{eq} . The ratio of $-\eta / j$ has resistance dimensions and is often called *charge transfer resistance*, R_{ct} .

$$R_{\text{ct}} = \frac{RT}{nF j_0} \quad [2.14]$$

(iii) for large values of η (either positive or negative) one of the two terms in eqn. [2.12] becomes negligible. For example, at large negative η it becomes

$$j = j_0 \exp(-\alpha n f \eta) \quad [2.15]$$

or

$$\eta = a - b \log j \quad [2.16]$$

where at 25°C parameters “a” and “b” are given as:

$$a = \frac{2.303RT}{\alpha nF} \log j_0 = \frac{0.0591}{\alpha n} \log j_0 \quad [2.17]$$

and

$$b = -\frac{2.303RT}{\alpha nF} = -\frac{0.0591}{\alpha n} \quad [2.18]$$

Eqn. [2.16] is known as *Tafel equation* in which “b” is known as *Tafel slope*. A plot of $\log j$ vs. η which is known as *Tafel plot*, is a useful device for evaluation of kinetic parameters.

$$\log j = \log j_0 - \frac{\alpha nF}{2.303RT} \eta \quad \text{or} \quad \log j = \log j_0 - \frac{1}{b} \eta \quad [2.19]$$

Parameters j_0 and b are sometimes reported as kinetic parameters of the electrode reactions. Since the values of these parameters usually depend on the range of overpotentials in which analysis is performed, another parameter which is more practical and indicates the electrode activity, is specified (26,192). That is overpotential at 250 mA cm⁻² current density with notation η_{250} .

$$\eta_{250} = -b \log \left(\frac{250}{j_0} \right) \quad [2.20]$$

where j_0 has dimensions as mA cm⁻². Of course to present the electrode activity, one may also show other overpotentials at any practically high current density, e.g., η_{200} , η_{300} , η_{500} , η_{1000} , etc.

2.2 Hydrogen evolution reaction (HER)

Several paths have been presented for the HER in aqueous solution among them three steps have been widely accepted (6,13,14,21,349).

2.2.1 Elementary reactions

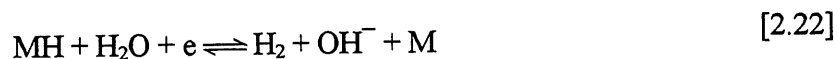
In alkaline solutions (13,14) these reactions contain:

(i) discharge of water molecules at the electrode surface with the formation of adsorbed hydrogen atoms on metallic sites,



known as Volmer step. This step is common to any mechanism that has been presented for the HER in alkaline solution, and should be followed by desorption step(s) in order to produce hydrogen molecules. Two possible steps have been proposed (both or one of them may be involved),

(ii) electrochemical desorption which is known as Heyrovský step,



and

(iii) chemical desorption which is known as Tafel step,



2.2.2 Adsorption isotherms

In the case when reaction mechanism passes through the adsorption of intermediates on the electrode surface, the amount of adsorbed species should be considered in formulating of the

mechanism. The involvement of intermediate adsorbed hydrogen, H, in the HER has been recognized by Horiuti and Polanyi (350) and Butler (351). The adsorption phenomenon depends on the nature of the surface and adsorbed species, concentration of the species, electrical state of the system, and temperature. The relation between surface coverage, θ , standard free energy of adsorption, ΔG_{ads}^0 , the activity of the species in bulk solution, and the solution-metal potential difference, E, at a given temperature, T, is called the *adsorption isotherm* (348,352). A number of adsorption isotherms have been proposed (26,348,353-360), some of them frequently are used in the HER (26-28,36,37,135,192,340,356-360) are presented here.

(i) The *Langmuir isotherm* involves assumptions of (a) no heterogeneity of the surface, (b) no interactions between the adsorbed species on the electrode surface, and (c) at high bulk activities, saturation coverage by adsorbate is reached, $\theta = 1$. Thus

$$\frac{\theta}{1-\theta} = ap\alpha_i \quad [2.24]$$

where “a” is a constant related to the standard free energy of adsorption, ΔG_{ads}^0 , as $a = \exp(-\Delta G_{\text{ads}}^0 / RT)$, and “p” is related to the metal-solution potential difference, E, as $p = \exp(-EF / RT)$, and $\alpha_i = \gamma_i C_i$, (α_i , γ_i and C_i are activity, activity coefficient, and concentration of species i). Inserting α_i , “a” and “p” in eqn. [2.24] will produce eqn. [2.25] which is known as Langmuir isotherm.

$$\frac{\theta}{1-\theta} = \gamma_i C_i \exp(-\Delta G_{\text{ads}}^0 / RT) \exp(-EF / RT) \quad [2.25]$$

Interactions between adsorbed species (lateral interactions) complicate the problem by making the energy of adsorption a function of surface coverage. Isotherms that include this possibility are the *Frumkin isotherm* and *Temkin isotherm*.

(ii) In Frumkin isotherm the free energy of adsorption changes linearly with surface coverage,

$$\Delta G_{\text{ads},\theta}^0 = \Delta G_{\text{ads}}^0 + r\theta \quad [2.26]$$

$$\frac{\theta}{1-\theta} = \gamma_i C_i \exp(-\Delta G_{\text{ads}}^0 / RT) \exp(-EF / RT) \exp(-g\theta) \quad [2.27]$$

where ΔG_{ads}^0 and $\Delta G_{\text{ads},\theta}^0$ are standard free energy of adsorption on the uncovered, $\theta \rightarrow 0$, and covered surface, $0 < \theta < 1$ respectively, $g = r / RT$, and r is a term considering the interactions energy (lateral interactions; $g < 0$ attraction, or $g > 0$, repulsion) (352).

(iii) Temkin proposed a linear relation between θ and E (360). At the intermediate values of θ , where $\theta / (1-\theta)$ reaches to one, the Frumkin isotherm becomes Temkin isotherm:

$$\exp(g\theta) = \gamma_i C_i \exp(-\Delta G_{\text{ads}}^0 / RT) \exp(EF / RT) \quad [2.28]$$

This equation predicts a linear relation between θ and E , although Temkin has never used it in this form. The parameter g can explain the heterogeneity arising from the surface sites. However, experimental results do not always show the linear dependence between $\Delta G_{\text{ads},\theta}^0$ and $r\theta$. Gileadi (352) has proposed the first approximation of eqn. [2.26] as:

$$\Delta G_{\text{ads},\theta}^0 = \Delta G_{\text{ads}}^0 + r\theta^m \quad [2.29]$$

where “ m ” is a number between 0.5 to 2. It seems that in some cases Temkin isotherm can explain the behavior of the systems very well (16).

2.2.3 Reaction rates

The Volmer step is a pure charge transfer reaction. Similarly to eqns. [2.6] and [2.7] the rate of this step under Langmuir isotherm may be written as (26,37,192):

$$v_1 = k_1^0 a_{\text{H}_2\text{O}} (1-\theta) \exp[-\beta_1 f(E - E^0)] - k_1^0 a_{\text{OH}^-} \theta \exp[(1-\beta_1) f(E - E^0)] \quad [2.30]$$

where k_1^0 is standard rate constant, θ is the surface coverage by adsorbed hydrogen, $a_{\text{H}_2\text{O}}$ is activity of water, a_{OH^-} is activity of hydroxyl ions, β_1 and $1-\beta_1$ are *symmetry factors* for the forward and backward reactions, and other parameters have they general meaning. The symmetry coefficient, β , is used instead of transfer coefficient, α , to recognize that reaction mechanism involves a multi-step reaction path with adsorbed intermediate (26,37,192,159,341,342). The equilibrium condition, $E = E_{\text{eq}}$ and $v_1 = 0$, leads to:

$$\frac{a_{\text{H}_2\text{O}}}{a_{\text{OH}^-}} \left(\frac{1-\theta_0}{\theta_0} \right) = \exp[f(E_{\text{eq}} - E^{0'})] \quad [2.31]$$

in which θ_0 denotes the surface coverage at these conditions. Combination of eqns. [2.30] and [2.31] will produce,

$$v_1 = k_1(1-\theta) \exp(-\beta_1 f\eta) - k_{-1}\theta \exp[(1-\beta_1) f\eta] \quad [2.32]$$

with

$$k_1 = k_1^0 a_{\text{H}_2\text{O}}^{1-\beta_1} a_{\text{OH}^-}^{\beta_1} \left(\frac{\theta_0}{1-\theta_0} \right)^{\beta_1} \quad [2.33]$$

and

$$k_{-1} = k_1^0 a_{\text{H}_2\text{O}}^{1-\beta_1} a_{\text{OH}^-}^{\beta_1} \left(\frac{1-\theta_0}{\theta_0} \right)^{1-\beta_1} \quad [2.34]$$

Similarly, one can develop equations for Heyrovský reaction as:

$$v_2 = k_2\theta \exp(-\beta_2 f\eta) - k_{-2}(1-\theta) \exp[(1-\beta_2) f\eta] \quad [2.35]$$

$$k_2 = k_2^0 a_{\text{H}_2\text{O}}^{1-\beta_2} a_{\text{OH}^-}^{\beta_2} p_{\text{H}_2}^{\beta_2} \left(\frac{1-\theta_0}{\theta_0} \right)^{\beta_2} \quad [2.36]$$

$$k_{-2} = k_2^0 a_{\text{H}_2\text{O}}^{1-\beta_2} a_{\text{OH}^-}^{\beta_2} p_{\text{H}_2}^{\beta_2} \left(\frac{\theta_0}{1-\theta_0} \right)^{1-\beta_2} \quad [2.37]$$

and the Tafel reaction:

$$v_3 = k_3\theta^2 - k_{-3}(1-\theta)^2 \quad [2.38]$$

$$k_{-3} = k_{-3}^0 p_{\text{H}_2} \quad [2.39]$$

2.2.4 Steady-state

The faradaic current of the HER is proportional to the rate of electron transfer at the electrode surface, r_0 , which is sum of the v_1 and v_2 ,

$$j = Fr_0(\theta, \eta) = F(v_1 + v_2) \quad [2.40]$$

where r_0 has dimensions of flux, $\text{mol cm}^{-2}\text{s}^{-1}$. It means that only Volmer and Heyrovský reactions contribute to the faradaic current. The rate of surface coverage changes, $d\theta / dt$, is proportional to the difference between the rate of hydrogen adsorption and desorption, r_1 ,

$$\left(\frac{d\theta}{dt} \right) \frac{\sigma_1}{F} = r_1(\theta, \eta) = v_1 - v_2 - 2v_3 \quad [2.41]$$

where σ_1 is the total charge required for one monolayer surface coverage by adsorbed hydrogen. At the steady-state, the rates of hydrogen adsorption and desorption will be equal, and the surface coverage will be constant,

$$\left(\frac{d\theta}{dt} \right) \frac{\sigma_1}{F} = r_1(\theta, \eta) = v_1 - v_2 - 2v_3 = 0 \quad [2.42]$$

Introducing eqns. [2.32], [2.35], and [2.38] in eqn. [2.41] will produce

$$\begin{aligned} \frac{d\theta}{dt} = \frac{F}{\sigma_1} \{ & [k_1 \exp(-\beta_1 f\eta) + [k_{-2} \exp((1 - \beta_2) f\eta) + 2k_{-3}] + \theta[-k_1 \exp(-\beta_1 f\eta) \\ & - k_{-1} \exp((1 - \beta_1) f\eta) - k_2 \exp(-\beta_2 f\eta) - k_{-2} \exp((1 - \beta_2) f\eta) - 4k_{-3}] \\ & + \theta^2[-2k_3 + 2k_{-3}] \} \end{aligned} \quad [2.43]$$

or more simply

$$\frac{d\theta}{dt} = \frac{F}{\sigma_1} (AA + BB\theta + CC\theta^2) \quad [2.44]$$

where

$$AA = k_1 \exp(-\beta_1 f\eta) + k_{-2} \exp[(1 - \beta_2) f\eta] + 2k_{-3} \quad [2.45]$$

$$BB = - \left\{ \begin{array}{l} k_1 \exp(-\beta_1 f\eta) + k_{-1} \exp[(1 - \beta_1) f\eta] \\ + k_2 \exp(-\beta_2 f\eta) + k_{-2} \exp[(1 - \beta_2) f\eta] + 4k_{-3} \end{array} \right\} \quad [2.46]$$

$$CC = -2k_3 + 2k_{-3} \quad [2.47]$$

2.2.5 Equilibrium conditions

At the equilibrium conditions, $E = E_{eq}$, the net of each individual step is zero, *i.e.*, $v_1 = v_2 = v_3 = 0$ (26-28,37,42-44,102,103,121-126,192,265-267,278), and the equilibrium surface coverage, θ_0 , can be calculated as:

$$\theta_0 = \frac{k_1}{k_1 + k_{-1}} = \frac{k_{-2}}{k_2 + k_{-2}} = \frac{\sqrt{k_{-3}}}{\sqrt{k_3} + \sqrt{k_{-3}}} \quad [2.48]$$

from which the following relation for rate constants can be obtained.

$$\frac{k_1 k_2}{k_{-1} k_{-2}} = \frac{k_1^2 k_{-3}}{k_{-1}^2 k_3} = 1 \quad [2.49]$$

To solve the kinetics of the HER it is necessary to determine four out of six rate constants and two symmetry coefficients.

2.2.6 Mechanism of the HER

A proper mechanism should be assumed and the experimental data modeled in order to evaluate the kinetics of the HER. Two limiting and one general case may be assumed that there is at least one *rate determining step* (rds) for each one.

2.2.6.1 Volmer–Heyrovský mechanism

In this mechanism it is assumed that the rate of hydrogen electrodesorption, Heyrovský reaction, is much faster than that of the Tafel step, *i.e.*, $v_2 \gg v_3$, and the latter can be neglected. At the steady-state $d\theta / dt = 0$, and the surface coverage can be derived from eqn. [2.42] in which k_3 and k_{-3} are equal to zero, *i.e.*,

$$\theta = \frac{A_1}{B_1} = \frac{\vec{k}_1 + \overset{\leftarrow}{k}_{-2}}{\vec{k}_1 + \overset{\leftarrow}{k}_{-1} + \vec{k}_2 + \overset{\leftarrow}{k}_{-2}} \quad [2.50]$$

in which $\vec{k}_1 = k_1 \exp(-\beta_1 f\eta)$, $\overset{\leftarrow}{k}_{-1} = k_{-1} \exp[(1 - \beta_1)f\eta]$, $\vec{k}_2 = k_2 \exp(-\beta_2 f\eta)$, and $\overset{\leftarrow}{k}_{-2} = k_{-2} \exp[(1 - \beta_2)f\eta]$ are potential dependent rate constants and

$$A_1 = k_1 \exp(-\beta_1 f\eta) + k_{-2} \exp[(1 - \beta_2)f\eta] \quad [2.51]$$

$$B_1 = \left\{ \begin{array}{l} k_1 \exp(-\beta_1 f\eta) + k_{-1} \exp[(1 - \beta_1)f\eta] \\ + k_2 \exp(-\beta_2 f\eta) + k_{-2} \exp[(1 - \beta_2)f\eta] \end{array} \right\} \quad [2.52]$$

The steady-state current density, j , may be presented as:

$$j = F \left\{ \begin{array}{l} k_1(1 - \theta) \exp(-\beta_1 f\eta) - k_{-1}\theta \exp[(1 - \beta_1)f\eta] \\ + k_2\theta \exp(-\beta_2 f\eta) - k_{-2}(1 - \theta) \exp[(1 - \beta_2)f\eta] \end{array} \right\} \quad [2.53]$$

Assuming $\beta_1 = \beta_2 = \beta$, after inserting eqn. [2.50], [2.51], and [2.52] in eqn. [2.53] one can obtain

$$j = 2F \frac{k_1 k_2 \exp(-\beta f\eta) [1 - \exp(2f\eta)]}{(k_1 + k_2) + (k_{-1} + k_{-2}) \exp(f\eta)} \quad [2.54]$$

The Tafel slope is defined here as $d\eta / d \log\{j / [1 - \exp(2f\eta)]\}$ (26). This equation may lead to different analysis.

(i) At large overpotentials eqn. [2.54] reduces always to:

$$j = 2F \frac{k_1 k_2}{k_1 + k_2} \exp(-\beta f\eta) \quad [2.55]$$

The Tafel slope is equal to $-2.303RT / \beta F$ or -118 mV dec^{-1} at 25°C , independent of rate determining step, and the corresponding j_0 is:

$$j_0 = 2F \frac{k_1 k_2}{k_1 + k_2} = 2F \frac{1}{\frac{1}{k_1} + \frac{1}{k_2}} \quad [2.56]$$

Therefore, in the limiting cases, the exchange current density may be equal to $2Fk_1$ or $2Fk_2$.

(ii) At very low overpotential, if $k_1 + k_2 \gg k_{-1} + k_{-2}$ the slope at 25°C for $\beta = 0.5$ will be -118 mV dec^{-1} , and j_0 as given above. However, when $k_1 + k_2 \ll k_{-1} + k_{-2}$ the slope is $-2.303RT / (1+\beta)F = -39 \text{ mV dec}^{-1}$, and the j_0 ,

$$j_0 = 2F \frac{k_1 k_2}{k_{-1} + k_{-2}} = 2F \frac{1}{\frac{1}{k_{-1}} + \frac{1}{k_{-2}}} \quad [2.57]$$

Therefore, in the limiting cases, the exchange current density may be equal to $2Fk_{-1}$ or $2Fk_{-2}$.

In the case when β_1 and β_2 are different, the corresponding steady-state current density may be expressed as:

$$j = 2F \frac{k_1 k_2 \exp(-\beta_1 f\eta) \exp(\gamma f\eta) [1 - \exp(2f\eta)]}{k_1 + k_2 \exp(\gamma f\eta) + [k_{-1} + k_{-2} \exp(\gamma f\eta)] \exp(f\eta)} \quad [2.58]$$

where $\gamma = \beta_1 - \beta_2$.

If γ is very small, at sufficiently negative overpotential and regardless the sign of γ , it may reduce to:

$$j = 2F \frac{k_1 k_2 \exp(-\beta_1 f\eta) \exp(\gamma f\eta)}{k_1 + k_2 \exp(\gamma f\eta)} \quad [2.59]$$

Two limit conditions exist for eqn. [2.59]:

(i) $k_1 < k_2$, *i.e.*, the Volmer step is rds, and eqn. [2.59] can be simplified as:

$$j = 2Fk_1 \exp(-\beta_1 f\eta) \quad [2.60]$$

with exchange current density of $j_0 = 2Fk_1$.

(ii) $k_1 > k_2$, *i.e.*, the Heyrovský step is the rds, and eqn. [2.59] can be simplified as:

$$j = 2Fk_2 \exp(-\beta_2 f\eta) \quad [2.61]$$

with exchange current density of $j_0 = 2Fk_2$.

2.2.6.2 Volmer–Tafel mechanism

When the desorption of hydrogen through of Heyrovský reaction, *i.e.*, electrodesorption reaction, is very slow, the HER proceeds through of Volmer–Tafel mechanism. The corresponding steady-state surface coverage can be obtained from eqns. [2.44], [2.45], [2.46], and [2.47] by setting $k_2 = k_{-2} = 0$.

$$\theta = \frac{-B_2 - \sqrt{B_2^2 - 4A_2C_2}}{2C_2} \quad [2.62]$$

where

$$A_2 = k_1 \exp(-\beta_1 f\eta) + 2k_{-3} \quad [2.63]$$

$$B_2 = -\{k_1 \exp(-\beta_1 f\eta) + k_{-1} \exp[(1-\beta_1) f\eta] + 4k_{-3}\} \quad [2.64]$$

$$C_2 = -2k_3 + 2k_{-3} \quad [2.65]$$

The current density in this mechanism may be obtained as:

$$j = Fv_1 = F\{k_1(1-\theta) \exp(-\beta_1 f\eta) - k_{-1}\theta \exp[(1-\beta_1) f\eta]\} \quad [2.66]$$

For this mechanism various limiting slopes may be obtained. At high negative overpotentials the rate of the *potential independent Tafel reaction* is always smaller than those of the Volmer reaction and the Tafel slope will be infinite (current will be potential independent). At low overpotentials; if $k_{-1} \gg k_1 \gg k_3 \gg k_{-3}$ the slope is $-2.303RT / 2F = -30 \text{ mV dec}^{-1}$, θ is small and exchange current density, $j_0 = 2Fk_{-3}$; if $k_1 \gg k_{-1} \gg k_3 \gg k_{-3}$ the slope is ∞ , $\theta \rightarrow 1$ and $j_0 = 2Fk_3$; if $k_3 \gg k_{-3} \gg k_1 \gg k_{-1}$ the slope is $-2.303RT / \beta F = -118 \text{ mV dec}^{-1}$, $\theta \rightarrow 1$ and $j_0 = Fk_{-1}$; and if $k_3 \gg k_{-3} \gg k_{-1} \gg k_1$ the slope is $-2.303RT / \beta F = -118 \text{ mV dec}^{-1}$, θ is small and $j_0 = Fk_1$. It is clear that the smallest reaction rate always limits the total current (26).

2.2.6.3 Volmer–Heyrovský–Tafel mechanism

If the rates of hydrogen desorption reaction through the Heyrovský and Tafel reactions are comparable, both reaction have to be considered in solving the mechanism of the HER. In this case, using eqn. [2.44] at the steady-state, the surface coverage, θ , is given as:

$$\theta = \frac{-BB - \sqrt{BB^2 - 4AA.CC}}{2CC} \quad [2.67]$$

where AA, BB, and CC are given by eqns. [2.45], [2.46], and [2.47]. The faradaic current here may be given after inserting eqn. [2.67] in eqn. [2.53]. In this mechanism, at high overvoltages, the rate of the HER through the Tafel reaction is almost negligible (because Tafel reaction is independent of potential), and the slope is the same as for the Volmer-Heyrovský mechanism. At low overpotentials, depending on the relative magnitude of rate constants, the slopes -30 and -120 mV dec^{-1} are possible (26).

2.3 Evaluation of the surface covered by adsorbed hydrogen and kinetic parameters

The basic studies on the adsorbed hydrogen in electrocatalysis were performed by Horiuti and Polanyi (350) and Butler (351) a few decades ago. Many subsequent papers treated the role of adsorbed intermediates in electrode processes in relation to the mechanism of the respective reactions. The behavior of adsorbed intermediates that are the kinetically involved species was thus only indirectly addressed, and more experimental procedures for characterization of their behavior have remained, until recently, undeveloped. The electrochemistry of UPD-H has been the subject of many original papers and reviews (358,362-365). However, very little work has been done until recently on the adsorbed intermediates that are involved in H_2 (26-28,37,62,121-123,192,287, 344,366), O_2 , and Cl_2 evolution reactions (358).

While it is easy to trace the small current densities associated with the changes of the coverage by adatoms, say hydrogen, deposited into or desorbed from the surface without interference from continuous faradaic currents in the UPD-H region, it is impossible to measure the small current densities that are involved in changing the coverage by adsorbed intermediates, for example H in the HER, that are kinetically involved, in the presence of a continuous net reaction. The currents in latter are sometimes 2 to 4 orders of magnitude larger than those partial currents which can be produced in changes of the coverage by intermediates. Therefore, the currents of the UPD-H, although often small, are not normally interfered by any other superimposed currents (except

impurities). Thus, changes of coverage by the OPD-H are not easily detectable under passage of a continuous faradaic current.

Involvement of adsorbed intermediates in electrocatalytic reactions has been manifested by various ways as: (i) in the values of Tafel slope (26,192,358), (ii) in the value of the reaction order of the process (20,205,343,356,358), (iii) in the pseudocapacitance behavior of the electrode interface (26,34,159,192,341,342,358,361), (iv) in the EIS measurements (26,31,37,192,350), (v) in the response of the reactions to the pulse or linear perturbation, or potential relaxation after polarization (26,192,358), and (vi) some spectroscopic methods as: Raman and IR reflectometry (358).

Although various techniques can be applied to study adsorbed intermediates in gas-solid heterogeneous catalysis successfully, most of these methods are inapplicable to the electrode-solution interface. More difficulties and limitations exist using these techniques for studying adsorbed intermediates in OPD-H, especially spectroelectrochemical methods are inapplicable in the case of porous and rough electrodes. Presence of the bubbles (358) and pores with different shapes (147,366,367,368) are additional difficulties in studying active electrodes. Only some of more advanced electrochemical techniques as potential relaxation and EIS (16,26,32,37,192,278,344,366-369) can give acceptable information. Such limitations rarely have been encompassed for study of the UPD species, making them easy to be studied by simple classical methods as cyclic voltammetry or IR and Raman spectroscopy (358). For determination of the adsorption (26,32,192) and absorption (36,62,70,135) behavior of OPD-H, in most of the cases, only *in situ* electrochemical techniques can be used.

2.3.1 Steady-state polarization curves (Tafel plots)

It should be emphasized that direct experimental information on the behavior of the adsorbed intermediates cannot be obtained from the steady-state current-potential relationship (Tafel plot)

alone. The above discussion (section 2.2) implied that measuring the exchange current density, j_0 , and Tafel slope is a primary evaluation of electrode kinetics. Usually j_0 is a complex function of the rate constants which cannot be separated and, in many cases a unique value may not be attributed to a rate constant. On the other hand Tafel slope may have the same value for different mechanisms which makes it difficult or impossible to evaluate the amount of adsorbed intermediates and surface coverage.

By comparison of the steady state current densities Wendt (147) has used the following relation for evaluation of the roughness factor, R , of Raney-nickel electrodes,

$$R = \frac{j_{1,\eta}}{j_{2,\eta}} \quad [2.68]$$

where $j_{1,\eta}$ and $j_{2,\eta}$ are steady-state current densities obtained on unknown and a smooth electrode surface (*e.g.*, smooth polycrystalline nickel) at a specified overvoltage, η , respectively. Of course any information (*e.g.*, R and C_{dl}) obtained on the kinetics by this method is only a rough estimation. This method may be used in a linear Tafel range only if the transfer coefficients are the same.

Some perturbation techniques are required in which a change of coverage by the kinetically involved species is included, and the resulting response of the system in a temporary non-steady-state is recorded. Three types of measurements can be envisaged; (i) controlled current pulses (current step technique), or controlled potential pulses (potential step technique); (ii) potential relaxation (open-circuit potential decay); and (iii) electrochemical impedance spectroscopy. All these techniques involve, in one way or another, a modulation of the kinetics in the course of the reaction time. The resulted response is then analyzable (26,31,192,358) in terms of (i) rate equations for various steps and (ii) potential dependence of surface coverage by adsorbed intermediates in those steps. The third technique is used in all parts of this thesis. However, in some cases the second one is also used to verify the results.

2.3.2 Open circuit potential decay

After a current interruption the electrode potential relaxes to the equilibrium value. During this process the double layer capacitance is discharged and the surface coverage by adsorbed hydrogen changes from the initial to equilibrium value through eqns. [2.21] to [2.23]. During the potential relaxation the pseudocapacitance is different from that measured at the steady state. In this case so called transient pseudocapacitance may be defined (31) as:

$$C_{\phi,t} = \sigma_1 \left(\frac{d\theta}{dt} \right) \left(\frac{d\eta}{dt} \right)^{-1} \quad [2.69]$$

but because

$$j = \frac{dQ}{dt} = \sigma_1 \left(\frac{d\theta}{dt} \right) \quad [2.70]$$

an operational pseudocapacitance, $C_{\phi,b}$, for potential relaxation technique was introduced as:

$$C_{\phi,b} = j \left(\frac{d\eta}{dt} \right)^{-1} \quad [2.71]$$

In order to analyze this equation the derivative, $d\eta / dt$ must be determined from the experimental relaxation curves. This derivative goes to zero at long times and the error of its determination increases. Besides, the faradaic current also decreases with decrease in the overvoltage and, at low η , it is usually less reproducible. Therefore, in the range of low overvoltage, where the changes of the surface coverage occur, $C_{\phi,b}$ is obtained with the greatest error and it is difficult to extract the kinetic parameters from the experimental data. However, at very short times and relatively high overvoltages the double layer capacitance may be determined (35,192) as:

$$C_{dl} = j \left(\left(\frac{d\eta}{dt} \right)_{t \rightarrow 0} \right)^{-1} \quad [2.72]$$

The η - t curves are obtained experimentally by fast recording the response of the current interruption. Analysis of η - t curves may be performed (192) using non-linear least-squares techniques, NLS.

2.3.3 Electrochemical impedance spectroscopy

The electrochemical impedance spectroscopy (EIS) was first applied to study the adsorbed species by Gerischer and Mehl (370a), Weininger and Breiter (370b), and with latter development by Armstrong and Henderson (371), Conway *et al.* (37), Lasia and Rami (192), and others (38,47,81,147,190,268,371-374). The possibility of use of the EIS to study electrode processes is due to: (i) Linear relation between logarithm of charge transfer resistance and overvoltage, (ii) Potential dependence of surface coverage (called pseudocapacitance, C_ϕ), (iii) Capacitive behavior of electrode-solution interface (called double-layer capacitance, C_{dl}).

The electrical behavior of the electrode-solution interface and the faradaic processes which may take place at it, can be treated in terms of an electrical equivalent circuit. The "circuits" of this type have a frequency-dependent impedance which may be experimentally measured. It should be mentioned that equivalent circuits do not necessarily uniquely represent the electrical behavior of the electrode-solution interface, and there may be other equivalent circuits with different arrangements and values of components which can present the same frequency-response behavior, especially for multi-step reactions. In these cases it is necessary to carry out a mathematical analysis of the response (26,37,192,371-375).

Although the impedance behavior of the electrode reactions is often complicated, they can be conveniently approximated with computer approximations, especially those based on kinetic equations (26,37,192,371-373). The form of real, Z' , and imaginary, Z'' , parts of impedance vector, Z , can be evaluated as a function of frequency, and plotted against each other. The resulted plot is named complex-plane-plot. The logarithmic relations between $|Z|$ or phase angle, ϕ , log of

angular frequency, ω , are called Bode plots. They characterize the reaction mechanism and presence of adsorbed intermediate(s) providing diagnostic bases for mechanism determination, complementary to those based on steady-state polarization responses and Tafel plots.

2.3.3.1 Fundamental concepts

In general, if an electrical circuit containing resistance, R, capacitance, C, and conductance, L, (each one or combination of them) be subjected to a sinusoidal signal (E or i), *e.g.*, $E(t) = E_0 \sin(\omega t)$, the response of the system will be a sinusoidal current as $i(t) = i_0 \sin(\omega t + \phi)$ in which $i_0 = E_0 / |Z|$, E_0 and i_0 are the maximum amplitude of applied and observed signals respectively, t is time, $\omega = 2\pi f$ is angular frequency, ϕ is phase angle between applied and observed signal, *i.e.*, E(t) and i(t), and Z is called impedance of the system (26,37,192,371-375). In the case when system containing only resistance, phase angle is equal to zero, in other cases a phase difference exists between input and output signal.

In order to simplify the calculations, impedances obtained from periodic perturbation of the electrical circuit may be represented using complex notation. For example for a circuit containing a series connection of R and C, the impedance may be represented as:

$$Z(j\omega) \equiv \hat{Z} = R + \frac{1}{j\omega C} = R - j\frac{1}{\omega C} \quad \text{or} \quad Z(j\omega) \equiv \hat{Z} = Z' + jZ'' \quad [2.73]$$

Therefore, the real and imaginary parts of impedance can be expressed as: $Z' = R$ and $Z'' = -1 / \omega C$, respectively. Thus

$$|Z| = \sqrt{(Z')^2 + (Z'')^2} = \sqrt{R^2 + (1 / \omega C)^2} \quad [2.74]$$

and $\tan \phi = Z'' / Z' = \tan(-1 / \omega RC)$. Using complex notation the impedance may be represented as:

$$Z(j\omega) = |Z| \exp(j\phi) = |Z| [\cos(\phi) + j \sin(\phi)] \quad [2.75]$$

$$E = E_0 \exp(j\omega t) \quad \text{and} \quad i = i_0 \exp[j(\omega t + \phi)] \quad [2.76]$$

These vectors rotate with frequency ω and the phase angle, ϕ , between them stays constant. Instead of showing rotating vectors in time space it is possible to present immobile vectors in the frequency space, separated by phase angle. They are called phasors.

In general, the complex impedance may be written for any circuit using R for resistance, $1/j\omega C$ for capacitance, and $j\omega L$ for inductance, and applying Ohm's and Kirchoff's laws to the connection of these elements. The two following examples will show the behavior of liquid electrodes as Hg or Ga etc. (*i.e.*, ideally smooth electrodes) in the absence and presence of faradaic reaction.

2.3.3.2 Ideally polarized electrode

Ideally polarized electrode has been already discussed implicitly in above. The impedance of a system consisting of an electrode, *e.g.*, mercury, in contact with electrolyte solution in which no faradaic reaction takes place at the electrode surface, *i.e.*, *ideally polarized*, may be represented as an electrical circuit consisting of a solution resistance, R_s , in series with a double layer capacitance, C_{dl} , Fig. 1a. Impedance of counter electrode is neglected. Therefore, the impedance of this system can be represented as $Z(j\omega) = R_s + 1/j\omega C = R - j/\omega C$. The complex plane plots of such a system show only a vertical line, Fig. 1b. In the case of solid smooth electrodes a deviation from vertical line is usually observed.

2.3.3.3 Faradaic reaction without mass transfer limitation

In this case the electrode impedance can be represented as an electrical circuit consisting of the solution resistance, R_s , in series with parallel connection of faradaic resistance, R_{ct} , and double layer

capacitance, C_{dl} , eqn. [2.77] and Fig. 2a. The complex plane plots of such a system show a perfect

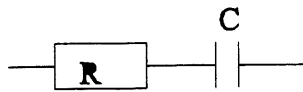


Figure 1a

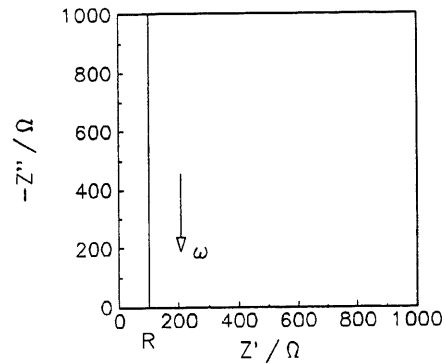


Figure 1b

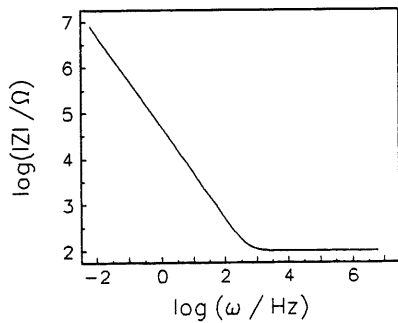


Figure 1c

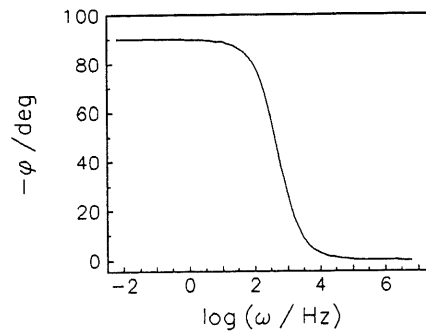


Figure 1d

Figure 1. Series connection of R_s and C (a), corresponding complex plane (b), Bode (c) and (d) plots; $R = 100 \Omega$, $C = 20 \mu\text{F}$ (375).

semicircle, Fig. 2b. The complex plane (Nyquist) plots are helpful for easy prediction of the circuit elements, however, they are not very informative to give the values of these component. On the

other hand Bode plots, Figs. 1 and 2 (c and d) contain all necessary information, and are mainly used in the circuit analysis.

$$Z(j\omega) \equiv \hat{Z} = R_s + \frac{1}{R_{ct} - j\frac{1}{\omega C}} \quad [2.77]$$

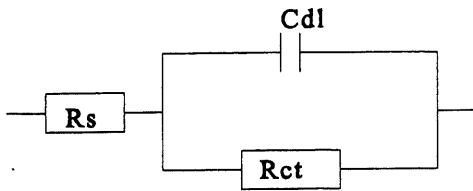


Figure 2a

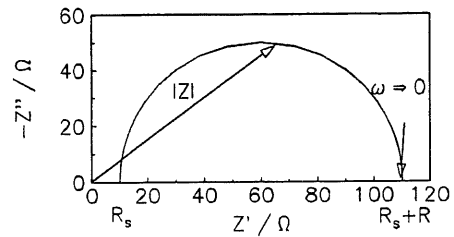


Figure 2 b

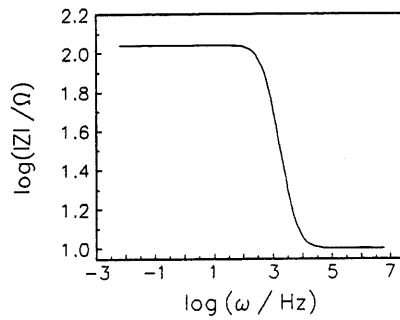


Figure 2c

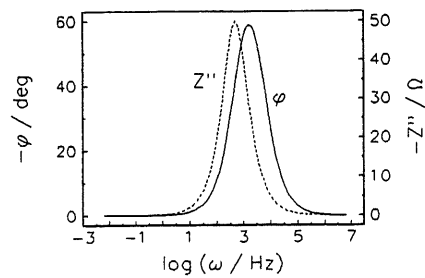


Figure 2d

Figure 2. Parallel connection of R_{ct} and C in series with R_s (a), corresponding complex plane (b), and Bode (c and d) plots; $R = 100 \Omega$, $C = 20 \mu\text{F}$ (375).

The above example was the classical Randles' model describing the ac impedance of *liquid electrodes*, e.g., Hg. However, it cannot explain the ac impedance of *solid electrodes*.

2.3.3.4 Impedance of faradaic reaction in the presence of adsorption of reacting species

In this case the reaction involves adsorbed species in the absence of diffusion effect, *i.e.*, there is no concentration gradient between the electrode and solution. Such a behavior can be observed in the HER. Here the state of the system which is under going a faradaic reaction at the steady-state may be explained by functions as:

$$i = i(\eta, \theta) = Fr_0(\eta, \theta), \text{ and } r_1 = r_1(\eta, \theta) \quad [2.78]$$

where r_0 and r_1 are given by eqns. [2.40] and [2.41]. In order to obtain the equation describing the impedance of the reaction, the state functions of the system should be linearized. Applying a small perturbing signal to the system which is at the steady-state (or at the equilibrium) will produce following changes (37):

$$\Delta i = \left(\frac{\partial i}{\partial \eta} \right)_{\theta} \Delta \eta + \left(\frac{\partial i}{\partial \theta} \right)_{\eta} \Delta \theta = F \left[\left(\frac{\partial r_0}{\partial \eta} \right)_{\theta} \Delta \eta + \left(\frac{\partial r_0}{\partial \theta} \right)_{\eta} \Delta \theta \right] \quad [2.79]$$

$$\frac{\sigma_1}{F} \frac{d\Delta \theta}{dt} = \Delta r_1 = \left(\frac{\partial r_1}{\partial \eta} \right)_{\theta} \Delta \eta + \left(\frac{\partial r_1}{\partial \theta} \right)_{\eta} \Delta \theta \quad [2.80]$$

where,

$$\Delta i = \tilde{i} \exp(j\omega t), \Delta r_1 = \tilde{r}_1 \exp(j\omega t), \Delta \eta = \tilde{\eta} \exp(j\omega t), \text{ and } \Delta \theta = \tilde{\theta} \exp(j\omega t) \quad [2.81]$$

and \tilde{i} , \tilde{r}_1 , $\tilde{\eta}$, and $\tilde{\theta}$ are phasors of the current, reaction rate, overvoltage, and surface coverage. Since only these small changes, eqns. [2.81], are contributors of ac impedance, the equations have to be solved for Δi , Δr_1 , $\Delta \eta$, and $\Delta \theta$.

Combination eqn. [2.81] with eqns. [2.79] and [2.80] and elimination θ between them gives

$$\hat{Y}_f = \frac{1}{\hat{Z}_f} = \frac{\tilde{i}}{\tilde{\eta}} = -F \left(\frac{\partial r_0}{\partial \eta} \right)_\theta - \frac{\frac{F^2}{\sigma_1} \left(\frac{\partial r_0}{\partial \theta} \right)_\eta \left(\frac{\partial r_1}{\partial \eta} \right)_\theta}{j\omega - \frac{F}{\sigma_1} \left(\frac{\partial r_1}{\partial \theta} \right)_\eta} = A + \frac{B}{j\omega + C} \quad [2.82]$$

where $A = -F \left(\frac{\partial r_0}{\partial \eta} \right)_\theta$, $B = -\frac{F^2}{\sigma_1} \left(\frac{\partial r_0}{\partial \theta} \right)_\eta \left(\frac{\partial r_1}{\partial \eta} \right)_\theta$, and $C = -\frac{F}{\sigma_1} \left(\frac{\partial r_1}{\partial \theta} \right)_\eta$ are terms

containing θ and potential dependent rate constants which can be easily obtain using r_0 and r_1 , *i.e.*, eqns. [2.32], [2.35], [2.40], and [2.41]. The total impedance of the electrode is given by a series connection of solution resistance with parallel connection of faradaic resistance and double layer capacitance, Fig. 3.

The physical meaning of parameters A, B, and C may be explained as (37): Parameter A is inverse of the charge transfer resistance, $A = 1 / R_{ct}$. Parameter B can be positive, negative, or very small so that $|B / C| \ll A$. In each case it has different physical meaning. If B is negative it produces a second semicircle in complex plane plot connected with the pores impedance, therefore, it indicates a porous behavior for electrodes. In the case when B is positive an inductive loop appears, and it will be difficult to attribute it a physical meaning simply. It may indicate corrosion of the electrode or oxidation of the surface. When $|B / C|$ is very small and negligible it indicates that the electrode surface is flat or flat-rough. Parameter C is the inverse of time constant, $C = 1 / \tau$, (37). The parameter τ measures how rapidly θ relaxes to its new value after the potential is changed. It has a precise meaning in the case when mechanism of the HER passes through the Volmer-Heyrovský reactions with Langmuir conditions, in other cases it is somewhat different (37). The mathematical discussion of the above meanings is presented in the following (37,375).

While A and C are always positive parameters, B may be negative, positive, or very small (near zero so that $|B/C| \ll A$) depending on the value of the rate constants. Eqn. [2.82] for $B < 0$ will produce

$$\hat{Z}_f = \frac{1}{\hat{Y}_f} = R_{ct} + \frac{R_{ct}^2 |B|}{j\omega + C - R_{ct} |B|} = R_{ct} + \frac{R_a}{1 + j\omega R_a C_a} = R_{ct} + \frac{1}{\frac{1}{R_a} + j\omega C_a} \quad [2.82a]$$

in which

$$R_a = \frac{R_{ct}^2 |B|}{C - R_{ct} |B|} \quad \text{and} \quad C_a = \frac{1}{R_{ct}^2 |B|} \quad [2.82b]$$

B is negative, and complex plane plot containing two semicircles, Fig. 4.

For $B > 0$ eqn. [2.82] will produce

$$\hat{Z}_f = \frac{1}{\frac{1}{R_{ct}} + \frac{1}{R_o + j\omega L}} \quad [2.82c]$$

in which

$$R_o = C / B \quad \text{and} \quad L = 1 / B \quad [2.82d]$$

In this case the capacitive semicircle is followed by an inductive one, Fig. 5. When $|B / C| \ll A$ the complex plane plot reduces to one semicircle, *i.e.*, the impedance corresponds to parallel connection of a resistance and capacitance in series with the solution resistance, Fig. 2.

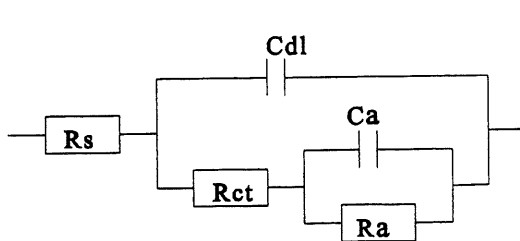


Figure 3a

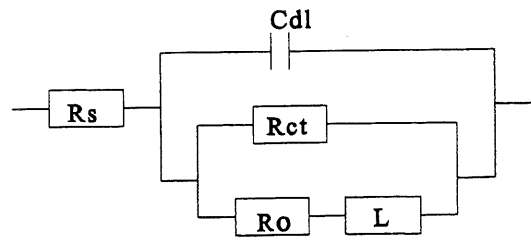


Figure 3b

Figure 3. Equivalent circuit in the case of one adsorbed species: (a) $B < 0$, (b) $B > 0$ (375).

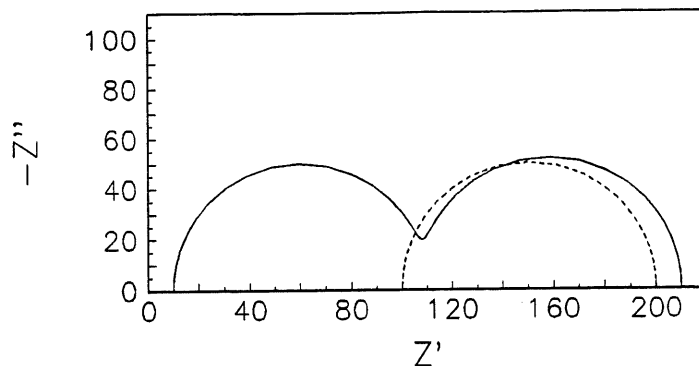


Figure 4. Complex plane plots in the case of one adsorbed species and $B < 0$; total impedance (continuous line), faradaic impedance (dashed line), parameters used: $R_{ct} = 100 \Omega$, $R_a = 40 \Omega$, $L = 0.2 \text{ H}$, $C_{dl} = 2 \times 10^{-5} \text{ F}$, $R_s = 10 \Omega$ (375).

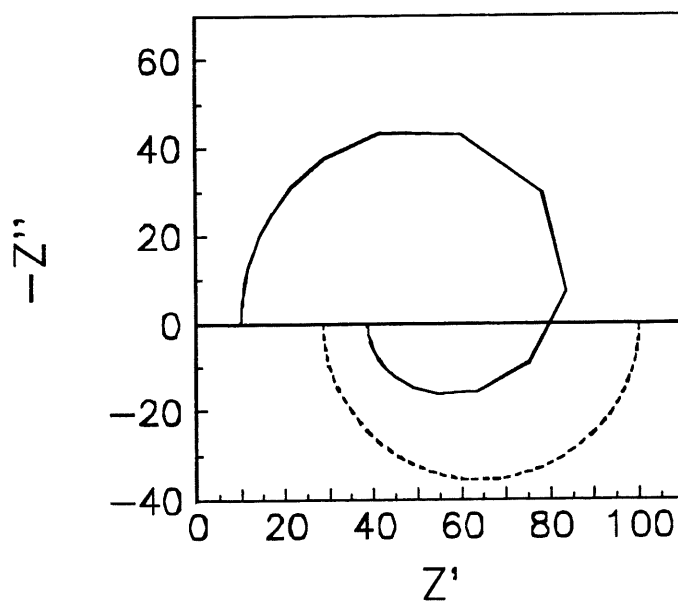


Figure 5. Complex plane plots in the case of one adsorbed species and $B > 0$; total impedance (continuous line), faradaic impedance (dashed line), parameters used : $R_{ct} = 100 \Omega$, $R_o = 40 \Omega$, $L = 0.2 \text{ H}$, $C_{dl} = 2 \times 10^{-5} \text{ F}$, $R_s = 10 \Omega$ (375).

This was another example of the classical Randles' model describing the ac impedance of *liquid electrodes, e.g., Hg*. It cannot also explain the ac impedance behavior of *solid electrodes*.

2.3.3.5 Impedance of solid electrodes

In practice only liquid electrodes as Hg and Ga show such an ideal behavior. In the case of solid electrodes, even smooth polycrystalline electrodes, a frequency dispersion is generally observed, it means that the impedance of the electrodes cannot be represented by connection of simple R-C-L elements. Moreover, in the case of porous electrodes, the penetration of ac signal in the pores contributes to the deviation of the electrodes from the ideal behavior. Therefore the classical Randles' model (see section 2.3.3.2 to 2.3.3.4) consisting of solution impedance, R_s , in series with a parallel connection of the double layer capacitance, C_{dl} , and the faradaic impedance, Z_f , describing the ac impedance of liquid electrode cannot explain the ac impedance behavior of solid electrodes. The typical models for the HER on solid, rough or porous electrodes are presented below (26,27,103,192,243):

2.3.3.5.1 Constant phase element, CPE, model

Even in the absence of a faradaic reaction a simple R-C circuit cannot describe the measured impedance of solid electrodes because dispersion of the time constants is observed, similarly to the Cole-Cole dielectric behavior.

Experimentally, this phenomenon causes rotation of a straight line, found for a simple series R-C circuit, clockwise by a constant angle $90^\circ(1-\phi)$ producing the so called constant phase element (CPE), its impedance is described as (38):

$$\hat{Z}_{\text{CPE}} = \frac{1}{T(j\omega)^\phi} \quad [2.83]$$

where T is the capacity parameter in $F\text{ cm}^{-2}\text{ s}^{\phi-1}$ and ϕ is a dimensionless parameter related to the rotation of the complex plane plot. Only if $\phi = 1$ then $T = C_{dl}$ and a purely capacitive behavior is obtained. In general, the average double layer capacitance, \bar{C}_{dl} , may be estimated from the value of T using method proposed by Brug *et al.* (38):

$$T = \bar{C}_{dl}^{\phi} [R_s^{-1} + R_{ct}^{-1}]^{1-\phi} \quad [2.84]$$

Since in this model CPE is used instead of C_{dl} in Randles' model the total electrode impedance, \hat{Z}_{el} , is given by :

$$\frac{1}{\hat{Z}_{el}} = T(j\omega)^{\phi} + \frac{1}{\hat{Z}_f} \quad [2.85]$$

where Z_f was given (37) by eqn. [2.82]. It has been suggested that deviation of the parameter ϕ from one is connected with the surface roughness, however, recent papers indicate that it may also be connected with ionic adsorption (376).

2.3.3.5.2 Porous electrode model

There is a great interest in increasing the real surface area in electrocatalysis, therefore, porous electrodes are used. Since the pores have different shapes and behavior (366-368) the modeling of the real surface area is difficult. De Levie (377) was the first who proposed a model for ac impedance of cylindrical pores. He found that the total impedance of the porous electrode can be given as:

$$\hat{Z}_t = R_s + \frac{\hat{Z}_{por}}{n} \quad [2.86]$$

where \hat{Z}_{por}

$$\hat{Z}_{por} = \left(\frac{1}{\pi r} \right) \left(\frac{\rho \hat{Z}_o}{2r} \right)^{1/2} \coth \left(\frac{2\rho l^2}{r \hat{Z}_o} \right)^{1/2} \quad [2.87]$$

n is the number of pores and Z_o stands for specific impedance per unit of the flat surface of a cylindrical pore, r and l are the pore radius and length, respectively, and ρ is the specific resistance of the solution. For a pure charge-transfer controlled process, \hat{Z}_o is described by a parallel connection of charge transfer resistance, R_{ct} and double-layer capacitance, C_{dl} , *i.e.*, $\hat{Z}_o = (1/R_{ct} + j\omega C_{dl})^{-1}$. The following equation can be obtained by rearrangement of eqns. [2.86] and [2.87] as:

$$\hat{Z}_t = R_s + R_{\Omega,p} \Lambda_1^{-1/2} \coth(\Lambda_1^{1/2}) \quad [2.88]$$

where

$$\Lambda_1 = \frac{1}{a} \left(\frac{1}{R_{ct}} + j\omega C_{dl} \right) \quad [2.89]$$

$$R_{\Omega,p} = \rho l / \pi r^2, \quad \text{and} \quad a = r / 2 \rho l^2 \quad [2.90]$$

The complex plane plot corresponding to the eqn. [2.88] is a 45° straight line at high frequencies followed by a semicircle at low frequencies.

Gassa *et al.* (378) considered the heterogeneity effects introduced by the porous cylindrical walls and suggested that the \hat{Z}_o may be described by

$$\hat{Z}_o = \frac{R_{ct}}{1 + (j\omega R_{ct} C_{dl})^\phi} \quad [2.91]$$

However, it is more justifiable to use $Z_{CPE} = 1 / [T(j\omega)^\phi]$ instead of C_{dl} , in parallel to R_{ct} to describe impedance of the surface of the pore walls (26,27,103,192,243). Thus

$$\hat{Z}_o = \frac{R_{ct}}{1 + (j\omega)^\phi R_{ct} T} \quad [2.92]$$

Replacing eqn. [2.92] in [2.87] and combining with eqn. [2.86] will produce the following relation for Z_t :

$$\hat{Z}_t = R_s + R_{\Omega,p} \Lambda^{-1/2} \coth(\Lambda^{1/2}) \quad [2.93]$$

in which

$$\Lambda = \frac{1}{A_p} \left[1 + (j\omega)^\phi A_p B_p \right] \quad [2.94]$$

where $A_p = a R_{ct}$, $B_p = T/a$ and other parameters were defined before. This model has five adjustable parameters, A_p , B_p , ϕ , $R_{\Omega,p}$, and R_s .

A complex plane plot corresponding to eqn. [2.93] is shown in Fig. 6a. The curve represents a straight line at high frequencies and a semicircle at low frequencies.

At very low frequencies, $\omega = 0$, the impedance becomes real. Thus eqns. [2.93] and [2.94] produce

$$\hat{Z}_t(\omega = 0) = R_p = R_s + \sqrt{\frac{\rho R_{ct}}{2\pi^2 r^3}} \coth\left(\sqrt{\frac{2\rho}{r R_{ct}} l}\right) \quad [2.95]$$

It is easy to show that the general eqn. [2.93] can be simplified to two limiting cases. The behavior of the pores depends on the penetration depth, λ , of the ac signal. This parameter is defined as $\lambda = (r\hat{Z}_0 / 2\rho)^{1/2}$, then $\Lambda = l/\lambda$ and two limits exist:

(a) for $l \ll \lambda$, $\Lambda \rightarrow 0$, $\coth \Lambda^{1/2} \rightarrow \Lambda^{1/2}$ and from eqns. [2.93]

$$\hat{Z}_t = R_s + \frac{R_{\Omega,p}}{\Lambda} = R_s + \frac{1}{2\pi r l} \hat{Z}_0 \quad [2.96]$$

In this case ac signal penetrates to the bottom of the pores (shallow pores), electrode behaves like a flat electrode, and for $\phi = 1$ complex plane plot will produce a semicircle with a diameter as $(R_{ct} R_{\Omega,p} a)$, Fig. 6b.

(b) for $l \gg \lambda$, *i.e.*, the pores behave as semi-infinite (deep pores), then $\Lambda \rightarrow \infty$, $\coth \Lambda^{1/2} \rightarrow 1$ and

$$\hat{Z}_t = R_s + \frac{R_{\Omega,p}}{\Lambda^{1/2}} = R_s + \left(\frac{\rho}{2\pi^2 r^3} \right)^{1/2} \hat{Z}_o^{1/2} \quad [2.97]$$

In this case electrode behaves like a porous surface and complex plane plot is a deformed semicircle, Fig. 6c.

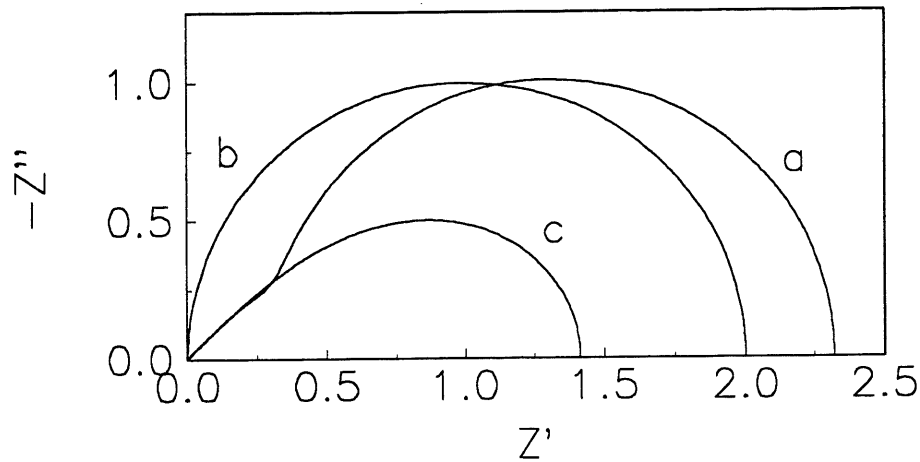


Figure 6. Complex plane plots for porous electrode according to de Levi's modified model: (a) general case, eqn. [2.93], (b) limiting case for shallow pores, eqn. [2.96], (c) limiting case for very deep pores, eqn. [2.97] (375).

2.3.3.5.3 Two-CPE model

The analysis presented above assumes right cylindrical pores, which is clearly a highly idealized representation of the structure of a real porous electrode. Therefore, the question arises to whether the shape of the pore can influence the impedance spectrum. Keiser *et al.* (367) have addressed in some depth to this question by numerical analysis of nonuniform electrical transmission line, assuming that the interface is purely capacitive, *i.e.*, in the absence of faradaic current. The results show that pore geometry does not have a profound effect on the complex plane plot shape at very high frequencies. The effects become more profound at moderate to low frequencies because of the

greater penetration depth of ac signal, and are greatest for the most occluded pores. Simply, when the pore shape changes from V shape to cylindrical and then pear shape a depression starts to appear in the middle range of frequencies. So that a 45° line for V shape and cylindrical pores and, a semicircle for pear shape pores appear in the complex plane plot at high and middle frequencies. The other pore shapes may be located between these two limits and their impedances too.

In the presence of the faradaic impedance, almost a second semicircle appears in the low frequencies range. Therefore, the complex plane plot of the pear shape pores becomes two semicircles. A two-CPE model has been used to explain the impedance of the pear shape pores in the presence of faradaic currents (26,27,42,121,243). This model may be represented as the solution resistance in series with the series of two parallel CPE-R elements. The model produces two semicircles on the complex plane plots. The high frequencies semicircle is related to the surface porosity predicted for pear shape pores (367). The low frequencies semicircle is related to the charge transfer process. The main assumption in this model is that the diameter of one semicircle (R_{ct1}) remains constant in the whole range of overpotentials. Therefore, the kinetic information can be obtained from the second semicircle in the same way as simple CPE model.

2.4 Approximation of rate constants and symmetry coefficients

Assuming that the HER proceeds through the Volmer–Heyrovský reaction without interference from Tafel reaction, the following relation exists between $\log A = \log (1 / R_{ct})$, and η .

$$\frac{1}{R_{ct}} = -F \left(\frac{\partial r_o}{\partial \eta} \right)_{\theta} = \frac{F^2}{RT} \left[\begin{array}{l} k_1 \beta_1 (1 - \theta) e^{-\beta_1 f \eta} + k_{-1} (1 - \beta_1) \theta e^{(1 - \beta_1) f \eta} \\ + k_2 \beta_2 \theta e^{-\beta_2 f \eta} + k_{-2} (1 - \beta_2) (1 - \theta) e^{(1 - \beta_2) f \eta} \end{array} \right] \quad [2.98]$$

At more negative overpotentials there is a linear relation between $\log (1 / R_{ct})$ and η . In these conditions for $\beta_1 = \beta_2 = \beta$ eqn. [2.98] may be simplified as:

$$\frac{1}{R_{ct}} = -F \left(\frac{\partial r_0}{\partial \eta} \right)_{\theta} = \frac{F^2}{RT} \frac{k_1 k_2}{k_1 + k_2} 2 e^{-\beta f \eta} \quad [2.99]$$

and a plot of $\log (R_{ct})$ vs. η will produce a line which theoretically has the same slope as Tafel plots, eqn. [2.59].

Eqn. [2.98], dependence of R_{ct} - η , and eqn. [2.53], together with the equilibrium conditions, eqn. [2.49] contain kinetic information about the process (26,192). In these conditions the rate constants and symmetry coefficients may be evaluated by simultaneous approximation of experimental data, *i.e.*, η - j and η - R_{ct} , using eqns. [2.53], [2.49], and [2.98]. This method has been followed in this thesis.

CHAPTER 3 EXPERIMENTAL

3.1 Introduction

A very important part in electrochemical studies is the electrode preparation. Paseka and Velicka (302) have shown that for a given electrode composition different activities may be obtained depending on the conditions of the electrode preparation, *e.g.*, temperature and current density. In our studies the electrodes have been prepared by electrodeposition in various ways and conditions, and their activities were evaluated towards the HER.

When high current densities are used, the HER at higher temperatures is preferable because of faster kinetics and lower solution resistance. In the case when porous electrodes are used, increase of temperature has other advantages as: (i) decreasing the viscosity of solution leading to better diffusion in the pores and (ii) easier releasing the gas bubbles from the pores. The kinetics of the HER in this study have been usually measured at 70°C, however, whenever it has been necessary experiments at 25°C have been done for comparison.

This chapter concerns with experimental parts of this thesis containing electrode preparation and treatments, techniques and methods for electrochemical measurements, instruments, and programs for data acquisition and analysis.

3.2 Electrodes

3.2.1 Reference electrode (preparation and potential calibration)

The electrode was made of Pyrex[®] glass consisted two compartments connected trough a

platinum wire (diameter ≤ 0.5 mm) sealed in the cobalt-glass. The Pt wire in one compartment was connected to HgO (ACS grade, Baker[®]) through metallic Hg. The HgO layer was wetted and covered with 1 M NaOH. The reference electrode was connected to the cell by a glass bridge. One branch of the bridge was connected to the cell (Luggin capillary). The ends of the bridge were filled with a glass frit. A Pt wire (0.1 mm diameter, 99.99%, Aldrich[®]) was immersed inside the bridge to reduce the noise and the solution resistance. The potential of this electrode was measured vs. activated platinized Pt electrode in solution studied and saturated with hydrogen (reversible hydrogen electrode, RHE).

To determine the equilibrium potential of the reference electrode, the platinized Pt was prepared using a Pt plate ($10 \times 10 \times 1$ mm, 99.99% Aldrich[®]). The plate was connected to a Pt wire, immersed in 3:1:4 HCl, HNO₃ and H₂O solution, washed with concentrated HNO₃ and then with H₂O. The plate was platinized during 2 min of cathodic polarization at $j = 15$ mA cm⁻² in platinizing solution (Mallinckrodt[®], Canada), 2% hexachloroplatinic acid solution. Then the platinized electrode was activated by 5 anodic-cathodic polarization cycles in 0.1 M H₂SO₄ (Fisher Scientific[®]) at $j = 500$ mA cm⁻², it was kept 15 seconds in each direction in each cycle, finishing by cathodic polarization.

The potential of RHE was equal to -0.895, -0.945 and -0.953 V vs. Hg/HgO/ 1 M NaOH electrode in 1 M NaOH, 25% and 30% KOH, respectively, at 70°C, and -0.928 V in 1 M NaOH at 25°C where the reference was always kept at room temperature.

3.2.2 Auxiliary electrode

Nickel foil ($150 \times 150 \times 0.125$ mm, 99.9%, Aldrich[®]) was used as a counter electrode.

3.2.3 Working electrodes

In this part preparation, determination of the composition, surface morphology, structure, and treatment of the working electrodes, Ni-P, Ni-Mo-P, Ni-Zn-P, and polycrystalline nickel, are presented. The chemicals used for preparation of deposition baths are of analytical grades otherwise it will be cited.

3.2.3.1 Preparation of nickel phosphorous, Ni-P, electrodes

Nickel-phosphorous electrodes were prepared by a constant current electrodeposition on a copper or nickel cylinder, cross-section surface area 0.314 cm^2 . Before electrodeposition the sides of the substrate were covered with thermoretractable plastic tube (Fit[®], Alpha Wire, N J USA) about 1 mm below than the edge. The electrode surface was polished with a sandpaper (P 600, Siawat[®]), washed with diluted HNO_3 and water, degreased with acetone, dried, immersed in a concentrated HNO_3 , again washed with water, and immediately introduced into the cell for electrodeposition. A two-compartment cell, separated by a Nafion[®] membrane (cationic, Dupont #117), was used. Nickel foil (Ni 99.9%, Aldrich[®]) served as a counter electrode. This configuration prevented transfer of gaseous oxygen, produced in the anodic compartment, to catholyte and further oxidation of phosphorous reagent, H_3PO_3 or NaH_2PO_2 .

After electrodeposition the tube was removed and the sides of the copper substrate were covered first with epoxy resin (Epofix Kit, Struers[®], Copenhagen, Denmark) and then with thermoretractable plastic tube to eliminate the edge effects. Three types of baths were used to obtain the Ni-P deposits as following.

(i) Bath A. Deposition from the bath containing 0.69 M H_3PO_4 , 1.52 M H_3PO_3 , 0.76 M Ni(II) obtained by dissolution of NiCO_3 in H_3PO_4 , (Aldrich[®]) and pH 1.25 to 1.3 (adjusted with H_3PO_4 or NaOH), at 70°C (94,98,118,293) at current densities from 200 to 250 mA cm^{-2} ,

gave alloys containing 30 at. % of P; decrease of H_3PO_3 concentration in the bath (to 0.025M) produced electrodes containing 30 to 19 at. % of P.

(ii) Bath B. Deposition from the bath containing 0.1 M NiSO_4 , 0.15 M H_3BO_3 , 0.1 M NH_4Cl (BDH[®]), and 0.3 M NaH_2PO_2 (Aldrich[®]) at a current density of 10 mA cm^{-2} , as in ref. 52, but at 18°C , the solution was stirred by magnetic stirrer (instead of rotating electrode), produced Ni_{92}P_8 .

(iii) Bath C. Deposition was carried out in two steps in two different baths, first by deposition of Ni from (a) 0.823 M NiCl_2 , 0.40 M NH_4Cl , and 0.10 M $\text{Na}_3\text{C}_6\text{H}_5\text{O}_7$ (sodium citrate, BDH[®]) followed by deposition of Ni-P from (b) 0.30 M NiSO_4 , 0.20 M NaH_2PO_2 , 0.30 M NH_4Cl , 0.12 M CH_3COONa (BDH[®]), 0.26 M H_3BO_3 and 0.14 M $\text{Na}_3\text{C}_6\text{H}_5\text{O}_7$, at a current density of 15 mA cm^{-2} at 22°C , produced $\text{Ni}_{73}\text{P}_{27}$.

3.2.3.2 Preparation of nickel molybdenum phosphorous, Ni-Mo-P, electrodes

Contrary to the electrodeposition of Ni-P electrodes, which can be performed in a wide range of pH, temperatures, and concentrations of the reagents, electrodeposition of Ni-Mo-P electrodes was sensitive to the conditions and concentration of the reagents. Electrodes were prepared using different methods. Several plating baths were examined and finally well adhered metallic deposits of Ni-Mo-P were obtained from aqueous baths as following:

(i) Electrodes A was prepared in one step from the bath containing: 0.15 M NiSO_4 , 0.02 M $(\text{NH}_4)_6\text{Mo}_7\text{O}_{24}$ (Aldrich[®]), 0.25 M NaH_2PO_2 , 0.30 M $\text{Na}_3\text{C}_6\text{H}_5\text{O}_7$, 2 M NaCl , pH = 9 (adjusted by NH_3 , BDH[®]), at 30°C . Deposition was carried out at a constant cathodic current, $j = 200 \text{ mA cm}^{-2}$ during 30 min, in a two compartments bath. Electrode A obtained using above mentioned conditions, had a bright metallic appearance. It was used at 25°C for the HER as it will be explained latter in this chapter.

(ii) Another electrode was prepared from the similar bath and exactly in the same conditions, but used for the HER at 70°C. This electrode was labeled as B. There is no any differences in the preparation method of these two electrodes (they are labeled as A and B to discriminate the kinetic results of the HER).

(iii) Electrode C was deposited from an aqueous bath in three steps. In step (a) a layer of nickel was deposited from the bath (solution volume 50 ml) containing 0.823 M NiCl₂, 0.40 M NH₄Cl, 0.10 M Na₃C₆H₅O₇, pH = 4.7, at 50°C, $j = 32 \text{ mA cm}^{-2}$ during 50 min; in step (b) a layer of nickel phosphorous was deposited from the bath containing the same components with the same concentrations as bath (a) plus 0.20 M NaH₂PO₂, deposition conditions were the same as in (a); finally in step (c) temperature of bath (b) was adjusted to 25°C and the solution was neutralized with NH₃ to pH = 7 to 8, and NaCl was added to obtain the concentration of 1 M, then deposition started and 10 ml of 0.57 M Na₂MoO₄ was added gradually during 50 min. The obtained electrode had a bright-gray appearance and a rough surface, but the top layer was somewhat fragile.

(iv) Electrode D was also deposited in three steps, the first step was the same as for electrode C, and the second carried out at lower current density (10 mA cm⁻²) and temperature (25°C). In step (c) pH was adjusted to 9.2 and 10 ml 0.57 M Na₂MoO₄ (Aldrich®) solution was gradually added to the bath (bath solution volume was 50 ml) as for electrode C, but at 10 mA cm⁻² and 25°C. This electrode had a black-brown metallic surface and showed a very good physical stability.

(v) Electrode E1 was a Ni-P electrode prepared as electrode D following steps (c) and (b) only.

(vi) Electrode E2 was a Ni-Mo electrode prepared similarly to D following steps (a) and (c), but without phosphorous, that is only Ni-Mo was deposited.

(vii) Electrode F was prepared in three steps : (a) first nickel was deposited in the absence of phosphorous using bath described in (52), (b) then Ni-P was deposited as in (52) and (c) finally the pH was adjusted to 9.2 by NH_3 and 10 ml of 0.57 M Na_2MoO_4 solution was added to the bath (bath solution volume 50 ml) gradually during 50 min.

(viii) Electrode G was prepared as F, but only $\text{Ni}_{192}\text{P}_8$ was deposited in steps (a) and (b).

(ix) We tried to deposit a Ni-Mo electrode using baths step (a) and (c) in the absence of phosphorous for comparison with electrode F, but the deposition was not successful.

Pretreatment of the substrate before electrodeposition was exactly the same as Ni-P electrodes. Also after electrodeposition the tube was removed and the sides of the copper substrate were covered first with epoxy resin and then with thermoretractable plastic tube.

3.2.3.3 Preparation of nickel zinc phosphorous, Ni-Zn-P, electrodes

Nickel–zinc–phosphorous alloys were deposited on cylindrical Cu substrates (0.314 cm^2) using four procedures.

(i) The first procedure consisted of deposition of Ni-Zn-P alloy from the bath AA containing 0.09 M ZnCl_2 , 0.823 M NiCl_2 , 0.10 M $\text{Na}_3\text{C}_6\text{H}_5\text{O}_7$, 0.40 M NH_4Cl , (analytical grade, BDH[®]), and 0.23 M NaH_2PO_2 , pH = 4.2, temperature 60°C , current density 320 mA cm^{-2} , using Ni foil as a counter electrode. A two-compartment cell was used as was mentioned for Ni-P electrodes. After deposition the electrode was leached for 4h in 30% KOH (analytical grade, BDH[®]) at 70°C

(ii) The second procedure consisted of deposition in three steps. First, a layer of Ni was deposited from the bath A containing 0.823 M NiCl₂, 0.10 M Na₃C₆H₅O₇, 0.40 M NH₄Cl, pH = 4.2, at 65°C, $j = 160 \text{ mA cm}^{-2}$, during 25 min. Bath B was prepared by dissolving 5.2 g of NaH₂PO₂ in 50 ml of solution A and adding it to 250 ml of bath A. Then, Ni-P alloy was deposited from this bath at $j = 200 \text{ mA cm}^{-2}$ during 25 min. Finally, 50 ml of the solution obtained by dissolving 3.08 g of ZnCl₂ in 50 ml of bath B was gradually added to 300 ml of bath B during 25 min (bath C). During this addition electrodeposition continued at $j = 230 \text{ mA cm}^{-2}$, the other conditions were always the same as in deposition from bath A. The deposition continued for the next 15 min. Similar procedure was used by Machado *et al.* (197,244,246) for electrodeposited Ni-Co-Zn electrodes.

(iii) Exactly after removing the three-step deposited electrodes another electrode was prepared in one step from bath C for comparison.

(iv) Another series of Ni-Zn-P electrodes was prepared by “three-step” method by the procedure mentioned above in (ii), but at higher temperature, 75°C, and lower current density, $j = 50 \text{ mA cm}^{-2}$. The temperature and current density were the same for all three steps. All other experimental techniques were the same as used for preparation and composition determination of Ni-Zn-P electrodes. After deposition, the electrodes were removed and leached in 30% KOH at 70°C for 24h, and used for surface studies. The advantage of this method was that the surface layers surface did not collapse after leaching, as compared with those prepared at higher current densities in method (ii). These series were used in studies of the surface behavior of Ni-Zn-P electrodes, chapter 7.

3.2.3.4 Preparation of polycrystalline nickel, Ni, electrode

Polycrystalline nickel electrode, area 0.314 cm^2 (99.99%, Aldrich®) was polished with 0.05

μm alumina suspended in distilled water (Buehler, Gamma Micropolish[®]), washed with water, 1:5 H_2SO_4 solution, again with water, connected to the cathodic potential immediately and then introduced to the cell. This electrode was used for the HER or CO adsorption and oxidation.

3.2.3.5 Composition, structure, and surface morphology of the working electrodes

The microscopic surface studies were carried out using scanning electron microscopy (SEM, Joel JSM-840-A). The composition of one step deposited electrodes, Ni-P (from bath A and B), Ni-Mo-P (A), and Ni-Zn-P (one step deposits), was studied by: (i) EDX, using K_α as analytical line, Ni 99.9%, Mo 99.5%, InP 99.9%, and Zn 99.5% as standards, and (ii) inductively coupled plasma (ICP) (or AAS, the case of Ni-Mo-P) after chemical dissolution.

Because “multi-step” deposited electrodes, Ni-P (C), Ni-Mo-P (C, D, E1, E2, F and G), and Ni-Zn-P had nonhomogeneous distribution of their components (*i.e.*, Ni, P, Mo, and Zn) from top of the surface to depth layers, wet analysis did not give the real surface composition of these electrodes, therefore the composition of the electrodes was studied by EDX quantitative microanalysis.

Suitable vertical cross-section of the electrodes were prepared by putting the electrode in an epoxy resin and cutting by diamond edge blade. Then the thickness of the electrode was determined by SEM.

X-Ray diffraction (XRD) analysis was performed on as deposited Ni-P samples directly, or after heating at 160 and 400°C in H_2 or air.

For thermogravimetric (TG) analysis of Ni-P electrodes, the sample was electrodeposited on a copper substrate for ~3h, cut out of the support, degreased with acetone, and heated in an aluminum dish at $20^{\circ}\text{C min}^{-1}$ from room temperature up to 600°C in nitrogen, N_2 , or air, and the variations in weight and the amount of absorbed energy were recorded as a function of temperature.

3.2.3.6 Electrode treatment

The aim of the electrode treatments was increase the electrode activity, besides in the case of Ni-P electrodes to verify the results exist in literature. Therefore, different treatments were applied as following:

Ni-P electrodes were studied either directly after preparation or after pretreatments as: 3h heating at 400°C in air; 6h oxidizing at $+0.200\text{ V vs. Hg/HgO}$ in 1 M NaOH at 70°C ; 40 min treating with 1 M HF at 25°C ; and heating 3h at 400°C in air then oxidation in 1 M NaOH, 70°C , one hour, at $+0.750\text{ V vs. Hg/HgO}$; and leaching in 30% NaOH, 70°C , 18h, N_2 atmosphere

Moreover Ni-P electrodes were cycled between -1.2 and $+0.6\text{ V vs. Hg/HgO}$ in 1 M NaOH at 70°C before and after heating in 400°C . Then these electrodes where used for the HER.

Ni-Mo-P electrodes were used directly after preparation or after pretreatments as: oxidation, cycling between the HER and OER, or leaching in KOH 30% solution at 70°C for 4h.

Ni-Zn-P electrodes were leached in 30% KOH solution at 70°C for 24h before to be used for electrochemical studies. After leaching, the tube was removed, electrode was covered first with epoxy resin up to the edge and then with shrinkable tube. The electrode composition and surface morphology were also studied after the HER experiments. It should be emphasized

that all the electrochemical measurements on Ni-Zn-P electrodes in this thesis were performed after leaching.

Ni-Zn-P electrodes were cycled between 0.6 to -1.2 V vs. Hg/HgO, the OER and HER, at 25 and 70°C in 1 M NaOH with different scan rates. The activity of the electrode towards the HER was measured before and after cv to find the effect of oxidation. Also cyclic voltammograms at different scan rates were used to estimate the double layer capacitance of the electrodes. These measurements were carried out in plateau region between -0.1 and -0.6 V and C_{dl} estimated from $j = C_{dl} v$, where v is the scan rate.

3.3 Cell, solutions, and instruments for kinetic measurements of the HER.

3.3.1 Cell

All the electrochemical measurements were performed in a two-compartment cell made of Pyrex[®] glass in which the anodic compartment was separated from the cathodic compartment by a Nafion[®] membrane (cationic, Dupont # 324). The temperature was controlled by a thermostated water bath through the cell jacket. Before each experiment cell was washed with hot water, H₂SO₄, many times with hot water, and finally with NaOH solution. Then it was kept under N₂ until be used.

3.3.2. Solutions

Electrochemical measurement were carried out in 1 M NaOH (semiconductor grade, Aldrich, 99.99 %) or 30% KOH (BDH, analytical grade) solutions using deionized water (Barnstead Nanopure, 17.4 MΩ cm). Oxygen was removed by bubbling of N₂ prior to start the experiments and continued during the experiments.

3.3.3 Instruments and data acquisition

The X-Ray diffractometer Rigaku-Geigerflex[®] using Cu K_α analytical line, 1° slit, 0.3° divergence, was used for the XRD measurements. The atomic emission spectroscopy (AES) and atomic absorption spectroscopy (AAS) analysis were carried out on ARL Fision[®] model 3560 AES working with argon inductively coupled plasma (ICP), and on Varian[®] AAS Specter AA-10 working with acetylene flame, respectively. The studies of the surface morphology and energy dispersive X-Ray diffraction (EDX) quantitative microanalysis were performed using the SEM, Joel JSM[®]-840-A.

The Diamond Wafering Blade on rotating plate, Isomet[™], Buehler[®] was used to cut the electrodes for studies of their cross section. Differential scanning calorimetric and thermogravimetric analysis were performed on DSC/320, and TG/320, Seiko Instruments[®], respectively.

The potentiostat EG&G PAR Model 273A and lock-in-amplifier EG&G Model 5210 controlled by an IBM compatible PC computer served for EIS, steady-state polarization, and cyclic voltammetric measurements. The digital oscilloscope Nicolet Pro[®] Model 92 was used for potential decay measurements. EG&G 175 Universal Programmer and a sub-commands software executable in M 273-81, Head Start were used for sampling analogue *cv* signal.

3.4 Studies of the hydrogen evolution reaction

3.4.1 Steady-state polarization curves (Tafel plots)

The steady-state was achieved approximately after 24h the HER at constant current, $j = 320 \text{ mA cm}^{-2}$ and then 24 to 36 cycles, each cycle consisting of 30 min galvanostatic electrolysis at 320 mA cm^{-2} and 55 min of polarization curve recording (45 seconds per point) at cathodic current densities ranging from 320 mA cm^{-2} to $0.04 \text{ } \mu\text{A cm}^{-2}$. At the steady-state, the

electrode potentials were corrected for iR drop, which was determined by the EIS or current interruption, and the current–overpotential data were used to determine the kinetics. The solution resistance, R_s , changed linearly with the overpotential, η , and these changes were considered for iR_s corrections.

3.4.2 Electrochemical impedance spectroscopy

All the EIS measurements were carried out at the steady-state where it was understood from polarization curves. The amplitude of applied ac signal was 5 mV. A frequency (f) range from 1×10^4 to 0.05 Hz was covered, the frequency being scanned step–wise, at a constant dc potential, with 10 steps per decade on logarithmic scale. For brevity, only the impedance spectra at few overpotentials will be shown in complex plane and phase angle plots in next chapters.

3.5 Surface behavior of Ni-Zn-P electrodes in alkaline solutions

This part contains the experiments related to the evaluation of the Tafel behavior, steady-state time, shift in the equilibrium potential, and determination of the surface roughness of Ni-Zn-P electrodes by new *in situ* methods developed in this work. All the measurements were performed in 1 M NaOH at 70°C except the experiments for CO which were performed at 25°C. Carbon monoxide was prepared from Linde Co., Union Carbide.

3.5.1 Steady-state and equilibrium time (shift in equilibrium potential)

For the steady-state polarization measurements in N_2 atmosphere, a positive shift in equilibrium potential was observed. To find the source, first the polarization curves were recorded for different polarization times (1,5,45,60, and 120 seconds per point) in 1 M

NaOH, 70°C and N₂ atmosphere. Then the experiments were repeated in H₂ atmosphere (solution was continuously bubbled with hydrogen).

3.5.2 Evaluation of the surface roughness of Ni-Zn-P electrodes by *in situ* methods

The following *in situ* methods were used for the determination of the roughness factor: the ratio of the steady-state polarization current densities, electrochemical impedance spectroscopy, coulometric oxidation of the electrode surface, cyclic voltammetry, and adsorption and electrooxidation of carbon monoxide (CO molecular probe). The experiments of the first two methods were explained earlier in this chapter, and the others will be explained here.

3.5.2.1 Coulometric oxidation of the electrode surface

Before coulometric measurements the electrode kinetics was measured using steady-state polarization and electrochemical impedance spectroscopy. Then the electrode was subjected to a cathodic current, $j = 2 \text{ mA cm}^{-2}$ for 5 min. For coulometric measurements an anodic current, $j = -2 \text{ mA cm}^{-2}$, was applied and the potential of the electrode was recorded as a function of time (chronopotentiometry). From the time and current density the amount of the charge needed to oxidize Ni to Ni(II) was determined. Assuming that the necessary charge for one monolayer oxidation of smooth Ni be known, 0.463 mC cm^{-2} , the roughness factor, R , and C_{dl} were determined (147).

3.5.2.2 Cyclic voltammetry

After the steady-state polarization and EIS measurements for the HER, Ni-Zn-P electrodes were cycled between -0.810 to -1.000 V vs. Hg/HgO with different scan rates at 70°C in 1 M NaOH, and at the steady-state the last cycle was recorded for each scan rate. The capacitive

current densities in each scan rate were extracted using average of current densities, $(j_a + j_c) / 2$, at 0.910 V vs. Hg/HgO, and plotted as functions of scan rate. The C_{dl} and R were determined from the slope of the linear part of j_{dl} vs. v .

Since the digital systems may produce different values for capacitive current densities depending on the selected acquisition mode (AM) in M270 software and due to the other limitations existing with this method (381), the data obtained using different AMs are compared with those obtained by the analogue sweep generator. The latter experiments were performed in the same conditions, but EG&G 175 Universal Programmer was used to generate the sweep. A sub-commands software executable in M 273-81, Head Start (382) was used for sampling of analogue cv signal instead of EG&G M270 software.

3.5.2.3 Adsorption and electrooxidation of carbon monoxide, CO molecular probe

Before preparing the working electrodes, the cell was arranged with the reference and counter electrodes, temperature was adjusted to 25°C, and the solution, 1 M NaOH, was bubbled with N₂ gas to remove the dissolved oxygen. First the measurements were performed on Ni electrode to optimize the conditions.

3.5.2.3.1 Adsorption of CO on polycrystalline Ni electrode

The cleaned electrode was connected to the cathodic potential immediately after preparation, and then introduced to the cell. The electrode was kept near the zero cathodic current density, $E = -0.935$ V vs. Hg/HgO (corresponding to $\sim 30 \mu\text{A cm}^{-2}$) for 30 min. The measurements consisted of the following parts.

(i) *Clean Ni electrode in 1 M NaOH.*—The electrode potential was cycled between -0.930 to 0.200 V (starting from -0.935 V), and the *first* and *second* cyclic voltammograms were recorded (clean electrode in pure NaOH).

(ii) *Ni electrode in 1 M NaOH saturated with CO.*— The electrode was prepared, washed with 1:5 H₂SO₄ solution, then with 1 M NaOH (deoxygenated with N₂, and then saturated with CO). While the electrode was kept near zero cathodic current, the solution was bubbled with CO gas for 25 min (solution volume was about 200 ml, longer time caused no changes). CO was passed over the solution, the electrode potential was cycled by the same way and, the first and second cyclic voltammograms were recorded (Ni electrode in 1 M NaOH saturated with CO).

(iii) *CO-adsorbed on Ni electrode and NaOH solution free of CO.*—Again the electrode was cleaned and introduced to the solution in the same way. The solution was bubbled with CO for 25 min then with N₂ in the same period (25 min) to remove dissolved CO, the path of the N₂ gas was changed to pass over the solution, and the first and second cyclic voltammograms were recorded. The experiment was repeated in the same conditions, but after 100 min of bubbling with N₂. In another experiment the solution was drained completely after CO bubbling was finished and replaced by pure and deoxygenated 1 M NaOH (CO-adsorbed on Ni electrode and NaOH solution free of CO), bubbled one hour with N₂, then N₂ was passed over the solution and the electrode potential was cycled as before. Reproducible data were obtained in these conditions for Ni electrode.

3.5.2.3.2 Adsorption of CO on Ni-Zn-P electrode

Ni-Zn-P electrodes were used just after 24h leaching in 30% KOH at 70°C and without any other treatment. The measurements consisted of following parts.

(i) *Clean Ni-Zn-P electrode in 1 M NaOH.*—The electrode was subjected to the HER at 25°C in 1 M NaOH for 24h at $j = 320 \text{ mA cm}^{-2}$, then steady-state polarization curve and EIS measurements were performed. Again the electrode was activated for the HER at $j = 320 \text{ mA cm}^{-2}$ in the same conditions for one hour, then it was kept at $E = -0.935 \text{ V vs. Hg/HgO}$ (note that current was cathodic and near to zero, $\sim 30 \mu\text{A cm}^{-2}$) and solution was bubbled with N_2 for 2.5h, N_2 was passed over the solution and the electrode potential was cycled in the same way as Ni (clean Ni-Zn-P electrode in 1 M NaOH).

(ii) *Ni-Zn-P electrode in 1 M NaOH solution saturated with CO.*—The experiment (i) was repeated, but solution was bubbled with CO (instead of N_2) for 2.5h, then CO was passed over the solution and the electrode potential was cycled as before (Ni-Zn-P electrode in 1 M NaOH saturated with CO).

(iii) *CO-adsorbed on Ni-Zn-P electrode and solution free of CO.*—The experiment (ii) was repeated, but before measuring the cyclic voltammogram solution was replaced by previously deoxygenated 1 M NaOH (CO-adsorbed and solution free of CO). The measurement was performed under N_2 atmosphere.

The first cyclic voltammogram was used and the amount of the charge was determined from irreversible anodic peaks around -0.490 and -0.650 V and attributed to the oxidation of active sites on the electrode surface for oxidation of Ni and Ni-Zn-P in pure 1 M NaOH, and from irreversible anodic peaks around -0.380 V to the oxidation of adsorbed CO on the Ni. For oxidation of adsorbed CO on Ni-Zn-P two peaks were observed, -0.380 and -0.650 V. Both of them were used to calculate the total charge.

3.6 Data analysis

The real, Z' , and imaginary, Z'' , components of impedances were analyzed using a modified

version of complex non-linear least squares fitting program, CNLS method (192,372-374, 379,380) and an equivalent electrical circuit from which the experimental parameters as R_s , $R_{ct} = 1 / A$, ϕ , and T were determined, then using eqn. [2.84] \bar{C}_{dl} was evaluated (see section 2.3.3.5.1). The EIS data of Ni-P, Ni-Mo-P, and Ni-Zn-P electrodes were approximated using various models. Three types of equivalent circuits were used to approximate the EIS data, CPE, two-CPE, and porous models. This matter will be discussed in chapters four to seven.

Using R_{ct} and current density, j , obtained from EIS and steady-state measurements respectively, as functions of overpotential, η , and non-linear least squares (NLS) methods (26,192,372,373,379,380) the rate constants, k_1 , k_{-1} , and k_2 and symmetry coefficients, β_i , together with their standard deviations were approximated, see eqns. [2.48], [2.53], and [2.98] in chapter 2.

CHAPTER 4

STUDIES OF THE HYDROGEN EVOLUTION REACTION ON Ni-P ELECTRODES IN ALKALINE SOLUTIONS

4.1 Introduction

Alkaline water electrolysis requires mechanically and chemically stable and electrochemically active electrodes. Nickel based electrodes, because of their chemical inertness, are among the most often used electrode materials for the hydrogen (HER) or oxygen (OER) evolution reactions in alkaline solutions. As it was suggested in first chapter (section 1.4), increase in the electrode activity can be achieved through: (i) increase of intrinsic activity, and (ii) increase in the real surface area. Because the main contribution to the total activity arises from increase of the real surface area (26) alloys which contain a leachable element are very promising in the high performance industrial water electrolysis. This element may be partially or totally removed leading to the increase in the real surface area and, in consequence, to increase the apparent electrocatalytic activity. The leachable alloys are of a general composition: Ni_yZ_x , where Z is a leachable element such as Al, Zn, Sn, S, P, etc.

Ni-P alloys are stable, resist to the corrosion (284,289-301), and their physical stability is better than that of nickel, as we found in our preliminary experimental tests. These properties encouraged us to try to increase the porosity of this material and obtain porous electrode. However, explanation of the electrode behavior will clear up the reaction mechanism and the source of activity.

In this chapter studies of the structure and electrocatalytic activity towards the HER of the Ni-P alloys, prepared by galvanostatic deposition and containing 8 to 30 at. % of P, are presented. The electrodes were studied directly after preparation or after pretreatment by

heating, leaching in HF solution, anodic oxidation, or potential cycling in the solution. The activity of these electrodes depended on the method of preparation and the phosphorous content: the activity was higher for the materials deposited at lower temperatures and for those containing smaller amount of phosphorous. The mechanism of the hydrogen evolution reaction was studied in 1 M NaOH and the kinetic parameters were determined using steady-state polarization and the EIS techniques.

4.2 Results and discussion

4.2.1 Composition, structure and surface morphology of Ni-P electrodes

The chemical composition of the alloys obtained from bath A by galvanostatic deposition at 200 mA cm^{-2} and determined by EDX and ICP analysis is $\text{Ni}_{70}\text{P}_{30}$. Figs. 7A and 8A show the cross-section and the surface of as-deposited $\text{Ni}_{70}\text{P}_{30}$ electrodes, respectively. The thickness of the deposit was 16 to 17 μm . Large crystals, covered by many smaller crystallites, are visible. Fig. 8D shows SEMs of the electrode Ni_{92}P_8 obtained from bath B. This surface is smoother than that of the samples prepared at high current densities and at higher temperatures. Similar pattern was also observed for the electrode $\text{Ni}_{73}\text{P}_{27}$ deposited in two steps from bath C.

Crystal structure of the electrodeposited materials was studied using XRD technique. All the electrodeposited materials, containing 8 to 30 at. % of P, deposited from different baths and at different temperatures (18 to 70°C) have shown amorphous structure; only very broad peaks are observed on the XRD spectra, Figs. 9A and C (the sharp peaks come from the diffraction by the copper substrate).

Heating these samples at 160°C for 4h in air or in hydrogen did not cause any transition to crystalline forms. This is in contradiction with the Paseka's (52) observation who found crystallization of amorphous Ni-P alloys containing 3 wt. % of P after heating them at 150°C .

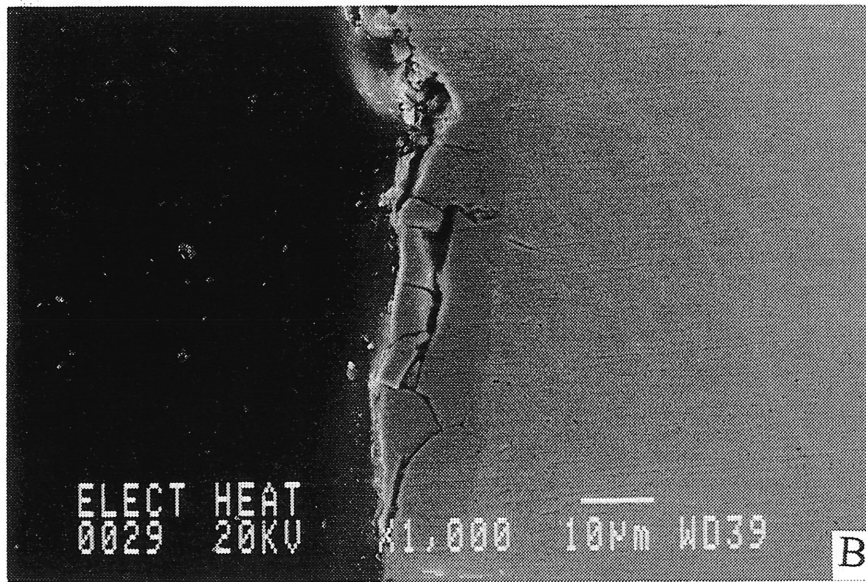
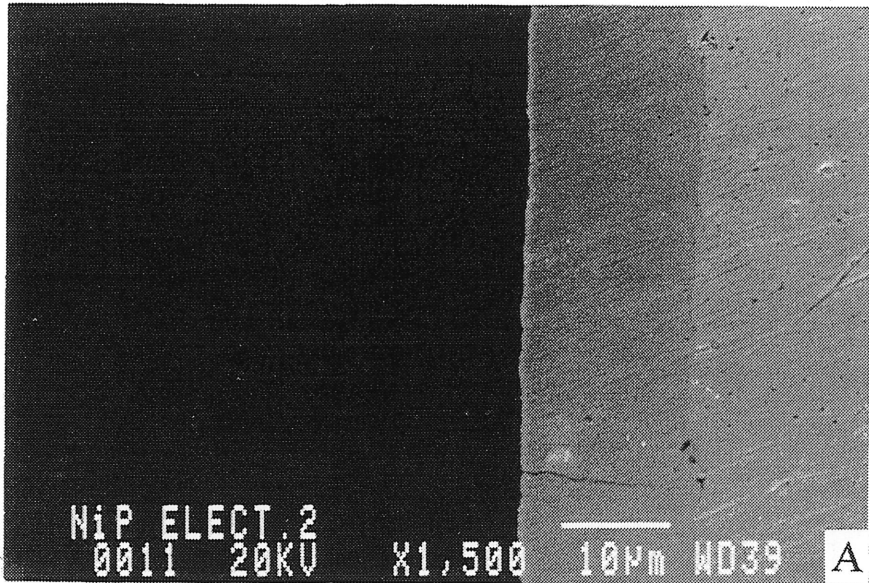


Figure 7. Scanning electron micrographs of the cross-section of Ni₇₀P₃₀ electrode, deposit thickness 16-17 μm : (A) before heating ; (B) after 3h heating at 400°C in air.

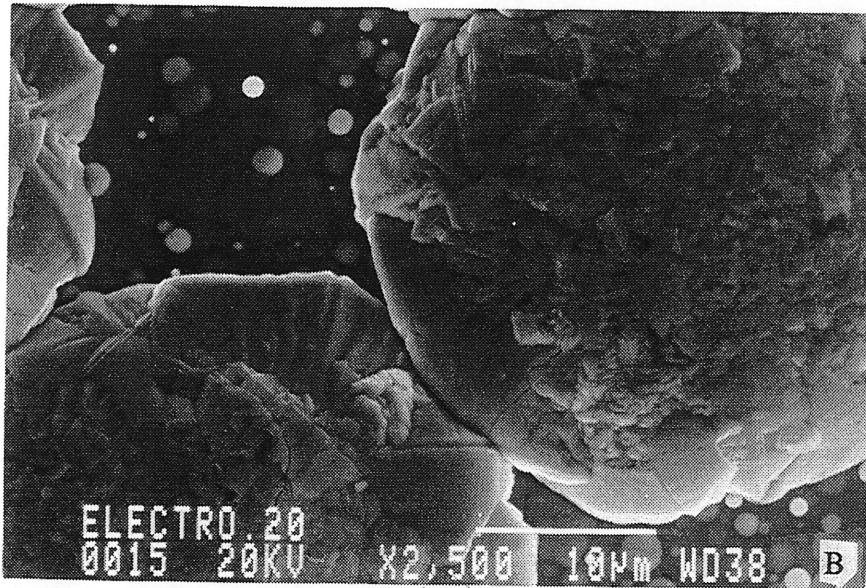
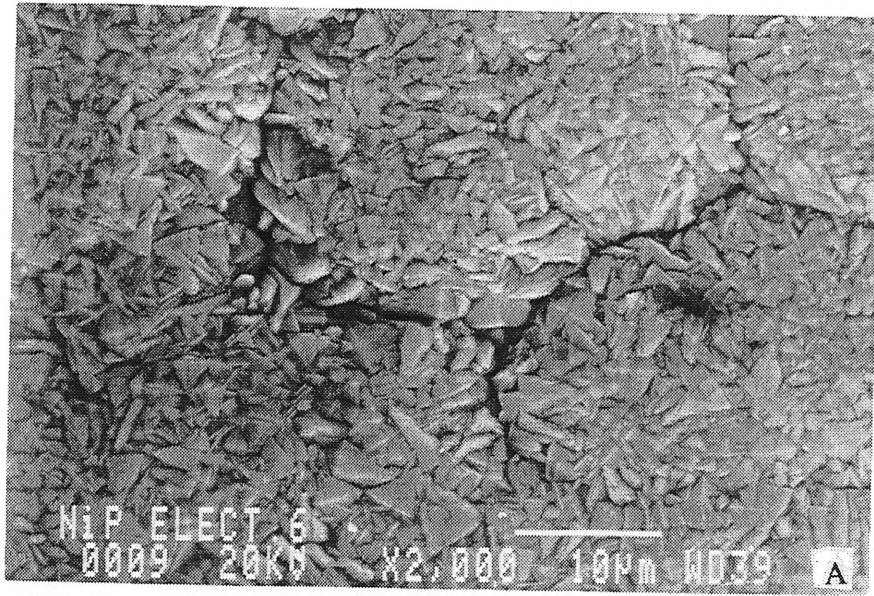


Figure 8A and B

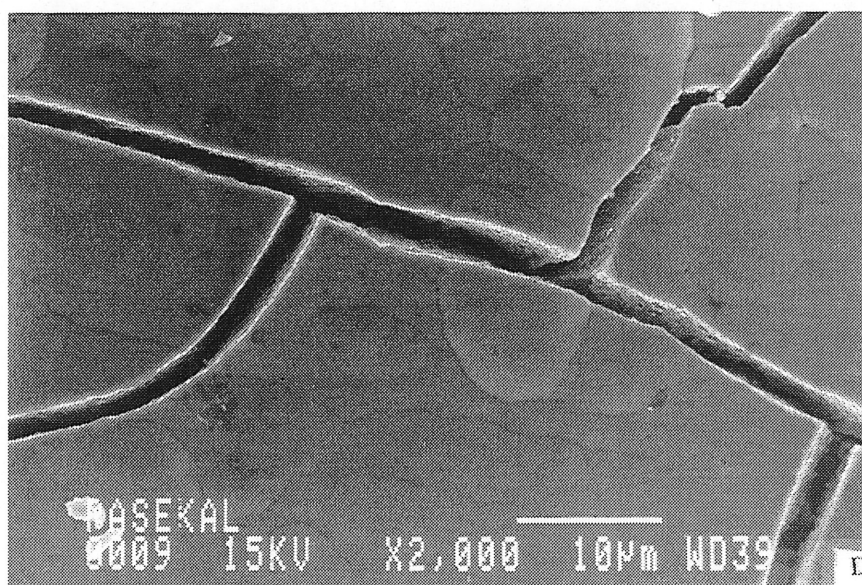
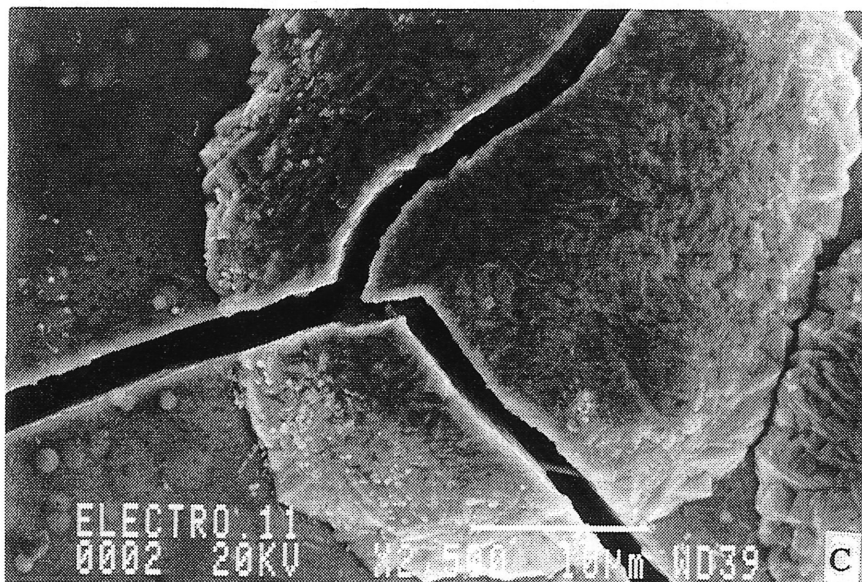


Figure 8C and D

Figure 8. Scanning electron micrographs of $\text{Ni}_{70}\text{P}_{30}$ electrode : (A) no pretreatment, (B) after leaching in 1 M HF at 25°C for 40 min, (C) after 3h heating at 400°C in air, and oxidation in 1 M NaOH at 30°C for 6h at +0.200 V vs. Hg/HgO, (D) as deposited Ni_{92}P_8 (from bath B).

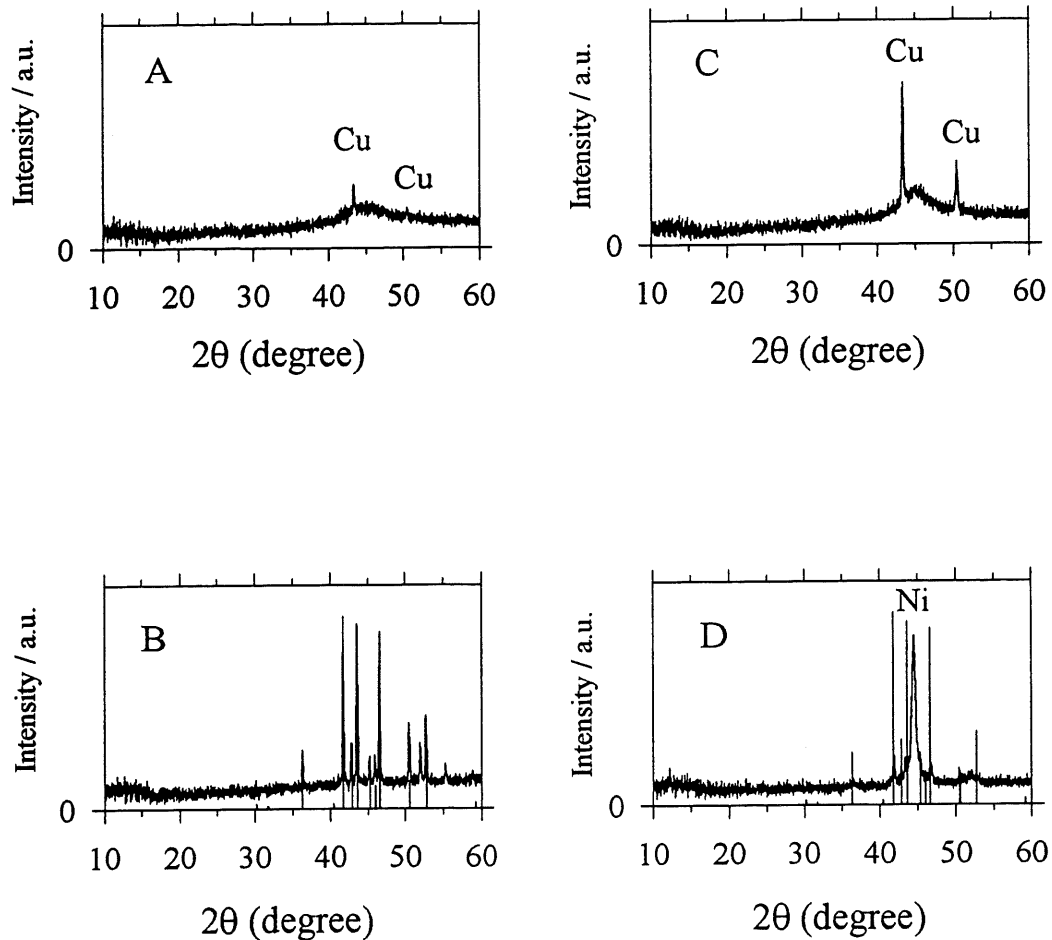


Figure 9. X-Ray diffraction patterns: of $\text{Ni}_{70}\text{P}_{30}$ electrodes, (A) as deposited and (B) after 3h heating at 400°C in air (similar patterns were observed for $\text{Ni}_{73}\text{P}_{27}$ electrodes); and of Ni_{92}P_8 electrodes, (C) as deposited and (D) after 3h heating at 400°C in air. The lines indicate Ni_3P phase.

However, heating at 400°C caused formation of peaks on XRD spectra and crystallization of samples, Fig. 9B and D. The peaks formed were attributed to Ni_3P (Fig. 9B), or Ni_3P and Ni crystals (Fig. 9D). The sharp peak in Fig. 9D implies that Ni_{92}P_8 is converted to Ni_3P and Ni.

It should be added that weak amorphous phase signals were measured using various sample holders (Plexiglass, plasticine or aluminum) in order to avoid artifacts. It was found that Plexiglass produced broad peaks at $2\theta = 13^\circ$, 30° and 42° and plasticine gave smaller, very broad peaks.

Table 1. Influence of pretreatment on the composition of Ni₇₀P₃₀ electrode deposited at $j = 200 \text{ mA cm}^{-2}$ from bath A.

Sample	pretreatment	Ni at. %	P at. %
1	no pretreatment	70	30
2	heating at 400°C, 3h, air	69	31
3	leaching in 30% NaOH, 70°C, 18h, N ₂ atmosphere	70	30
4	cathodic current, 90 mA cm ⁻² , 18h, 1 M NaOH, 70°C	70	30
5	leaching in 1 M HF, 40 min, 25°C	73	27
6	heating at 400°C, 3h, air, then oxidation at +0.200 V vs. Hg/HgO, 6h, 1 M NaOH 25 and 70°C	73	27

To increase the electrocatalytic activity these electrodes were treated in various ways: heated in air at 400°C, leached in 1 M HF, electrochemically oxidized at +0.200 V vs. Hg/HgO electrode and underwent long time (8 days) the hydrogen evolution reaction. Table 1 presents the EDX analysis of the deposit after these treatments. It is obvious that they did not cause any important changes in the alloy composition, at least in the layer producing X-rays (few μm). Habazaki *et al.* (297) have suggested that after heating of the Ni-P electrodes with high phosphorous content, elemental phosphorous may exist on the surface of Ni₃P. However, the surface composition could be only studied by surface sensitive techniques, *e.g.*, electron spectroscopy for chemical analysis (ESCA) or auger electron spectroscopy (AES). Figs. 7B,

8B and 8C show SEMs of treated electrodes. Heating and oxidation produce rougher surface and cause formation of cracks, whereas leaching in HF produces a smoother surface. The stability of nickel alloys is discussed in pages 96 to 102 in this thesis. It seems that Ni-P alloys are stable in HF solution (92). There were no distinguishable differences between the results obtained on samples deposited on copper or nickel substrates. Since oxidation peak of copper was not observed on cyclic voltammograms, the cracks observed on the surface do not continue to the substrate, *i.e.*, copper. The cracks may cause partial increase in the surface roughness and activity of the electrodes. The cyclic voltammograms and roughness factors will be presented subsequently in this chapter.

4.2.2 HER on Ni-P electrodes obtained from bath A

The steady-state polarization curves of the HER, obtained on amorphous Ni₇₀P₃₀ electrodes (from bath A) at 70°C in 1 M NaOH are displayed in Fig. 10 and the kinetic parameters obtained from the steady-state polarization curves before and after different pretreatments are presented in Table 2. These pretreatments did not increase the electrode activity towards the HER.

An increase of the Tafel slope with overpotential was often observed at very negative overpotentials. However, this phenomenon depended on the current used for the electrode activation before recording the Tafel curves (higher slope for larger currents) and longer times were necessary for the stabilization of currents at higher overpotentials. This behavior was probably connected with the formation of hydrides in the surface layer (327,341,342) and it was not studied in more details.

Electrochemical impedance spectroscopy was also used to study the interfacial properties and the kinetics of the HER. Fig. 11 presents complex plane plots obtained on Ni₇₀P₃₀ electrodes in 1 M NaOH at 70°C. One semicircle was obtained in the whole potential range studied.

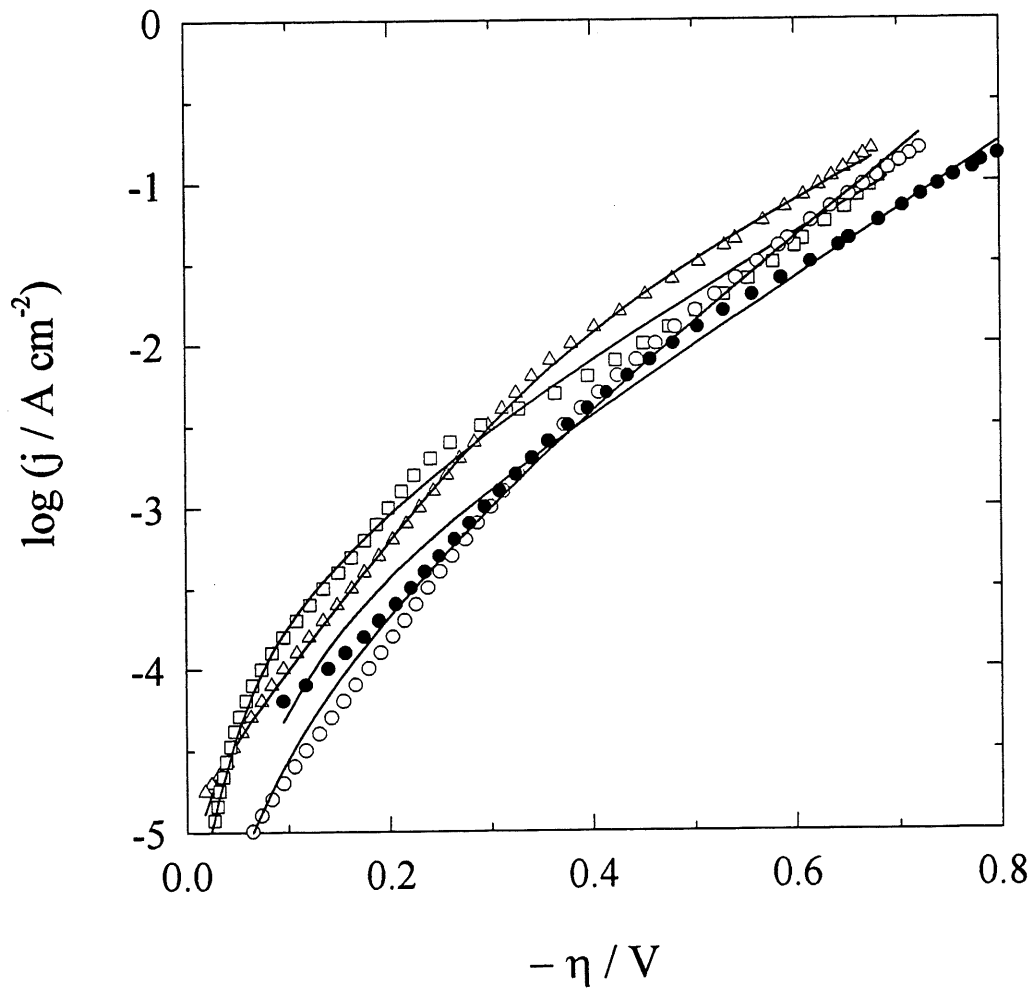


Figure 10. Steady-state polarization curves obtained on $\text{Ni}_{70}\text{P}_{30}$ in 1 M NaOH at 70°C ; (Δ) no pretreatment, (\square) after 3h heating at 400°C in air, (O) after 6h oxidizing at $+0.200$ V vs. Hg/HgO in 1 M NaOH at 70°C , and (\bullet) after 40 min treating with 1 M HF at 25°C . The continuous lines were obtained using data in Table 3.

Table 2. Kinetic parameters of HER obtained on Ni₇₀P₃₀ electrodes from the steady-state polarization curves in 1 M NaOH at 70°C.

Pretreatment	b / mV dec ⁻¹ *	j ₀ / A cm ⁻²	η ₂₅₀ / mV
no pretreatment	(1) -136	3.0 · 10 ⁻⁵	
	(2) -244	3.5 · 10 ⁻⁴	-698
400°C, 3h, air	(1) -127	3.4 · 10 ⁻⁵	
	(2) -264	2.3 · 10 ⁻⁴	-801
oxidation, 1 M NaOH, 70°C, 6h, +0.200 V vs. Hg/HgO	(1) -119	5 · 10 ⁻⁶	
	(2) -204	6.7 · 10 ⁻⁵	-727
oxidation, 1 M NaOH, 70°C, 1 hour, +0.750 V vs. Hg/HgO	(1) -87	1.7 · 10 ⁻⁵	
	(2) -201	2.9 · 10 ⁻⁴	-590
400°C, 3h in air, then oxidation in 1 M NaOH, 70°C, 1 hour, +0.750 V vs. Hg/HgO	(1) -130	6.4 · 10 ⁻⁵	
	(2) -237	4.1 · 10 ⁻⁴	-661
1 M HF, 40 min, 25°C	(1) -219	3.2 · 10 ⁻⁵	
	(2) -256	1.5 · 10 ⁻⁴	-823

*: Two Tafel slopes observed, at low current densities ($j \leq 20 \text{ mA cm}^{-2}$) and high current densities ($j \geq 25 \text{ mA cm}^{-2}$) labeled by (1) and (2) respectively.

Similar behavior was observed for other electrodes obtained from bath A. Complex nonlinear least-squares (CNLS) approximations (26,38,192,372-374,379), showed that impedances may be well described by a circuit consisting of the solution resistance in series with the parallel connection of the charge transfer resistance and a constant phase element (CPE) instead of the electrode capacitance. Impedance of the CPE was described in section 2.3.3.5.1, chapter 2,

$A \gg |B/C|$. The results of the CNLS approximations, *i.e.* \bar{C}_{dl} and ϕ , are displayed in Fig. 12. The average of double layer capacitance, \bar{C}_{dl} , was estimated using formula proposed by Brug *et al.* (38) and subsequently applied to Ni based electrodes (26,42-44,104,121-123,125,192, 243,279). The capacitance of the electrode heated in air was larger, but there were no noticeable differences in the capacitances of other electrodes. The parameter ϕ changes with overpotential, between 0.8 to 1.0. This mater will be discussed more in details in chapter five.

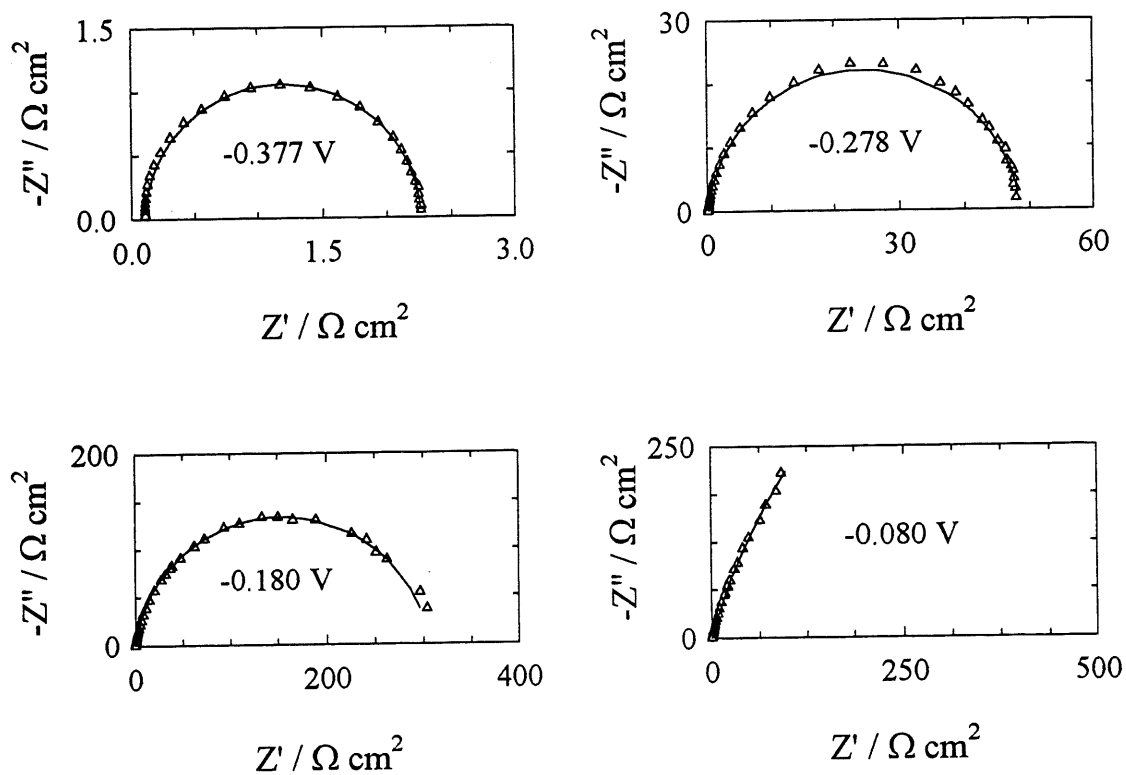


Figure 11. Complex plane plots obtained on untreated $\text{Ni}_{70}\text{P}_{30}$ electrodes in 1 M NaOH at 70°C . The continued lines indicate the fitted data using the CNLS method and CPE model.

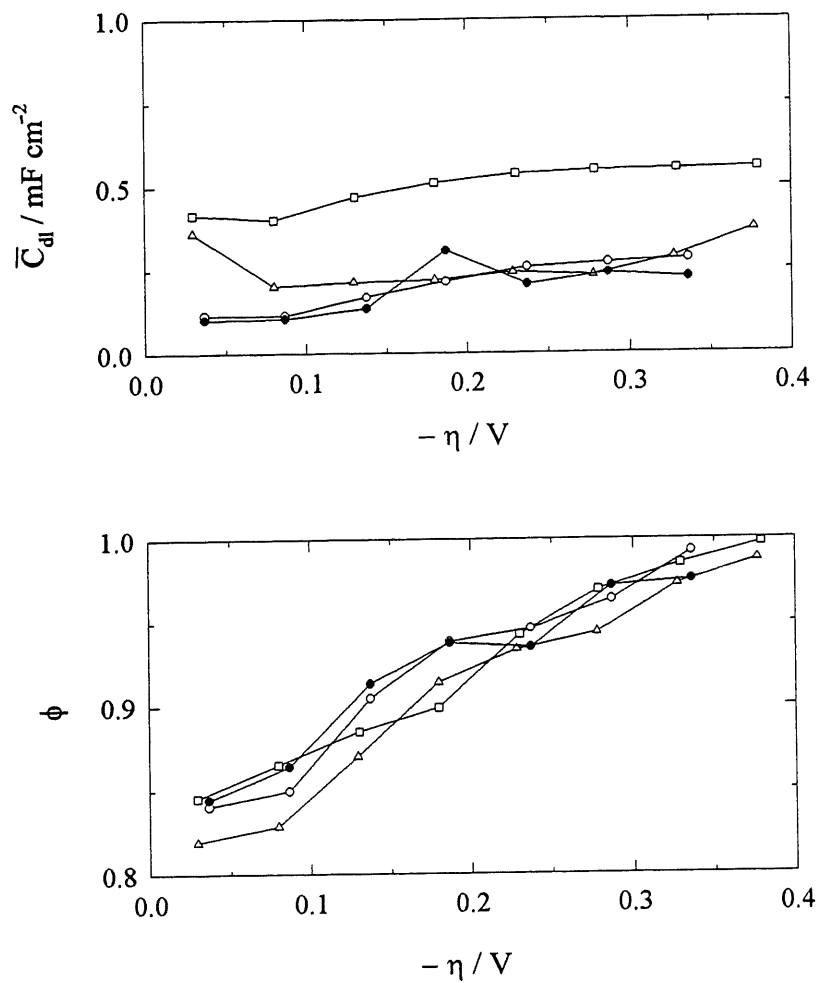


Figure 12. Dependence of the average of double layer capacitance, \bar{C}_{dl} , and parameter ϕ on overpotential obtained for the HER on $\text{Ni}_{170}\text{P}_{30}$ electors in 1 M NaOH at 70°C : (Δ) untreated electrode, (\square) heated at 400°C for 3h in air, (\circ) oxidized at $+0.200\text{ V vs. Hg/HgO}$, 1 M NaOH, 70°C for 6h (\bullet) kept in 1 M HF, 40 min under N_2 at 25°C . See table 1

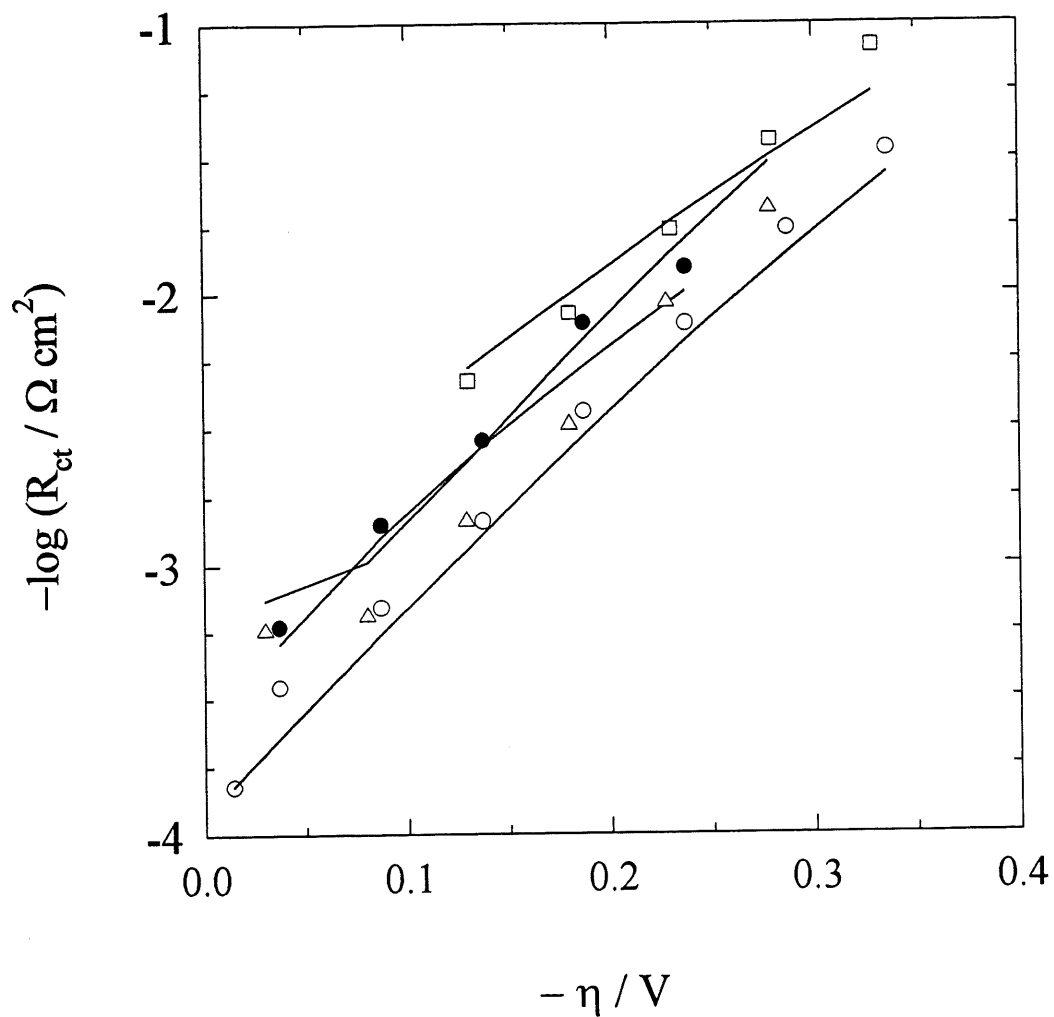


Figure 13. Dependence of the charge transfer resistance, R_{ct} , on overpotential obtained for the HER on $\text{Ni}_{70}\text{P}_{30}$ electrodes in 1 M NaOH at 70°C : (Δ) untreated, (\square) after 3h heating at 400°C in air, (\circ) after 6h oxidizing at $+0.200 \text{ V vs. Hg/HgO}$ in 1 M NaOH at 70°C , and (\bullet) after 40 min treatment with 1 M HF at 25°C . The continuous lines were obtained using data in Table 3.

Table 3. Kinetic parameters of the HER obtained on Ni₇₀P₃₀ electrode from steady-state polarization curves and the EIS measurements in 1 M NaOH on Ni₇₀P₃₀ at 70°C before and after various treatments^a.

Pretreatment	k_1 mol cm ⁻² s ⁻¹	k_{-1} mol cm ⁻² s ⁻¹	k_2 mol cm ⁻² s ⁻¹
no pretreatment	$(2.49 \pm 0.93) \cdot 10^{-8}$	$(1.79 \pm 0.45) \cdot 10^{-10}$	$(1.09 \pm 0.04) \cdot 10^{-10}$
3h heating at 400°C in air	$(1.20 \pm 0.32) \cdot 10^{-9}$	$(2.79 \pm 0.88) \cdot 10^{-8}$	$(5.1 \pm 2.2) \cdot 10^{-10}$
6h oxidation at +0.200 V vs. Hg/HgO	$(1.17 \pm 0.44) \cdot 10^{-9}$	$(4.69 \pm 0.49) \cdot 10^{-12}$	$(4.76 \pm 0.33) \cdot 10^{-11}$
40 min in 1 M HF	$(8.1 \pm 1.8) \cdot 10^{-10}$	$(8.1 \pm 2.3) \cdot 10^{-12}$	$(1.24 \pm 0.16) \cdot 10^{-10}$

^aTransfer coefficient β_1 varies between 0.20 to 0.32, β_2 was fixed as 0.5 in all the cases.

The dependence of the logarithm of the inverse charge transfer resistance, R_{ct} ($A = 1 / R_{ct}$), on overpotential is shown in Fig. 13. The kinetic parameters were obtained by fitting the steady-state polarization curves and the charge transfer resistances from the EIS to the corresponding kinetic equations using the NLS method (26,192,379), see eqns. [2.49], [2.58], and [2.98] in chapter 2. It was sufficient to assume the Volmer-Heyrovský mechanism, with the Heyrovský reaction as the rate-determining step, to explain the experimental data. The rate constants obtained are presented in Table 3.

Intrinsic activities are related to the real (per unit of a real surface area) exchange current densities and the real rate constants. These parameters are determined from the apparent

Table 4. Comparison of the roughness factors, R , and the real exchange current densities, j_0 / R , obtained on $\text{Ni}_{70}\text{P}_{30}$ electrodes at 70°C in 1 M NaOH.

Pretreatment	\bar{C}_{dl} / $\mu\text{F cm}^{-2}$	$R =$ $\bar{C}_{dl} / 20$	j_0 / $R \text{ A cm}^{-2} *$	k_2 / $R \text{ mol cm}^{-2} \text{ s}^{-1}$
no pretreatment	366	18.3	(1) $1.7 \cdot 10^{-6}$ (2) $1.9 \cdot 10^{-5}$	$(5.95 \pm 0.21) \cdot 10^{-12}$
400°C, 3h, air oxidation, 1 M NaOH, 70°C, 6h, +0.200 V vs. Hg/HgO	486	24	(1) $1.4 \cdot 10^{-6}$ (2) $9.5 \cdot 10^{-6}$	$(2.11 \pm 0.90) \cdot 10^{-11}$
1 M HF, 40 min, 25°C	198	10	(1) $5.1 \cdot 10^{-7}$ (2) $6.8 \cdot 10^{-6}$	$(4.76 \pm 0.33) \cdot 10^{-12}$
	163	8	(1) $2.6 \cdot 10^{-7}$ (2) $1.9 \cdot 10^{-5}$	$(1.55 \pm 0.20) \cdot 10^{-11}$

*: Labels (1) and (2) indicate the j_0 / R corresponding to the Tafel slopes in Table 2.

experimental values divided by the roughness factor (43). The roughness factor, R , was estimated from the ratio of the average double layer capacitance of the studied electrode, \bar{C}_{dl} , and the average of double layer capacitance of a smooth metallic electrode, $R = \bar{C}_{dl} / 20 \mu\text{F cm}^{-2}$. The obtained results are presented in Table 4. The real activities and roughness factors also do not show big changes due to different treatments. These results confirm earlier findings (268) that these Ni-P alloys are not very active electrodes for the HER.

Machida *et al.* (129,346) reported that the activity of nickel alloys, Ni-Ti and Ni-Zr, for the HER increased after treatment with 1 M HF. However, Zhang *et al.* (92) reported that the phosphorous content in Ni-P alloy (19 at. % of P) did not decrease after 3h leaching with 47%

HF solution, but the surface layer was significantly enriched in P after this treatment. These authors detected a large amount of phosphate groups on the surface using XPS technique. Our results presented in Table 2 show that the activity of the Ni₇₀P₃₀ electrode is decreased after treating with HF and the electrode surface becomes smoother (Fig. 8B). Higher intrinsic activity is observed for heated and HF treated electrodes although the apparent activities are low, Table 2. The large Tafel slopes at high current densities are probably due to the deposition of impurities or electrode deactivation (52).

4.2.3 Activation by anodic oxidation and potential cycling

Oxidation of the surface may increase the activity of the electrodes towards the HER (28,44,192) or OER (149,258,265). It was found earlier that oxidation of polycrystalline Ni increased the electrode activity towards the HER approximately 10 times (192). In the following experiments Ni-P alloys were produced using method A and different H₃PO₃ concentrations, from 0.015 to 1.52 M. Alloys containing 19 to 30 at. % of P were obtained.

It was suggested in the literature (298,299) that anodic oxidation at +0.200 V vs. Hg/HgO caused partial leaching of phosphorous from the alloy, however, using EDX we have not noticed any important changes in phosphorous content. Such changes might occur in the surface layer, however, they were not be detected by EDX but could be detected by surface sensitive techniques (ESCA, AES). Further oxidation of the electrode at +0.75 V did not affect the electrode activity (Table 2). This observation is in accordance with the model presented by Hoffmann and Well (265,300), Habazaki *et al.* (297), and Lo *et al.* (114) stating that hypophosphite groups block the surface of Ni-P electrodes and passivate them. This behavior may explain why it was not possible to leach out phosphorous from Ni-P electrodes. It was also suggested that the charge transfer resistance, R_{ct}, increases with the increase in the phosphorous content of Ni-P electrodes.

Despite the expectation that (a) heating would change the alloy morphology from amorphous to crystalline and (b) the anodic oxidation would decrease the surface phosphorous content and increase the surface roughness and activity for the HER, the results in Table 2 and 5 show that the activity of the electrode is not high. In fact, Wronkowska (304) reported that a stable nickel hydroxide layer may be formed on Ni-P electrodes by cycling them between the potentials corresponding to oxygen and hydrogen evolution reactions. These layers passivate the electrode surface. Using AES and XRD analysis she showed that a solid surface layer contained oxidized phosphorous presented between the alloy and the hydrated nickel oxide layer. The passivity of the surface depended mainly on P content rather than on the structural effects.

In subsequent experiments the electrode potential was cycled between -1.2 V and +0.6V vs. Hg/HgO at 50 mV s^{-1} in 1 M NaOH at 70°C . The aim of this treatment was to study the possibility of dissolution of phosphorous from crystalline and/or amorphous $\text{Ni}_{70}\text{P}_{30}$ electrodes and increase the electrode activity (298,299), also to increase the surface roughness and consequently the electrode activity through oxidation-reduction of the nickel sites on the surface (192-194). The Tafel curves were measured after 100 and 180 cycles. Thereafter the electrode was oxidized by applying a constant potential of +0.75 V for 1 hour and again the activity towards the HER was determined. Table 5 shows the obtained results. Two Tafel slopes were observed in most of the cases. The effect of oxidation on the activity of $\text{Ni}_{77}\text{P}_{23}$ is the most pronounced. Although this electrode is more active than the polycrystalline nickel (126,192), yet its activity is relatively low (Table 5).

An example of a cyclic voltammogram obtained on $\text{Ni}_{70}\text{P}_{30}$ electrode (without any pretreatment) is presented in Fig. 14 (continuous line). Similar pattern was observed for the electrodes with lower P content. Three anodic (A_1 , A_2 and A_3) and two cathodic (B_1 and B_2) peaks are found. Comparison of this cyclic voltammogram with those of nickel and Ni-P

Table 5. Kinetic parameters of the HER obtained in 1 M NaOH at 70°C from steady-state polarization experiments on untreated and heated (3h at 400°C in air) Ni-P electrodes before and after electrochemical treatment by cycling (between -1.2 and +0.6 V vs. Hg/HgO) and constant potential oxidation (one hour at +0.75 V vs. Hg/HgO).

Electrode	b / mV dec ⁻¹ *		j ₀ / μA cm ⁻²		η ₂₅₀ / mV		electrochemical pretreatment
	untreated	400°C	untreated	400°C	untreated	400°C	
Ni ₇₀ P ₃₀	(1) -93	-264	15	560			100 cycles
	(2) -220		291		-646	-700	
	(1) -84	-115	23	54			180 cycles
	(2) -202	-246	207	452	-624	-675	
	(1) -87	-131	17	64			oxidation
	(2) -201	-237	292	409	-590	-661	
Ni ₇₇ P ₂₃	(1) -132		73				none
	(2) -183		187		-571		
	(1) -142		44				100 cycles
	(2) -247		325		-714		
	(1) -132		55				180 cycles
	(2) -252		696		-643		
Ni ₇₅ P ₂₅	(1) -56		63				oxidation
	(2) -151		215		-462		
	(1) -87		17				none
	(2) -201		293		-590		
	(1) -193		72				100 cycles
	(2) -202		222		-684		
Ni ₇₉ P ₂₁	(1) -125		29				180 cycles
	(2) -190		203		-586		
	(1) -123		18				oxidation
	(2) -209		216		-640		
	(1) -94	-110	8.5	109			none
	(2) -261	-145	103	382	-885	-407	
Ni ₈₁ P ₁₉	(1) -203		12		-701		100 cycles
	(1) -180	-135	61	44	-650		180 cycles
	(2) -193			197		-597	
	(1) -158	-108	44	41	-592		oxidation
	(2) -202		158			-648	
	(1) -50		30				
Ni ₈₁ P ₁₉	(2) -246		140		-800		none

*: Labels (1) and (2) have the same meaning as defined in Table 2.

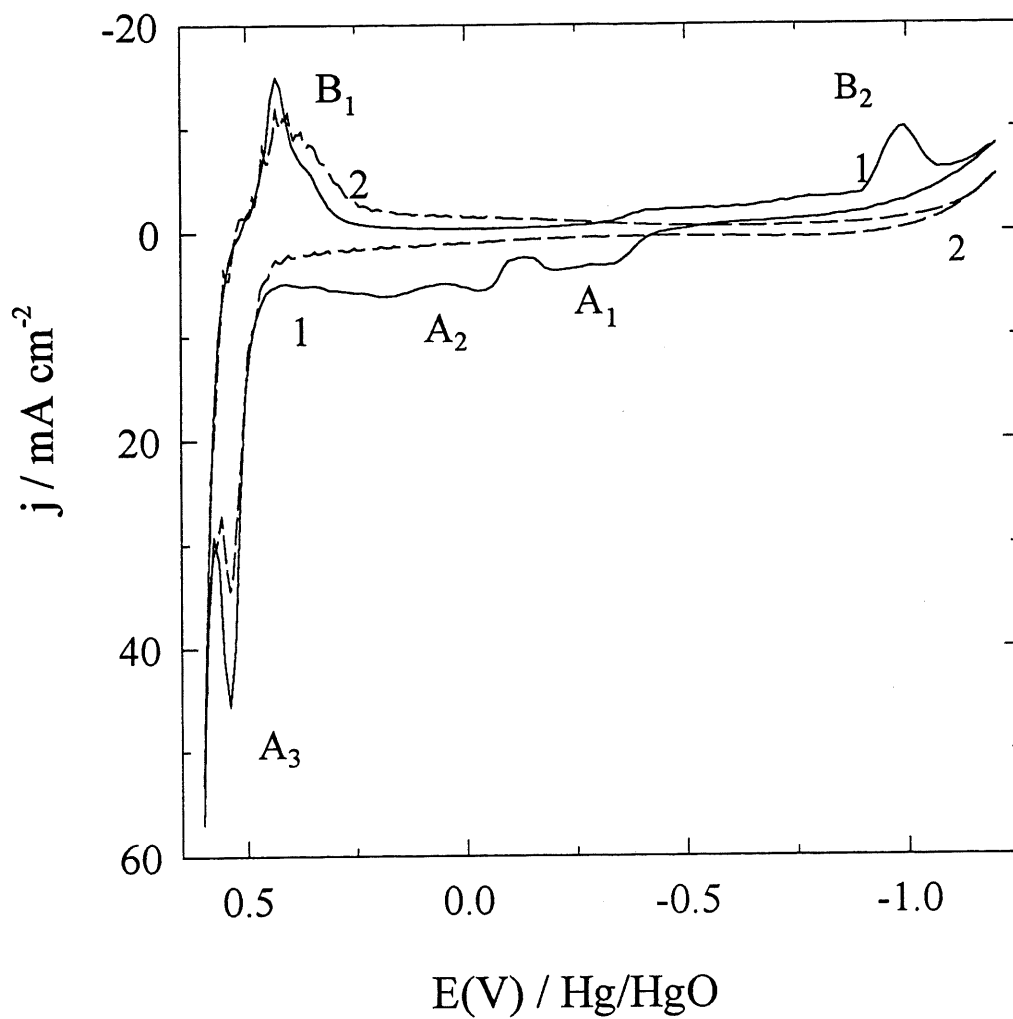


Figure 14. Cyclic voltammograms obtained on $\text{Ni}_{70}\text{P}_{30}$ electrodes in 1 M NaOH at a sweep rate of 50 mV s^{-1} at 70°C ; continuous line 1 : 180th cycle for untreated electrode, dashed line 2 : electrode heated at 400°C for 3h in air.

electrodes (255,265,295,304) in alkaline solutions shows that peak A_1 and hump-like peak A_2 may be assigned to the adsorption of OH and simultaneous oxidation of Ni to α -Ni(OH)₂ and P to hypophosphite groups (255,265,295,297,301,304). Besides, conversion of α -Ni(OH)₂ to a more stable β -Ni(OH)₂ may occur in this region. Oxidation of Ni(II), *i.e.*, α or β -Ni(OH)₂ to Ni(III), β or γ -NiOOH [or to Ni(IV)] (250-259,307,312-314) and phosphorous oxides to higher oxidation states occurs in the region of anodic peak A_3 . The most probable process is, β -Ni(OH)₂ to β -NiOOH transition, α - γ transition is also possible at $T \leq 70^\circ\text{C}$ (250). Broad cathodic peak B_1 is connected with the reduction of high valency nickel oxides to Ni(II). However, the origin of the cathodic peak B_2 and the hump preceding it is not clear.

Heated samples behaved similarly to nickel polycrystalline electrode, and only peaks A_3 and B_1 were observed (Fig. 14, dashed line). The experiments showed that the peak heights and their surface area were not influenced by the number of cycles which implies that quantities of Ni(OH)₂ and hypophosphite do not increase with time. However, phosphate (92) and hypophosphite (265,300) groups can passivate the surface. It seems that these groups, present on Ni-P electrodes, decrease their activity.

4.2.4 Heating of Ni-P at 550°C

Heating of the Ni₇₀P₃₀ electrode at higher temperatures (550°C) in air changed the color of the deposit from bright metallic to green-yellow and showed decrease in the phosphorous content to Ni₈₁P₁₉ (EDX). The sample was highly fragile, layered and broke before electrochemical measurements.

Thermogravimetric analysis (TGA) showed that there was no mass change during the heating of Ni₇₀P₃₀ alloy from 23 to 600°C in N₂ atmosphere. Differential Scanning Calorimetric (DSC) analysis of the alloy in the same temperature range showed two phase transitions around 287°C and 534°C. Because similar behavior was observed when the experiment was carried

out in air it may be concluded that there was no bulk oxidation or reduction reactions in this range of temperatures.

4.2.5 HER on Ni-P electrodes obtained from baths B and C.

The activities of the electrodes, prepared at low current densities at 18 and 22°C from baths B and C, were also studied. The steady-state conditions were reached after 12h of activation at the cathodic current density of 320 mA cm⁻². The obtained electrodes were chemically and electrochemically stable during our studies (over a three day period). Fig. 15 presents the steady-state polarization curves and the corresponding parameters obtained are presented in Table 6. These electrodes are more active than those obtained from bath A. Electrodes prepared from bath B are characterized by low Tafel slopes of 57 mV dec⁻¹ and low $\eta_{250} = -171$ mV. It should also be stressed that the electrode containing 27 at. % of P obtained from bath C is much more active than those of similar composition obtained from bath A (see Tables 2, 5 and 6). Heating these electrodes at 400°C caused formation of crystal phases (see Fig. 9) and a decrease in their electrocatalytic activity (see Table 6).

Table 6. Kinetic parameters of the HER obtained on amorphous Ni-P electrodes from steady-state polarization curves in 1 M NaOH at 70°C.

Electrode	b / mV dec ⁻¹	j ₀ / mA cm ⁻²	η_{250} / mV
Ni ₇₃ P ₂₇ * (bath C)	-109	0.07	-358
Ni ₇₃ P ₂₇ ** (bath C)	-123	0.07	-433
Ni ₉₂ P ₈ * (bath B)	-57	0.24	-171
Ni ₉₂ P ₈ ** (bath B)	-120	0.44	-330

* as-deposited; ** after 4h heating at 400°C in air.

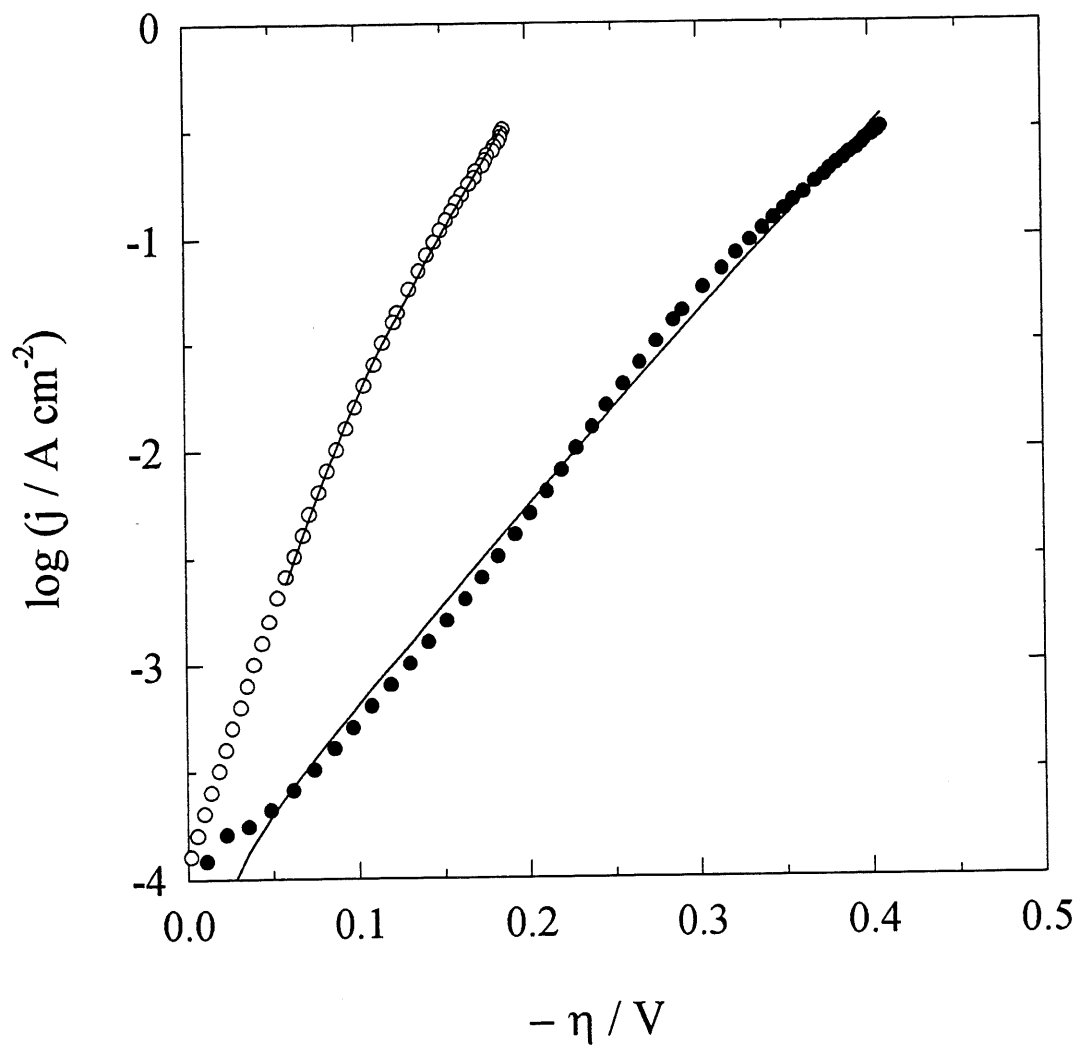


Figure 15. Steady-state polarization curves obtained on untreated (O) Ni_{92}P_8 and (●) $\text{Ni}_{73}\text{P}_{27}$ electrodes in 1 M NaOH at 70°C. The continued lines were obtained using data in Table 7.

The slopes observed for electrode obtained from bath C may be explained by Volmer-Heyrovský mechanism, see section 2.2.6.1. However, the small Tafel slope, -57 mV dec^{-1} , observed for electrode obtained from bath B (as-deposited) can be explained by Temkin isotherm (predicted Tafel slopes are around 69 mV dec^{-1}).

The EIS measurements of Ni_{92}P_8 electrodes (from bath B) showed formation of a high frequency straight line followed by a semicircle on the complex plane plots. This behavior is characteristic for porous electrodes containing cylindrical pores (26,368,377-379,383), see eqn. [2.93] in section 2.3.3.5.2 of chapter 2. The electrodes $\text{Ni}_{73}\text{P}_{27}$ (from bath C) displayed different EIS behavior, their complex plane plots represented two semicircles. This behavior is also characteristic for porous electrodes composed of pear shape pores (384), and it has been confirmed experimentally for some electrodes (42,121). In this case the equivalent circuit may be represented by a series connection of two CPE-R elements, in which the first one is connected with the electrode porosity and the second one with the HER. Although such pores are not visible on SEM pictures, Figs. 7 and 9, they may exist as nanopores (273). Neglecting the high frequency features and analyzing the lower frequency semi-circle gave similar values of \bar{C}_{dl} and R_{ct} .

Fig. 16 illustrates few complex plane plots for Ni_{92}P_8 electrodes and Fig. 17 displays the results of analysis of these curves, *i.e.*, $-\log R_{ct}$ (where $A = 1 / R_{ct}$) as function of overpotential. The average double layer capacitances, \bar{C}_{dl} , were from 30 mF cm^{-2} at lower overpotentials to 50 mF cm^{-2} at higher overpotentials for Ni_{92}P_8 and $\sim 3 \text{ mF cm}^{-2}$ for $\text{Ni}_{73}\text{P}_{27}$ electrode, corresponding to the roughness factor of 1500 to 2500 and 140, respectively.

Paseka (52) studied the electrode containing 3 wt. % of P (corresponding to Ni_{94}P_6) using the open circuit potential relaxation data extrapolated to very short times (35). He has found

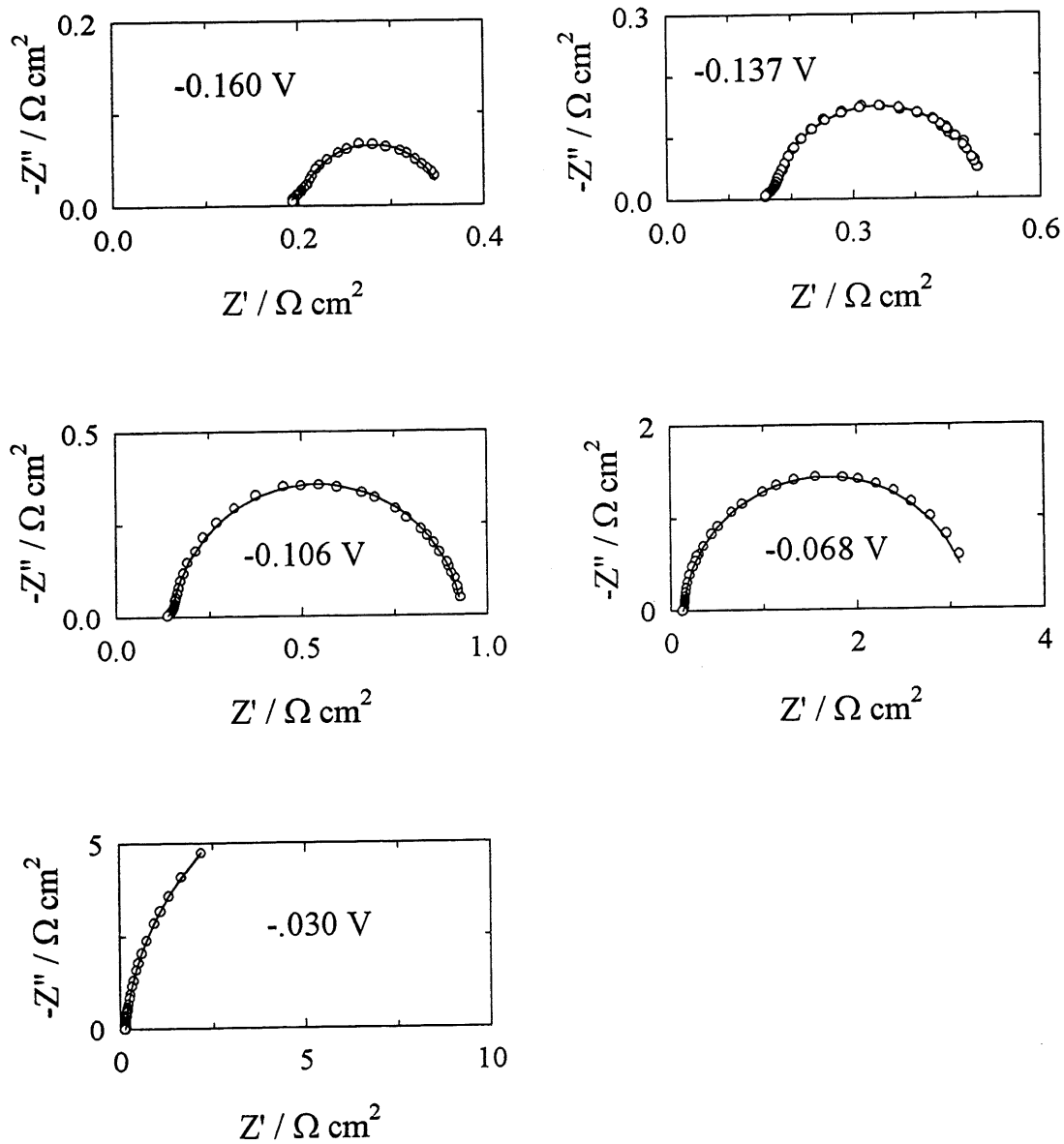


Figure 16. Complex plane plots obtained on untreated Ni_{92}P_8 electrodes in 1 M NaOH at 70°C . The continuous lines indicate fitted results using the CNLS method and porous model.

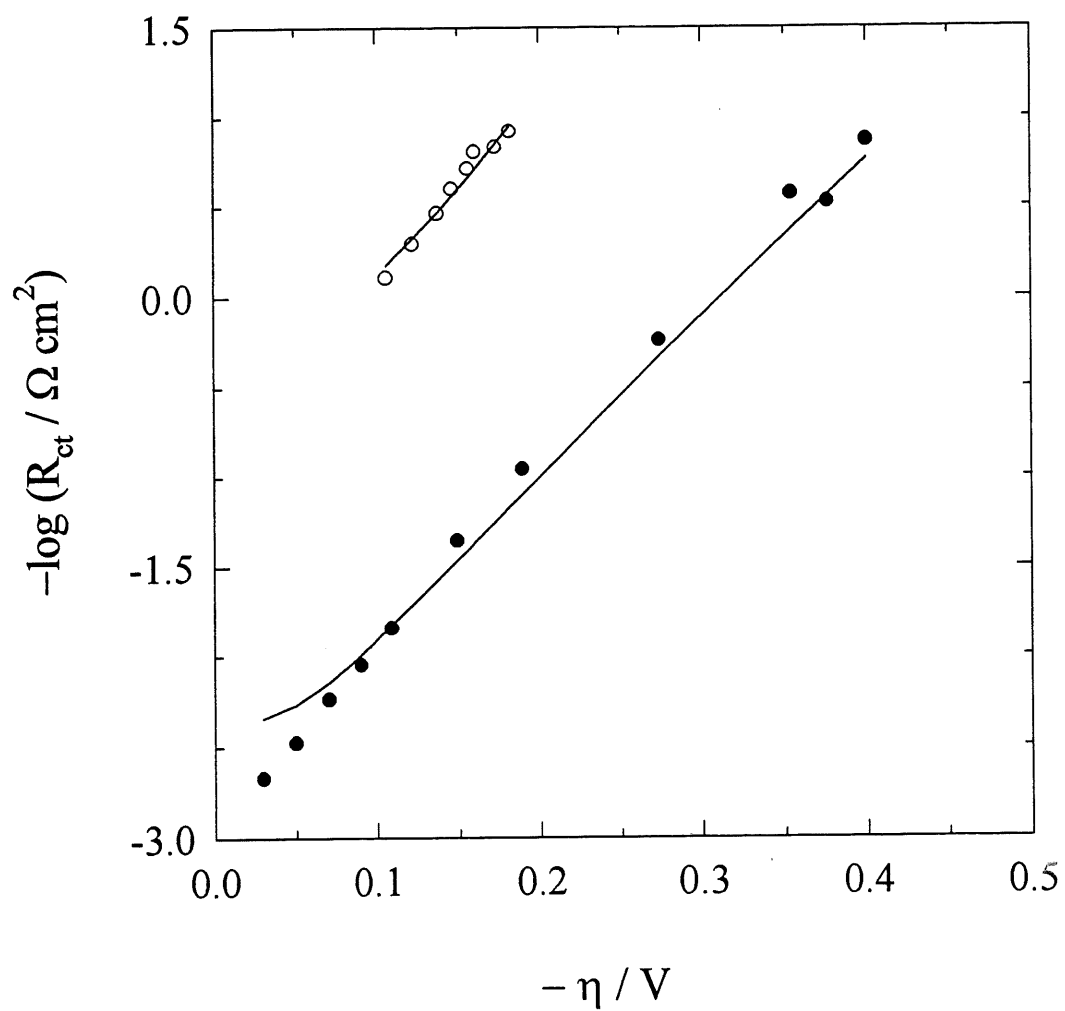


Figure 17. Dependence of the charge transfer resistance, R_{ct} , on overpotential for the HER obtained on untreated (O) Ni₉₂P₈ and (●) Ni₇₃P₂₇ electrodes in 1 M NaOH at 70°C. The continuous lines were obtained using data in Table 7.

pseudocapacitances from 60 mF cm⁻² (at lower overpotentials) to 25 mF cm⁻² (at higher overpotentials) and attributed them to the hydride formation reaction. Our EIS measurements gave similar values of the double layer capacitances of 50 to 30 mF cm⁻². However, assuming hydride formation the pseudocapacitances should be larger at more negative potentials. Besides, decomposition of hydrides should appear mainly at longer times. Therefore, as indicated above, the obtained capacitances may be attributed to the surface roughness.

It should be mentioned that the relaxation experiments are more difficult to interpret (31,32,192,385). At lower overpotentials the potential relaxation is very slow and difficult to measure and at longer times they are of pseudocapacitive nature and involve changes in the surface coverage by the adsorbed hydrogen. Therefore, in practice, it is not possible to determine the double layer capacitances from the potential relaxation experiments at low overpotentials. Only analysis of the system of the differential equations describing relaxing system (26,31,192,385) may give the correct results.

Table 7. Kinetic parameters of the HER obtained on amorphous Ni-P electrodes from steady-state polarization curves and the EIS measurements in 1 M NaOH at 70°C.

Electrode	k_1 mol cm ⁻² s ⁻¹	k_{-1} mol cm ⁻² s ⁻¹	k_2 mol cm ⁻² s ⁻¹
Ni ₇₃ P ₂₇ *	$(1.57 \pm 2.15) \cdot 10^{-8}$	$(1.14 \pm 0.14) \cdot 10^{-9}$	$(4.12 \pm 0.72) \cdot 10^{-10}$
Ni ₉₂ P ₈ **	$(3.77 \pm 0.39) \cdot 10^{-8}$	$(7.6 \pm 3.1) \cdot 10^{-7}$	$(9.3 \pm 1.8) \cdot 10^{-9}$

* $\beta_1 = 0.43$ and $\beta_2 = 0.64$. ** $\beta_1 = 0.86$ and β_2 was fixed as 0.5.

Paseka (52) also attributed low Tafel slopes to a barrierless discharge of hydrogen. Although such a possibility was predicted theoretically, it is not very probable for the overpotential hydrogen evolution. Such a low Tafel slopes may be explained assuming Temkin adsorption

isotherm for adsorbed hydrogen or distributed kinetics on a heterogeneous surfaces (16,199,200).

The rate constants were evaluated in the same way as for the electrodes from bath A. They are presented in Table 7 and the intrinsic activities are presented in Table 8. Comparison of these values with those shown in Table 4 implies that increase of the activity arises mostly from the increase in the surface roughness. These electrodes are apparently much more active for the HER than the electrodes prepared from bath A, but the intrinsic activity (related to the limiting rate constant k_2) of the most active electrode, Ni_{92}P_8 , is similar to that electrodeposited from bath A.

Table 8. Comparison of the roughness factors, R , and real exchange current densities, j_0 / R , obtained on $\text{Ni}_{73}\text{P}_{27}$ and Ni_{92}P_8 electrodes in 1 M NaOH at 70°C.

Electrode	$\bar{C}_{dl} / \mu\text{F cm}^{-2}$	$R = \bar{C}_{dl} / 20 \mu\text{F cm}^{-2}$	$j_0 / R \text{ A cm}^{-2}$	$k_2 / R \text{ mol cm}^{-2} \text{ s}^{-1}$
$\text{Ni}_{73}\text{P}_{27}$	$2.74 \cdot 10^3$	140	$5.11 \cdot 10^{-7}$	$(2.95 \pm 0.52) \cdot 10^{-12}$
Ni_{92}P_8	$38.24 \cdot 10^3$	1900	$1.26 \cdot 10^{-7}$	$(4.9 \pm 1.1) \cdot 10^{-12}$

Larger intrinsic activities were found for the electrodes obtained from bath C, although the apparent activities were low. It has been reported (52) that the activity of these electrodes decreases after heating them up to 150°C or leaving them at the open circuit potential, however, we have not seen any decrease in the activity during three days of the HER at 70°C. Oxidation of the electrodes in 1 M NaOH at 70°C for one hour at +0.200 or +0.70 V vs. Hg/HgO did not cause large decrease in their activity for the HER (e.g. for Ni_{92}P_8 before oxidation $\eta_{250} = -171$ and after that $\eta_{250} = -195 \text{ mV dec}^{-1}$). Recently, Paseka has corrected (302) his previous report (52) that the deactivation which he had observed during long time electrolysis with Ni-P electrode (containing 3 at. % of P) had been due to impurities

presented in the electrolyte solution. He has used very pure electrolyte solution (302) and did not find any deactivation after 560h the HER at 0.240 A cm^{-2} in 1 M KOH at room temperature. He has also found that high activity of Ni-P alloys is not due to low content of P, but to the method of preparation. We found both of these points earlier and reported in our studies here (344) criticizing Paseka's work (52). However, again Paseka has emphasized that the high activity of these materials is due to their great ability for hydrogen absorption (52,286,302) which is of course in disagreements with our finding.

4.3 Summary

Ni-P electrodes containing 8 to 30 at. % of P were obtained by electroplating. All the deposited alloys were amorphous and changed into crystalline form after heating at 400°C . Steady-state polarization curves and electrochemical impedance measurements, were used to determine mechanism and kinetics of the HER on Ni-P electrodes. It was found that the reaction proceeds through the Volmer-Heyrovský mechanism with the Heyrovský reaction as the rate determining step. Different procedures were used to increase the activity of the electrode. Oxidation and also heating the electrodes at 400°C increased their roughness factor but not their intrinsic activity. The amorphous Ni-P electrodes change to a more stable crystalline phase during heating, however, this process decreases their activity. The electrodes prepared at low current densities and at lower temperatures (from bath B), Ni_{92}P_8 , showed good activity for the HER. This electrode is more porous with the roughness factor of 2,000. It was found that the differences in the electrode activities are principally due to the differences in the real surface area. The obtained electrodes showed high physical and chemical stability and good electrocatalytic activity ($\eta_{250} = -171 \text{ mV}$) for the HER as compared with other electrode materials.

CHAPTER 5
KINETICS OF THE HYDROGEN EVOLUTION REACTION ON Ni-Mo-P
ELECTRODES IN ALKALINE SOLUTIONS

5.1 Introduction

In order to increase the activity and keep the stability of the pure metal, nickel is often alloyed with different elements (26,48,243,343,386). Alloying with metals which may be leached out in the alkaline solutions, as Al or Zn, increases the real surface area while alloying with phosphorus increases the stability. Alloying of Ni with other metals may increase the intrinsic electrocatalytic activity (48,189,243). Divisek *et al.* (46) reported enhancement of the catalytic activity of Raney nickel (Ni-Al) by deposition of Mo and attributed it to the synergetic effects. However, prediction of the stability and electrocatalytic activities of the alloys is difficult (183,278,305,342,387). In some cases the stability of the alloy produced from two metals, *e.g.*, Ni-Mo, is lower than the alloy produced from a metal and a non-metal, *e.g.*, Ni-P. In the latter case the hardness of Ni-P is larger than that of pure Ni. In the case of lower physical stability, if the catalyst can be deposited on a porous matrix its lifetime can be increased, but it is not clear that if the activity will be increased as well.

In order to increase the adherence of the deposit to the surface and also its activity a “multi-step” electrodeposition procedure (197,278), see also section 1.5.2 in chapter 1, creating a composition gradient in the deposit may be used.

The studies of preparation, structure and corrosion resistance of Ni-Mo-P alloys have been reported in the literature (192,193,388-397). However, there is no quantitative information about the kinetics and mechanism of the HER on these electrodes. A knowledge of the

detailed mechanism and kinetics of the HER is necessary in order to determine the source of the activity, change the catalyst structure and improve it for obtaining higher activity.

The present chapter is concerned with nickel-molybdenum-phosphorous electrodes. They were prepared by alloy electrodeposition and their activity for the hydrogen evolution reaction was studied in 1 M NaOH using the electrochemical impedance spectroscopy (EIS) and steady-state polarization technique. Active electrodes were obtained creating a concentration gradient in the deposit (multi-step technique). It was found that the increase in the electrode activity was due to increase in both surface roughness and intrinsic activity, as compared with Ni-P, Ni-Mo and Ni electrodes. The reaction mechanism and the kinetic parameters were determined.

5.2 Results and discussion

5.2.1 Composition and surface morphology of electrodes

The composition, physical stability and activity of the Ni-Mo-P electrodes for the HER depend on pH, current density, temperature and concentration of the chemical reagents (394) in the deposition bath. At high current densities and in the absence of NaCl a black powder-like deposit was obtained in the center of the electrode and the edges were covered with metallic deposit. In the presence of NaCl the metallic deposit, electrodes A and B, which did not show the desired activity, were deposited. At low current densities and using “one-step” deposition method only black powder with low adherence was obtained. But electrodes C and D prepared at low current density in a “three-step” method showed good activity and good physical stability.

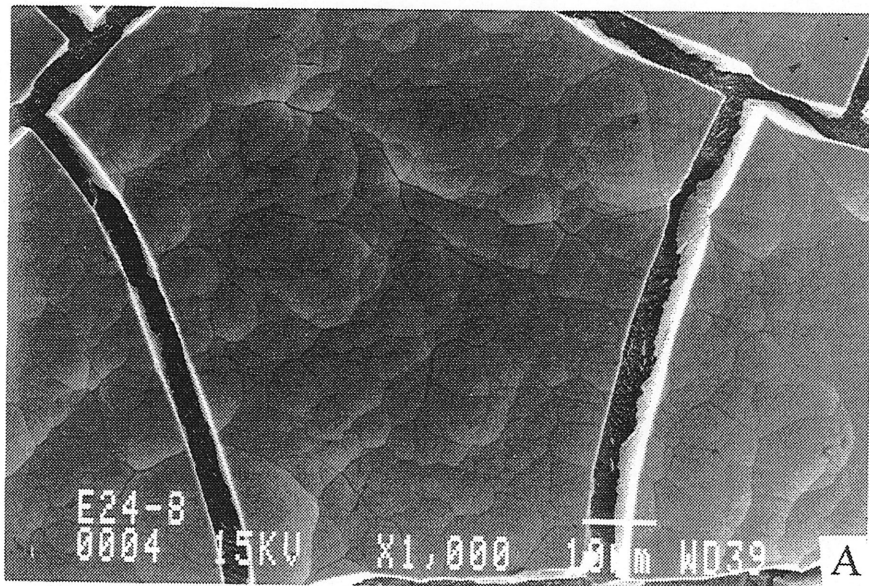
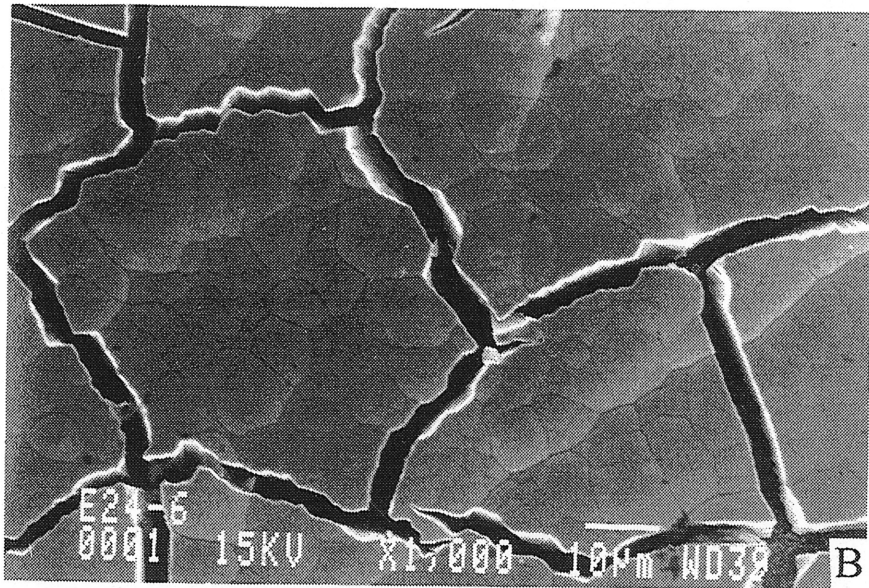


Figure 18A and B

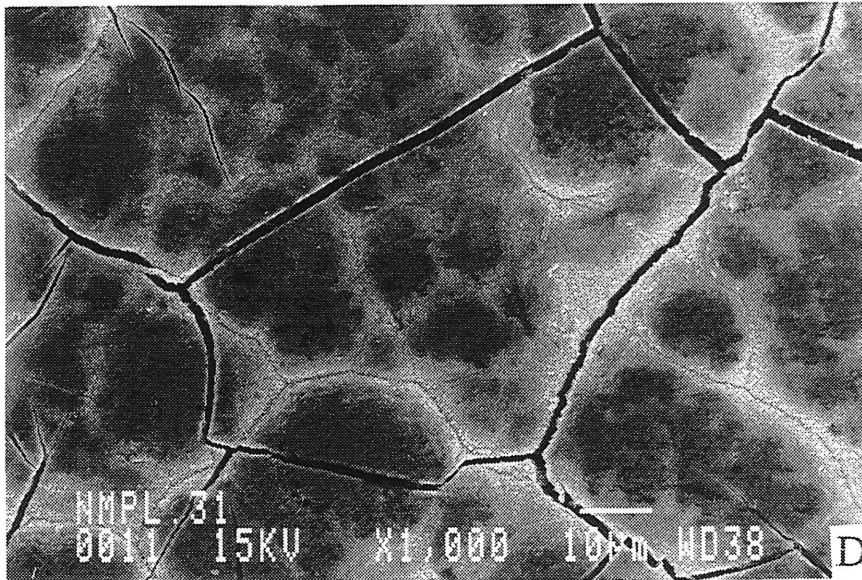
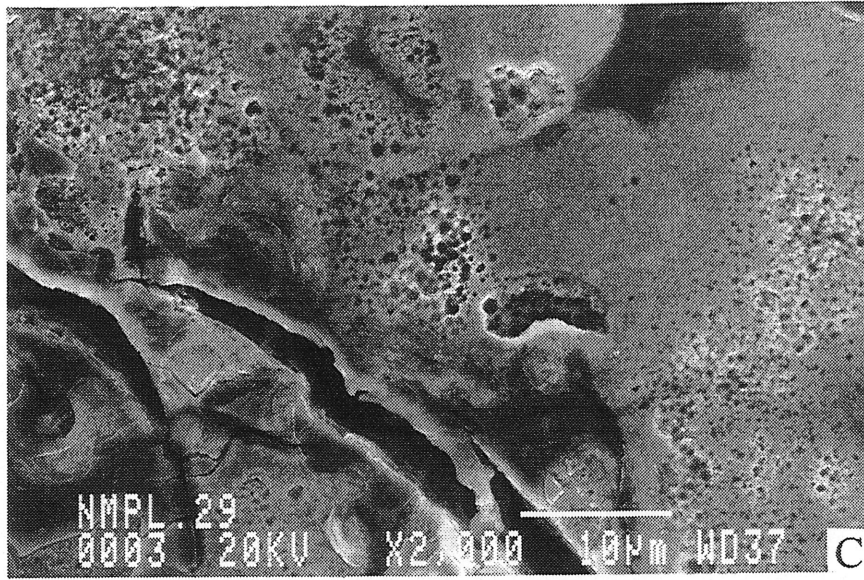


Figure 18C and D

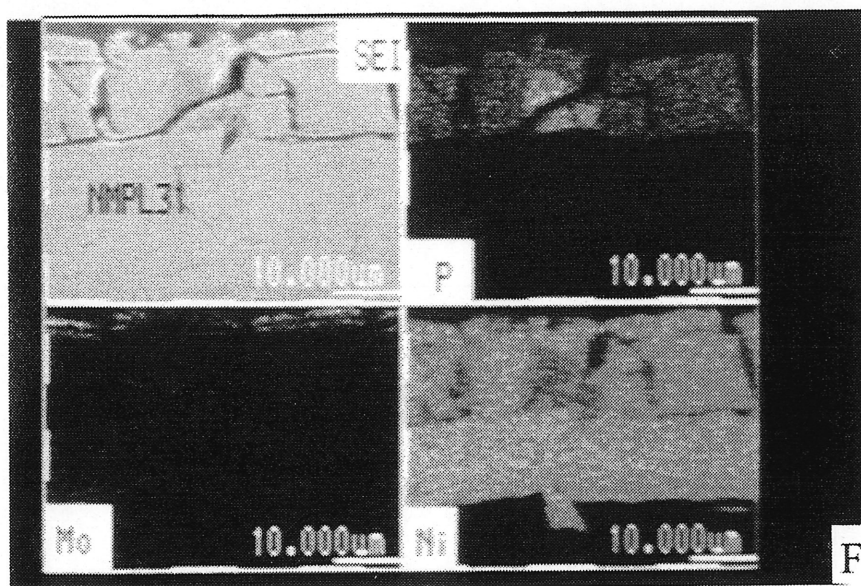
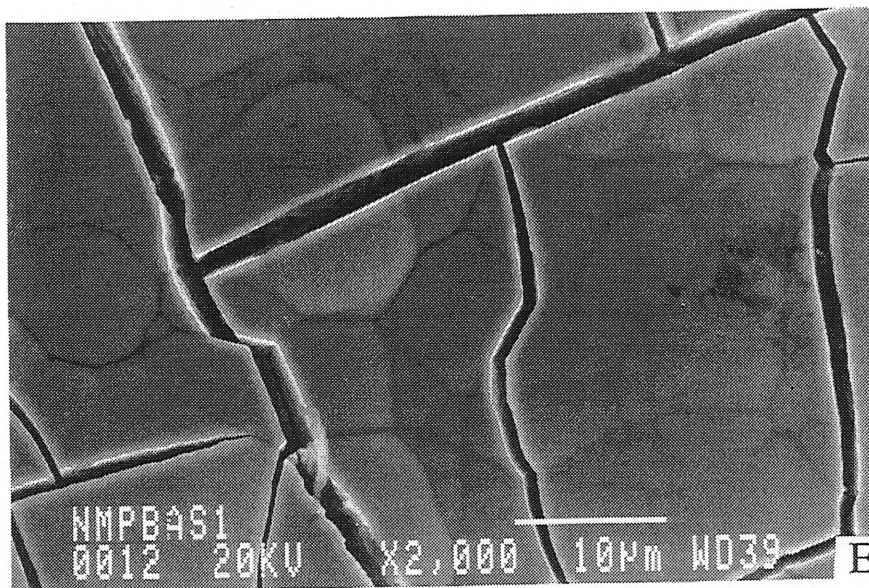


Figure 18E and F

Figure 18. Scanning electron micrographs prepared from the surface of Ni-Mo-P electrodes, letters indicate the electrodes in Table 9. Fig. 18F presents the cross section of the three-step deposited electrode, D. The thickness of the Ni, Ni-P, and Ni-Mo-P layers are respectively 20, 20, and 7 μm .

To determine the global composition of the electrodes, deposit was dissolved in HNO_3 and analyzed by ICP, AAS, and EDX methods. This electrode had a composition of $\text{Ni}_{74}\text{Mo}_{16}\text{P}_{10}$. Electrodes A and B did not show high activity for the HER, yet their activity were higher than that of nickel polycrystalline (192). Electrodes C and D were prepared at low current density in three steps as mentioned in the experimental part. The main difference between electrode C and D is the pH of deposition bath. Electrode C prepared at $\text{pH} = 7$ to 8 had a bright-gray metallic and rough surface, but the top layer was somewhat fragile while electrode D prepared at $\text{pH} = 9.2$ had a black-brown metallic appearance with a good physical stability. Electrode F was not as stable as D. Because “multi-step” deposited electrodes had nonhomogeneous distribution of Ni, Mo and P from top of the surface to depth layers, wet analysis did not give the real surface composition of these electrodes, therefore the surface morphology and composition of the electrodes were studied by EDX quantitative microanalysis, see section 3.2.3.5 in chapter 3. The composition of the electrodes prepared and used in this study are presented in Table 9.

The SEM micrographs of these electrodes are presented in Fig. 18A to E. The cross-section of the electrode is presented in Fig. 18F. The approximate thickness of three layers, Ni, Ni-P and Ni-Mo-P are 20, 20, 7 μm , respectively. For “one-step” deposited electrodes the thickness was ~ 60 μm . The deposit was hard and well adhered to the surface, therefore, it was difficult to remove it by polishing with a sand paper (SiC).

5.2.2 HER on Ni-Mo-P electrodes

5.2.2.1 Steady-state polarization

The steady state polarization curves obtained on different Ni-Mo-P electrodes are presented in Fig. 19. Only one slope was observed in the whole studied potential range . The kinetic

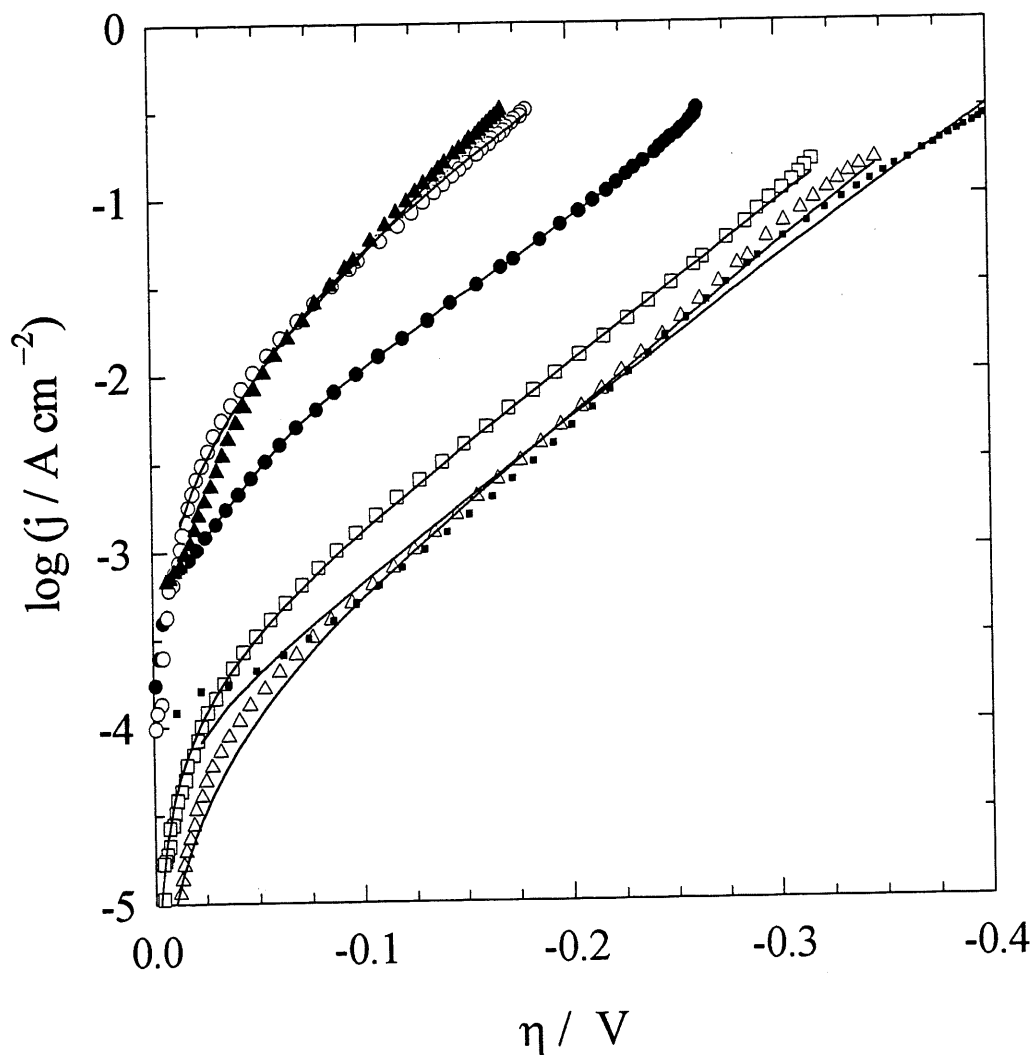


Figure 19. Steady-state polarization curves obtained for the HER in 1 M NaOH on “one-step” deposited $\text{Ni}_{74}\text{Mo}_{16}\text{P}_{10}$ (Δ) at 25°C , (\square) at 70°C , “three-step” deposited (\bullet) $\text{Ni}_{86}\text{Mo}_{12}\text{P}_2$, (\circ) $\text{Ni}_{71}\text{Mo}_{27}\text{P}_2$, (\blacktriangle) $\text{Ni}_{50}\text{Mo}_{45}\text{P}_5$, and “two-step deposited” (\blacksquare) $\text{Ni}_{73}\text{P}_{27}$, (the substrate of electrode C and D) at 70°C . The continued lines are obtained from fitted data using NLS.

parameters are presented in Table 9. The slopes of the Ni-Mo-P electrodes changed between -74 and -112 mV dec⁻¹. Although the activity of electrode Ni₇₄Mo₁₆P₁₀ is better than that of Ni (192) and Ni-P electrodes prepared in the similar conditions (ref. 344, Ni-P electrode prepared at $j = 200 \text{ mA cm}^{-2}$), yet it was not very active (28,42-44,103,106,121-123, 243,278,344).

Electrode C prepared by a "three-step" method has higher activity, but the third layer of this electrode was somewhat fragile and did not show the desired physical stability.

An increase in the electrode activity was observed for electrode D. This electrode is characterized by a low overpotential, Table 9. It seems that the electrode activity not only depends on the deposition conditions of Ni-Mo-P but also on the porosity of the predeposited layer, Ni-P. The physical properties and electrochemical activity of the electrode remained unchanged for three days of the HER at 70°C, $j = 320 \text{ mA cm}^{-2}$ in 1 M NaOH.

The activity of the electrode F is somewhat higher than D. This electrode is compared with its substrate, *i.e.*, electrode G. Electrode F had black surface. Physically this electrode was not as stable as electrode D.

5.2.2.2 Activation by anodic oxidation and potential cycling

We tried to increase the activity of the Ni-Mo-P electrodes by cycling the electrode potential. First the electrode was cycled between -1.20 to 0.70 V vs. Hg/HgO at 50 mV s⁻¹ in 1 M NaOH at 25°C and then the kinetic parameters were extracted for the HER from steady-state polarization curves. Then the electrode was oxidized at 0.70 V vs. Hg/HgO in 1 M NaOH (OER) for more than 5h and again kinetic parameters were extracted by the same way (Table 10).

The last cyclic voltammograms were recorded for Ni₇₄Mo₁₆P₁₀ electrodes at 25 and 70°C. The same behavior was observed at both temperatures. For brevity only one of cyclic voltammograms, obtained at the steady state (280th cycle at 25°C), is presented, Fig. 20. The voltammograms were similar to those were reported for nickel in alkaline solutions (251).

Table 9. Kinetics of the HER from steady-state polarization curves obtained on Ni-Mo-P electrodes in 1 M NaOH without any special treatment.

Electrode composition		T / °C	b / mV dec ⁻¹	j _o / mA cm ⁻²	η ₂₅₀ / mV
Ni ₇₄ Mo ₁₆ P ₁₀	(A)	25	-97	0.05	-359
Ni ₇₄ Mo ₁₆ P ₁₀	(B)	70	-103	0.12	-339
Ni ₈₆ Mo ₁₂ P ₂	(C)	70	-112	1.29	-257
Ni ₇₁ Mo ₂₇ P ₂	(D)	70	-89	3.10	-170
Ni ₇₃ P ₂₇	(E1)	70	-109	0.07	-385
Ni ₈₉ Mo ₁₁	(E2)	70	-180	12.7	-234
Ni ₅₀ Mo ₄₅ P ₅	(F)	70	-74	1.98	-155
Ni ₉₂ P ₈	(G)	70	-57	0.24	-171
Ni	(H)	25	-115	0.002	-591

(A), (B) Prepared in “one-step” and at high current density ($j = 200 \text{ mA cm}^{-2}$); (C) prepared in “three step” pH = 7 to 8; and (D) pH = 9.2; see the text for more detail; (E1) deposited as C and D just up to the end of step two, *i.e.*, without continuing step three; (E2) deposited as D in the absent of phosphorous; (F) prepared in three steps as C and D but from different bath and conditions, see the text; (G) substrate of electrode F; (H) data for Ni polycrystalline at 25°C in 1 M NaOH are taken from ref. 192.

The electrode composition changed from Ni₇₄Mo₁₆P₁₀ (A and B) and Ni₇₁Mo₂₇P₂ (D) to Ni₈₈Mo₂P₁₀ (A and B) and Ni₈₅Mo₁₃P₂ (D) after experiments (Table 10). Although the Mo was partially removed, the remainder did not dissolve during further oxidation.

Table 10. Kinetics of the HER obtained on Ni-Mo-P electrodes from steady-state polarization curves in 1 M NaOH after electrochemical pretreatments.

Electrode	T / °C	b / mV dec ⁻¹	j ₀ / mA cm ⁻²	η ₂₅₀ / mV	pretreatment
Ni ₇₄ Mo ₁₆ P ₁₀ (A)	25	-96	0.05	-357	no
Ni ₇₄ Mo ₁₆ P ₁₀ (A)	25	-96	0.06	-352	280 cycles
Ni ₇₄ Mo ₁₆ P ₁₀ (A)	25	-107	0.12	-356	oxidation
Ni ₇₄ Mo ₁₆ P ₁₀ (B)	70	-103	0.12	-340	no
Ni ₇₄ Mo ₁₆ P ₁₀ (B)	70	-128	0.43	-357	280 cycles
Ni ₇₄ Mo ₁₆ P ₁₀ (B)	70	-145	0.93	-352	oxidation
Ni ₇₄ Mo ₁₆ P ₁₀ (A)	25	-210	0.71	-512	leaching*
Ni ₇₄ Mo ₁₆ P ₁₀ (A)	25	-168	0.69	-430	280 cycles
Ni ₇₁ Mo ₂₇ P ₂ (D)	70	-89	3.10	-170	no
Ni ₇₁ Mo ₂₇ P ₂ (D)	70	-115	0.78	-290	oxidation

(A), (B) Prepared in “one-step” and at high current density ($j = 200 \text{ mA cm}^{-2}$); (C) prepared in “three step” pH = 7 to 8 and (D) pH = 9.2, see the text for more detail; the electrodes C and F didn't show very good stability in oxidation and cycling experiments, therefore there is no data for them in the Table.

*: Leaching in KOH 30% solution at 70°C for 4h.

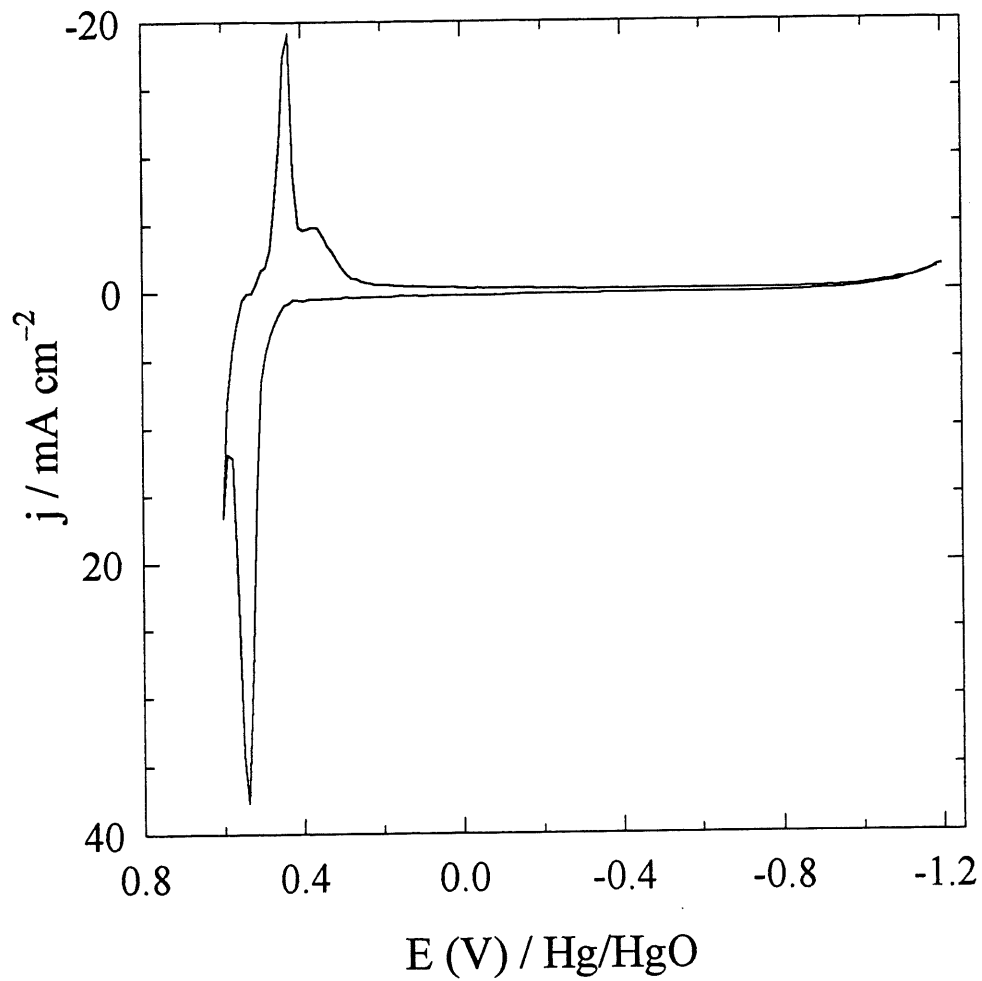


Figure 20. A typical cyclic voltammogram obtained on $\text{Ni}_{74}\text{Mo}_{16}\text{P}_{10}$ electrode in 1 M NaOH at 25°C at 50 mV s^{-1} scan rate. The same pattern was observed at 70°C .

Activities of the Ni-Mo-P electrodes decrease after anodic polarization or cycling the electrode potential between the HER and OER (-1.2 to 0.7 V vs. Hg/HgO), Table 10. This behavior is different from that of nickel (192,193) or nickel alloys (194).

It has been reported that oxidation of nickel increased the activity of this electrode for the HER (192,193). Oxidation or cycling of nickel cobalt, Ni-Co, electrodes between anodic (OER) and cathodic potential (HER) increased their activity for electrolysis of alkaline water solutions (194). Since the studied electrodes are of nickel-based categories here, we expected that such treatments (192-194) increase the activity of our electrodes.

Any treatment that removes the Mo will deactivate the Ni-Mo-P electrodes. This will be discussed subsequently in this chapter. However, the best activity and physical stability was observed for as-deposited electrode D (see Table 9 and 10). Although the electrode F is more active, considering other aspects as physical stability D is the best one.

5.2.2.3 Electrochemical impedance spectroscopy

The EIS measurements was performed on Ni-Mo-P electrodes in the potential range in which steady-state polarization curves were recorded covering the current density 0 to 320 mA cm⁻². For electrodes A, B, C and E1 at high frequencies the complex plane plot was a straight line of 45°, and at low frequencies a semi-circle was observed similar to those observed for porous electrodes (26,42,44,123,243,344,377,380,398-403). The complex plane plots of the electrodes D, E2 and F were different from the others. Only one semi-circle was observed for these electrodes in the whole range of frequencies and overpotentials. This behavior was similar to that was observed for flat electrodes (26,192,243,379), Fig. 21. The EIS data of each electrode was fitted in three models (Fig. 21), and kinetic parameters, especially R_{ct} , were extracted. Then η - j , from steady-state polarization measurements, and η - R_{ct} data, from

the EIS, were used for approximation of rate constants, see eqns. [2.49], [2.58], and [2.98] in chapter 2.

For each electrode one of the models gave the best approximation. When the R_{ct} from two other models were used, the approximated parameters were unreal, e.g., β_1 and/or β_2 greater than *one* were obtained. In general, if the approximation errors values for two models were similar, we selected the model with less number of parameter. This procedure of model selection has been used elsewhere in this work (278). This matter will be discussed in next chapter.

Different models were attributed to the electrodes: The approximation of the EIS experimental data of electrodes A, B and C was attained using modified de Levie's porous model, eqns. [2.93] and [2.94] (26,28,121,377,378,380), see section 2.3.3.5.2 in chapter 2. This model has five adjustable parameters, A_p , B_p , ϕ , $R_{\Omega,p}$, and R_s , and explains the impedance of cylindrical pores.

A simple CPE model (26,37,192,243) that its faradaic impedance is given by eqns. [2.83] to [2.85], the case that $A \gg |B/C|$ leading to $Z_f = 1/A = R_{ct}$, and the impedance of its double layer capacitance as $Z_{CPE} = 1/T(j\omega)^\phi$, was used for approximation of the EIS data of electrodes D, E2 and F, Fig. 21 (only data for electrode D are presented here). This model has four adjustable parameters: A , R_s , T and ϕ .

From the two-CPE model that was used for E1 (121) seven parameter may be obtained, A_1 , A_2 , R_s , T_1 , ϕ_1 , T_2 and ϕ_2 . The main assumption of this model is that the diameter of one semicircle remains constant in the whole range of overpotentials. In this case from the second semicircle kinetic parameters can be determined in the same way as for simple CPE model. The model explains the impedance of pear shape pores (26,27,42,121,243).

The real and imaginary components, Z' and Z'' , of the electrode impedance obtained in the whole frequency range at various overpotentials were analyzed using the CNLS program (372,404). The kinetic parameters, R_{ct} and T were directly obtained from CPE and two-CPE models. From five parameters obtained from porous model, A_p , B_p , ϕ , $R_{\Omega,p}$ and R_s (solution resistance), the charge transfer resistance (R_{ct}) and the average of double layer capacitance (\bar{C}_{dl}) are extracted, $R_{ct} = A_p R_{\Omega,p}$, $T = B_p / R_{\Omega,p}$, where T is given by eqn. [2.84] the \bar{C}_{dl} is obtained.

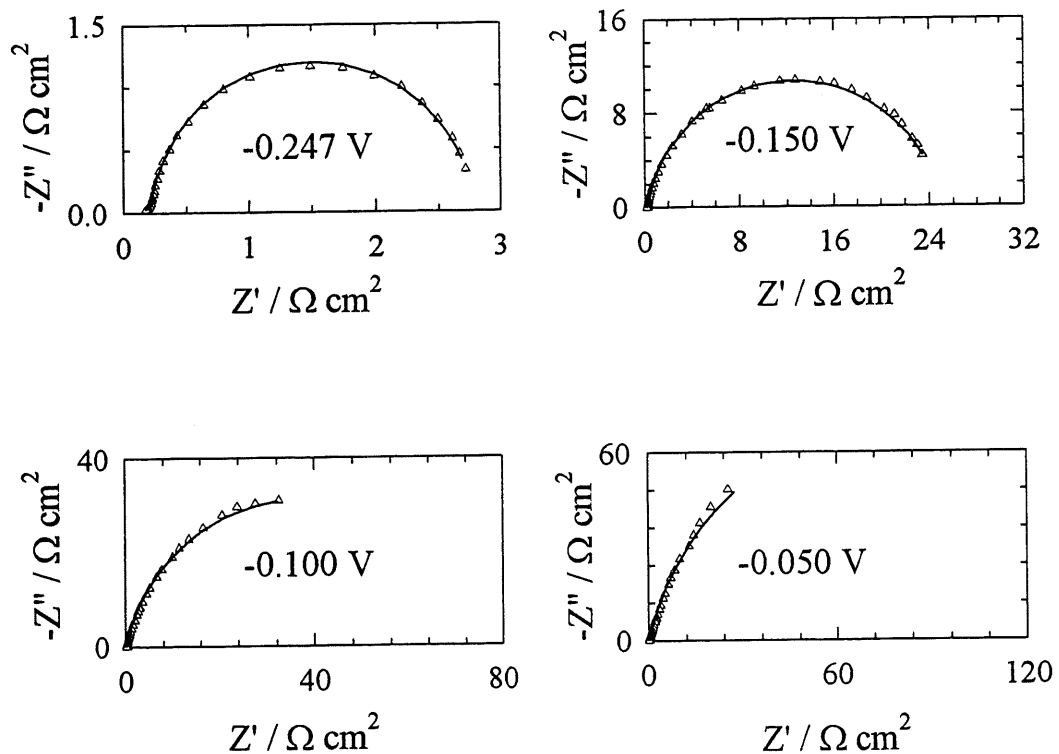


Figure 21A

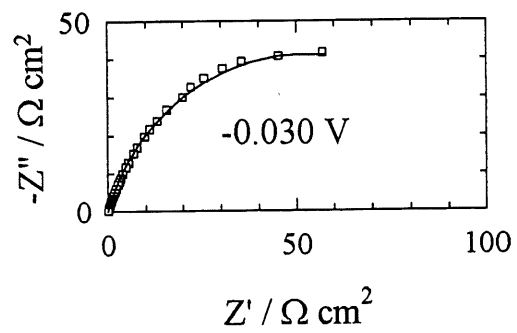
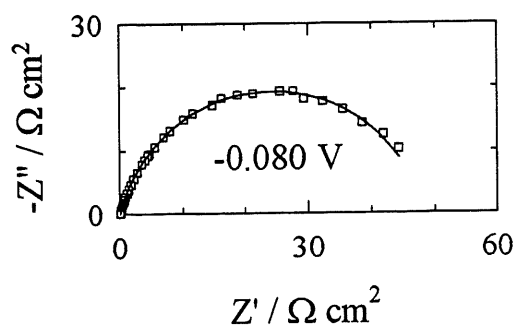
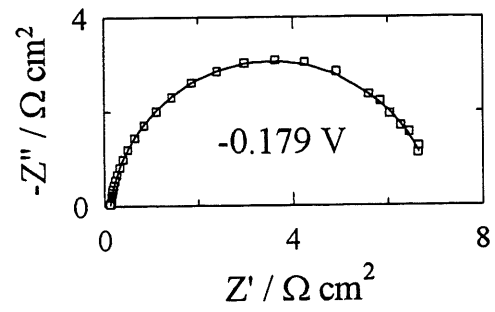
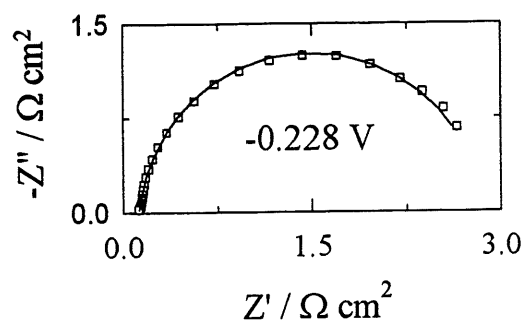


Figure 21B

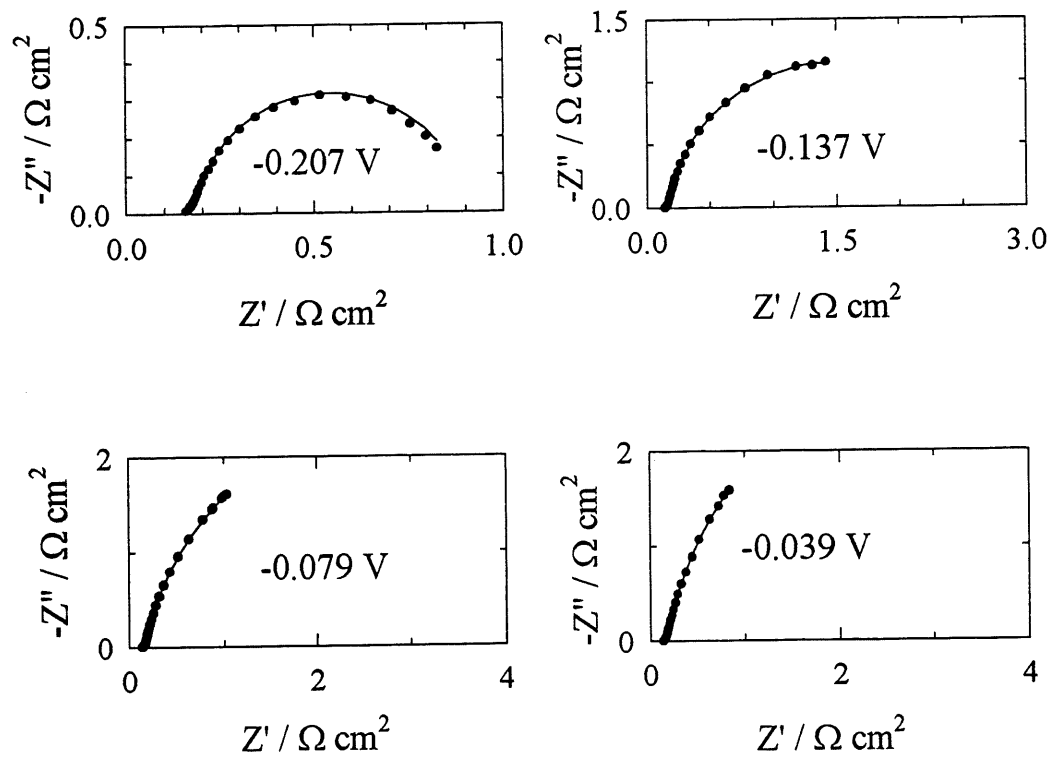


Figure 21C

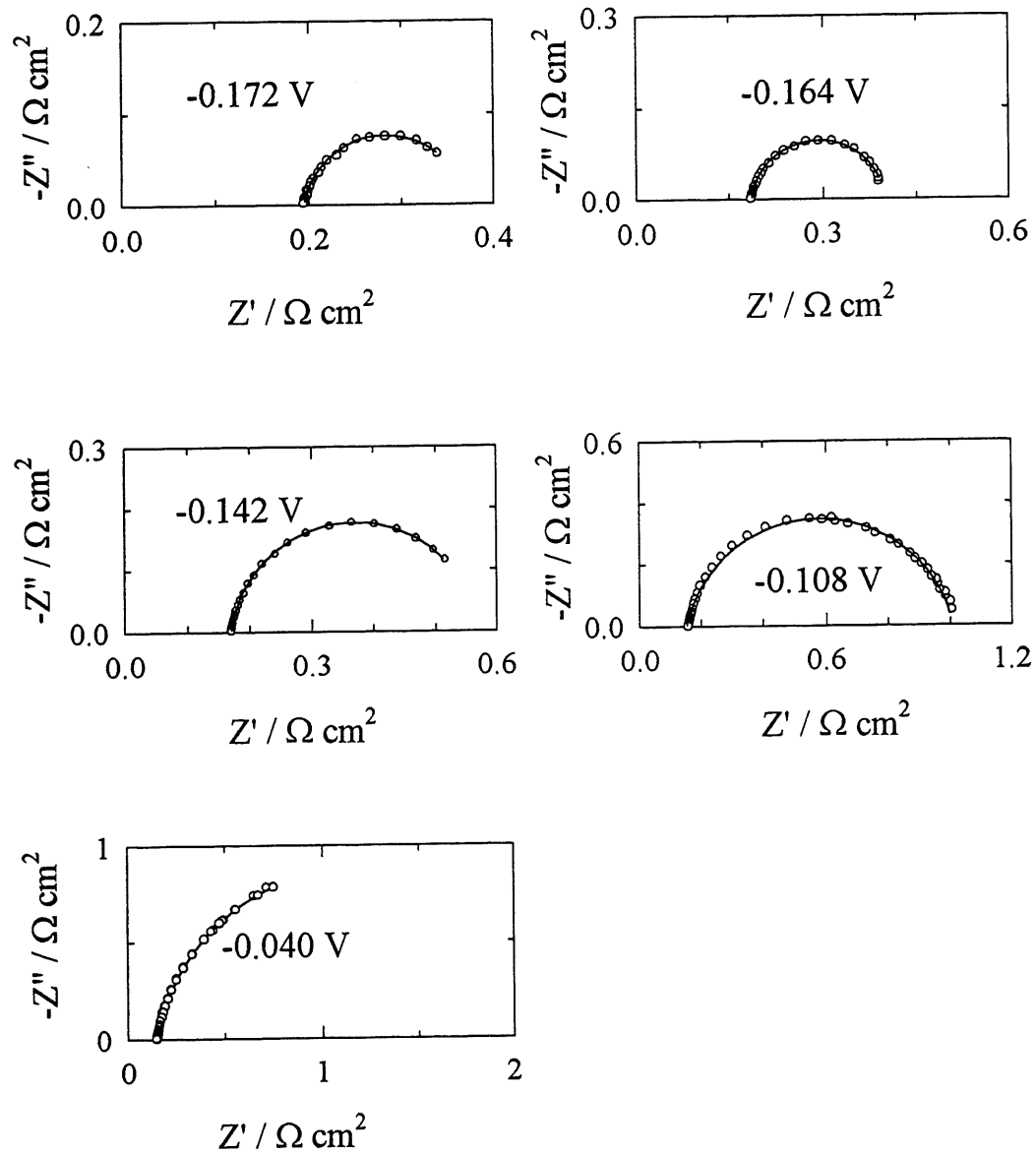


Figure 21D

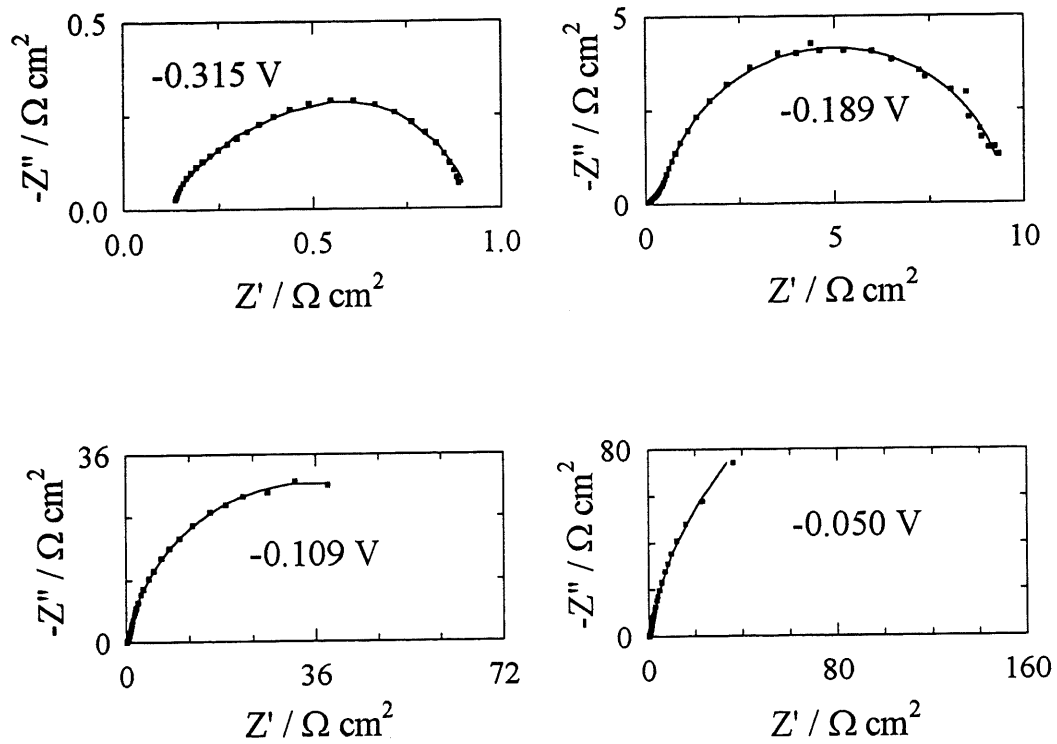


Figure 21E

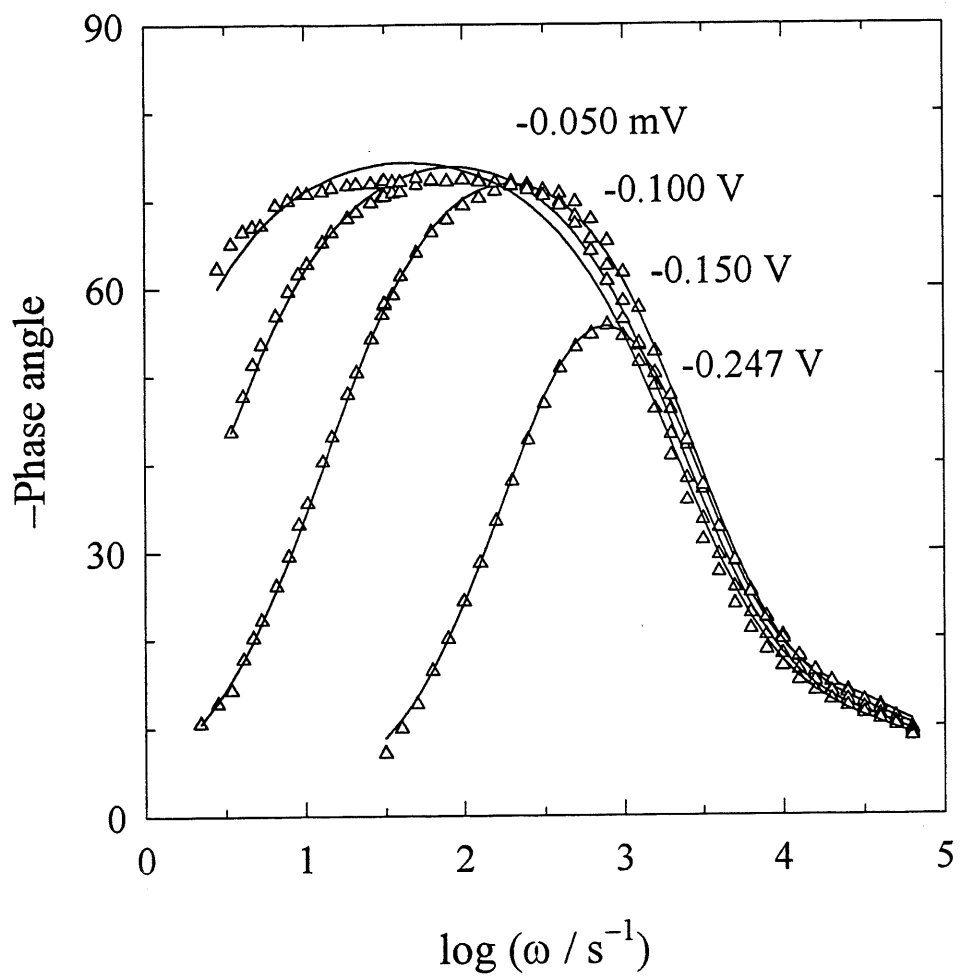


Figure 21F

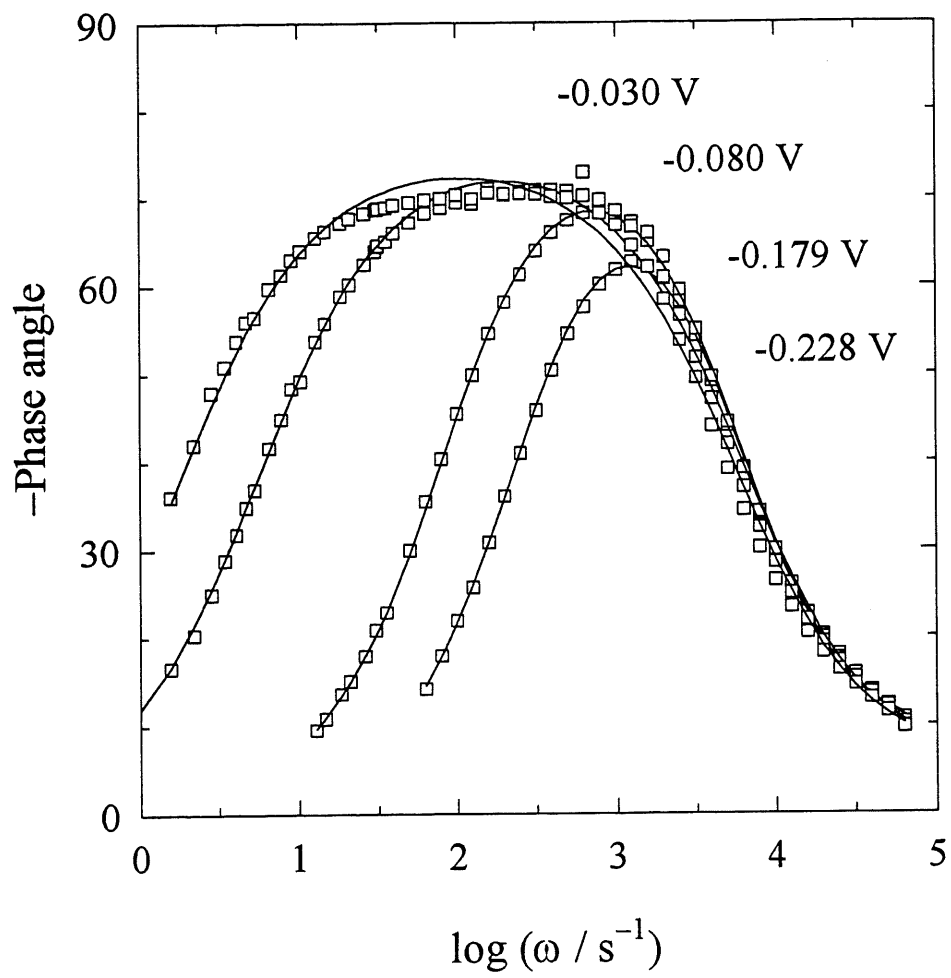


Figure 21G

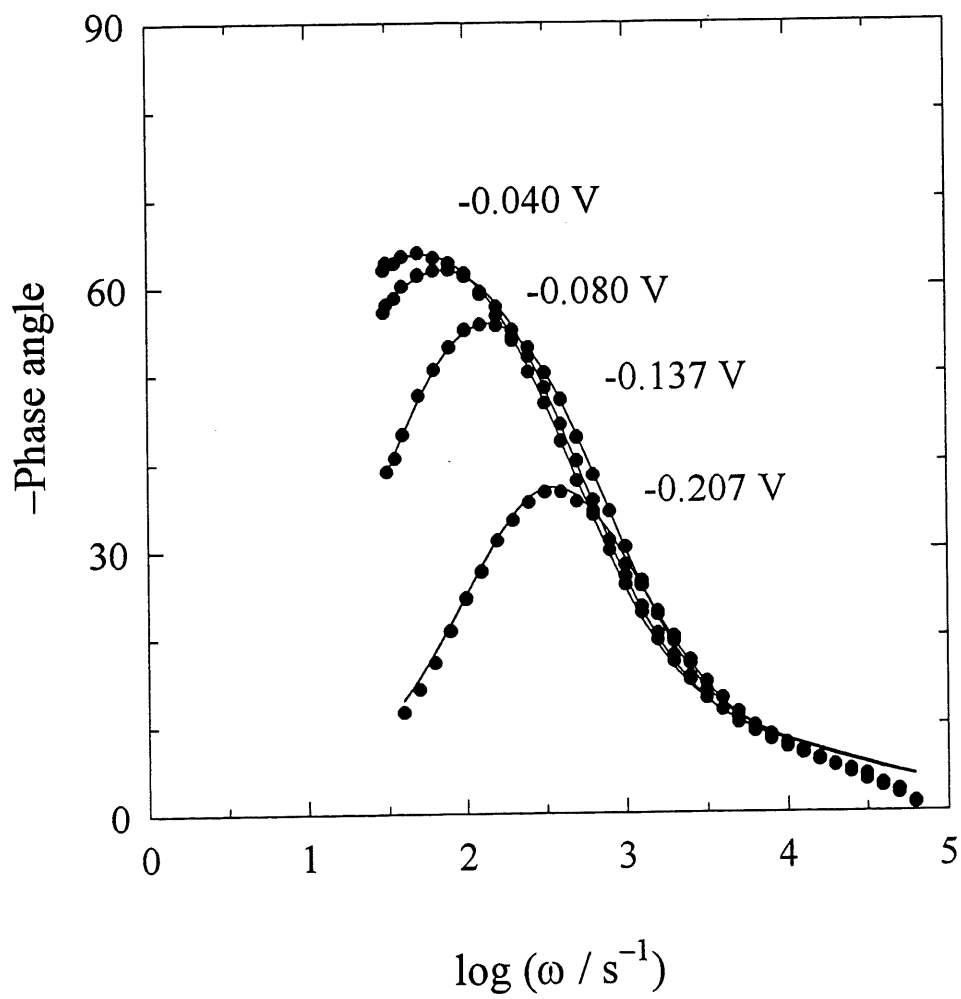


Figure 21H

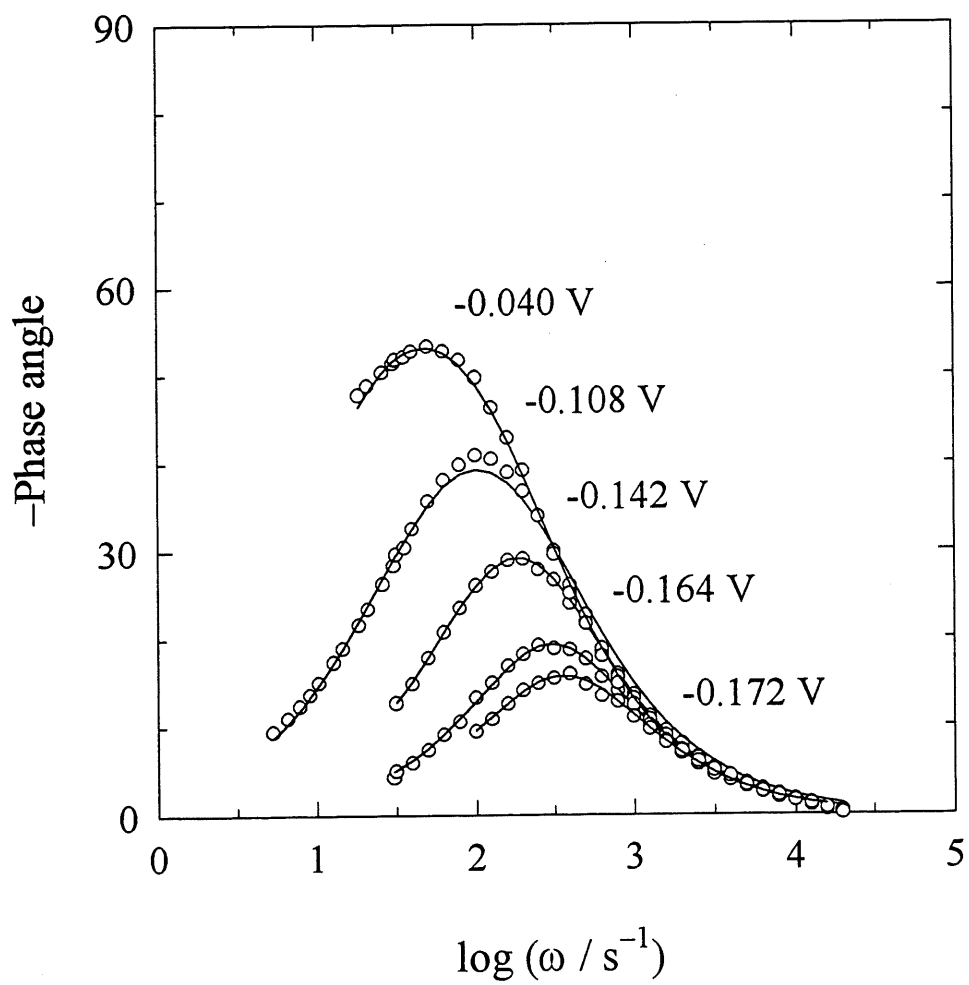


Figure 21I

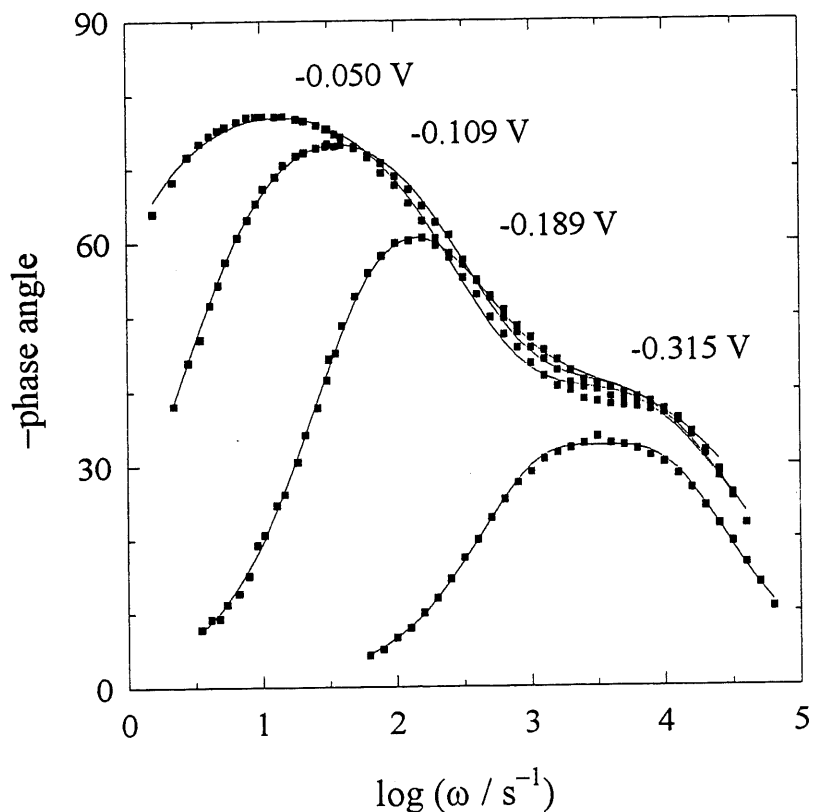


Figure 21J

Figure 21. Complex plane and phase angle plots obtained for the HER in 1 M NaOH on “one-step” deposited $\text{Ni}_{74}\text{Mo}_{16}\text{P}_{10}$ (A,F) at 25°C, (B,G) at 70°C; “three-step” deposited (C,H) $\text{Ni}_{86}\text{Mo}_{12}\text{P}_2$, (D,I) $\text{Ni}_{71}\text{Mo}_{27}\text{P}_2$; and “two-step deposited” (E,J) $\text{Ni}_{73}\text{P}_{27}$ (the substrate of electrode C and D) at 70°C. The behavior of electrode $\text{Ni}_{50}\text{Mo}_{45}\text{P}_5$ (*i.e.*, electrode F, Table 9) was similar to $\text{Ni}_{71}\text{Mo}_{27}\text{P}_2$ (*i.e.*, electrode D, Table 9) with smaller R_{ct} . The continuous lines indicate fitted results using the CNLS method, see section 5.2.2.3 for models. The first letters in the parentheses indicate the complex plane plots as well as the electrode *name*, the second letters indicate only the complex plane plots.

The variations of the \bar{C}_{dl} and parameters ϕ as functions of η is displayed in Fig. 22. For all the electrodes except F the parameter ϕ was between 0.8 to 1.0. The origins of this effect was recently studied by Pajkossy *et al.* (376). It can be due to various reasons as: (i) the nature of electrode metal, (ii) type of electrolyte, (iii) the microscopic surface roughness and (iv) specific ionic adsorption.

The exceptional behavior of electrode F may has different reasons; (i) physical instability of the electrode, or (ii) distribution of adsorption energies.

An approximation of the dependence of charge transfer resistance ($A = 1 / R_{ct}$) and j as functions of η , was carried out by adjusting the rate constants k_1 , k_{-1} , k_2 and transfer coefficients, β_1 and β_2 , and using NLS method assuming Volmer-Heyrovský mechanism (192). A good approximation was observed using, R_{ct} and η from the EIS measurements, current density, j , and η from steady-state measurements, and eqns. [2.49], [2.58], and [2.98] in chapter 2, (see Figs. 19 and 23). The kinetic parameters together with their standard deviations are presented in Table 11. It was found that the reaction proceeds through the Volmer-Heyrovský mechanism with the Heyrovský reaction as rate determining step (rds).

We couldn't fit simultaneously the steady-state and the EIS data of electrode F by this method. The reason may come from distribution of adsorption energies which is not considered in this method (16).

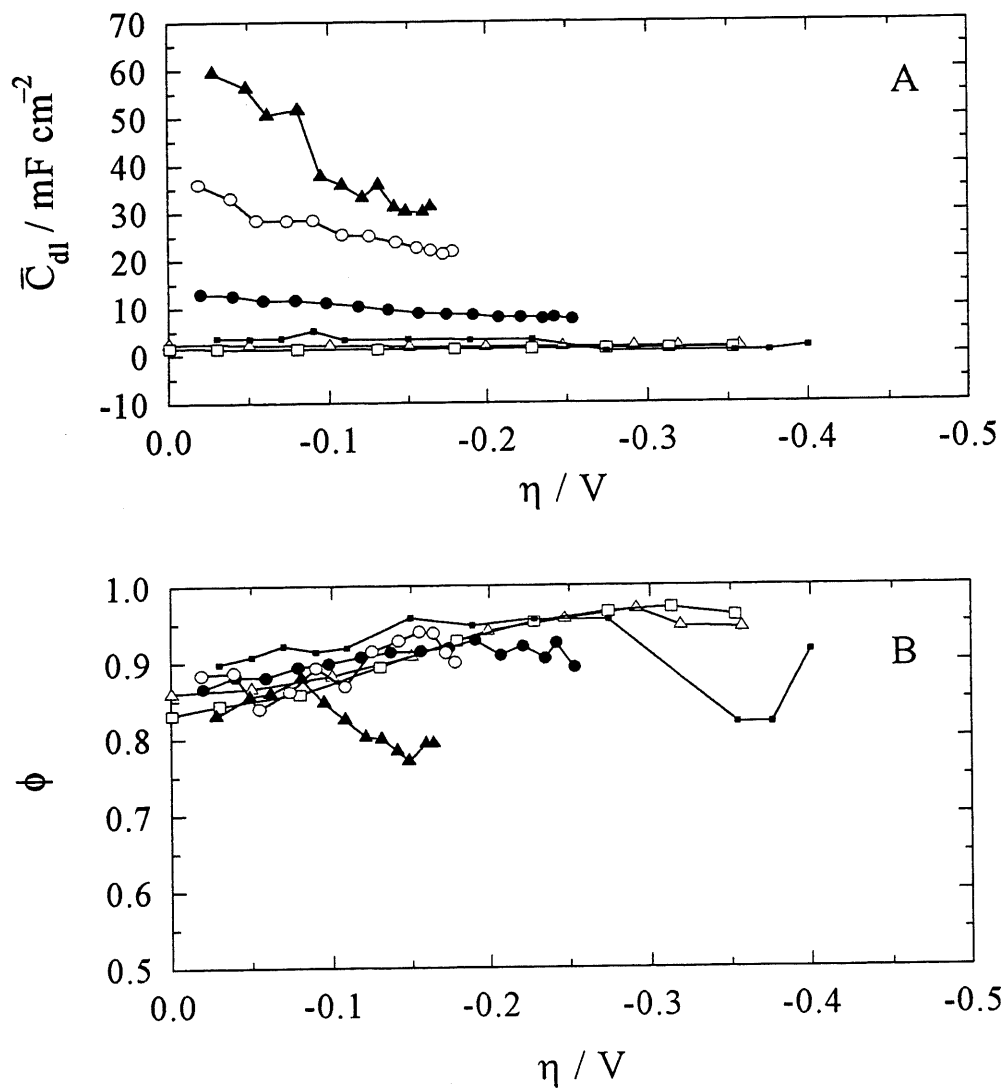


Figure 22. (A) Dependence of the average of double layer capacitance, \bar{C}_{dl} , and (B) parameter ϕ on overpotential for the HER in 1 M NaOH on "one-step" deposited Ni₇₄Mo₁₆P₁₀ (Δ) at 25°C, (\square) at 70°C, "three-step" deposited (\bullet) Ni₈₆Mo₁₂P₂, (\circ) Ni₇₁Mo₂₇P₂, (\blacktriangle) Ni₅₀Mo₄₅P₅, and "two-step deposited" (\blacksquare) Ni₇₃P₂₇ (the substrate of electrode C and D), at 70°C.

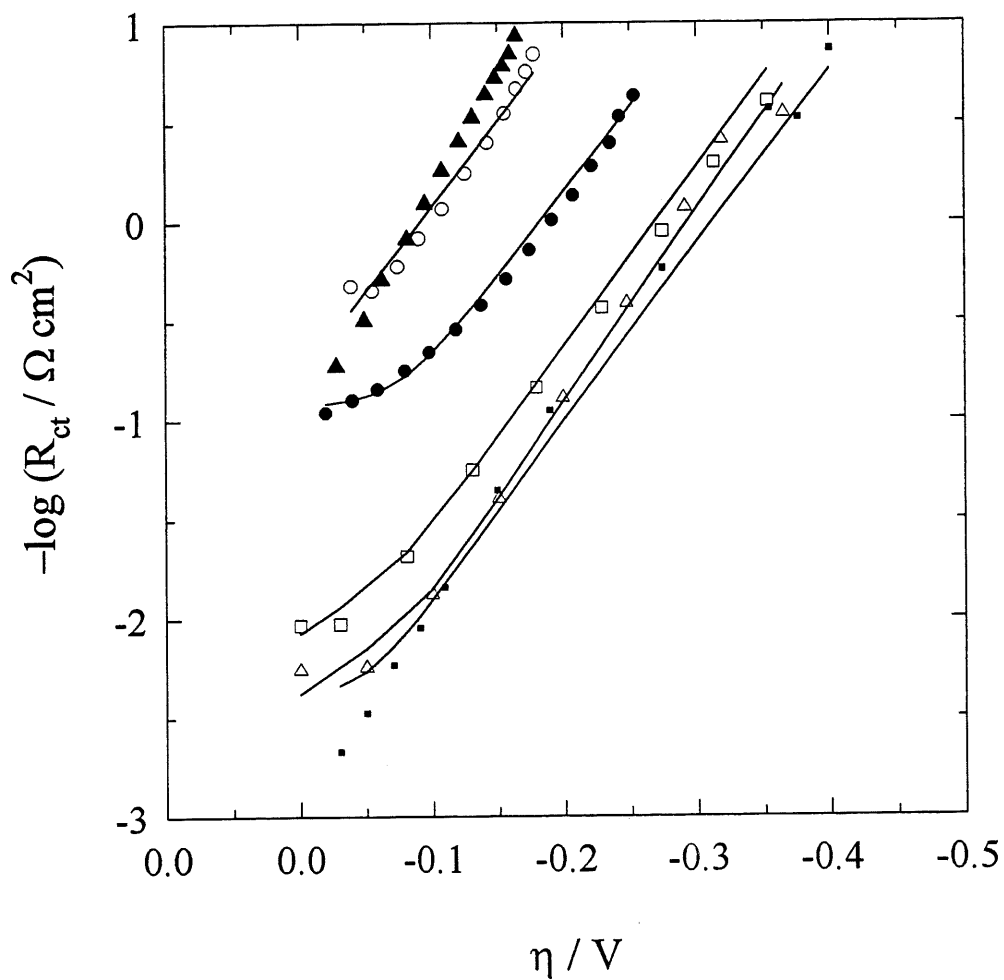


Figure 23. Dependence of charge transfer resistance, R_{ct} , on overpotential for the HER in 1 M NaOH on “one-step” deposited $Ni_{74}Mo_{16}P_{10}$ (Δ) at 25°C, (\square) at 70°C, “three-step” deposited (\bullet) $Ni_{86}Mo_{12}P_2$, (O) $Ni_{71}Mo_{27}P_2$, (\blacktriangle) $Ni_{50}Mo_{45}P_5$, and “two-step deposited” (\blacksquare) $Ni_{73}P_{27}$ (the substrate of electrode C and D), at 70°C. The continued lines are obtained from fitted data using NLS method.

Table 11. Kinetic parameters of the HER obtained on Ni-Mo-P electrodes from the steady-state polarization curves and the EIS measurements in 1 M NaOH, using NLS program.

Electrode	k_1 / mol cm ⁻² s ⁻¹	k_{-1} / mol cm ⁻² s ⁻¹	k_2 / mol cm ⁻² s ⁻¹	β_1	β_2
Ni ₇₄ Mo ₁₆ P ₁₀ (A)	$(1.25 \pm 0.43) \cdot 10^{-9}$	$(6.681 \pm 7.32) \cdot 10^{-9}$	$(3.64 \pm 2.11) \cdot 10^{-10}$	0.64 ± 0.12	0.51 ± 0.08
Ni ₇₄ Mo ₁₆ P ₁₀ (B)	$(3.10 \pm 0.68) \cdot 10^{-9}$	$(8.77 \pm 4.82) \cdot 10^{-9}$	$(1.12 \pm 0.34) \cdot 10^{-9}$	0.67 ± 0.08	0.57 ± 0.07
Ni ₈₆ Mo ₁₂ P ₂ (C)	$(5.36 \pm 0.88) \cdot 10^{-8}$	$(7.91 \pm 0.68) \cdot 10^{-8}$	$(8.03 \pm 0.64) \cdot 10^{-9}$	0.63 ± 0.01	0.48 ± 0.04
Ni ₇₁ Mo ₂₇ P ₂ (D)	$(1.92 \pm 0.77) \cdot 10^{-7}$	$(7.99 \pm 0.55) \cdot 10^{-9}$	$(4.70 \pm 0.43) \cdot 10^{-8}$	0.500*	0.65 ± 0.04
Ni ₇₃ P ₂₇ (E)	$(1.57 \pm 2.15) \cdot 10^{-8}$	$(1.14 \pm 0.14) \cdot 10^{-9}$	$(4.12 \pm 0.72) \cdot 10^{-10}$	0.43 ± 0.08	0.64 ± 0.04

(A), (B) Prepared in "one-step" and at high current density ($j = 200$ mA cm⁻²); (C) prepared in "three step" pH = 7 to 8 and (D) pH = 9.2, see the text for more detail; (E) deposited as C and D just up to the end of step two, *i.e.*, without continuing step three. See also Table 9.

*: Was fixed.

Referring to the experimental information obtained from the EIS measurements the surface of the electrode after step two (*i.e.*, Ni-P deposition) had a porous structure (Figs. 21E and J), while after step three (*i.e.*, Ni-Mo-P deposition) behaves as a flat electrode (electrode D, Figs. 21D and I). Another important point is the relation between the shape of the substrate (Ni-P) pores and stability of the catalyst, Ni-Mo-P. Electrode D showed a good stability (substrate had pear shape pores), while electrode F did not show a good stability (substrate had cylindrical pores), see section 5.2.2.3 for more detailed discussion about the model and shape of the pores.

Intrinsic activity of the electrodes may be evaluated by comparison of the real rate constants obtained from apparent rate constants of the rate determining step, k_{rds} , divided by roughness factor. The results are presented in Table 12. They are compared with E1 (*i.e.*, Ni-P, the base of electrodes C and D) and Ni. The best activity for the HER was observed at 70°C on electrode D. The intrinsic activity, k_{rds} / R , of this electrode is one order of magnitude larger than that of its substrate, Ni-P, in the same conditions. If the apparent activity in Table 11 (k_2) is compared, it reveals that the apparent activity of electrode D is two orders of magnitude larger than that of Ni-P, $k_2(D) / k_2(E1) = 110$ (Table 11), considering one order of magnitude that is originated from increase in intrinsic activity, $k_{real}(D) / k_{real}(E) \cong 10$, (Table 12), one order of magnitude increase in apparent activity arises from increase in the surface roughness, $R(D) / R(E) \cong 10$, (Table 12). In other words the activity of electrode D is two orders of magnitude larger than that its substrate (electrode E1). Such a comparison for other Ni-Mo-P electrodes in Table 11 and 12 reveals this interesting aspect of these electrodes that increase in the activity of Ni-Mo-P electrode is achieved with increase of surface roughness and intrinsic activity (synergetic effect) (46,48,189,343,397,405).

It seems that the synergetic effect, which is responsible here for the electrode activity, arises from Mo, because it has been decreased by removing the Mo or Mo-P from the surface by

Table 12. Roughness factors and intrinsic activities of the HER obtained on Ni-Mo-P electrodes in 1 M NaOH.

Electrode	T / °C	R	j_o / R / mA cm ⁻²	$k_{real} = k_{rds} / R$ / mol cm ⁻² s ⁻¹
Ni ₇₄ Mo ₁₆ P ₁₀ (A)	25	95	$5.26 \cdot 10^{-4}$	$(3.83 \pm 2.22) \cdot 10^{-12}$
Ni ₇₄ Mo ₁₆ P ₁₀ (B)	70	68	$1.77 \cdot 10^{-3}$	$(1.65 \pm 0.50) \cdot 10^{-11}$
Ni ₈₆ Mo ₁₂ P ₂ (C)	70	479	$2.69 \cdot 10^{-3}$	$(1.67 \pm 0.14) \cdot 10^{-11}$
Ni ₇₁ Mo ₂₇ P ₂ (D)	70	1315	$2.36 \cdot 10^{-3}$	$(3.58 \pm 0.33) \cdot 10^{-11}$
Ni ₇₃ P ₂₇ (E1)	70	137	$5.30 \cdot 10^{-4}$	$(3.01 \pm 0.53) \cdot 10^{-12}$
Ni ₅₀ Mo ₄₅ P ₅ (F)	70	2015	$1.00 \cdot 10^{-3}$	-----
Ni ₉₂ P ₈ (G)	70	1900	$1.26 \cdot 10^{-4}$	$(2.43 \pm 0.12) \cdot 10^{-13}$
Ni (H)	25	2	$9.0 \cdot 10^{-4}$	$(2.10 \pm 0.50) \cdot 10^{-12}$

(A), (B) Prepared in “one-step” and at high current density ($j = 200 \text{ mA cm}^{-2}$); (C) prepared in “three step” pH = 7 to 8 and (D) pH = 9.2, see the text for more detail; (E) deposited as C and D just up to the end of step two, *i.e.*, without continuing step three; (F) prepared in three steps as C and D but from different bath and conditions, see the text; (G) substrate of electrode F; (H) data for nickel polycrystalline at 25°C in 1 M NaOH taken from ref 192.

means of oxidation or leaching. For example for electrode A and D the composition before oxidation is (A): Ni₇₄Mo₁₆P₁₀ and (D): Ni₇₁Mo₂₇P₂ and after oxidation (A): Ni₈₈Mo₂P₁₀ and (D): Ni₈₅Mo₁₃P₂. Most probably the decrease observed in the electrode activity for the HER (Table 10) is due to the decrease of the number of Ni-Mo or Mo-P bonds. However,

formation of phosphorous oxides during oxidation or cycling process and blocking some of the active sites is also possible (344).

A considerable amount of the gas was evolving from the surface of the electrode D after 20h activation at cathodic current $j = 320 \text{ mA cm}^{-2}$ at 70°C (getting steady-state) and then leaving it at the open-circuit potential. This phenomenon continued for a few minutes and then with less intensity up to 10 min. Such an observation was reported for glassy metal electrodes (340,342) and can have various reasons as: (i) trapping of the gas in the electrode pores: this one is not the case here, because electrode D behaves as a flat electrode as was concluded from the EIS measurements, (ii) hydride formation: it is probably the reason for this behavior (340-343). Hydride formation on Ni-Mo alloys was also observed by Divisek *et al.* (48). It was suggested that hydrogen can diffuse to the matrix of Ni-Mo and Ni-Al-Mo alloys and form metal hydride. However, our EIS measurements revealed that the behavior of the electrode D before Ni-Mo-P deposition (porous) and after that (as flat) is different (Figs. 21D, E, I and J). Probably the Ni-Mo-P is deposited onto the Ni-P pores leading to increase its stability. Fig. 18 D and F also shows the deposition of Ni-Mo-P onto Ni-P layer.

5.3 Summary

Ni-Mo-P electrodes of different composition were prepared and their activities toward the HER were studied by the EIS and steady-state polarization techniques. An increase in the electrode activity was observed for the electrodes prepared by a “three-step” method, at $\text{pH} = 9.2$, (electrodes D and F). The increase in the electrode activity was due to increase in: (i) surface roughness and (ii) intrinsic activity. The “three-step” deposited electrode D showed gas evolution behavior on leaving at the open-circuit potential which may be related to the “hydride formation”. Probably the Ni-Mo-P catalyst is deposited in pear shape pores of Ni-P substrate leading to stabilization of Ni-Mo-P catalyst.

CHAPTER 6
KINETICS OF HYDROGEN EVOLUTION REACTION ON
Ni-Zn-P ELECTRODES IN ALKALINE SOLUTIONS

6.1 Introduction

In the previous chapters it was found that Ni-P electrodes have high physical and chemical stability, but relatively low electrocatalytic activity for the HER (344). It seemed promising to prepare Ni-Zn-P electrodes by combination of good physical and chemical stability of Ni-P with high activity (large surface area) of Ni-Zn (28,42,268).

In the present chapter Ni-Zn-P electrodes were electrodeposited from an aqueous solution and, after leaching out zinc in alkaline solution, studied for the HER. The kinetics was determined using steady-state polarization and electrochemical impedance spectroscopy (EIS) techniques. The obtained electrodes are more stable and more active towards the hydrogen evolution reaction than Ni-Zn alloys. They are characterized by low Tafel slopes and large surface roughness of 10^4 . They may be attractive candidates for the alkaline water electrolysis.

6.2 Results and discussion

6.2.1 Electrode composition and surface morphology

The Ni-Zn-P electrodes that were prepared in one step deposition from bath AA (containing all the reagents Ni, Zn, and P, see procedure (i) and (iii) for preparation of Ni-Zn-P electrodes in chapter 3, and those prepared in three steps deposition, see procedure (ii), Ni, Ni-P, and Ni-Zn-P from baths A (containing Ni reagent), B (containing Ni and P reagents), and C (containing Ni, Zn, and P reagents) had similar SEM and EDX surface patterns. However, the

physical stability of Ni-Zn-P electrodes obtained in one step (from bath AA) and three-step (from baths A, B, C), after leaching out the Zn, were completely different. While one step deposited electrodes did not show good physical stability, the three-step deposited electrodes were very stable.

Fig. 24A presents a scanning electron micrograph of the electrode deposited in one step from bath AA. Its composition is $\text{Ni}_{55}\text{Zn}_{38}\text{P}_7$ and its surface is relatively smooth. The SEM micrograph, Fig. 24B, shows a smooth surface covered by flat hemispheres obtained from surface of three-step deposited electrode. The same pattern was observed for electrode obtained in one step from bath C. The electrode deposited in three steps was characterized by a surface composition $\text{Ni}_{54}\text{Zn}_{20}\text{P}_{26}$, and the electrode deposited in one step from bath C by $\text{Ni}_{56}\text{Zn}_{27}\text{P}_{17}$, as determined by EDX.

However, after leaching three-step deposited electrodes in 30% KOH at 70°C for 24h, rough surface of a “dry mud” structure, Fig. 24C, was observed because the leaching process decreased the deposit volume. The leached sample had a composition $\text{Ni}_{83}\text{Zn}_5\text{P}_{12}$ and zinc was not leached out completely. This residual zinc is important for the electrode activity (406). The structure and composition did not change after 8 days of a constant current polarization in 30% KOH at $j = 500 \text{ mA cm}^{-2}$ at 70°C, Fig. 24D and the composition was $\text{Ni}_{84}\text{Zn}_5\text{P}_{11}$.

The one step deposited electrodes did not show a good physical stability after leaching in 30% KOH at 70°C for 4h and we could not determine their surface composition after leaching very well. The deposit was easily removed by a lab knife after 10 days the HER. The kinetics of the electrode will be discussed latter in this chapter.

Crosssection mapping displayed that the thickness of the Ni, Ni-P and Ni-Zn-P layers was 70, 30 and 100 μm , respectively, Fig. 25A. After leaching, several cracks perpendicular to the surface were clearly visible in the Ni-Zn-P layer, Fig. 25B.

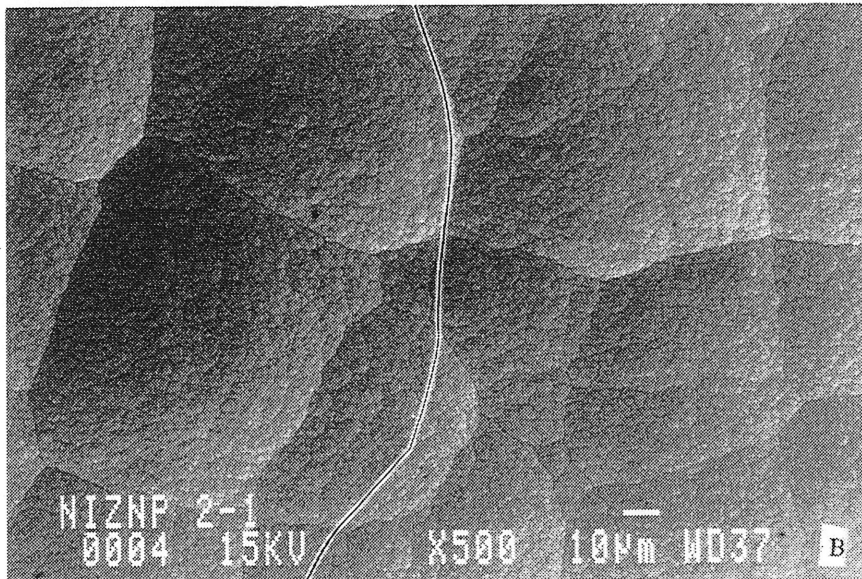
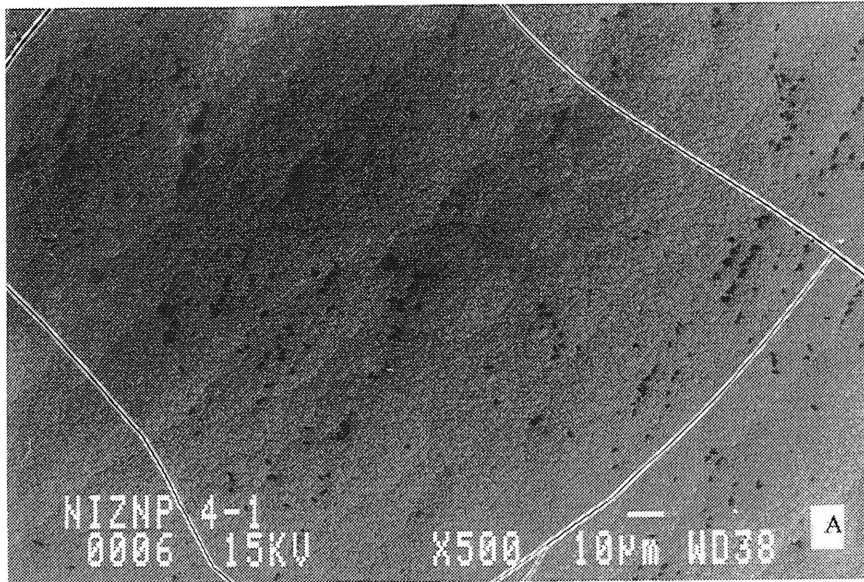


Figure-24A and B

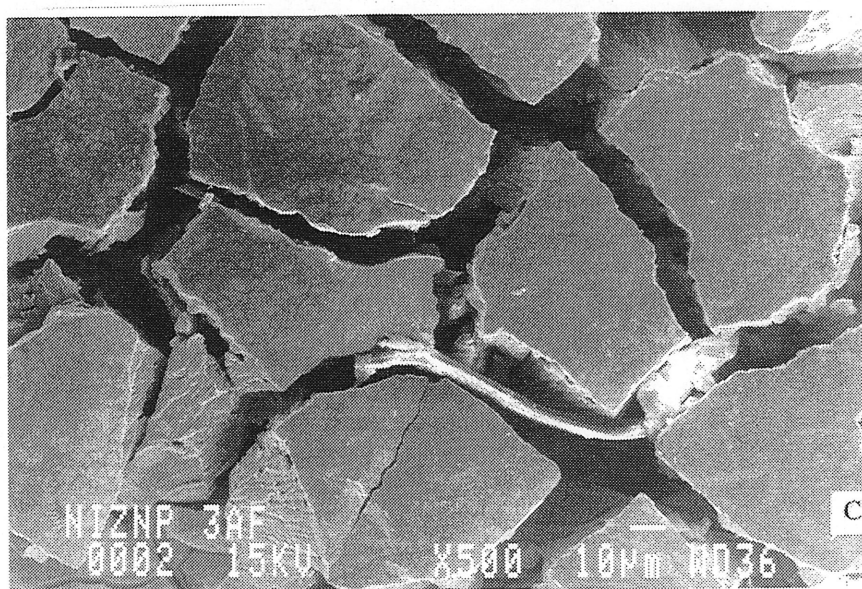
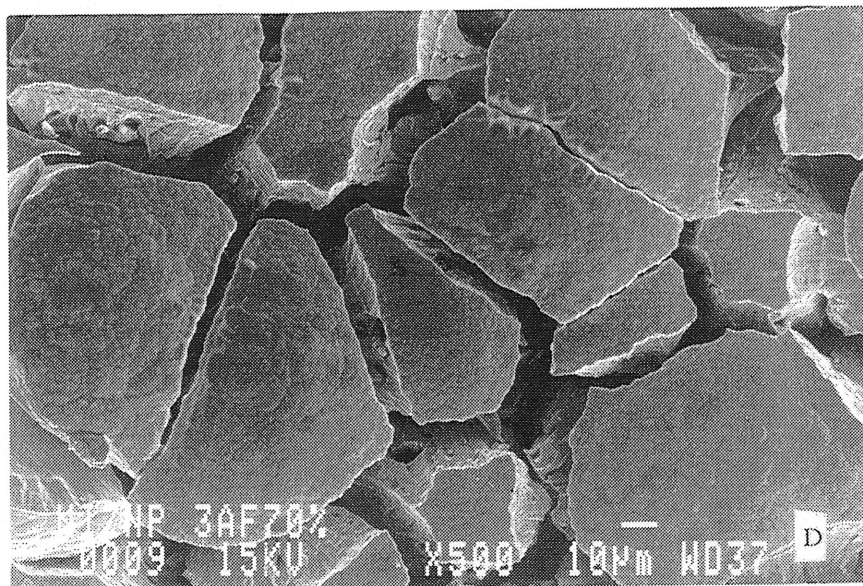


Figure 24C and D

Figure 24. Scanning electron micrographs prepared from the surface of Ni-Zn-P electrode, (A) as deposited in “one-step”, (B) as deposited in “three-step”, (C) electrode “B”, but after leaching at 70°C in 30% KOH for 24h, (D) electrode “C” after 8 days the HER at constant current, $j = 500 \text{ mA cm}^{-2}$, and 70°C in 30% KOH.

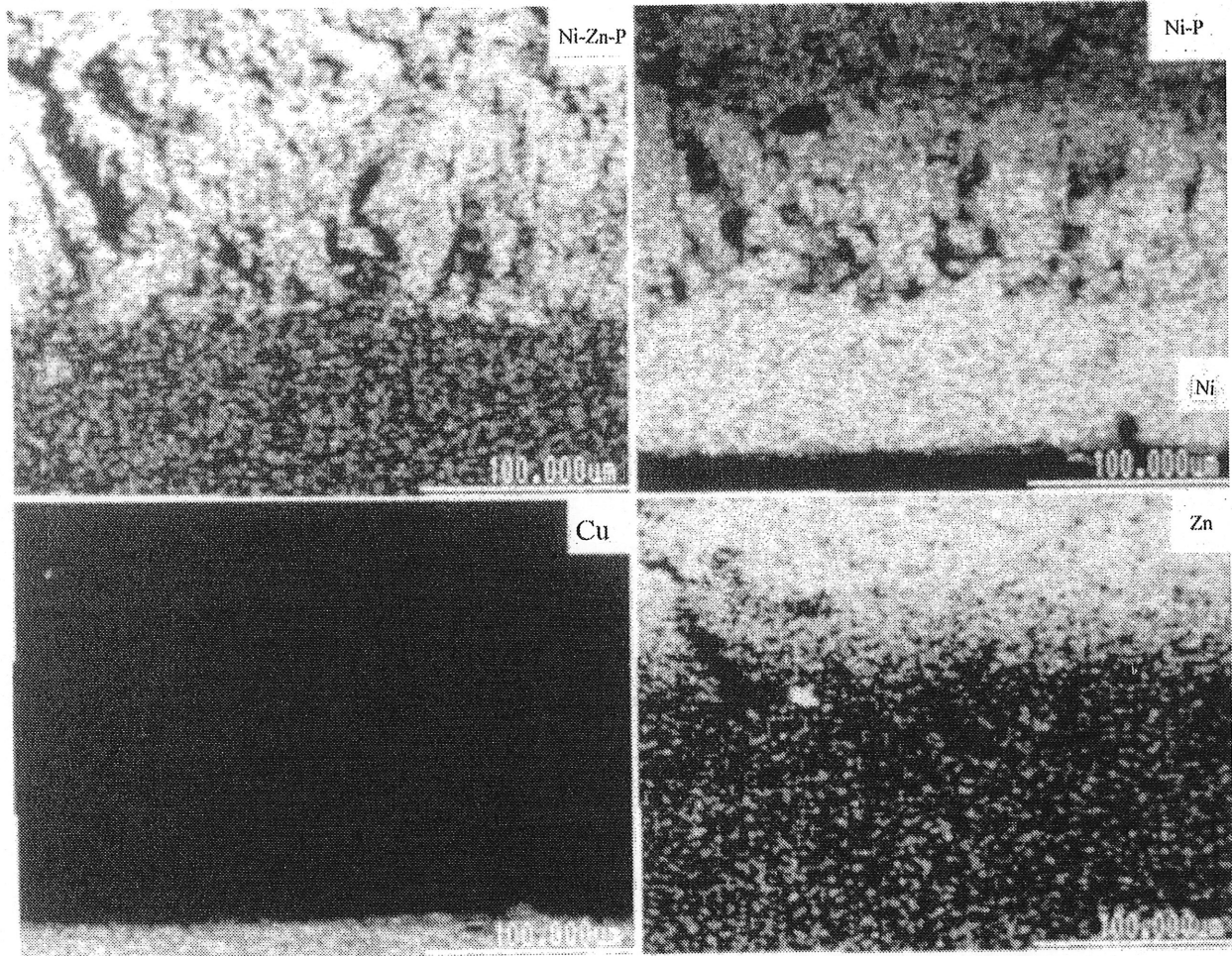


Figure 25A

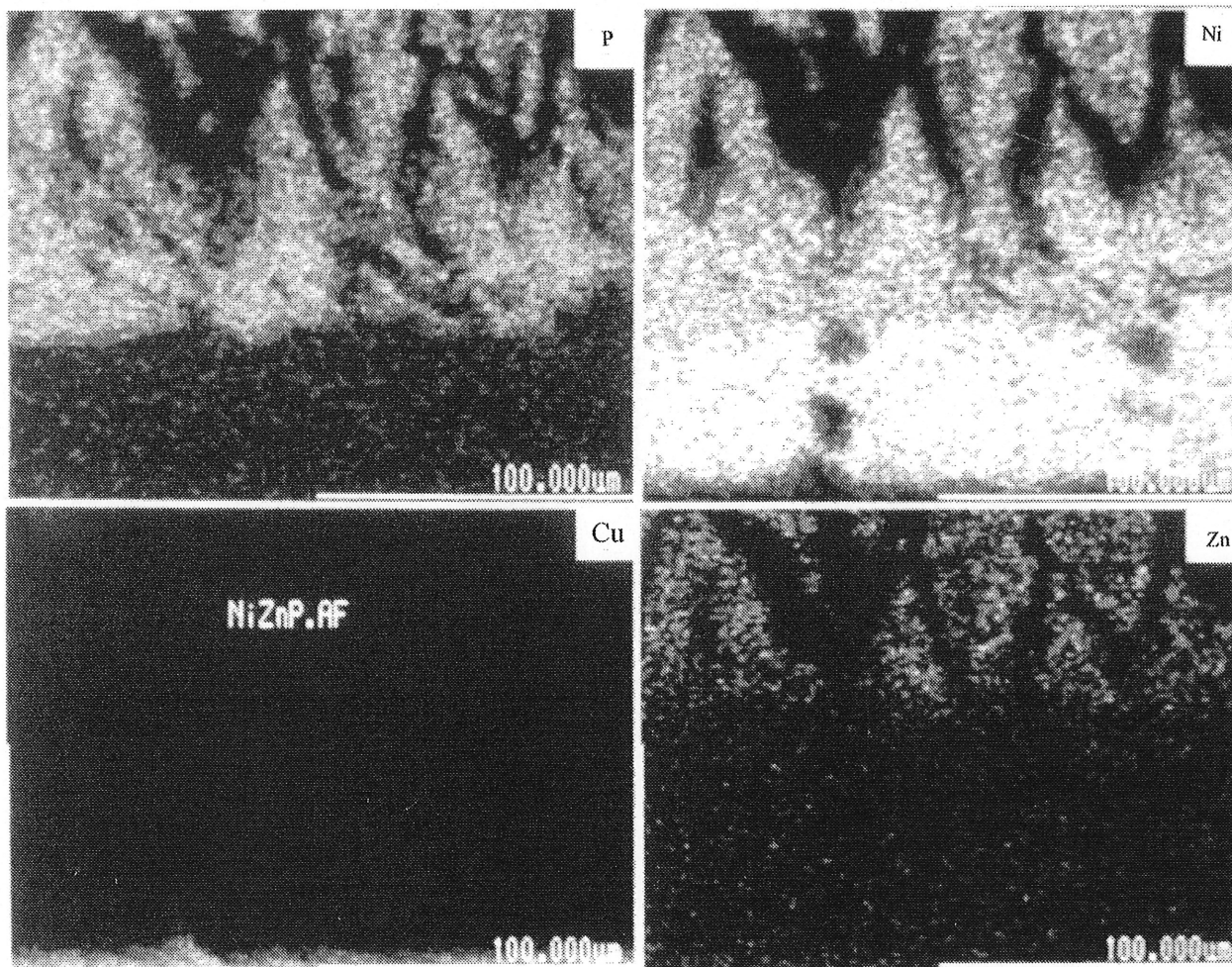


Figure 25B

Figure 25. Scanning electron micrographs prepared from the cross-section of "three-step" deposited Ni-Zn-P electrodes, (A) as-deposited, and (B) after 24h leaching at 70°C in 30% KOH. The bright regions show the alloy which is indicated on the picture.

It should be emphasized that all the electrochemical measurements on Ni-Zn-P electrodes in this thesis are performed on the electrodes after leaching in 30% KOH at 70°C, whether they have been cited or not.

6.2.2 Steady-state polarization

All Tafel curves obtained on Ni-Zn-P electrodes had only one slope in the whole potential range studied, Fig. 26. They were measured at different times after perpolarization at the constant current density, $j = 320 \text{ mA cm}^{-2}$ for a constant time period of 1800 s. It was found that the current measurements were reproducible after 24h. In Tafel curves measurements, potential was recorded 45 seconds after application of each constant current (see section 3.4.1 in chapter 3). The kinetic parameters, *i.e.*, Tafel slope, b , exchange current density, j_0 , and the overpotential at 250 mA cm^{-2} , η_{250} , are presented in Table 13 and compared with those obtained on Ni, Ni-P, and Ni-Zn electrodes in the same experimental conditions. The electrode deposited in one step from bath AA is characterized by small Tafel slope of -42 mV dec^{-1} . However, its physical stability is not good. Although the electrode worked properly and the electrochemical response was stable, it was fragile and the adhesion of the top-most layer was poor; it was possible to remove it with a knife after 10 days of polarization with $j = 130 \text{ mA cm}^{-2}$ at 25°C. The electrode prepared in three steps is also characterized by low Tafel slope which is decreasing with increase in temperature and, at 70°C, after four days of polarization, it equals -50 mV dec^{-1} and η_{250} equals -125 mV . This electrode continues to be active in 30% KOH after 8 days of polarization.

6.2.3 Electrochemical impedance spectroscopy

The EIS experiments were performed on Ni-Zn-P electrodes in the whole range of overpotential in which polarization curves were studied, *i.e.*, up to $\eta = -0.142$, corresponding to $j = 320 \text{ mA cm}^{-2}$. Very good reproducibility of results was observed. The effect of stirring

on charge transfer resistance ($A = 1 / R_{ct}$) was negligible (less than 2% at high overpotentials). Examples of the complex plane plots are displayed in Fig. 27. At high frequencies a small section of a straight line was observed on the complex plane plots followed by a semicircle. This behavior is similar to that found for porous electrodes (26,243,377,379,378,401,403).

Table 13. Kinetic parameters of the HER obtained on nickel based electrodes from the steady-state polarization curves.

Composition	Remarks	T / °C	Solution	b / mV dec ⁻¹	j ₀ / mA cm ⁻²	η ₂₅₀ mV
Ni	this work	25	1M NaOH	-165	0.02	-675
Ni ₇₀ P ₃₀	ref. 344	70	1M NaOH	-130	0.01	-576
Ni ₂₈ Zn ₇₂	ref. 42	25	1M NaOH	-69	0.31	-206
Ni ₅₅ Zn ₃₈ P ₇	one step*	25	1M NaOH	-42	0.13	-125
Ni ₅₄ Zn ₂₀ P ₂₆	three steps***	25	1M NaOH	-58	0.23	-176
Ni ₅₄ Zn ₂₀ P ₂₆	A***	70	1M NaOH	-50	0.72	-125
Ni ₅₄ Zn ₂₀ P ₂₆	B***	70	30% KOH	-47	0.11	-157
Ni ₅₆ Zn ₂₇ P ₁₇	one step**	25	1M NaOH	-53	0.33	-153

* deposited in one step from bath AA; ** deposited in one-step from bath C; *** deposited in three steps; A - after 4 days of polarization at $j = 320 \text{ mA cm}^{-2}$. B - after 8 days polarization at $j = 500 \text{ mA cm}^{-2}$.

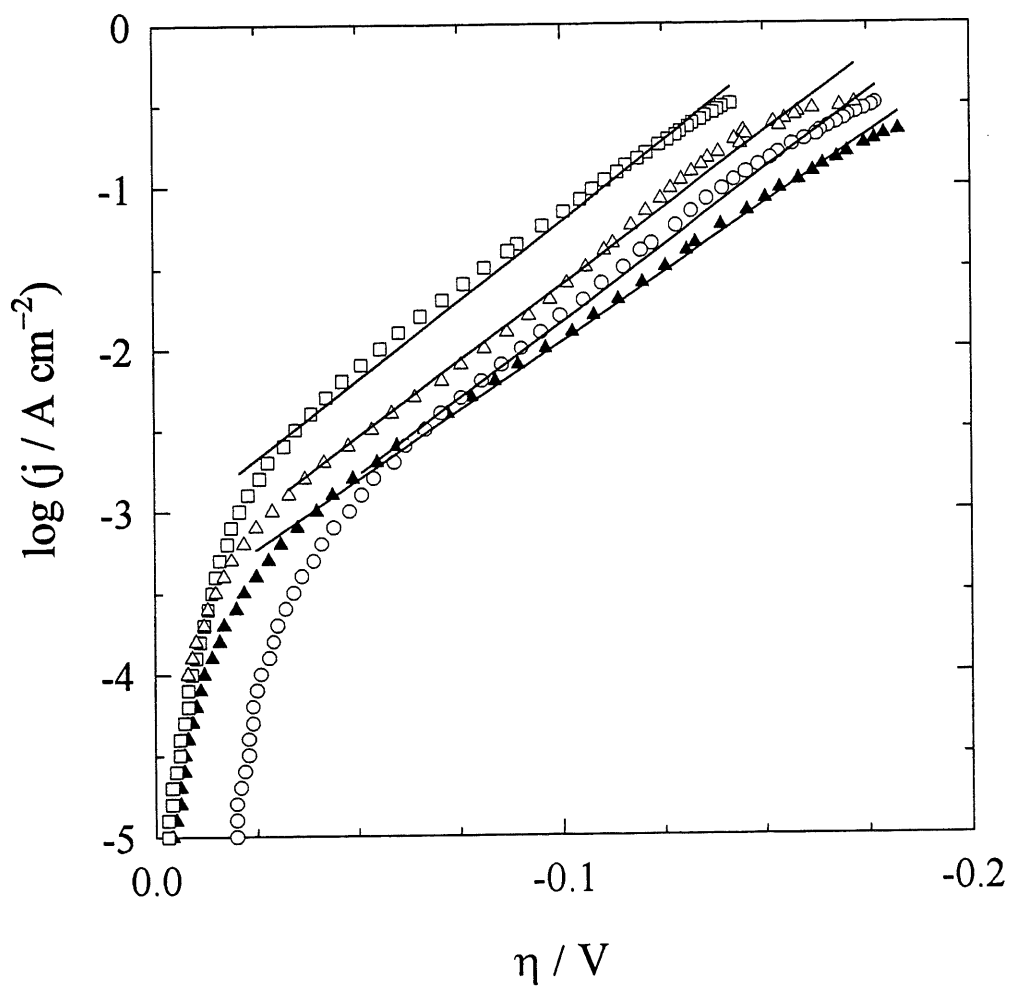


Figure 26. Steady-state polarization curves obtained for the HER on “three-step” deposited $\text{Ni}_{54}\text{Zn}_{20}\text{P}_{26}$ electrodes (after leaching in 30% KOH at 70°C for 24h): (\blacktriangle) in 1 M NaOH at 25°C , (\square) in 1 M NaOH at 70°C , (O) after 8 days activation in 30% KOH at 70°C , (\triangle) in 1 M NaOH at 25°C on “one-step” deposited $\text{Ni}_{56}\text{Zn}_{27}\text{P}_{17}$. The continued lines are obtained using linear regression method.

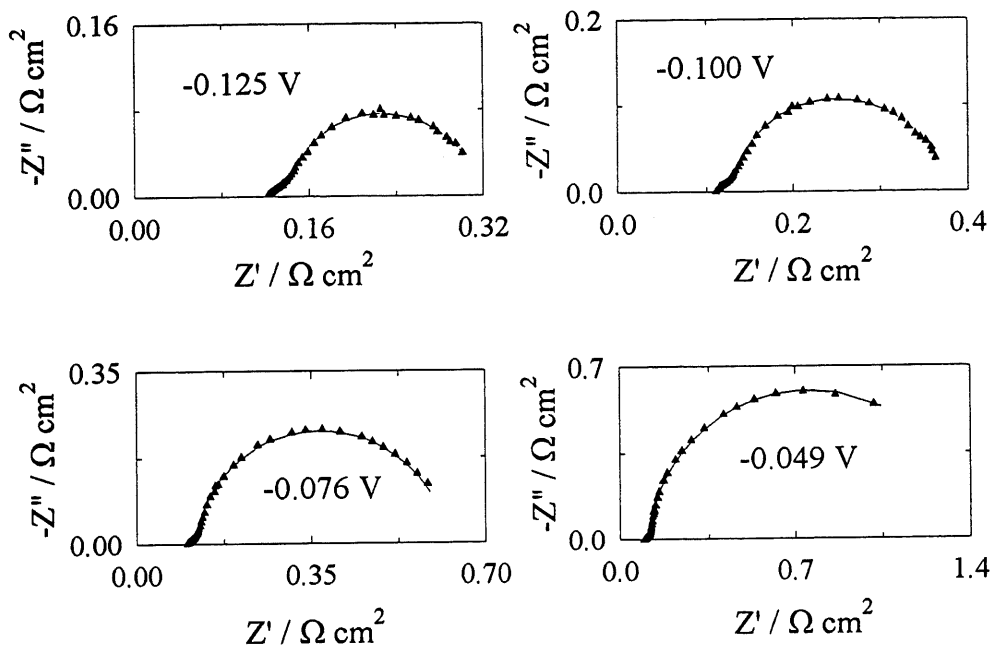


Figure 27A

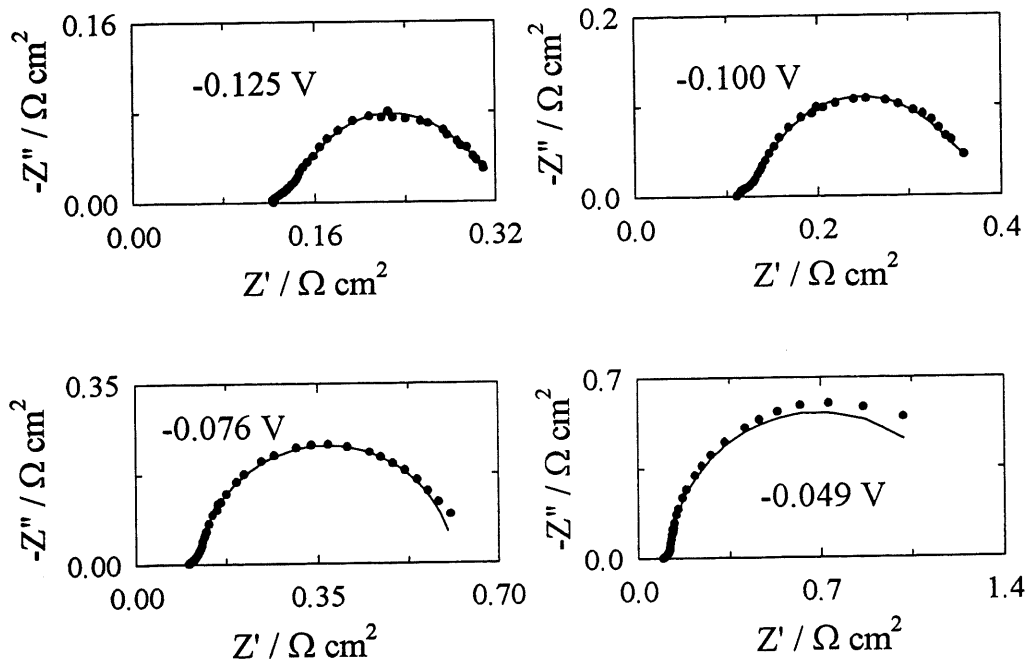


Figure 27B

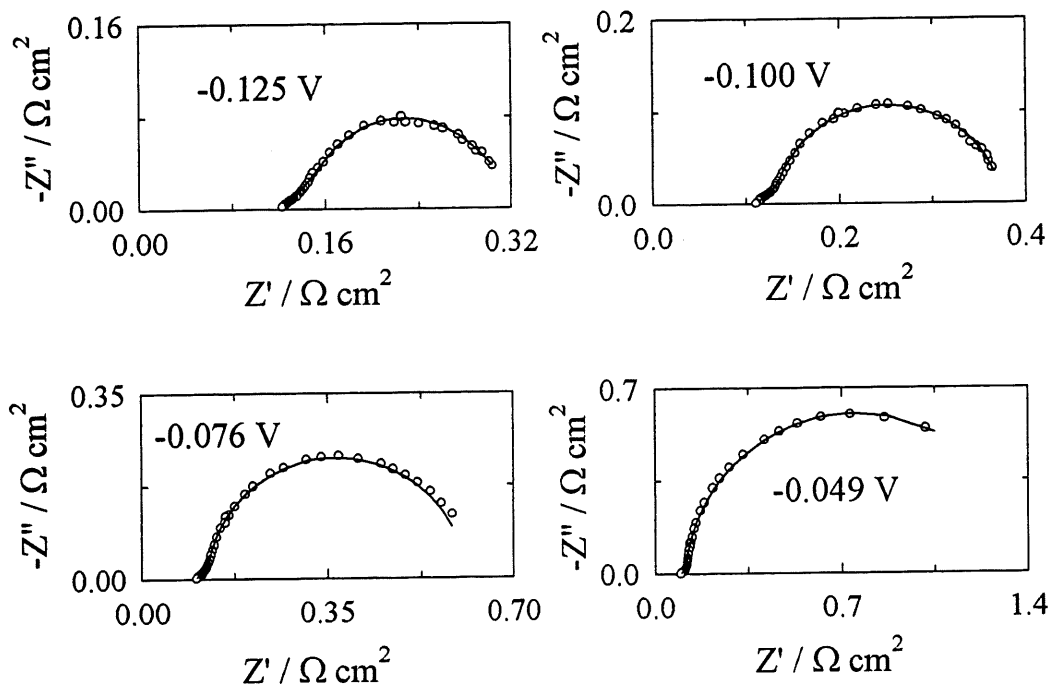


Figure 27C

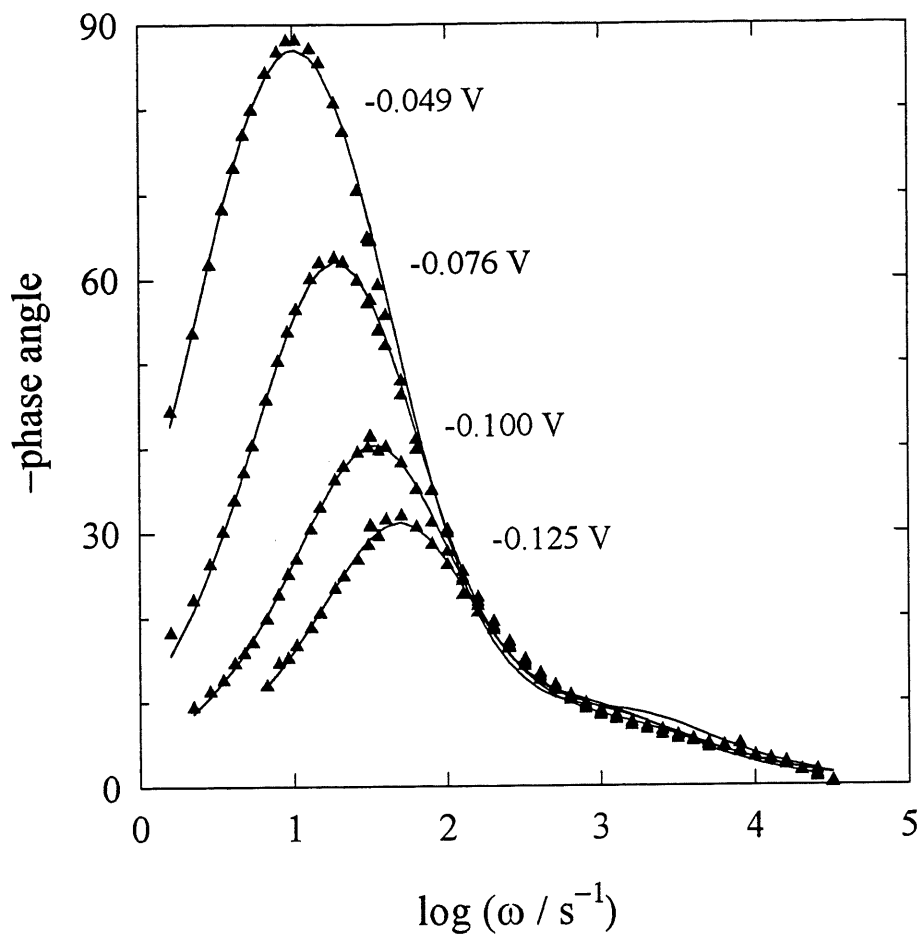


Figure 27D

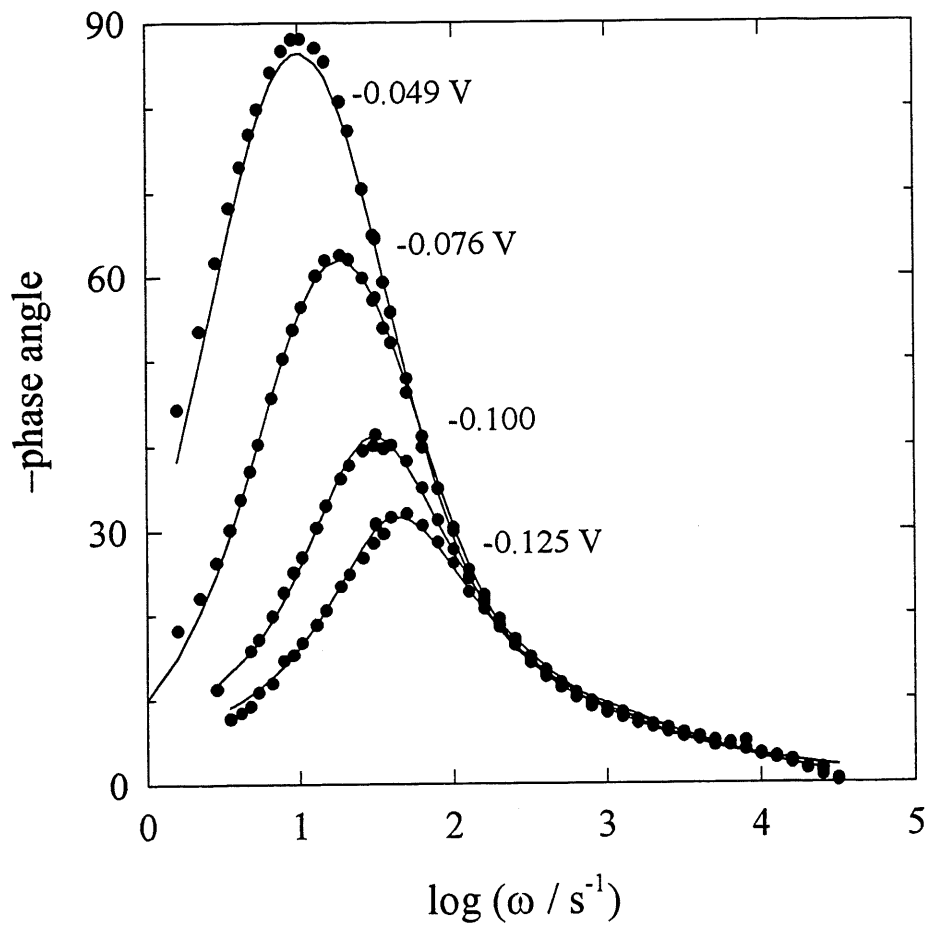


Figure 27E

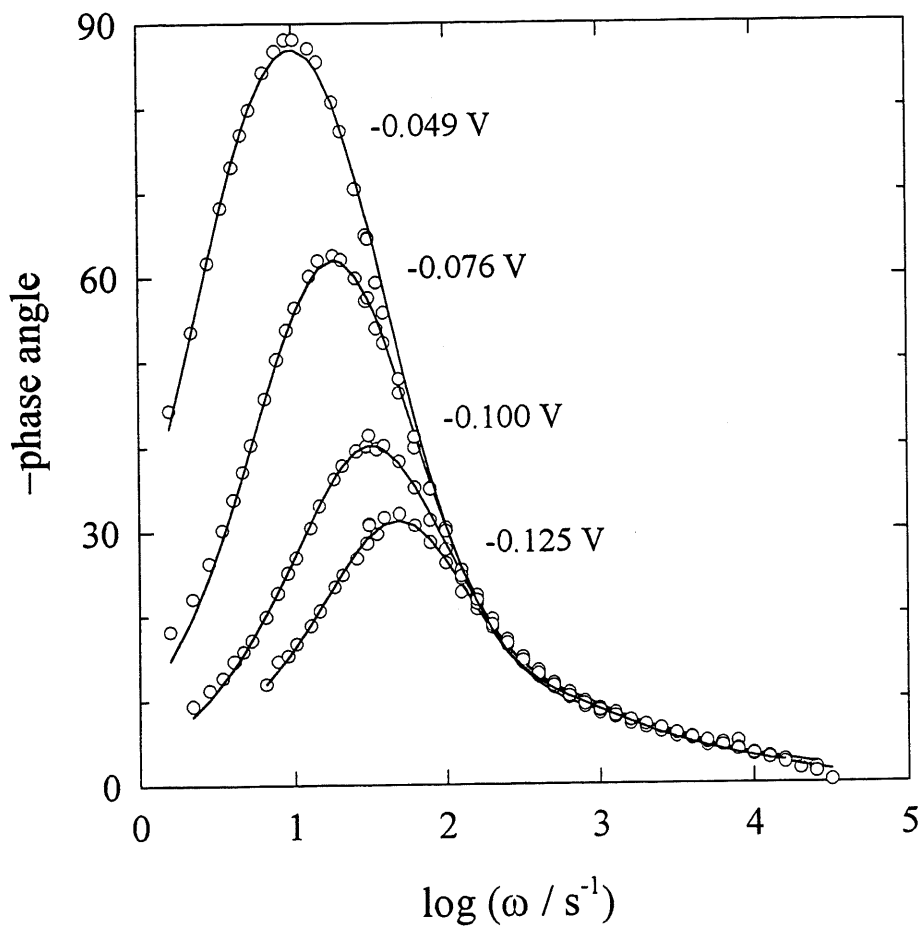


Figure 27F

Figure 27. Complex plane plots, $-Z''$ vs. Z' , and Bode plot, phase angle vs. $\log \omega$ ($\omega = 2\pi f$) for the HER obtained on “three-step” deposited $\text{Ni}_{54}\text{Zn}_{20}\text{P}_{26}$ electrodes in 1 M NaOH at 70°C and using CPE (A,D), two-CPE (B,E), and porous (C,F) models. The continued lines are obtained from fitted data CNLS method.

6.2.4 Model selection (criteria)

There is an ambiguity in selecting the model (42,106,121,123,379) when the EIS experimental data can be fitted to different models (equivalent circuits), especially when the values of standard deviations of the parameters obtained from different models are similar (407). The way is the validation of experimental data by K-K transformation, fitting the valid data to the models, comparing the quality of fit, the values of the standard deviation of parameters obtained from fitting data to equivalent circuits in all the range of overpotential and temperature, then selecting the model containing smaller number of parameters if all other conditions are the same (372,407-409). In some cases this method has not been followed by some authors instead, they have used their own procedure for model selection (410a). A more practical and simple way was followed in our lab (26,192). It is based on simultaneous fitting the experimental kinetic data of the HER obtained by two techniques, the steady-state polarization and the EIS, see eqns. [2.49], [2.54], and [2.98] in chapter 2. This is practically interesting. If model for the EIS experimental data fitting, or assumed mechanism for the HER are wrong, or data have been acquired in non-steady-state, it is usually impossible to get a good fit with acceptable values of parameters and their standard deviations.

In our study here we have compared the number of adjustable parameters of equivalent circuits, and their standard deviations as functions of variable, *e.g.*, η .

Three models were selected, CPE, two-CPE, and porous. These models have been used generally to explained the behavior of porous electrodes (26,42,43,121-124,192,243). The EIS experimental data were fitted to these models and the parameters with their standard deviations were extracted using CNLS program (372,373,404,409). Figs. 27A to F show the complex plane plots, Z' vs. Z'' , and Bode plots, phase angle vs. $\log \omega$ ($\omega = 2\pi f$).

There are no statistical differences in the values of S_F which are 1.45×10^{-3} , 1.37×10^{-3} , and 1.21×10^{-3} for porous, two-CPE, and CPE models, respectively, the parameter indicating the quality of the fits ($S_F = \sum_{i=1}^k \left\{ \left| \frac{Z'_{ei} - Z'_{ci}}{Z'_{ei}} \right|^2 + \left| \frac{Z''_{ei} - Z''_{ci}}{Z''_{ei}} \right|^2 \right\}$ where k is number of data points, Z'_{ci} and Z''_{ci} are the values of Z' and Z'' calculated for each point and, Z'_{ei} and Z''_{ei} are the corresponding experimental values for each point) (372).

Table 14. Parameters values and their standard deviations obtained using the CPE model to approximate the EIS data obtained on $Ni_{54}Zn_{20}P_{26}$ electrode in 1 M NaOH at 70°C.

$-\eta / V$	$A / \Omega^{-1} cm^{-2}$	$-B / \Omega^{-1} cm^{-2} s^{-1}$	C / s^{-1}	$R_s \Omega cm^2$	$T / F cm^{-2} s^{-\phi-1}$	ϕ
0.135	24.0 ± 1.7	$(4.88 \pm 0.88) \cdot 10^3$	294 ± 28	0.140 ± 0.001	0.29 ± 0.02	0.67 ± 0.02
0.130	25.7 ± 1.9	$(6.0 \pm 1.0) \cdot 10^3$	312 ± 28	0.131 ± 0.001	0.25 ± 0.02	0.70 ± 0.02
0.125	27.3 ± 0.9	$(6.04 \pm 0.45) \cdot 10^3$	287 ± 12	0.130 ± 0.001	0.19 ± 0.02	0.74 ± 0.02
0.116	26.9 ± 0.9	$(5.98 \pm 0.45) \cdot 10^3$	274 ± 11	0.120 ± 0.001	0.18 ± 0.01	0.75 ± 0.01
0.109	26.1 ± 0.8	$(5.48 \pm 0.35) \cdot 10^3$	247 ± 8	0.120 ± 0.001	0.16 ± 0.01	0.78 ± 0.01
0.100	27.8 ± 1.0	$(5.22 \pm 0.38) \cdot 10^3$	213 ± 8	0.108 ± 0.001	0.18 ± 0.01	0.77 ± 0.01
0.092	28.8 ± 1.0	$(6.52 \pm 0.47) \cdot 10^3$	258 ± 9	0.115 ± 0.001	0.16 ± 0.01	0.78 ± 0.01
0.080	26.3 ± 0.9	$(4.88 \pm 0.34) \cdot 10^3$	216 ± 8	0.112 ± 0.001	0.18 ± 0.01	0.76 ± 0.01
0.076	28.9 ± 1.0	$(5.20 \pm 0.37) \cdot 10^3$	197 ± 7	0.105 ± 0.001	0.15 ± 0.01	0.80 ± 0.01
0.067	30.5 ± 1.6	$(5.63 \pm 0.57) \cdot 10^3$	197 ± 10	0.103 ± 0.001	0.14 ± 0.01	0.83 ± 0.01
0.058	35.2 ± 2.6	$(6.35 \pm 0.98) \cdot 10^3$	186 ± 16	0.970 ± 0.001	0.11 ± 0.01	0.82 ± 0.02
0.049	35.7 ± 2.9	$(6.2 \pm 1.1) \cdot 10^3$	178 ± 17	0.10 ± 0.001	0.10 ± 0.01	0.83 ± 0.02

Apparently good agreement was observed between the EIS experimental data and model using CPE model (26,106,123,243), Fig. 27 and D, but the standard deviations were somewhat large, around 10%, Table 14.

Also using two-CPE (121,123) model it was observed that the EIS experimental data can be fitted very well, Fig. 27B. Logarithm of A_2 changed linearly with overpotential while the values of A_1 parameter were constant only for overpotentials lower than -0.09V, Table 15. This is in contradiction with the main supposition of this model that the A_1 is constant in the whole range of overpotential, and is not affected by the pore texture (26,121,123,243,378,379).

The EIS experimental data also agreed very well with modified de Levie porous model, eqns. [2.93] and [2.94], chapter 2. The real and imaginary components, Z' and Z'' , of the electrode impedance obtained in the whole range of frequencies at various overpotentials were analyzed (372,373,404,409), Fig. 27C and F. All the parameters were defined earlier in chapter 2 and their values are presented in Table 16.

The standard deviations of the parameters of CPE model (Table 14) in some cases, (parameters B and C) are relatively large. For two-CPE model (Table 15) they are lower than those of CPE model, but yet in some cases they are large (parameters A_1 and T_1). For the porous model (Table 16) the maximum error is observed for A_p . They are around 5% which is relatively lower than those observed for CPE and two-CPE. In all other cases the errors for porous model are relatively small (around 1%). This may let to select (407) porous model, but with caution.

The number of adjustable parameters in each model is different, the porous model contains 5 (R_s , $R_{\Omega,p}$, A_p , B_p , ϕ), the one CPE model contains 6 (R_s , T , ϕ , A, B, C), and the two-CPE model contains 7 (R_s , T_1 , ϕ_1 , A_1 , T_2 , ϕ_2 , A_2) parameters. In the case of a similar quality of fit, a

model containing the smallest number of parameters should be selected. This also let to select the porous model.

Table 15. Parameters values and their standard deviations obtained using the two-CPE model to approximate the EIS data obtained on Ni₅₄Zn₂₀P₂₆ electrode in 1 M NaOH at 70°C.

$-\eta$ / V	A_1 / $\Omega^{-1} \text{ cm}^{-2}$	A_2 / $\Omega^{-1} \text{ cm}^{-2}$	R_s / $\Omega \text{ cm}^2$	T_1 / $\text{F cm}^{-2} \text{ s}^{\phi_1}$	ϕ_1	T_2 / $\text{F cm}^{-2} \text{ s}^{\phi_2}$	ϕ_2
0.142	11.36 ± 0.62	37.0 ± 5.9	0.138 ± 0.001	0.28 ± 0.01	0.93 ± 0.02	0.39 ± 0.14	0.64 ± 0.05
0.139	8.14 ± 0.12	69.1 ± 6.2	0.136 ± 0.001	0.33 ± 0.01	0.84 ± 0.01	0.090 ± 0.03	0.86 ± 0.05
0.135	8.53 ± 0.39	37.4 ± 7.7	0.130 ± 0.001	0.261 ± 0.01	0.94 ± 0.02	0.42 ± 0.24	0.64 ± 0.08
0.130	8.41 ± 0.95	11.8 ± 0.7	0.122 ± 0.001	3.23 ± 0.48	0.35 ± 0.03	0.25 ± 0.01	1.04 ± 0.02
0.125	9.23 ± 0.69	7.97 ± 0.42	0.118 ± 0.001	3.59 ± 0.70	0.36 ± 0.04	0.26 ± 0.01	1.00 ± 0.02
0.116	12.1 ± 1.1	5.08 ± 0.15	0.113 ± 0.001	4.01 ± 0.56	0.34 ± 0.04	0.27 ± 0.01	0.97 ± 0.01
0.106	8.4 ± 1.4	4.30 ± 0.11	0.106 ± 0.001	6.4 ± 1.3	0.26 ± 0.05	0.26 ± 0.01	0.97 ± 0.01
0.100	6.45 ± 0.51	5.63 ± 0.17	0.107 ± 0.001	4.50 ± 0.61	0.33 ± 0.03	0.29 ± 0.01	1.01 ± 0.01
0.092	55.6 ± 6.3	3.49 ± 0.03	0.109 ± 0.001	0.11 ± 0.07	0.81 ± 0.09	0.29 ± 0.01	0.92 ± 0.01
0.080	44.8 ± 5.2	2.68 ± 0.02	0.103 ± 0.002	0.23 ± 0.11	0.70 ± 0.08	0.28 ± 0.01	0.95 ± 0.01
0.076	51.8 ± 9.5	2.01 ± 0.01	0.101 ± 0.002	0.26 ± 0.21	0.71 ± 0.13	0.29 ± 0.01	0.95 ± 0.01
0.067	48.5 ± 5.8	1.49 ± 0.01	0.099 ± 0.002	0.18 ± 0.12	0.76 ± 0.10	0.29 ± 0.01	0.96 ± 0.01
0.058	65 ± 12	1.08 ± 0.01	0.097 ± 0.002	0.08 ± 0.09	0.90 ± 0.17	0.30 ± 0.02	0.96 ± 0.01
0.049	64 ± 12	0.78 ± 0.01	0.094 ± 0.003	0.08 ± 0.09	0.92 ± 0.18	0.30 ± 0.01	0.96 ± 0.01
0.039	36.7 ± 2.2	0.10 ± 0.01	0.093 ± 0.001	0.64 ± 0.15	0.62 ± 0.04	0.28 ± 0.01	1.01 ± 0.01

Table 16. Parameters values and their standard deviations obtained using porous model to approximation the EIS data obtained on Ni₁₅₄Zn₂₀P₂₆ electrode in 1 M NaOH at 70°C.

$-\eta$ / V	A_p	B_p / $1 \cdot 10^{-2} s^\phi$	ϕ	$R_{\Omega,p}$ / $1 \cdot 10^{-2} \Omega cm^2$	R_s / $1 \cdot 10^{-2} \Omega cm^2 *$
0.139	1.80 ± 0.12	(2.10 ± 0.08)	0.87 ± 0.02	6.5 ± 0.3	13.0 ± 0.1
0.135	1.77 ± 0.12	(1.70 ± 0.09)	0.93 ± 0.01	6.9 ± 0.4	13.0 ± 0.1
0.130	2.39 ± 0.15	(1.80 ± 0.07)	0.89 ± 0.01	6.3 ± 0.3	13.0 ± 0.1
0.125	2.63 ± 0.11	(1.60 ± 0.05)	0.93 ± 0.01	6.6 ± 0.2	12.0 ± 0.1
0.116	3.88 ± 0.15	(1.60 ± 0.06)	0.92 ± 0.01	6.2 ± 0.2	12.0 ± 0.1
0.109	4.84 ± 0.22	(1.50 ± 0.06)	0.92 ± 0.01	5.7 ± 0.3	11.0 ± 0.1
0.100	3.92 ± 0.19	(1.80 ± 0.08)	0.92 ± 0.01	6.3 ± 0.4	11.0 ± 0.1
0.092	4.72 ± 0.25	(1.80 ± 0.08)	0.92 ± 0.01	6.1 ± 0.3	11.0 ± 0.1
0.080	5.91 ± 0.25	(1.80 ± 0.07)	0.95 ± 0.01	6.4 ± 0.3	10.0 ± 0.1
0.076	7.92 ± 0.33	(1.80 ± 0.07)	0.95 ± 0.01	6.2 ± 0.3	10.0 ± 0.1
0.067	11.10 ± 0.60	(1.80 ± 0.09)	0.96 ± 0.01	6.0 ± 0.3	10.0 ± 0.1
0.058	15.3 ± 1.1	(1.70 ± 0.11)	0.97 ± 0.01	5.8 ± 0.4	10.0 ± 0.2
0.049	23.4 ± 2.7	(1.60 ± 0.18)	0.96 ± 0.01	5.5 ± 0.6	10.0 ± 0.2

$A_p = a R_{ct}$, $B_p = T / a$, $a = r / 2\rho l$, and $R_{\Omega,p} = \rho l / \pi r^2$, r - pore radius, l - pore length, ρ - specific resistance of the solution (192,243,378,379).

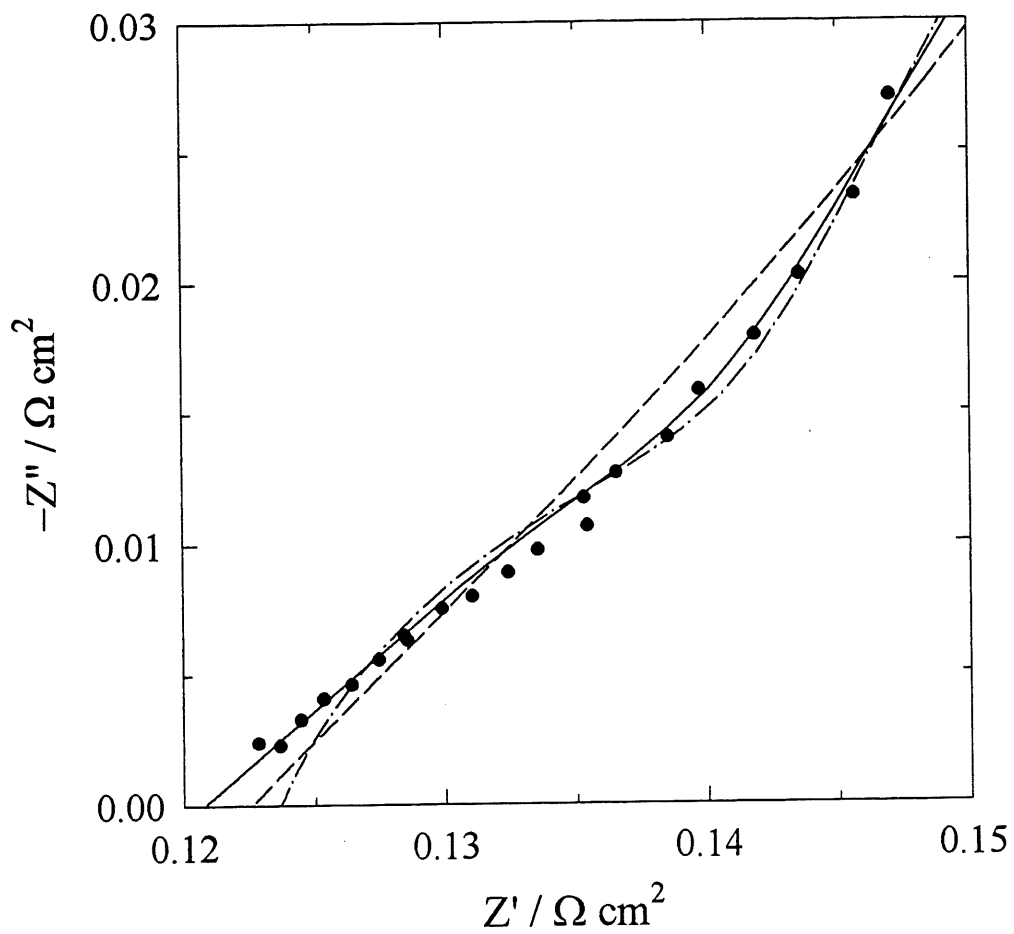


Figure 28A

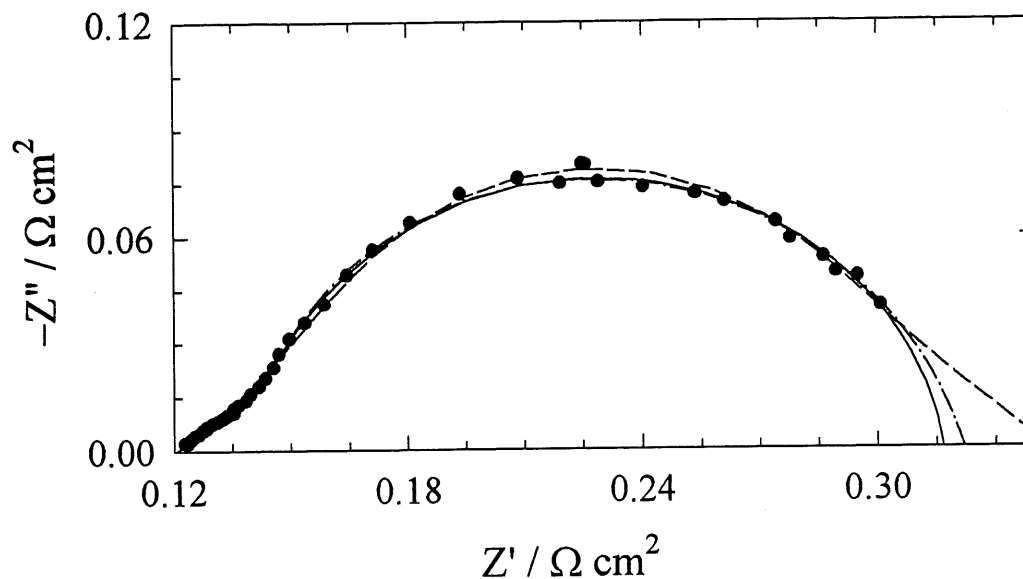


Figure 28B

Figure 28. Complex plane plots obtained on $\text{Ni}_{54}\text{Zn}_{20}\text{P}_{26}$ electrode at $\eta = -0.125$ V, in 1 M NaOH at 70°C , fitted to different models: continuous line - porous model, dashed line - "two-CPE" model, dashed-dotted line - "one CPE" model; (A) in high frequencies range and (B) in the whole range of frequencies.

The one CPE model led to the charge transfer resistances almost independent of overpotential. Besides, their values were often very small and determined with large errors because the high frequency feature was relatively small at more positive potentials. It is very unlikely that this feature corresponds to the charge transfer resistance. The two-CPE and porous models usually produced similar values of the charge transfer resistances, however, the

former sometimes gave worse approximations. Fig. 28 presents an example of the CNLS approximation of impedances obtained in 1 M NaOH at $\eta = -0.125$ V at 70°C on the electrode deposited in three steps. The high frequency part, Fig. 28A, of the plot contains systematic differences for the CPE and two-CPE models. The low frequency part, Fig. 28B, is deformed in the two-CPE model and the value of the parameter ϕ is much larger than 1 (for the low frequency semicircle). Therefore, in further approximations the porous model was used.

The results obtained in 1 M NaOH at 70°C on the electrode prepared in three steps are presented in Table 17. They show that the CPE parameter $\phi \geq 0.92$ except the highest overpotentials where the diffusion starts to change from finite pore length to semi-infinite pore model. The parameter $R_{\Omega,P}$ is practically constant confirming the validity of the model. Using the obtained parameters the charge transfer resistances, values of parameter T and the double layer capacitances were determined (379).

Fig. 29 presents the parameter ϕ and the double layer capacitance as functions of the overpotential. The values of the parameter ϕ , Fig. 29A, for the electrode deposited in three steps are close to one at 25°C. They decrease to ~ 0.92 – 0.96 at higher temperature (70°C). For the electrode deposited in one step they are also close to one. It has been suggested that deviation of the parameter ϕ from one is connected with the surface roughness, however, recent papers indicate that it may also be connected with ionic adsorption (376).

The double layer capacitances obtained on the electrode prepared in three steps, Fig. 29B, are practically potential independent, the average value at 70°C is 0.25 F cm^{-2} with the standard deviation 0.02 F cm^{-2} . At 25°C \bar{C}_{dl} values are slightly lower, 0.21 F cm^{-2} and after 8 days polarization in 30% KOH are $\sim 0.16 \text{ F cm}^{-2}$. Only the electrode prepared in one step from bath C shows double layer capacitances about four times larger than those on the electrodes prepared in three steps. Assuming that the average double layer capacitance of a smooth metal

surface is $20 \mu\text{F cm}^{-2}$ the surface roughness may be estimated as: $R = \bar{C}_{dl} / 20 \mu\text{F cm}^{-2}$ (26,42,192,123,243).

Table 17. Kinetic parameters obtained using porous model data in Table 16.

$-\eta / \text{V}$	$R_{ct} = A_p R_{\Omega,p} / \Omega \text{ cm}^2$	$T = (B_p / R_{\Omega,p}) / \text{F cm}^2 \text{ s}^{\phi-1}$	$\bar{C}_{dl} / \text{F cm}^{-2}$
0.139	0.11719	0.30915	0.25
0.135	0.12165	0.25148	0.22
0.130	0.15057	0.28707	0.24
0.125	0.17186	0.24905	0.22
0.116	0.23732	0.25823	0.23
0.109	0.27634	0.25764	0.23
0.100	0.24453	0.28923	0.25
0.092	0.28674	0.29285	0.26
0.080	0.37511	0.28024	0.26
0.076	0.49033	0.28101	0.26
0.067	0.67818	0.28631	0.27
0.058	0.89267	0.29196	0.28
0.049	1.28270	0.29781	0.28

The average surface roughness of the electrode prepared in three steps is 1.25×10^4 , 1.1×10^4 and 8×10^3 at 70°C and 25°C in 1 M NaOH and at 70°C in 30% KOH, respectively (and 4.6×10^4 for one step deposited from bath C). It is larger than those found for Ni-Zn

electrodes ($R = 1-1.25 \times 10^3$) (28,42,147), but smaller than those for Ni-Al electrodes (44,106,121). At higher temperature, the surface roughness is larger, indicating better accessibility of pores by the solution. It is smaller in more viscous 30% KOH.

An approximation of the dependence of charge transfer resistance ($A = 1 / R_{ct}$) and j as functions of η , was carried out by adjusting the rate constants k_1 , k_{-1} , k_2 and transfer coefficients, β_1 and β_2 , using NLS method and assuming the Volmer-Heyrovský mechanism. A big gap between fitted and experimental data with very small and unacceptable value for β_1 and β_2 (0.04 and 0.07×10^{-7}) was observed when the data of CPE model were used in eqn. [2.98]. However, when data of two-CPE model were used, A_2 , in eqn [2.98]. the fit was good, but the values obtained were unreal (1.00 ± 0.07 and 1.11 ± 0.64 for β_1 and β_2). Better approximation was observed when charge transfer resistance, $1 / A = R_{ct}$, from porous model was used, (Figs. 30, and 31). The kinetic parameters together with their stds are presented in Table 18. Even in this case the transfer coefficients are approaching one and unacceptable. The reason may be discussed as following.

The dependence of the logarithm of the charge transfer resistance on overpotential is shown in Fig. 31. This dependence is linear with the slope of -75 and -89 mV dec^{-1} at 25 and 70°C in 1 M NaOH and -73 mV dec^{-1} in $30\% \text{ KOH}$. These slopes are slightly larger than the Tafel slopes, Table 13. The slopes obtained on the electrode prepared in one step from bath C are identical, -53 mV dec^{-1} . All these logarithmic slopes are much lower than those predicted for the Volmer-Heyrovský reaction mechanism (-120 mV dec^{-1}) (26). Because of the small Tafel and charge transfer resistance slopes the approximation led to unrealistic, close to unity, values of charge transfer coefficients. Such slopes cannot be explained in terms of the Volmer-Heyrovský-Tafel reaction mechanism. They may indicate Temkin isotherm for the hydrogen adsorption or the distributed kinetics (16,199,200).

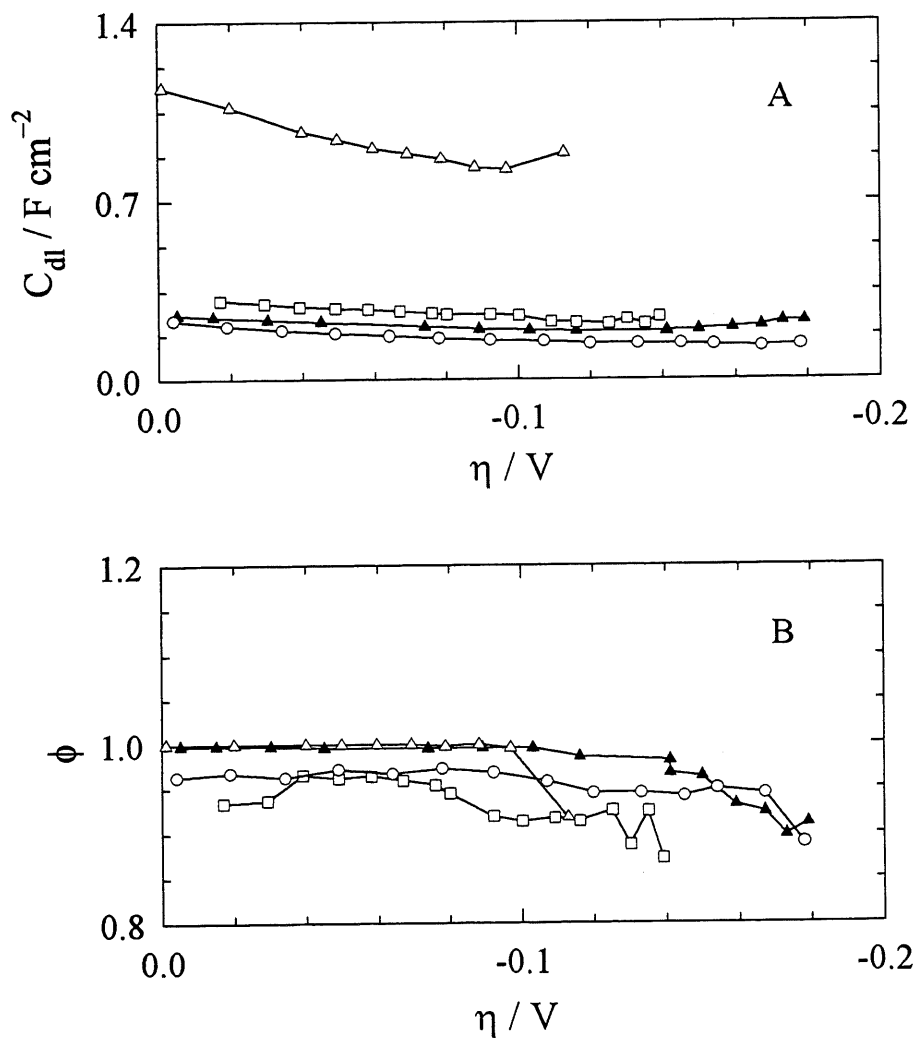


Figure 29. Dependence of (A) the average of double layer capacitance, \bar{C}_{dl} , and (B) parameter ϕ on overpotential obtained for the HER on "three-step" deposited $\text{Ni}_{54}\text{Zn}_{20}\text{P}_{26}$, (\blacktriangle) in 1 M NaOH at 25°C, (\square) in 1 M NaOH at 70°C, (\circ) after 8 days activation in 30% KOH at 70°C, (Δ) on "one-step" deposited $\text{Ni}_{56}\text{Zn}_{27}\text{P}_{17}$ in 1 M NaOH at 25°C (porous model was used in all these cases).

Table 18. Kinetic parameters for the HER obtained from the steady-state polarization and the EIS measurements on Ni-Zn-P electrodes, using porous model.

Electrode*	k_1 mol cm ⁻² s ⁻¹	k_{-1} mol cm ⁻² s ⁻¹	k_2 mol cm ⁻² s ⁻¹	β_1	β_2
A	$(6.79 \pm 0.62) \cdot 10^{-9}$	$(1.5 \pm 1.7) \cdot 10^{-6}$	$(1.26 \pm 0.89) \cdot 10^{-7}$	0.77 ± 0.38	0.50**
B	$(7.02 \pm 0.38) \cdot 10^{-8}$	$(7.6 \pm 3.5) \cdot 10^{-6}$	$(3.4 \pm 2.2) \cdot 10^{-7}$	0.78 ± 0.03	0.61 ± 0.05
C	$(1.55 \pm 0.14) \cdot 10^{-8}$	$(1.50 \pm 0.70) \cdot 10^{-6}$	$(3.3 \pm 2.9) \cdot 10^{-8}$	0.96 ± 0.05	0.77 ± 0.10
D	$(5.9 \pm 1.1) \cdot 10^{-9}$	$(4.9 \pm 2.1) \cdot 10^{-7}$	$(1.03 \pm 0.17) \cdot 10^{-7}$	1.00 ± 0.05	0.50**

*: The “three-step” deposited Ni₅₄Zn₂₀P₂₆ electrodes (after leaching in 30% KOH at 70°C for 24h): (A) in 1 M NaOH at 25°C, (B) in 1 M NaOH at 70°C, (C) after 8 days activation in 30% KOH at 70°C; and (D) in 1 M NaOH at 25°C on “one-step” deposited Ni₅₆Zn₂₇P₁₇ electrode.

** : β_2 was fixed.

6.2.5 Electrode oxidation

The Ni-Zn-P electrodes were also cycled between 0.6 to -1.2 V vs. Hg/HgO at 25 and 70°C in 1 M NaOH. The shape of cyclic voltammograms was similar to that observed for unheated Ni-P electrodes, Fig. 32, (see also chapter 4). Cyclic voltammograms at different sweep rates were used to estimate the double layer capacitance. These measurements were carried out between -0.1 and -0.6 V and C_{dl} estimated from $j_{dl} = C_{dl} \nu$, where ν is the scan-rate. The dependence of j as a function of ν was linear. The slopes, $dj_{dl} / d\nu$, obtained on the electrode deposited in three steps, are 0.036 and 0.128 F cm⁻² at 25 and 70°C, respectively. The corresponding double layer capacitance values are 7 and 2 times smaller than those obtained

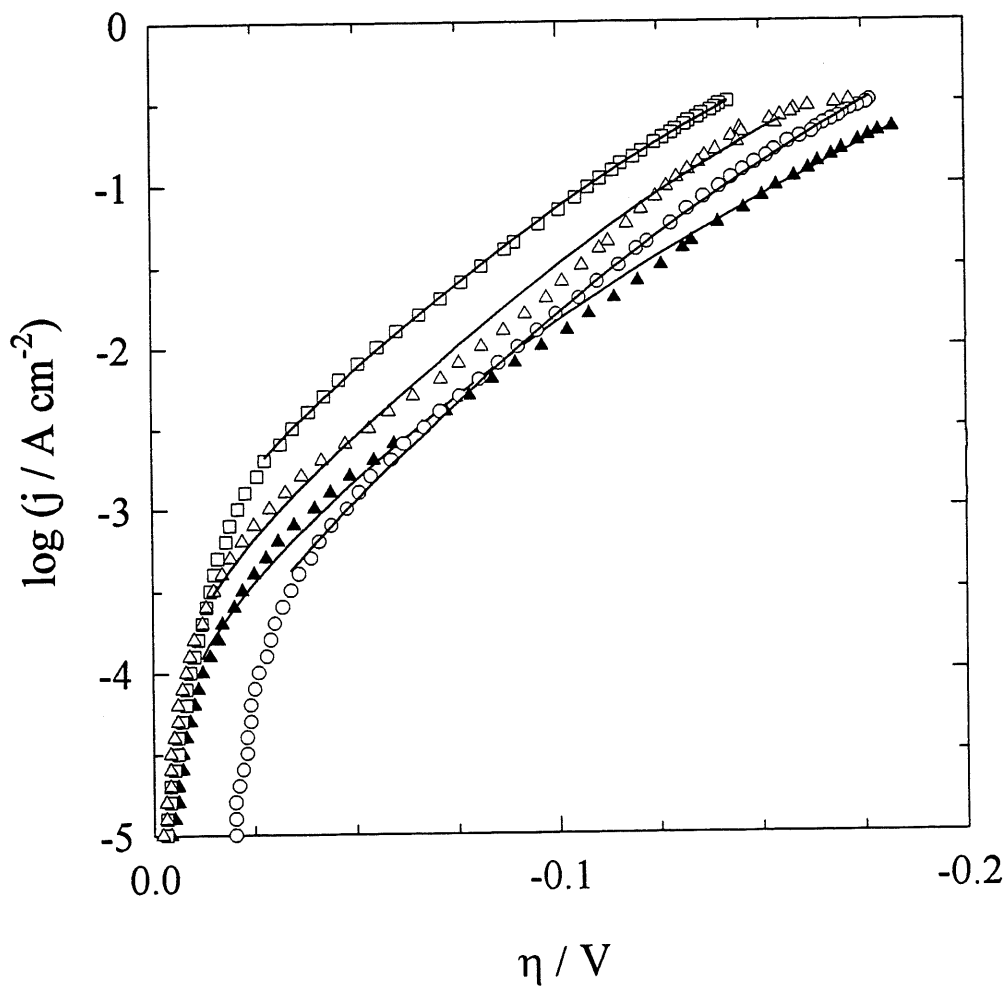


Figure 30. Steady-state polarization curves obtained for the HER on “three-step” deposited $\text{Ni}_{54}\text{Zn}_{20}\text{P}_{26}$ electrode, (▲) in 1 M NaOH at 25°C, (□) in 1 M NaOH at 70°C, (O) after 8 days activation in 30% KOH at 70°C, (Δ) in 1 M NaOH at 25°C on “one-step” deposited $\text{Ni}_{56}\text{Zn}_{27}\text{P}_{17}$. The continued lines are obtained from fitted data using NLS method.

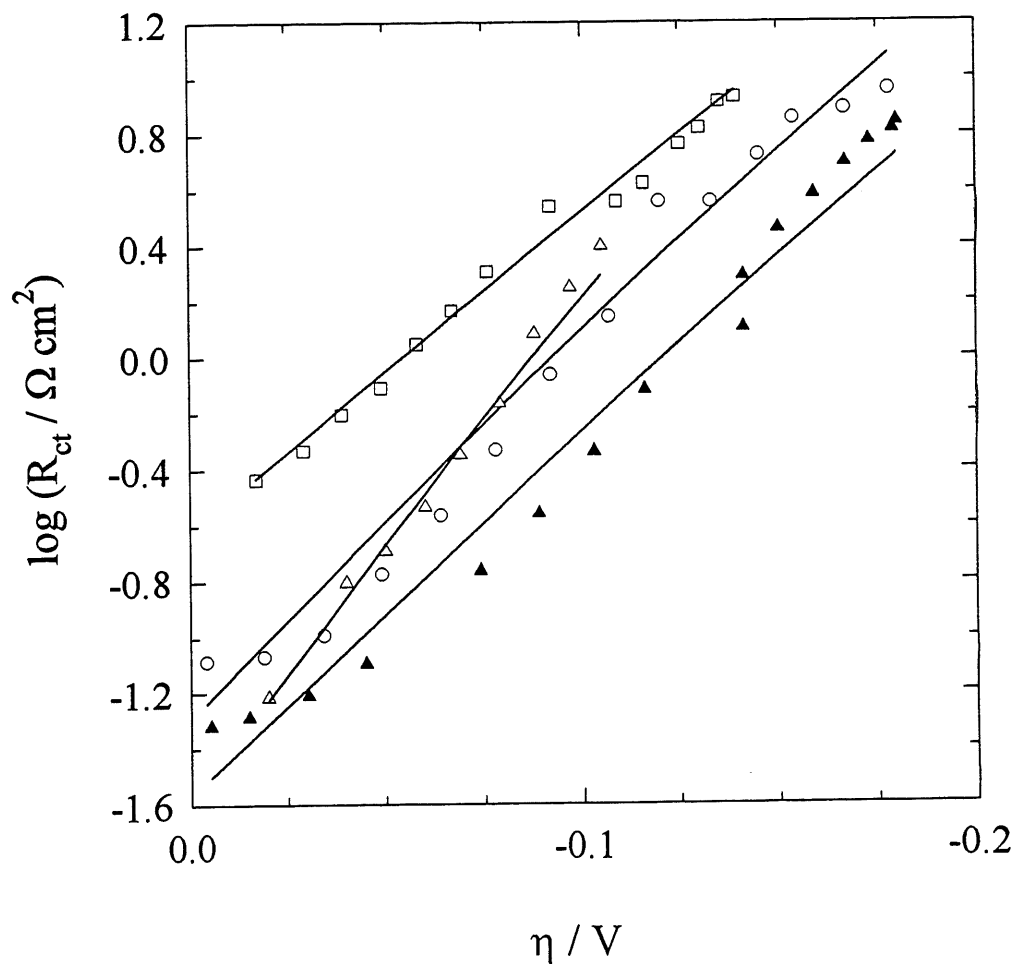


Figure 31. Dependence of charge transfer resistance, R_{ct} , on overpotential for the HER obtained on “three-step” deposited $Ni_{54}Zn_{20}P_{26}$ electrode, (▲) in 1 M NaOH at 25°C, (□) in 1 M NaOH at 70°C, (○) after 8 days activation in 30% KOH at 70°C, (Δ) in 1 M NaOH at 25°C for “one-step” deposited $Ni_{56}Zn_{27}P_{17}$. The continued lines are obtained from fitted data using NLS (R_{ct} from porous model was used in all these cases).

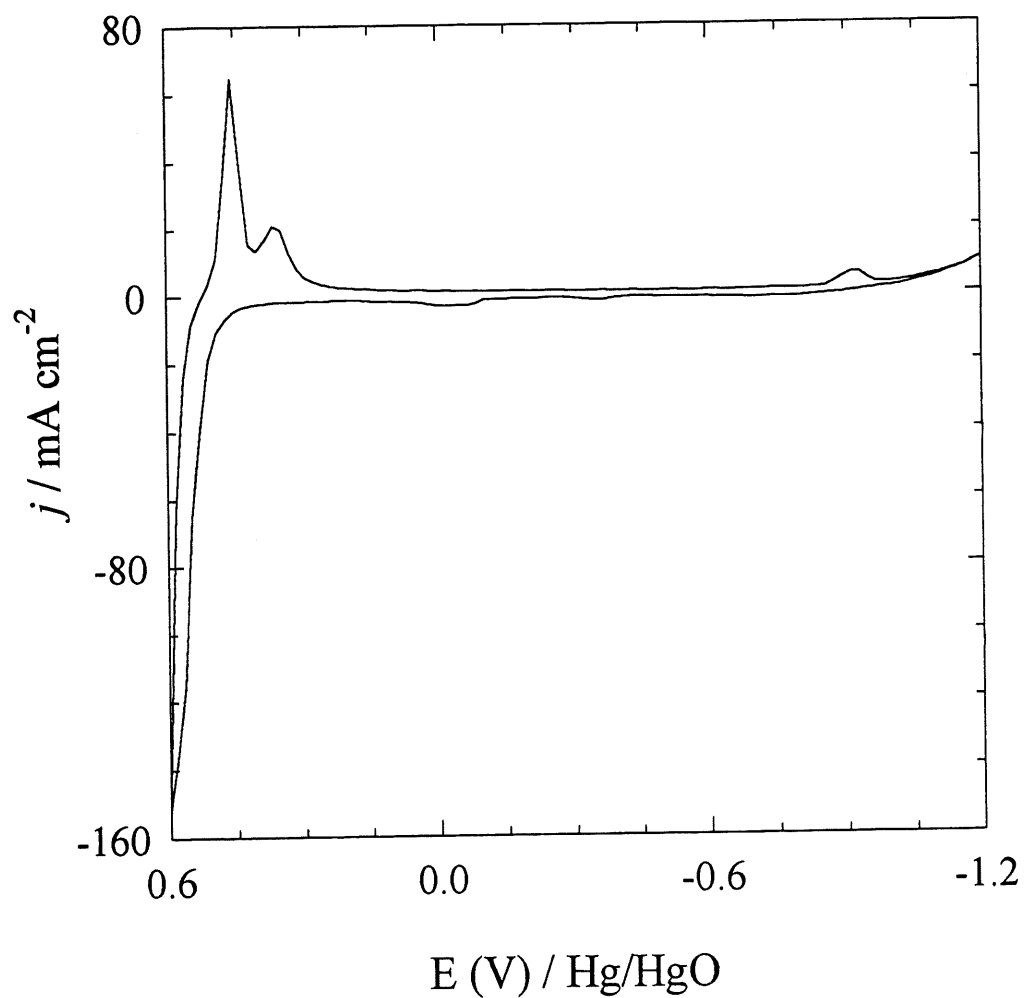


Figure 32. A typical cyclic voltammogram obtained on $\text{Ni}_{54}\text{Zn}_{20}\text{P}_{26}$ electrode at 70°C , in 1 M NaOH, with 20 mV s^{-1} scan rate. The same pattern was observed at 25°C .

from the EIS measurements at negative potentials. The largest difference is found at 25°C. However, cycling in this potential range oxidizes the electrode surface and, the capacitive current is measured on the oxidized surface, covered by nickel and phosphorous oxides. These compounds are much more bulky than metallic nickel and some smaller pores may be clogged by them leading to a decrease in the surface roughness. At higher temperature, the solution viscosity is smaller and the solution may better penetrate into small pores.

After oxidation the electrode activity (electrode A, Table 13, $\eta_{250} = -125$ mV and $b = -50$ mV dec⁻¹) decreased partially ($\eta_{250} = -158$ mV and $b = -58$ mV dec⁻¹). This may be due to the irreversible formation of β -Ni(OH)₂ and phosphorous containing compounds on the electrode surface (344).

The surface roughness, R , of Raney nickel electrodes, Ni₅₄Zn₂₀P₂₆, may also be evaluated using Ni(III)/Ni(II) redox reaction provided to only one monolayer of active sites undergoes the redox reaction (251) without interference of any other reaction. After leaching the Ni₅₄Zn₂₀P₂₆ electrode in 30% KOH, it was subjected to the HER, $j = 320$ mA cm⁻², in 1 M NaOH at 25 and 70°C for 24h, left at the open circuit potential for a few minutes, and then cyclic voltammograms were recorded. The experiment was performed in different scan rate increased from 0.75 to 640 mV s⁻¹. The cyclic voltammograms obtained on Ni₅₄Zn₂₀P₂₆ electrodes were similar to that presented in Fig. 32. From the cathodic peak between 0.400 to 0.500 V vs. Hg/HgO the total cathodic charge, Q_p , was extracted in each scan rate, from which the roughness factor, R , was determined assuming the total charge for one monolayer reduction reaction, Ni(III)/Ni(II), be equal to 0.1 mC cm⁻² (410b).

Variation of Q_p , R , and peak current, j_p , at 0.450V (vs. Hg/HgO) as functions of scan rate, ν , is presented in Fig. 33. As the scan rate decreases R increases and around 1 mV s⁻¹ the value obtained by this method, $R = 4800$, approaches to the value obtained by the EIS, 1×10^4 , for this electrode ($R_{\text{redox}} / R_{\text{EIS}} = 0.48$).

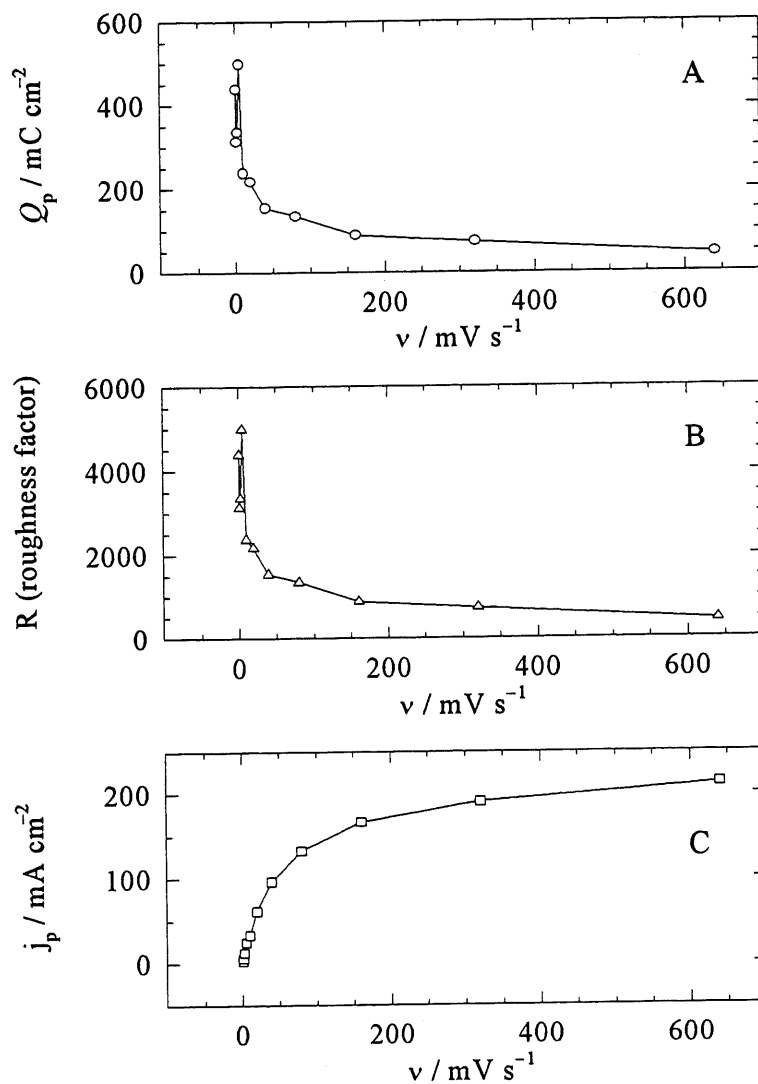


Figure 33. Variation of (A) peak charge, Q_p ; (B) roughness factor, $R = Q_p / 0.1$; and (C) the peak current (at 0.450 V /Hg/HgO, see Fig. 32), j_p , as functions of scan rate, obtained on $\text{Ni}_{54}\text{Zn}_{20}\text{P}_{26}$ electrode from cathodic peak between 0.400 to 0.500V vs. Hg/HgO, at 70°C, in 1 M NaOH.

Although the difference is less than one order of magnitude, but at high scan rate the differences are much large and out of the range of the accepted experimental error, *i.e.*, one order of magnitude. This indicates that this method is valid at low scan rates ($v \leq 20 \text{ mV s}^{-1}$).

However, only at high scan rates ($v \geq 200 \text{ mV s}^{-1}$), Q_p is almost independent of scan rate. At low scan rates Q_p is scan rate dependent. This may be explained as the following: The electrode surface is oxidized in this method and oxides fill the pores. Therefore, the whole surface of the electrode does not participate in redox reaction at higher scan rates. At lower scan rates probably the time is sufficient for oxidation of the pores surface. Another reason might be the oxidation of more than one monolayer (251). These might be the reasons that better agreement was observed between R obtained by Ni(III)/Ni(II) redox reaction at low scan rates and those obtained by the EIS.

Evaluation of surface roughness of porous electrodes needs more investigation. Until now the information obtained by the EIS has explained their behavior very well. This will be left to be studied in more detailed in next chapter.

6.3 Summary

New Ni-Zn-P electrodes were prepared by electrodeposition in three steps. A gradient of zinc concentration was obtained in the deposits. The composition of the top layer is $\text{Ni}_{54}\text{Zn}_{20}\text{P}_{26}$ and it is changed, after leaching, to as $\text{Ni}_{83}\text{Zn}_3\text{P}_{12}$. These electrodes are characterized by low Tafel slopes and high activity towards the HER; $\eta_{250} = -125 \text{ mV}$ in 1 M NaOH at 70°C . The obtained electrodes show also good physical stability, much better than those prepared in one step deposition. Their the EIS behavior may be explained using porous electrode model. These electrodes have quite high surface roughness of 10^4 , much larger than Ni-Zn electrodes. However, their behavior cannot be explained in terms of the Volmer-Heyrovský,

Volmer-Tafel or Volmer-Heyrovský-Tafel reaction mechanisms and it indicates the influence of the surface heterogeneity on the reaction kinetics. These electrodes are potential candidates for the alkaline water electrolysis.

CHAPTER 7
SURFACE BEHAVIOR OF Ni-Zn-P ELECTRODES IN ALKALINE SOLUTIONS
AND EVALUATION OF THE SURFACE ROUGHNESS BY *IN SITU* METHODS

7.1 Introduction

Evaluation of the double layer capacitance, C_{dl} , and roughness factor, R , of the electrode is an important aspect in the studies of electrode kinetics to understand the mechanism of the reactions, the intrinsic activity, and the electrode properties. Two types of methods may be used; *in situ* and *ex situ* (24). *In situ* methods are preferred because the surface of the electrode does not change. It is not clear how the predicted values by different methods are close together and in agreement with the electrode behavior (27,43,48,49,106,147,196,244, 273,278,379,411,412,413).

In the previous chapter a new porous electrode ($Ni_{54}Zn_{20}P_{26}$) was prepared and its activity for the HER was studied by the EIS and steady-state measurements (278). The C_{dl} that was measured by the EIS explained the behavior of this electrode very well. Since the electrode showed the best physical, chemical, and electrochemical stability and activity, among the electrodes studied in this work and also by some other authors (196,197), it will be valuable to study its surface behavior.

The purpose of the present chapter is evaluation and comparison of the double layer capacitance, C_{dl} , and roughness factor, R , of Ni-Zn-P electrode by several *in situ* methods. The following methods were used: electrochemical impedance spectroscopy (EIS), coulometric oxidation of the surface, cyclic voltammetry (*cv*), ratio of the polarization currents, and oxidation of CO adsorbed "CO molecular probe".

Adsorption and electrooxidation of carbon monoxide, CO, on Pt single-crystal electrodes in acidic solutions was studied earlier by *cv* and the structure of electrosorbed CO was determined (411,412). An irreversible anodic wave was observed on the cyclic voltammogram and attributed to the oxidation of adsorbed CO. It was reported that the charge consumed in the whole anodic wave was independent of the potential sweep rate (412). Adsorption of CO on nickel single-crystal electrode in ultrahigh vacuum chamber and subsequently electrooxidation by *cv* in 0.1 M KOH was also studied and the irreversible peak for oxidation of adsorbed CO was observed around 0.77 V vs. RHE (413). The cyclic voltammogram of polycrystalline nickel electrode has shown an irreversible anodic peak in pure 0.1 M KOH. The same behavior was observed on a cyclic voltammogram obtained on the electrode placed in the solution saturated with CO followed by removing of dissolved CO. The only difference between these two peaks was few tens of millivolts positive shift in the peak-potential in the presence of CO (414).

Recently there have been two suggestions on adsorption and electrooxidation of CO on Ni electrodes in alkaline solutions (415,416). Zinola *et al.* (415) have found that adsorbed CO can be oxidized to CO₂ in alkaline solution on electrodeposited nickel. They have confirmed this point that was reported earlier by Wang *et al.* (413). Cuesta *et al.* (416) have suggested electrooxidation of dissolved CO on nickel. In the present case the priority in evaluation of the Ni-Zn-P behavior in the presence of CO is the determination of the surface roughness. Therefore, we studied electrooxidation of CO on Ni and Ni-Zn-P electrodes in 1 M NaOH.

As a comparison, CO adsorbs on nickel electrodes more strongly than hydrogen. Adsorption of hydrogen is a redox reaction while adsorption of CO is chemisorption reaction. CO can be adsorbed on nickel electrodes in gas phase or in the solution around equilibrium potential by one monolayer while adsorption of hydrogen is potential dependent and at very high negative overpotentials the nickel surface can be saturated by adsorbed hydrogen.

A positive shift in equilibrium potential has been observed for some nickel based electrodes, especially Raney nickel electrodes like Ni-Al, Ni-Zn, etc. (28,32,42,278). The source of this behavior is not clear. In our previous studies on this electrode we also selected 45 seconds per point for recording polarization curves (278) without more detailed explanation of the reasons of this choice. We will also clarify this behavior and document our choice. We will show that this time is sufficient for Ni-Zn-P electrodes to reach steady-state.

7.2 Results and discussion

7.2.1 Electrode composition and surface morphology

For these studies we have selected the Ni-Zn-P electrode, because it was the best electrode among the electrodes were studied in this thesis as well as the best electrode among those were prepared by electrodeposition for the HER until now, *e.g.*, Co-Zn-P, regarding physical and chemical stability as well as its electrocatalytic activity and stability. The surface composition of the electrode was Ni₆₆Zn₁₄P₂₀ (before leaching) and Ni₈₆Zn₂P₁₂ (after leaching) as studied by EDX-SEM quantitative microanalysis (278), Fig. 34A and B. The top layer of the electrode was stable and did not collapse during the leaching and the HER (278). The appearance of the electrodes was metallic, bright and showed excellent physical stability remaining stable after ten days the HER ($j = 320 \text{ mA cm}^{-2}$) in 1 M NaOH or 30% KOH at 70°C. In the text the electrode is indicated as Ni₆₆Zn₁₄P₂₀, but of course all the measurements was performed on leached electrodes (*i.e.*, Ni₈₆Zn₂P₁₂).

7.2.2 Evaluation of the surface roughness of Ni-Zn-P electrodes by *in situ* methods

Surface roughness of the electrode may be evaluated by *ex situ* or *in situ* methods (24). *In situ* methods were used in this study.

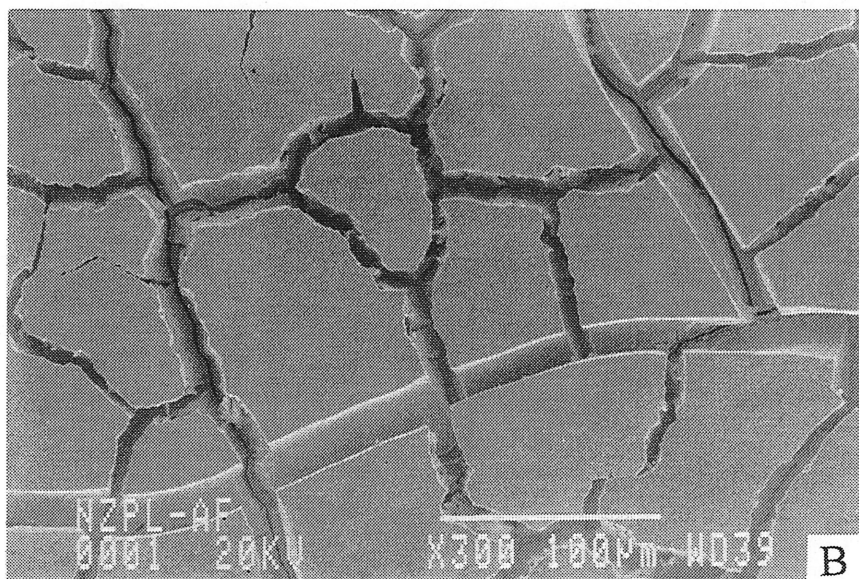
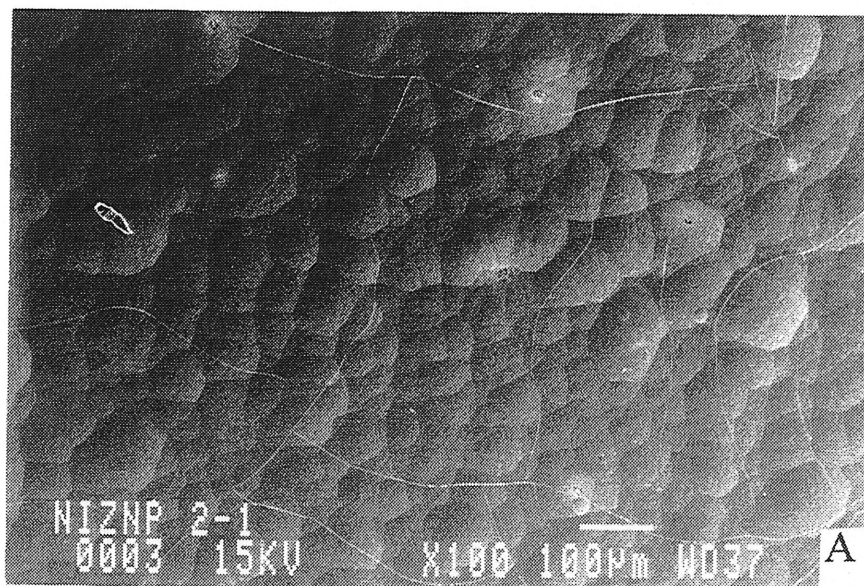


Figure 34. Scanning electron micrographs prepared from the surface of $\text{Ni}_{66}\text{Zn}_{14}\text{P}_{20}$ electrode, (A) as deposited and (B) after leaching in 30% KOH at 70°C for 24h.

7.2.2.1 Ratio of the steady-state polarization current densities

Fig. 35 presents steady-state polarization curves obtained on $\text{Ni}_{66}\text{Zn}_{14}\text{P}_{20}$ electrode at different polarization times per point, at 70°C in 1 M NaOH saturated with N_2 . This series of electrodes were characterized by $b = -72 \text{ mV dec}^{-1}$, $\eta_{250} = -163 \text{ mV}$ and $j_o = 2.5 \times 10^{-4} \text{ A cm}^{-2}$ (Fig. 35, case 45 seconds per point). In fact two slopes can be observed, $b = -33 \text{ mV dec}^{-1}$ (at low overpotentials range) and $b = -72 \text{ mV dec}^{-1}$ at (high overpotentials range). Since a part of the curve (at low overpotentials) extends towards positive overpotentials, the slope of this range is not related to the HER. As the time per point increases from 1 to 120 seconds E_{eq} shifts in a positive direction. For 60 and 120 seconds per point we observed almost the same value of E_{eq} . We assumed that this behavior is related to the absence of hydrogen in the solution (because equilibrium potential that was used for determination of the overpotential was measured between Hg/HgO and platinized platinum in solution saturated with H_2). Fig. 36 presents the Tafel plots which were obtained for different time per point, 1 to 120 seconds, in the solution saturated with H_2 . Two points may be highlighted from Figs. 35 and 36: (i) There is a negative shift in E_{eq} for 1 and 5 seconds per point which disappears for 45 seconds and more. It means that the "time" which is necessary for $\text{Ni}_{66}\text{Zn}_{14}\text{P}_{20}$ electrodes to reach the steady-state is at least 45 seconds in these conditions. Besides, measurements which are performed in non-steady-state conditions produce smaller Tafel slopes showing an unreal activity; (ii) Small slopes at positive overpotentials and also positive shift in E_{eq} are only artifacts, because they do not exist in the presence of hydrogen. In fact, the real Tafel plots can be obtained from a solution saturated with H_2 . In the absence of H_2 bubbling from an external source, such a condition (solution saturated with H_2) exists only at high overpotentials, because electrode itself produce sufficient amount of H_2 to saturate the solution. Therefore, the Tafel slopes which are determined at high overpotential ranges are correct. At low overpotentials H_2 is not produced in sufficient quantities at the electrode, its concentration (in the absence of external H_2 bubbling) is small and consequently, the positive shift is observed (note that solubility of H_2 at 70°C is very small).

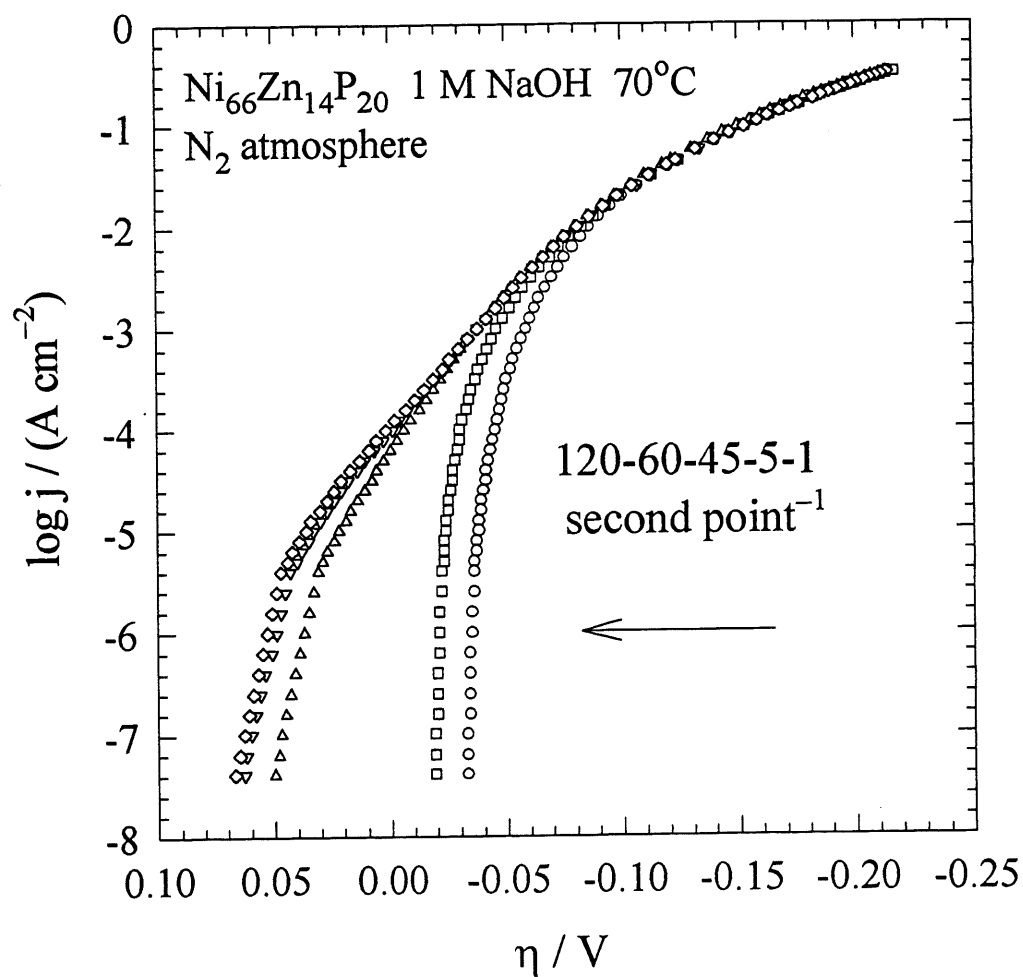


Figure 35. Steady-state polarization curves obtained for the HER on $\text{Ni}_{66}\text{Zn}_{14}\text{P}_{20}$ electrode in 1 M NaOH at 70°C in N_2 atmosphere with different polarization time. A negative shift in E_{eq} for 1 and 5 seconds per point polarization time, and a positive shift for longer times is observed.

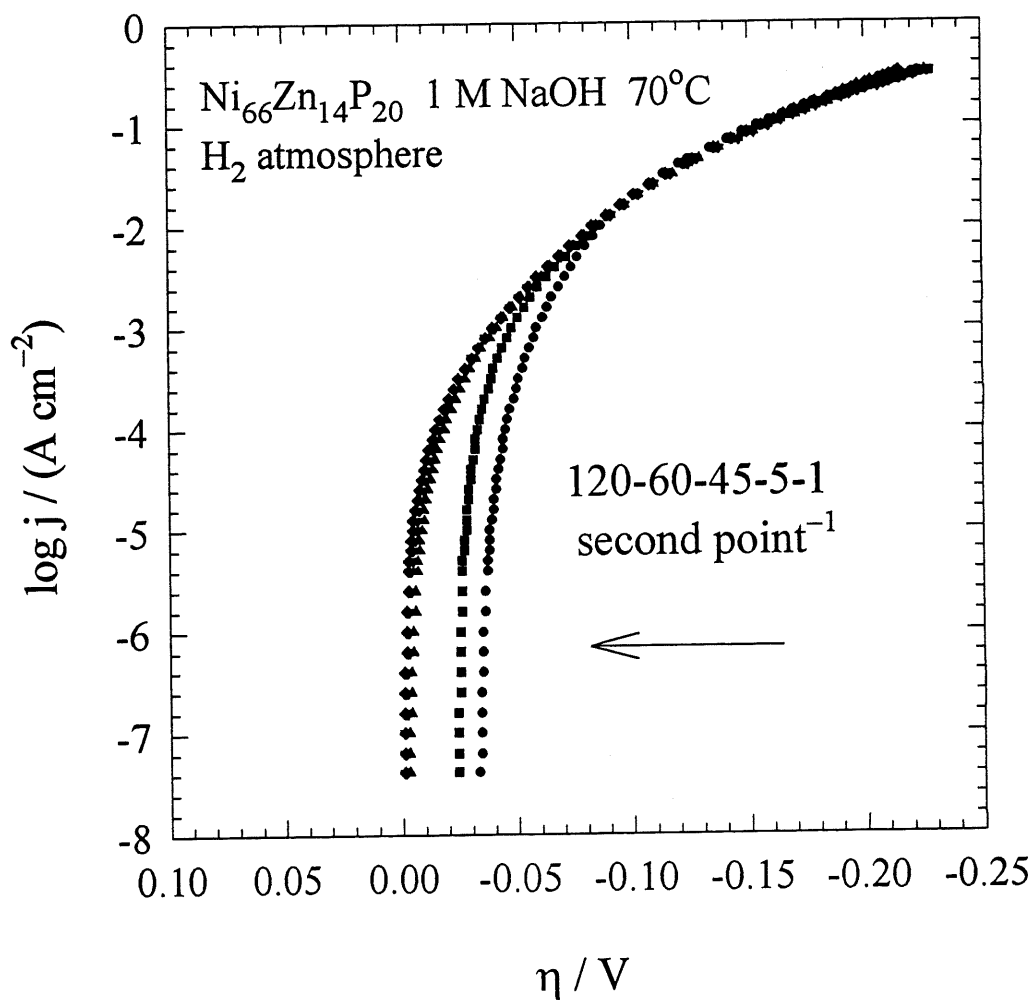


Figure 36. Steady-state polarization curves obtained for the HER on $\text{Ni}_{66}\text{Zn}_{14}\text{P}_{20}$ electrode in 1 M NaOH at 70°C in H_2 atmosphere with different polarization time. While a negative shift in E_{eq} is observed for 1 and 5 seconds per point polarization time, no shift is observed for longer times.

At $\eta = -173$ mV the current densities for $\text{Ni}_{66}\text{Zn}_{14}\text{P}_{20}$ and smooth Ni electrodes were 318 and 0.16 mA cm^{-2} respectively. Using Butler–Volmer equation and assuming similar α , similar and constant concentration at the surface of both electrodes for η , from the ratio of current densities one may obtain a roughness factor as $R = j_{1,\eta} / j_{2,\eta}$, where $j_{1,\eta}$ and $j_{2,\eta}$ are referred to the current density at η on $\text{Ni}_{66}\text{Zn}_{14}\text{P}_{20}$ and smooth electrode respectively. For smooth Ni, R was considered as 2 (192) and the resulted R was corrected for a smooth electrode. The value obtained by this method on $\text{Ni}_{66}\text{Zn}_{14}\text{P}_{20}$ is 5.0×10^3 which is 0.78 of the value obtained by the EIS. The C_{dl} was calculated considering a C_{dl} as $40 \mu\text{F cm}^{-2}$ for Ni or $20 \mu\text{F cm}^{-2}$ for smooth electrodes (192). The value obtained was 0.78 F cm^{-2} . When η changes from -128 to -173 mV the roughness factor changes from 2.2×10^3 to 5.0×10^3 . These values are in good agreement with those obtained by other techniques. For overpotentials more than 120 mV this method gives values for R which are comparable with those were obtained by other techniques.

7.2.2.2 Electrochemical impedance spectroscopy

The behavior of $\text{Ni}_{66}\text{Zn}_{14}\text{P}_{20}$ electrodes as studied by the EIS was similar to those reported in our previous paper (278). Before evaluation of C_{dl} by each technique the electrode was activated by the HER and at the steady-state, Tafel curve was recorded and the EIS measurements were performed in the whole range of overpotentials. The complex plane plots of electrodes used in coulometric, cyclic voltammetry, and adsorption of CO were the same and similar to those were observed for porous electrodes (26,192,243,278,379). At each overpotential a distorted semicircle in low and middle frequencies range followed by a 45°C line in high frequencies range was observed. For brevity and space saving only one example of complex plane and phase angle plots will be presented in this work. Approximation of data was achieved using improved porous model (26,27,103,192,243,278,379), see eqns. [2.92], [2.93], and [2.94] and Fig. 6 in section 2.3.3.5.2 in chapter 2, the model parameters were extracted, R_{ct} , R_s , T , and ϕ were determined, and \bar{C}_{dl} , was obtained using

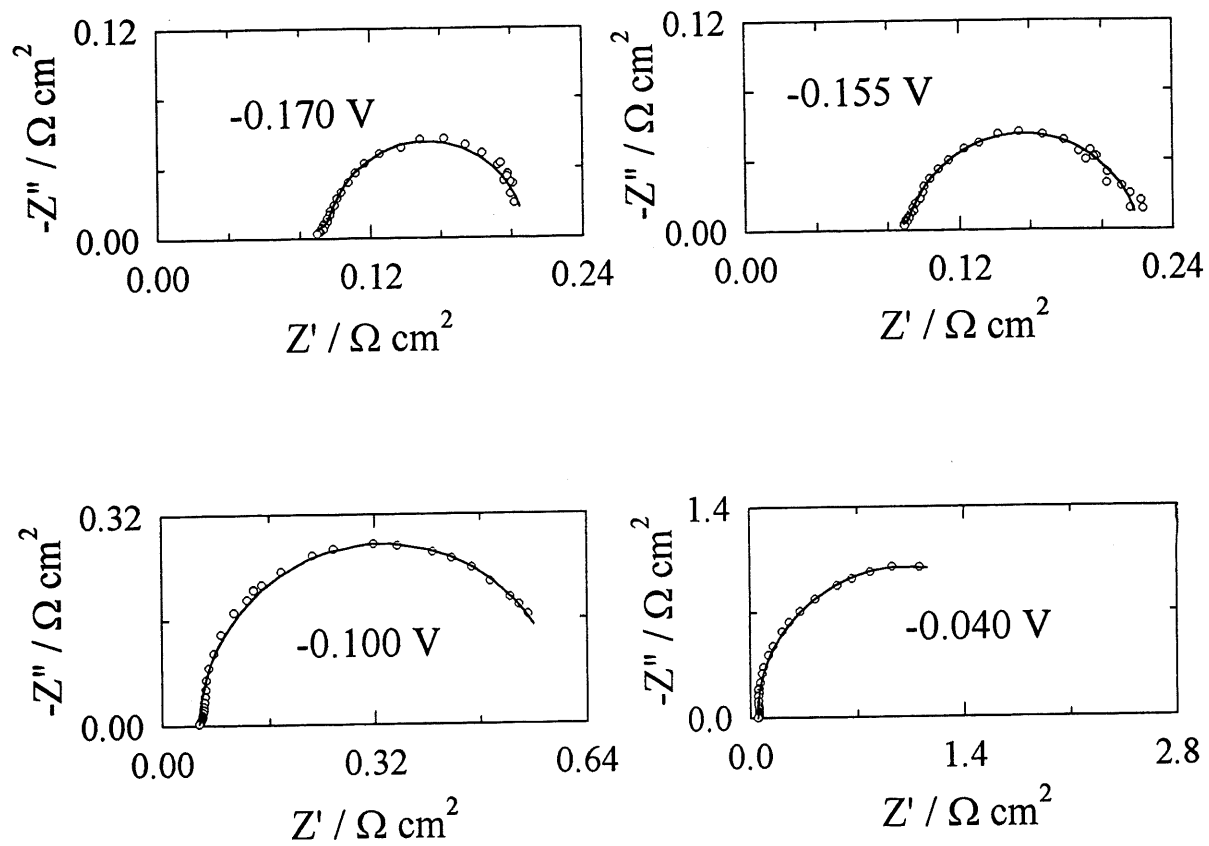


Figure 37A

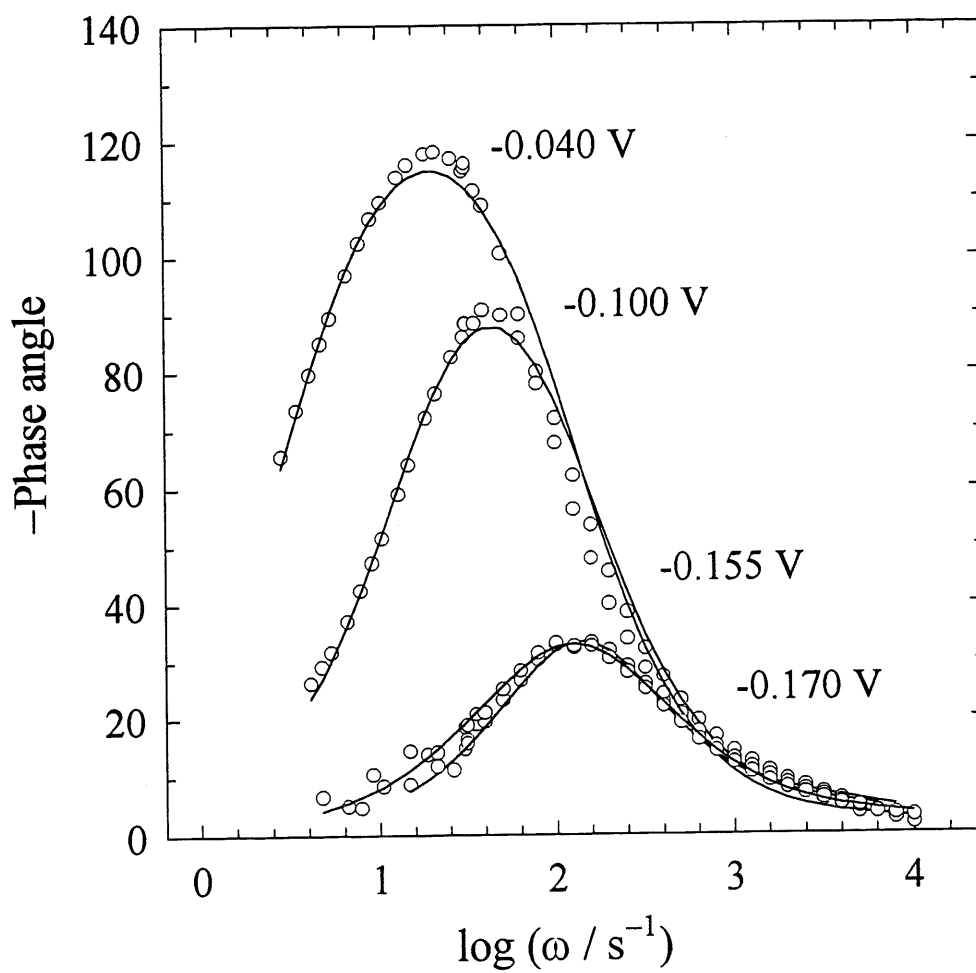


Figure 37B

Figure 37. (A) Complex plane and (B) phase angle plots obtained on $Ni_{66}Zn_{14}P_{20}$ in 1 M NaOH at 70°C. The continued lines are obtained from fitted data in porous model using CNLS method.

$T = \bar{C}_{dl}^{\phi} (R_s^{-1} + R_{ct}^{-1})^{1-\phi}$ (26,192,279). Figs. 37A and B present a sample of complex plane plot, $-Z''$ vs. Z' , and Bode plot, phase angle vs. $\log \omega$, ($\omega = 2\pi f$). The value obtained for Cdl was 0.128 F cm^{-2} and, the roughness factor determined was 6.4×10^3 .

The CPE model which was used here and elsewhere in this thesis is a semi-empirical model, but it explains the EIS behaviors of many solid electrodes very well, see section 2.3.3 in chapter two.

7.2.2.3 Coulometric oxidation of the electrode surface

The chronopotentiogram obtained on $\text{Ni}_{66}\text{Zn}_{14}\text{P}_{20}$ electrodes consisted of three parts, Fig. 38. The first part corresponds to the oxidation of adsorbed hydrogen (from 0.0 to ~ 120 mV). The second part may be attributed to the oxidation reaction of $\text{Ni} + 2\text{OH}^- \rightleftharpoons \text{Ni}(\text{OH})_2 + 2e$ (from ~ 120 to ~ 300 mV vs. RHE). This part was followed by a large increase in the electrode potential which implies the transition of $\text{Ni}(\text{OH})_2$ to NiOOH (147,251,273,344,417).

It has been suggested that the total charge consumed in the second range is related to the formation of one monolayer of $\text{Ni}(\text{OH})_2$ on the nanocrystals constituting the metallic matrix of the Raney nickel electrodes (147,273). From time and current density in this part one may obtain 3.98 C cm^{-2} for the oxidation of Ni to Ni(II). Based on Wendt papers (147,273), one monolayer of $\text{Ni}(\text{OH})_2$ correspond to $2.4 \times 10^{-9} \text{ mol cm}^{-2}$, or $4.63 \times 10^{-4} \text{ C cm}^{-2}$. The surface roughness obtained in this way is 8.6×10^3 which is 1.34 time of value was obtained by the EIS. The reason for this differences may be due to: (i) more than one monolayer oxidation (251), and (ii) oxidation of the phosphorous (344). If these phenomena occur, the consumed charge increases leading to increase the value obtained for C_{dl} and R by this method. Therefore values obtained by coulometric oxidation of the surface may be a little larger than those of obtained by the EIS.

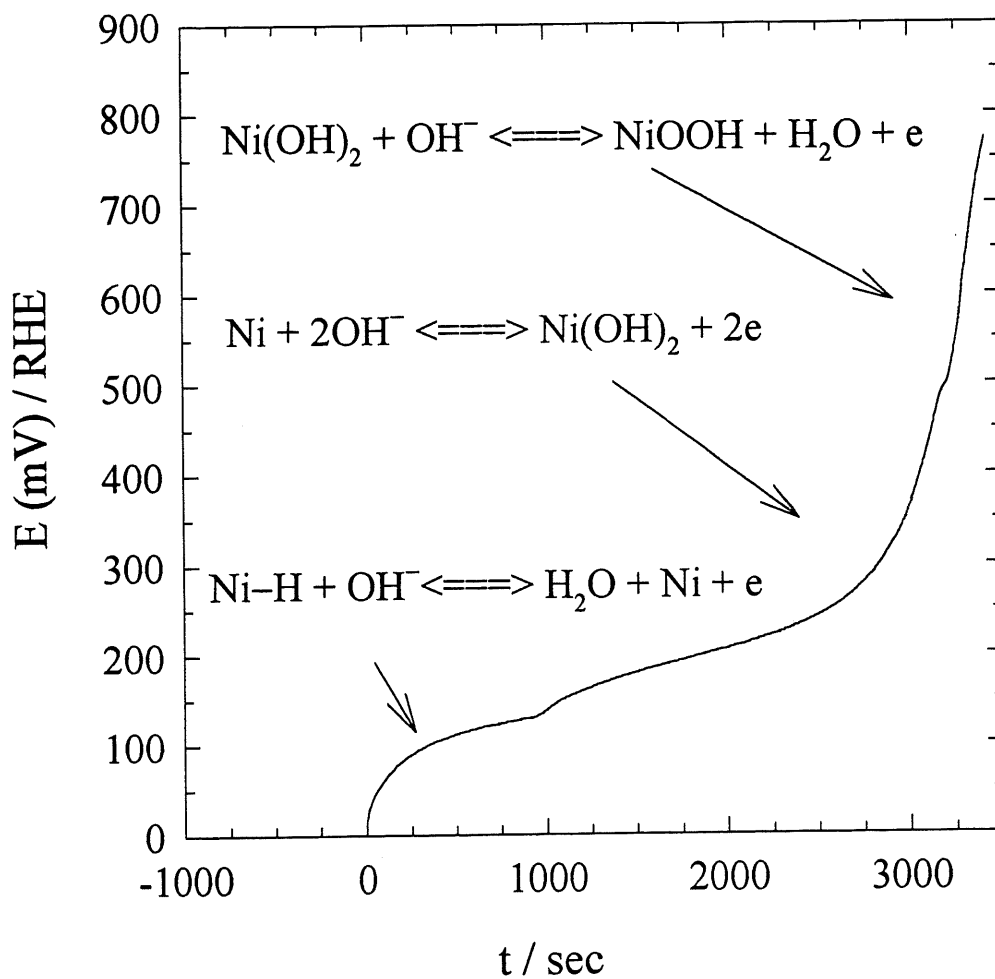


Figure 38. Chronopotentiogram obtained on $\text{Ni}_{66}\text{Zn}_{14}\text{P}_{20}$ electrodes in 1 M NaOH at 70°C under 2 mA cm^{-2} anodic current-step. The expected reactions are presented on the figure.

7.2.2.4 Cyclic voltammetry

Fig. 39A displays the cyclic voltammograms obtained on $\text{Ni}_{66}\text{Zn}_{14}\text{P}_{20}$ in 1 M NaOH at 70°C using analogue potential sweep generation. The same pattern was observed using different digital data Acquisition Modes (AMs), 1/4, 2/4, 3/4, and 4/4 by EG&G M270 software (381). A plateau region was observed between -0.820 to -0.950 V vs. Hg/HgO. The capacitive current densities, j_{dl} , at each scan rate were extracted using average of current densities, $(j_a + j_c) / 2$, at -0.910 V vs. Hg/HgO. However, the capacitive currents were different for different AMs as well as for analogue signal generation Fig. 39B. Provided to a linear relation exists between capacitive current density and scan-rate, $j_{dl} = C_{dl} \nu$, C_{dl} and R may be evaluated from the slope (348). Fig. 40 presents the plots obtained from j_{dl} as a function of scan rate, ν . The slopes of lines represent the C_{dl} in F cm^{-2} . It is clear that values obtained using different AMs are not the same. Also they are lower than that obtained using analogue method. The roughness factors were obtained using the C_{dl} divided by $20 \times 10^{-6} \text{ F cm}^{-2}$ and are presented in Table 19.

The values obtained for C_{dl} from the slopes varied from 0.04 to 0.07 F cm^{-2} , the slopes in Fig. 40. These values gave roughness factors ranged from 2.1×10^3 to 3.5×10^3 which are 0.32 to 0.55 that obtained by the EIS measurements (see Table 19). The nearest value to the EIS is obtained by *cv* analogue method.

For porous electrodes the experimental errors lower than one order of magnitude in R are acceptable. The largest difference in R values exists between the value given by the EIS and *cv* method (AM 4/4). Table 19 shows that the value given by CV 4 (*i.e.*, AM 4/4) is 3 times smaller than that of the EIS. For other acquisition modes (or even other techniques) differences are lower than this. In *cv* method, the best agreement was observed between values given by analogue method and that by the EIS. However, all the values in Table 19 are

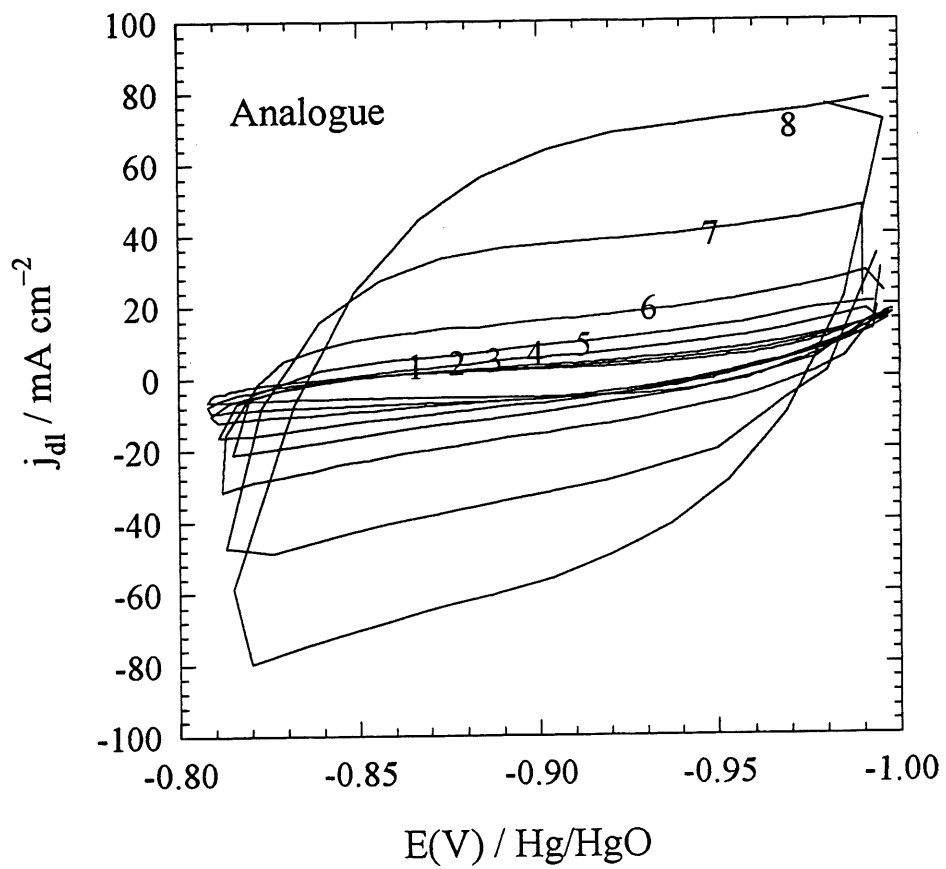


Figure 39A

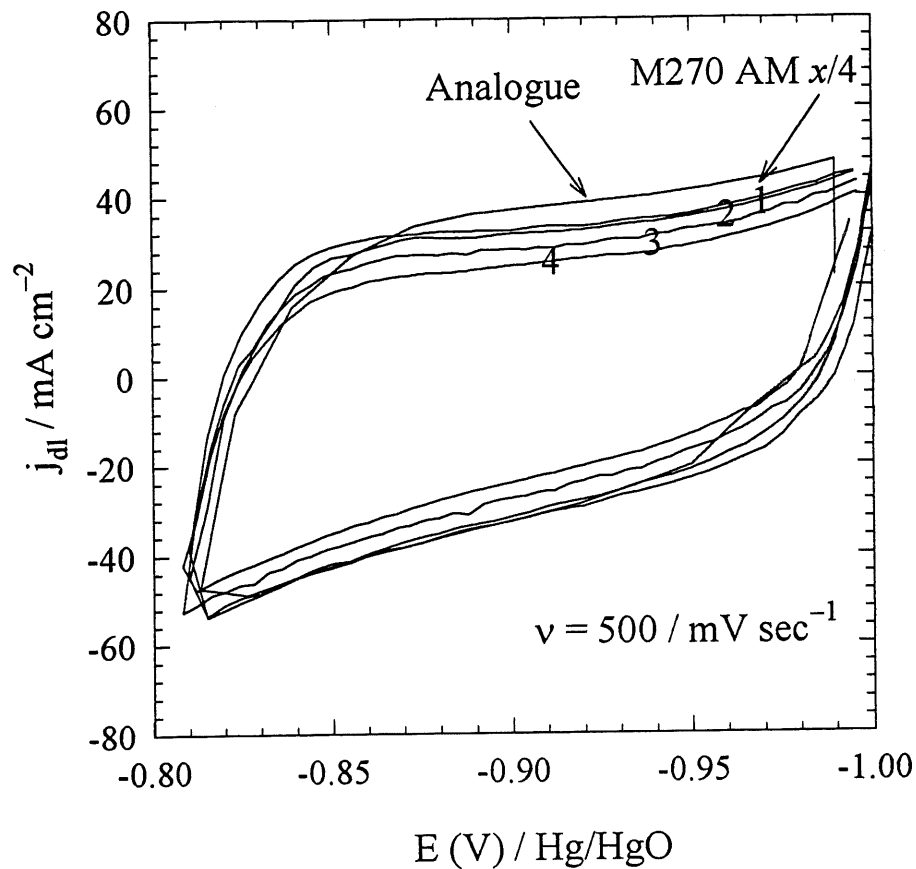
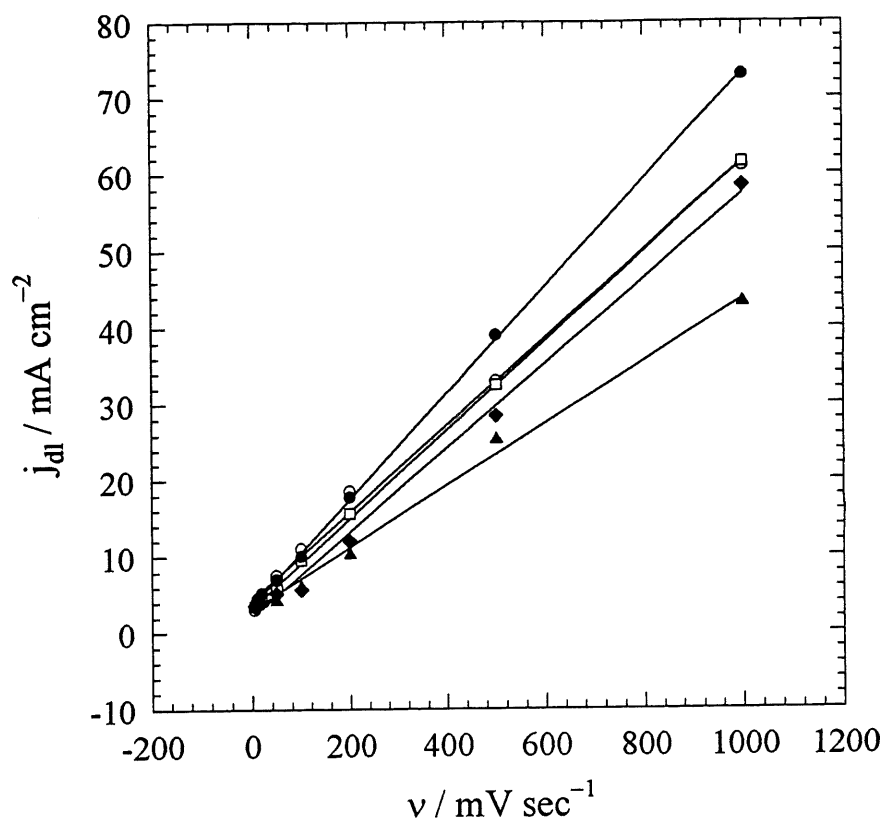


Figure 39B

Figure 39. Cyclic voltammograms obtained on $\text{Ni}_{66}\text{Zn}_{14}\text{P}_{20}$ electrode at 70°C in 1 M NaOH in the range of -0.810 to -1.000 V vs. Hg/HgO with different scan rates: (A) (1) 5, (2) 10, (3) 20, (4) 50, (5) 100, (6) 200, (7) 500, and (8) 1000 mV s^{-1} . (B) Comparison one of the cyclic voltammograms obtained at 500 mV s^{-1} for different data acquisition modes (AM $x/4$, x varies from 1 to 4) using M270 software as well as for analogue method, see the text.



- Analogue $y = 3.59216 + 0.06969x$ $r^2 = 0.999$
- AM = 1/4 $y = 4.39501 + 0.05721x$ $r^2 = 0.995$
- AM = 2/4 $y = 3.34960 + 0.05828x$ $r^2 = 0.999$
- ◆ AM = 3/4 $y = 2.15910 + 0.05529x$ $r^2 = 0.995$
- ▲ AM = 4/4 $y = 3.12677 + 0.04064x$ $r^2 = 0.994$

Figure 40. Dependence of capacitive current density on scan-rate at 70°C in 1 M NaOH extracted from cyclic voltammograms obtained on Ni₆₆Zn₁₄P₂₀ electrode from average of the current densities, $(j_c + j_a) / 2$ at -0.910; analogue (●), and digital with different acquisition mode, AM, in EG&G M270 software; (○) 1/4, (□) 2/4, (▲) 3/4, and (◆) 4/4.

Table 19. Average of the double layer capacitance, \bar{C}_{dl}^* , and roughness factors, R, obtained on Ni₆₆Zn₁₄P₂₀ electrode in 1 M NaOH at 70°C using different techniques.

Method	$C_{dl} / F \text{ cm}^{-2}$	R	R / R _{EIS}
EIS	0.128	6.4×10^3	1.00
Coulometric Ni(II)/Ni	0.172	8.6×10^3	1.34
Tafel plot	0.10	5.0×10^3	0.78
CV 1	0.0572	2.9×10^3	0.45
CV 2	0.0583	3.0×10^3	0.47
CV 3	0.0553	2.8×10^3	0.44
CV 4	0.0407	2.1×10^3	0.32
CV (analogue)	0.070	3.5×10^3	0.55
CO molecular probe	0.084	4.2×10^3	0.66

*: C_{dl} reported for the EIS may be given as: $C_{dl}(\text{EIS}) = \frac{\sum_{i=1}^n \bar{C}_{dl,i}}{n}$ where \bar{C}_{dl} is average of the double layer capacitance in the whole frequencies range at constant η , “n” is the number of measurement points of \bar{C}_{dl} in the whole range of overpotentials, in this work n was varied (8 to 14).

in agreement, even they are apparently different. The best estimation of R is given by the EIS, other values are distributed around this value with differences of lower than one order of magnitude. The EIS is not a destructive method (contrary to surface oxidation), and the obtained \bar{C}_{dl} values are practically independent of η in the cathodic potentials range.

7.2.2.5 Adsorption of carbon monoxide, CO

Different tests were performed to find the appropriate conditions for studying the adsorption of CO on Ni₆₆Zn₁₄P₂₀ electrodes. First, polycrystalline nickel electrode was used to optimize the conditions.

7.2.2.5.1 Adsorption of CO on polycrystalline Ni electrode

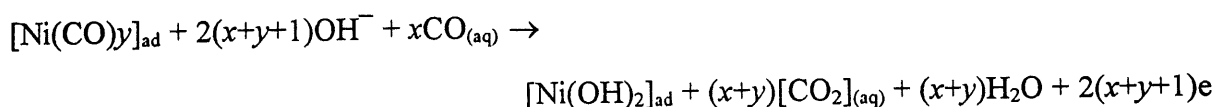
The best method for surface preparation was to wash the polished and cleaned Ni electrode with 1:5 sulfuric acid, then with water (previously deoxygenated), connecting it to the cathode (which was subjected to a cathodic current near zero, 30 $\mu\text{A cm}^{-2}$ corresponding to -0.935 V vs. Hg/HgO) and immersing in the cell containing previously deoxygenated 1 M NaOH solution at 25°C, under N₂ atmosphere, and keeping at these conditions for 25 min while the nitrogen was passing over the solution and then running the experiment. In these conditions reproducible cyclic voltammograms were obtained.

(i) *Clean Ni electrode in 1 M NaOH.* –Fig. 41, curve 1 presents the first cyclic voltammogram obtained on Ni in the absence of CO. An irreversible anodic peak around -0.490 V was observed which was attributed to the oxidation of nickel, $\text{Ni} + 2\text{OH}^- \rightleftharpoons \text{Ni}(\text{OH})_2 + 2e$ (413-415).

(ii) *Ni electrode in 1 M NaOH saturated with CO.* –For CO studies the Ni electrode was prepared, washed with 1:5 H₂SO₄ solution (but in the last step with 1 M NaOH was deoxygenated with N₂ for 6h and then bubbled with CO for 6h) and immersed in the solution in the same way, the solution was bubbled with CO for 25 min, then CO was passed over the solution. Fig. 41, curve 2 presents the first cyclic voltammogram. The peak was shifted to more positive potentials and its intensity was increased. It is clear that CO is oxidized

(413,415), but it is not clear if dissolved CO, adsorbed CO, or both of them are oxidized. The experiment was repeated but after bubbling with CO, solution was bubbled with N₂ for 25 min. Fig. 41, curve 3 presents the first cyclic voltammogram obtained in these conditions. When the bubbling time with N₂ (after CO bubbling) was increased from 25 to 100 min, the peak area around -0.380 V decreased slightly, Fig. 41, curve 4. Bubbling for longer time did not change the peak area. It means that dissolved CO oxidizes at the same potential as adsorbed CO. The charge under anodic peak around -0.380 mV (in Fig. 41, curve 4) may be attributed to the oxidation of adsorbed CO (413-415), and around -0.380 mV (in Fig. 41, curve 2) to the oxidation of both adsorbed and dissolved CO, on nickel electrode.

(iii) *CO-adsorbed on Ni electrode and NaOH solution free of CO.*—We repeated the experiment but before cv measurements replaced the solution (drained it) by a new one free of CO, bubbled it for one hour with N₂ and then cycled the electrode as before. The first (Fig. 41, curve 4) and second cyclic voltammograms were the same as observed before for 100 min bubbling with N₂. It means that the peak around -0.380 V in curve 4 is related to the oxidation of adsorbed CO. This experiment also confirms that dissolved CO oxidizes at the same potential. The following relation may be attributed to oxidation of CO, of course in the absence of CO $x = y = 0$ and for clean solution $x = 0$.



The second cyclic voltammograms were the same in all the cases, Fig. 41, curve 5. It implies that CO can not be oxidized on oxidized Ni surface.

The first cyclic voltammogram was used in calculations and the amount of the charge was determined from the irreversible anodic peak around -0.490 V, Fig. 41, curve 1, and attributed

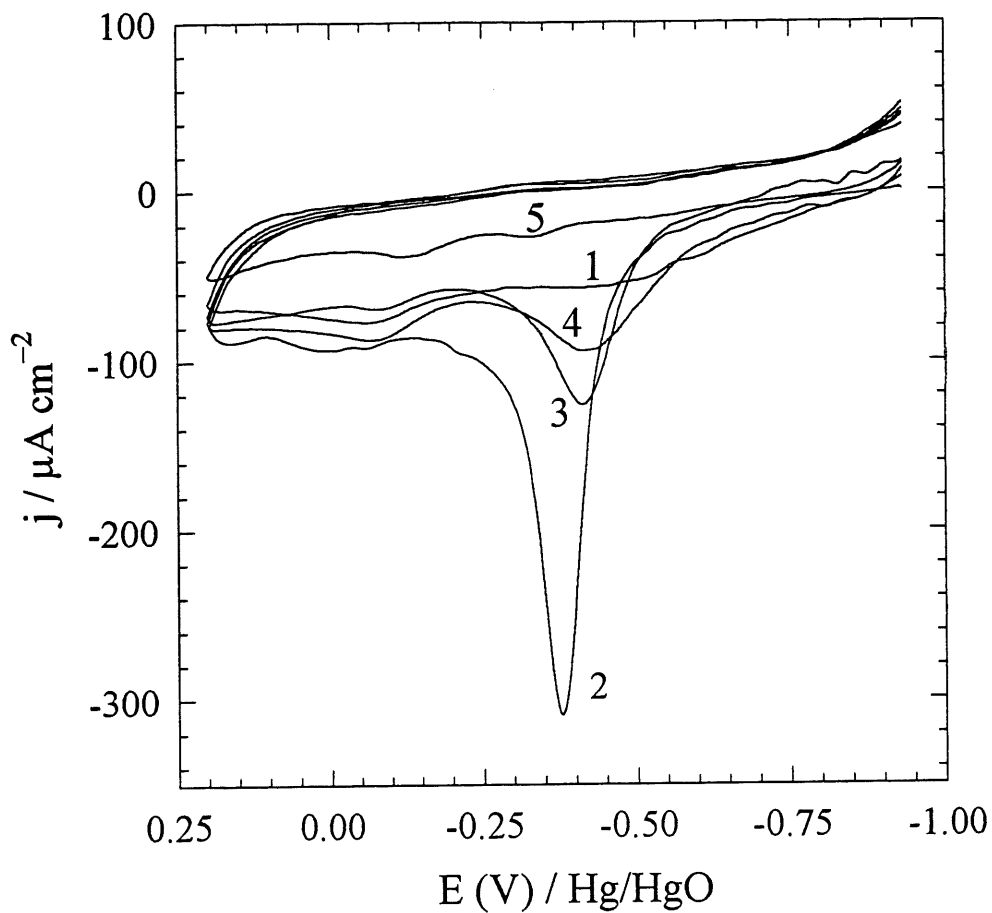


Figure 41. Cyclic voltammograms obtained on polycrystalline nickel electrode at 25°C in 1 M NaOH and 20 mV s^{-1} scan rate; the first cycle (1) in the absence of CO, (2) in the solution saturated with CO, (3) after 25 min bubbling with CO followed by 25 min bubbling with N_2 , (4) after one 25 min bubbling with CO followed by 100 min bubbling with N_2 or replacing the solution by a new and deoxygenated pure 1 M NaOH, and (5) the second cycle for all the cases.

to the oxidation of active sites on the Ni electrode surface, and from irreversible anodic peak around -0.380 V, Fig. 41, curve 4, to the oxidation of adsorbed CO. Fig. 42 shows our method for extraction of data.

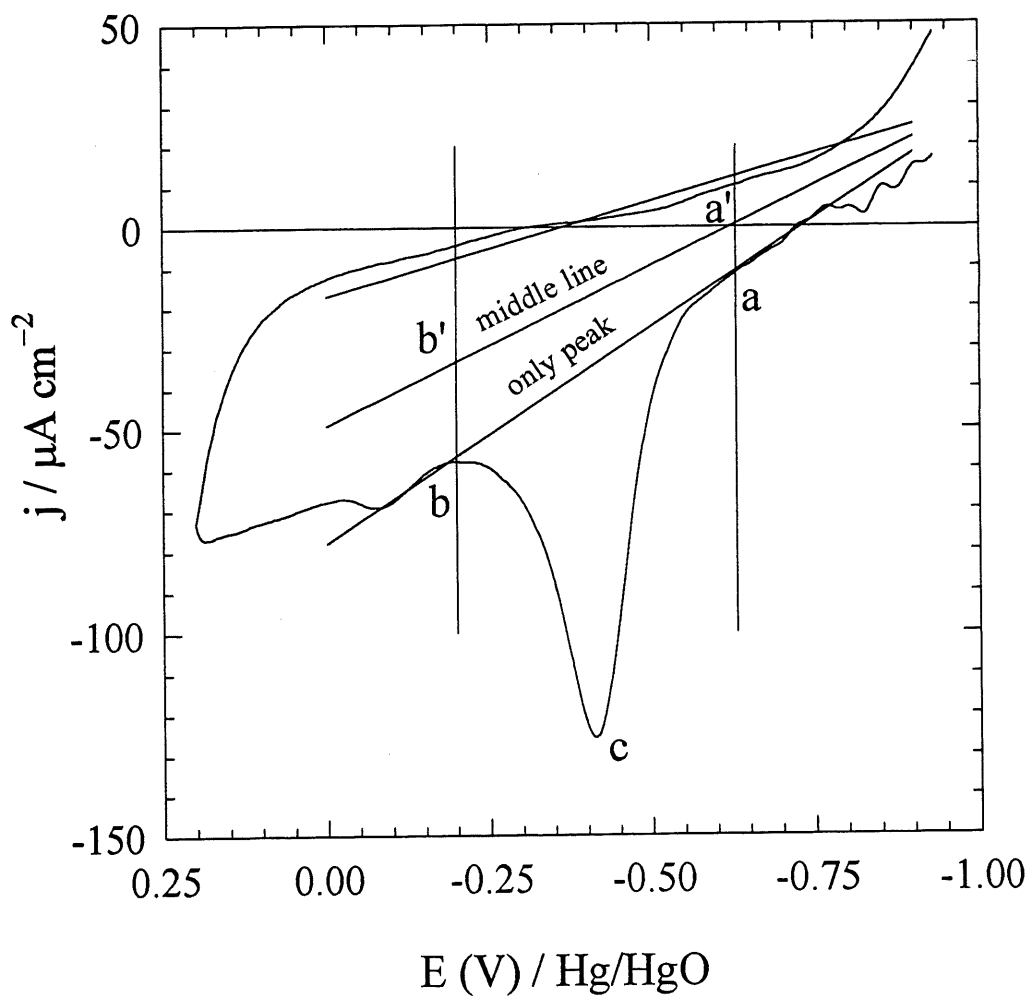


Figure 42. A typical cyclic voltammogram selected from Fig. 41, curve 3, to show our method for extraction of data, only peak (abc area), and up to middle line (a'b'c area).

Considering that the total charge for oxidation of one monolayer of Ni electrode is 0.463 mC cm^{-2} and for one monolayer of Ni-CO is 0.926 mC cm^{-2} , the roughness factor was obtained. The total charge calculated from curve 4 in Fig. 41, was 1.17 mC cm^{-2} . It produced roughness factor 1.26 for this electrode. We also used the oxidation charge for Ni electrode and got roughness factor 1.4. These values are in good agreement (Table 20). It means that CO molecular probe can be used for estimation surface roughness of nickel based electrodes.

7.2.2.5.2 Adsorption of CO on Ni-Zn-P electrodes

Fig. 43 displays the cyclic voltammograms obtained on $\text{Ni}_{166}\text{Zn}_{14}\text{P}_{20}$ electrodes in 1 M NaOH at 25°C and different conditions.

(i) *Clean Ni-Zn-P electrode in 1 M NaOH.*—The charge under irreversible anodic oxidation peak in the absence of CO was 2.03 C cm^{-2} , Fig. 43, curve 1.

(ii) *Ni-Zn-P electrode in 1 M NaOH solution saturated with CO.*—Fig. 43, curve 2 shows one large and one small anodic peak. The total charge under anodic irreversible oxidation peaks curve 3, is 5.70 C cm^{-2} .

(iii) *CO-adsorbed on Ni-Zn-P electrode and solution free of CO.*—When CO was adsorbed and solution was replaced by a new one the total charge under irreversible peaks was 3.88 C cm^{-2} Fig. 43, curve 3. The ratio of the anodic peaks in curves 1 and 2 was 1.9, Table 21. It implies that this method is suitable for surface roughness determination of porous electrodes. However, this information also show that both adsorbed CO and covered nickel site can be oxidized in the first cycle.

The total charge under anodic irreversible oxidation peaks in Fig. 43, curve 2, 5.70 C cm^{-2} , is

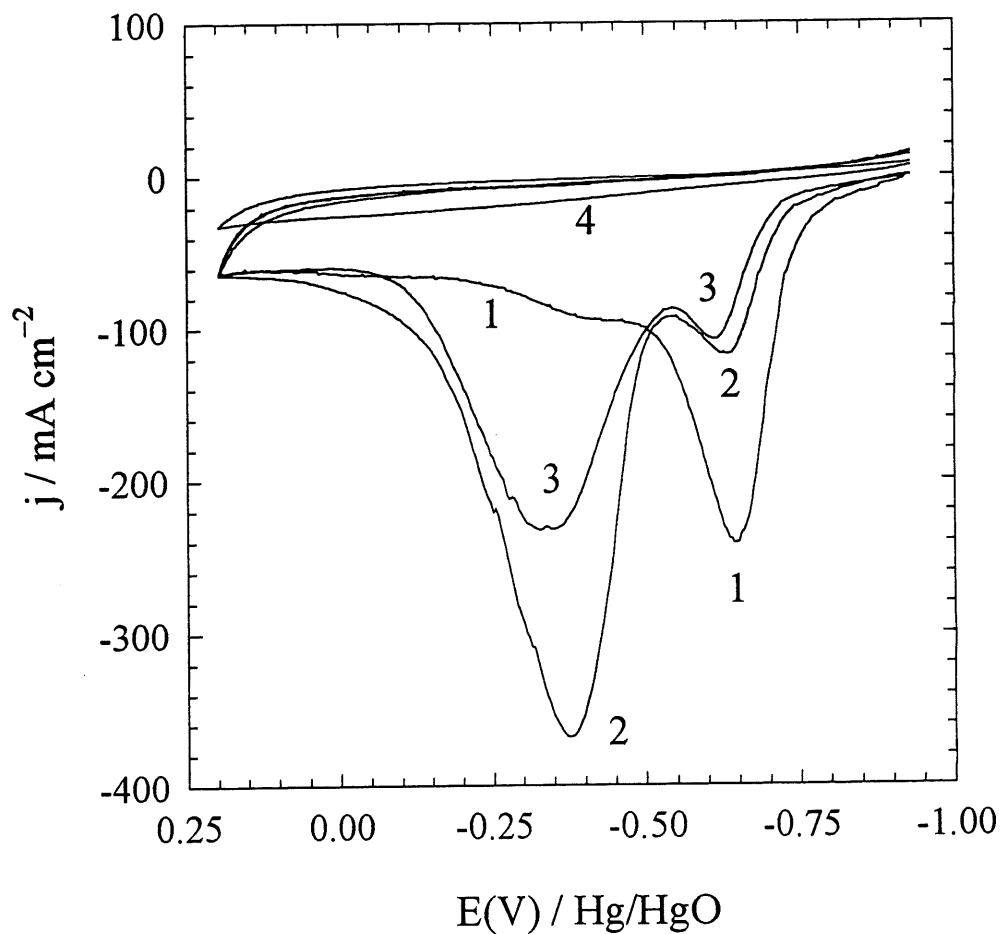


Figure 43. Cyclic Voltammograms obtained on $\text{Ni}_{66}\text{Zn}_{14}\text{P}_{20}$ at 25°C in 1 M NaOH and 20 mV s^{-1} scan rate; the first cycle, (1) in the absence of CO, (2) after 2.5h bubbling with CO, and (3) after 2.5h bubbling with CO followed by replacing the solution with a new and deoxygenated pure 1 M NaOH solution, and (4) the second cycle in all the cases.

Table 20. Electrooxidation charges of CO and corresponding surface roughness obtained on Ni electrode in 1 M NaOH at 25°C, $Q_{Ni,theory} = 0.463 \text{ mC cm}^{-2}$.

Conditions	$Q_1 / \text{mC cm}^{-2}$ from the middle	$Q_2 / \text{mC cm}^{-2}$ only peak	Q_1 / Q_{01}	Q_2 / Q_{02}	R_{Q1}	R / R_{EIS}
A	0.65 = Q_{01}	0.2034 = Q_{02}	1	1	1.41	0.71
B	2.15	1.315	3.3	6.5	2.33	1.17
C	1.2	0.668	1.85	3.3	1.3	0.65
D	1.17	0.54	1.8	2.66	1.26	0.63

(A) 1 M NaOH, (B) 1 M NaOH + CO saturated, (C) 1 M NaOH + CO + 25 min N_2 , (D) 1 M NaOH + CO (saturated) + changing the solution.

Table 21. Electrooxidation charges of CO and corresponding surface roughness obtained on $Ni_{66}Zn_{14}P_{20}$ electrode in 1 M NaOH at 25°C.

Conditions	$Q_1 / \text{C cm}^{-2}$ from the middle	$Q_2 / \text{C cm}^{-2}$ only peaks	Q_1 / Q_{01}	Q_2 / Q_{02}	$R_{Q-1-tot}$	R / R_{EIS}
A	2.026 = Q_{01}	1.56 = Q_{02}	1	1	4.38×10^3	0.69
B	5.7	4.69	2.8	3	6.16×10^3	0.96
C	3.88	3.09	1.92	2	4.19×10^3	0.66

(A) 1 M NaOH, (B) 1 M NaOH + CO saturated, (C) 1 M NaOH + CO (saturated) + changing the solution.

larger than that obtained for Fig. 43, curve 3. It means that dissolved CO can also be oxidized on this electrode at the same potential as the adsorbed CO. Finally, Fig. 43, curve 4 shows the second cycle for all the cases. It simply shows that CO can not be adsorbed on oxidized $\text{Ni}_{66}\text{Zn}_{14}\text{P}_{20}$ and also dissolved CO can not be oxidized in this case (see Table 21).

The double layer capacitance was obtained assuming $9.2 \times 10^{-4} \text{ C cm}^{-2}$ for oxidation of one monolayer adsorbed CO, Table 19 and 21.

Another point which may be suggested here is the presence of two peaks for oxidation of CO on $\text{Ni}_{66}\text{Zn}_{14}\text{P}_{20}$ electrode. Probably two kinds of sites exist on $\text{Ni}_{66}\text{Zn}_{14}\text{P}_{20}$ electrode and the number of the sites at more positive potentials is higher (comparing peaks area in Fig. 41). Comparing Fig. 41 curve 4 (for Ni) and Fig. 43 curve 3 (for $\text{Ni}_{66}\text{Zn}_{14}\text{P}_{20}$) one will find that there is a new small peak for $\text{Ni}_{66}\text{Zn}_{14}\text{P}_{20}$ in the same conditions. The first probable reason for this peak is oxidation of CO in more negative potentials as compared with Ni. This is probably due to little amount of Zn which is left after leaching. This behavior has been well known for Sn when it alloys with Pt (138). If this is the case, it will be a useful behavior for this electrode as a candidate for fuel cell. Yet it does not have ideal behavior in this case and more improvements are necessary. In the ideal case oxidation potential of CO as a poison in fuel cells has to be more negative than oxidation of hydrogen, H_2 (138), to be oxidized and removed before oxidation of H_2 . Such an ideal electrode will have always a clean surface free of CO. The electrodes of this kind (Pt_3Sn) now have been well known and their behavior has carefully studied, although they are expensive (138).

Since the small peak appears exactly in the same potential as surface oxidation in the absence of CO, another probable reason for this peak is oxidation of uncovered sites inside the pores. To check such a possibility one may try to keep the potential somewhere around -0.575 mV vs. Hg/HgO and then verifies if the intensity of the second peak will decrease but, the peaks are irreversible and it is impossible to get such a result.

However, the intensity of the small peak also increases in the solution saturated of CO. This is a good evidence to confirm the first probable reason which considers this peak also as oxidation of adsorbed CO together with its Ni sites (Ni and CO) but, with a negative shift.

7.3 Summary

The double layer capacitance, and roughness factor obtained for the HER on porous $\text{Ni}_{66}\text{Zn}_{14}\text{P}_{20}$ electrodes by the EIS measurements was in good agreements with values obtained from other techniques as *cv*, ratio of the polarization current densities, coulometric oxidation of the surface, and adsorption-oxidation of CO molecular probe. CO can adsorb on $\text{Ni}_{66}\text{Zn}_{14}\text{P}_{20}$ as well as Ni electrodes, and be oxidized together with Ni sites shift into anodic direction. Dissolved CO in alkaline solution oxidizes on nickel based electrodes at the same potential as adsorbed CO. It is possible to determine the surface roughness and double layer capacitance of nickel based electrodes, Ni-Zn-P, by adsorption-oxidation of CO. A positive shift in equilibrium potentials is due to the absence of H_2 . However, negative shift in E_{eq} is due to non-steady-state measurements.

FINAL CONCLUSIONS AND CONTRIBUTIONS TO ORIGINAL RESEARCH

During the course of this study, preparation of new electrode materials, mechanistic studies of their activities towards the HER in alkaline solutions, and development and comparison of new techniques for evaluation of the surface roughness have been investigated.

Three types of the electrodes, namely Ni-P, Ni-Mo-P, and Ni-Zn-P, were prepared by “one-step” and “multi-step” electrodeposition. The activities of the electrodes were studied by EIS, steady-state polarization, and cyclic voltammetry. With the aid of adsorption-electrooxidation of carbon monoxide a new *in situ* technique was developed, “CO molecular probe” for surface roughness evaluation. The surface roughness of Ni-Zn-P electrodes was evaluated by *in situ* techniques as: EIS, cv, coulometric oxidation of the surface, ratio of the steady-state polarization current densities, and compared with CO adsorption. A good agreement was observed between all the techniques, implying that increase in the electrode activity is due to increase in the surface roughness of the electrode.

Contributions to original research

(A) Preparation and kinetic studies of new, active, and stable electrodes for the HER

1. A literature review carried out at the beginning of this study showed that conflicting results had been published in literature on the activity of Ni-P electrodes towards the HER. The results covered a range of claims from active to non-active as compared with a polycrystalline nickel. The results in this study show that generally Ni-P electrodes are not very active for the HER in alkaline solutions. In this study Ni-P electrodes were prepared with a range of phosphorous content. Phosphorous could not be removed by means as

leaching the electrodes in HF, alkaline solutions, heating, and/or oxidation to produce a rough surface, in opposite to what was expected. None of these treatments caused noticeable changes in the electrode activity. Ni-P alloys deposited at high current densities and temperatures were characterized by higher hardness than Ni. Finally, active electrodes were obtained by galvanostatic deposition at low current density and temperature. The increase in electrode activity is due to increase in the surface roughness. Reaction mechanism passes through the Volmer-Heyrovský mechanism with the Heyrovský reaction as the rate determining step.

2. XRD patterns of Ni-P electrodes show that all the deposited samples have an amorphous structure. After heating at 400°C the structure of the electrodes containing high quantity of phosphorous changed to crystalline, with domination of Ni₃P phase, and without changes in their activity. Activity of the electrodes deposited at low current density and temperature decreased upon heating at 400°C, while no changes were observed up to 160°C. After heating at 400°C their structure changed to crystalline with domination of Ni and Ni₃P phases. These results provide excellent reasons that amorphous Ni-P alloys, prepared at low current density and temperature, are active materials for the HER. In contradiction with results reported in the literature, heating did not increased the activity of Ni-P electrodes.
3. Active and stable Ni-Mo-P electrodes were prepared by “three-step” electrodeposition at low current density and temperature. Oxidation or cycling of the electrodes between the HER and OER decreased the electrode activity. The reason is removing of Mo and loosing Ni-Mo, or Mo-P bonds, implying that a part of increase in the electrode activity is due to synergetic effect induced by these bonds. As-deposited electrodes were active for the HER in alkaline solutions and remained stable for more than 72h. Ni-Mo-P catalyst shows very interesting behavior: (i) The electrode activity is increased through both increase in intrinsic activity and increase in the surface roughness. (ii) The activity and stability of the electrodes

depend on the porosity and pore type of substrate, as well as on the method of preparation. $\text{Ni}_{71}\text{Mo}_{27}\text{P}_2$ electrodes prepared in three steps at low current density and temperature show very good activity and stability in this study. (iii) Experimental results suggest hydride formation by this electrode during cathodic polarization in alkaline solutions.

4. New electrode material, Ni-Zn-P, was prepared with different Zn content, from 14 to 35 at.%. Electrodes were prepared through one-step or three-step electrodeposition method by plating Ni, Ni-P, and Ni-Zn-P. The method works very well so that in a range of pH, temperature, and concentrations of the reagents very stable and active electrodes were obtained. After leaching deposited electrodes in 30% KOH, Zn was mostly removed leading to a porous electrode with a large surface area. While one step deposited electrodes did not show high stability after leaching, excellent stability was observed for the electrodes prepared in three-steps. Electrochemical activities of the electrodes prepared in different conditions and concentration of alkaline solutions show that among three-step deposited electrodes, those prepared at high current densities are the most active electrodes with surface roughness of $\sim 10^4$. The electrodes deposited at high current densities ($\text{Ni}_{54}\text{Zn}_{20}\text{P}_{26}$), after leaching ($\text{Ni}_{83}\text{Zn}_5\text{P}_{12}$) contained more zinc than that ($\text{Ni}_{86}\text{Zn}_2\text{P}_{12}$) deposited at low current density (initial composition $\text{Ni}_{66}\text{Zn}_{14}\text{P}_{20}$). The role of Zn does not seem to be simply that of a sacrificial component, *i.e.*, insertion followed by leaching and leaving a large surface area. Residual Zn present in the structure probably plays a role in the electrode activity.

5. The EIS data were fitted to three models. The criteria for model selection were presented and applied in this case. The best model for EIS data of Ni-Zn-P electrodes here is a modified porous model. The slopes of $\log R_{ct}$ vs. η were somewhat larger than those of steady-state polarization curves. All the logarithmic slopes were smaller than those expected by Volmer-Heyrovský-Tafel mechanism. This remains as a matter of further studies.

(B) Comparison of different methods of surface area determination.

1. Electrochemical impedance spectroscopy explained well the kinetics of the all three groups of electrodes studied. Surface roughness of Ni-Zn-P electrodes as representative of porous electrodes (because of high activity and excellent stability) was evaluated by EIS and compared with the values obtained by other techniques. Very good agreement was observed between the values obtained by all the techniques. The values obtained by other techniques are distributed around that obtained by EIS. The differences change between of 1.4 to 3 times of the value obtained by the EIS. Coulometric oxidation of the surface gave values slightly larger (1.4 time) than that obtained by the EIS. On the other hand, the values obtained by cv using AMs in EG&G M270 software as well as using the analogue sweep generator were slightly (3 to 1.8 times, for AMs 4/4 to analogue, respectively) lower than values obtained by the EIS. The value obtained by ratio of the polarization current densities was also (1.2 time) lower than that of the EIS, but showed better agreement. The comparison really shows that a good agreement exists between the values obtained for roughness factors by these techniques (note that the surface area is very large and the maximum difference is lower than 3 times).
2. Adsorption of carbon monoxide on clean Ni protects the surface from oxidation in air or alkaline solutions at normal conditions. When potential is swept into anodic direction, both CO and covered Ni sites are oxidized. Surface roughness of Ni-Zn-P electrodes was evaluated using the amount of the charge under irreversible anodic peak resulted from oxidation of adsorbed CO referred to the same measurements on Ni polycrystalline. The results were in good agreement with those obtained by other techniques (1.5 time lower than the value obtained by EIS).

3. Finally, it should be pointed out that Raney electrodes as Ni-Co-Zn, Ni-Zn-P, Ni-Mo-Zn, and Ni-Al-Mo, seem to be highly promising for the HER. Deposition by three steps was proposed for Ni-Co-Zn by Machado *et al.* (196,197) and for Ni-Zn-P by us (278). A roughness factor of 4400 for Ni-Co-Zn and 12500 for Ni-Zn-P (278) have been reported for the most active electrodes, see also chapter 6. This method has other interesting benefits as using a simple aqueous bath and wide range of conditions for electrodeposition. The technique is straightforward and seems to be applicable in preparation of other Raney nickel materials. Ni-Al-Mo materials had been prepared by vacuum plasma spray and studied earlier (46,106). The bath given in literature for preparation of Ni-Mo-Zn (277) did not work. My attempts to improve the conditions has not been successful until now.

BIBLIOGRAPHY

1. TRASATTI, Int. J. Hydrogen Energy, **20**, 835 (1995).
2. G. NICOLETTI, Int. J. Hydrogen Energy, **20**, 759 (1995).
3. G. BELANGER, and A. K. VIJH, Int. J. Hydrogen Energy, **9**, 285 (1984).
4. H. VANDENBORRE, R. LEYSEM, H. NACKAERTS, and PH. VAN ASBROEK, Int. J. Hydrogen Energy, **9**, 277 (1984).
5. S. D. FRITTS, and R. GOPAL, J. Electrochem. Soc., **140**, 3337 (1993).
6. R. PARSONS, Trans. Faraday Soc., **54**, 1053 (1958).
7. S. TRASATTI, J. Electroanal. Chem. **111**, 125 (1980).
8. D. PLETCHER, J. Appl. Electrochem., **14**, 403 (1984).
9. D. BARONETTO, I. M. KODINTSEV, and S. TRASATTI, J. Appl. Electrochem., **24**, 189 (1994).
10. S. TRASATTI, Electrochim. Act., **36** 225 (1991).
11. D. E. HALL, J. Electrochem. Soc., **128**, 740 (1981).
12. B. E. CONWAY, J. Electrochem. Soc., **124**, 410 (1977).
13. J. O'M. BOCKRIS and E. C. POTTER, J. Chem. Phys., **20**, 614 (1952).
14. A. C. MAKRIDES, J. Electrochem. Soc., **109**, 977 (1962).
15. A. REINTJES-SARABY, Electrochim. Acta, **31**, 251 (1986).
16. A. LASIA, "Influence of Adsorption of Organic Compounds on the Hydrogen Evolution Reaction," 189th Electrochemical Society Meeting, Los Angeles, May, 1996, Abstract No. 886.
17. R. L. LEROY, Int. J. Hydrogen Energy, **8**, 401 (1983).
18. F. GUTMANN and O. J. MURPHY, *in*: Modern Aspects of Electrochemistry, *Edited* by R. E. White, J. O'M. Bockris, and B. E. Conway, Plenum Press, New York, 1983, Vol. **15**, p.1.
19. K. TENNAKONE, Int. J. Hydrogen Energy, **14**, 681 (1989).

20. K. WISWANATHAN and B. V. TILAK, *J. Electrochem. Soc.*, **131**, 1551 (1984).
21. J. O'M BOCKRIS and E. C. POTTER, *J. Electrochem. Soc.*, **99**, 169 (1952).
22. S. TRASATTI, *in: Advances in Electrochemical Science and Engineering*, Edited by H. Gerischer and C. W. Tobias, VCH, Weinheim, 1992, Vol. 2, p. 1.
23. A. FRUMKIN, N. POLIANOVSKAYA, I. BAGOTSKAYA, and N. GRIGORYEV, *J. Electroanal. Chem.*, **33**, 319 (1971).
24. S. TRASATTI and O. A. PETRII, *Pure Appl. Chem.* **63**, 701 (1991).
25. K. MACHIDA, M. ENYO, G. ADACHI, and J. CHIYOKAWA, *J. Electrochim. Acta*, **29**, 807 (1984).
26. A. LASIA, *Current Topics in Electrochemistry*, **2**, 239 (1993).
27. A. LASIA, *Polish. J. Chem.*, **69**, 639 (1995).
28. A. C. D. ANGELO and A. LASIA, *J. Electrochem. Soc.*, **142**, 3313 (1995).
29. B. E. CONWAY, L. BAI, and D. F. TESSIER, *J. Electroanal. Chem.*, **161**, 39 (1984).
30. M. ELAM and B. E. COMWAY, *J. Appl. Electrochem.*, **17**, 1002 (1987).
31. D. A. HARRINGTON and B. E. CONWAY, *J. Electroanal. Chem.* **221**, 1 (1987).
32. L. BAI, L. GAO, and B. E. CONWAY, *J. Chem. Soc. Faraday Trans.*, **89**, 235 (1993).
33. E. LAMY-PITARA, L. LGHOUZOUANI, Y. TAINON, and J. BARBIER, *J. Electroanal. Chem.*, **260**, 157 (1989).
34. B. E. CONWAY and L. BAI, *J. Chem. Soc., Faraday Trans. 1*, **81**, 1841 (1985).
35. P. Gu, L. BAI, L. GAO, R. BROUSSEAU, and B. E. CONWAY, *Electrochim. Acta*, **37**, 2145 (1992).
36. B. E. CONWAY and L. BAI, *Electrochim. Acta*, **31**, 1013 (1986). G. JERKIEWICZ, J. J. BORODZINSKI, W. CHRZANOWSKI, and B. E. CONWAY, *J. Electrochem. Soc.*, **142**, 3755 (1995).
37. D. A. HARRINGTON and B. E. CONWAY, *Electrochim. Acta*, **32**, 1703 (1987).
38. G. J. BRUG, M. SLUYTERS-REHBACH, and J. H. SLUYTERS, *J. Electroanal. Chem.*, **181**, 245 (1984). G. J. BRUG, A. L. G. VAN DEN EEDEN, M.

- SLUYTERS-REHBACH, and J. H. SLUYTERS, *J. Electroanal. Chem.*, **176**, 275 (1984).
39. A. SARABY-REINTJES, *J. Chem. Soc., Faraday Trans. 1*, **82**, 3343 (1986).
 40. D. SCHÖNFUß, H.-J. SPITZER, and L. MÜLLER, *Russ. J. Electrochem.* **31**, 930 (1995).
 41. R. L. LEROY, M. B. JANJUA, R. RENAUD, and U. LEUENBERGER, *J. Electrochem. Soc.*, **126**, 1674 (1979).
 42. L. CHEN and A. LASIA, *J. Electrochem. Soc.*, **138**, 3321 (1991).
 43. L. CHEN and A. LASIA, *J. Electrochem. Soc.*, **139**, 1058 (1992).
 44. P. LOS, A. RAMI, and A. LASIA, *J. Appl. Electrochem.*, **23**, 135 (1993).
 45. J. DIVISEK, J. MERGEL, and H. F. NESSEN, *Int. J. Hydrogen Energy*, **5**, 151 (1979).
 46. J. DIVISEK, H. SCHMITZ, and J. BELAJ, *J. Appl. Electrochem.*, **19**, 519 (1989).
 47. T. SCHMIDT and H. WENDT, *Electrochim. Acta*, **39**, 1763 (1994).
 48. J. DIVISEK, H. SCHMITZ, and B. STEFFEN, *Electrochim. Acta*, **39**, 1723 (1994).
 49. J. DIVISEK, P. MLINOWSKI, J. MERGEL, and H. SCHMITZ, *Int. J. Hydrogen Energy*, **13**, 141 (1988).
 50. N. YOSHIDA and T. MORIMOTO, *Electrochim. Acta*, **39**, 1733 (1994).
 51. M. B. I. JANJUA, R. L. LEROY, and L. CHEN, *Int. J. Hydrogen Energy*, **10**, 11 (1985).
 52. I. PASEKA, *Electrochim. Acta*, **40**, 1633 (1995).
 53. E. ENDOH, H. OTOUMA, and T. MORIMOTO, *Int. J. Hydrogen Energy*, **13**, 207 (1988).
 54. R. TUNOLD, J. BRUN, B. JOHANSEN, and M. M. JAKŠIĆ, *Russ. J. Electrochem.*, **31**, 638 (1995).
 55. J. DIVISEK, J. MERGEL, and H. SCHMITZ, *Int. J. Hydrogen Energy*, **15**, 105 (1990).
 56. M. E. MARTINS, J. J. PODESTÀ, and A. J. ARVIA, *Electrochim. Acta*, **32**, 1013 (1987).
 57. K. MACHIDA and M. ENYO, *BULL. Chem. Soc. Jpn.* **59**, 725 (1987).

58. S. HADŽI-JORDANOV, H. ANGERSTIEN-KOZLOWSKA, M. VUKOVIĆ, and B. E. CONWAY, *J. Phys. Chem.* **81**, 2271 (1977).
59. M. W. BREITER, *J. Electroanal. Chem.*, **178**, 53 (1984).
60. A. M. SUKHOTIN, M. N. SHLEPAKOV, P. YU. KOSTIKOV, and V. S. STRYKANOV, *Elektrokhimiya*, **17**, 1361 (1981).
61. E. A. MALEEVA, K. S. PEDAN, and V. N. KUDRYAVTSEV, *Russ. J. Electrochem.*, **32**, 770 (1996).
62. A. LASIA and D. GRÉGOIRE, *J. Electrochem. Soc.*, **142**, 3393 (1995).
63. E. A. MALEEVA, K. S. PEDAN, and V. N. KUDRYAVTSEV, *Russ. J. Electrochem.*, **30**, 1118 (1994).
64. R. N. IYER and H. W. PICKERING, *J. Electrochem. Soc.*, **136**, 2463 (1989).
65. G. JERKIEWICZ, J. J. BORODZINSKI, and W. CHRZANOWSKI, **142**, 3755 (1995).
66. A. E. KOZACHINSKII, A. P. PCHEL'NIKOV, Y. B. SKURATNIK, and V. V. LOSEV, *Russ. J. Electrochem.*, **30**, 446 (1994).
67. H. M. LEE, *J. Mater. Sci. Lett.* **14**, 1002 (1979).
68. S. TRASATTI, *in: Electrochemical Hydrogen Technology, Edited by H. Wendt, Elsevier, Amsterdam, 1990.*
69. B. E. CONWAY and L. BAI, *in: Hydrogen Energy Progress, Edited by T. N. Veziroğlu, J. B. Taylor, Pergamon Press, Oxford, 1984, Vol. 2, p. 879.*
70. H. E. G. ROMMAL and P. J. MORAN, *J. Electrochem. Soc.*, **135**, 343 (1988).
71. Y. M. KOLOTYRKIN, P. J. MORGAN, and A. N. CHEMODANOV, *Mat. Chem. Phys.* **19**, 1 (1988).
72. H. J. FLIT and J. O'M. BOCKRIS, *Int. J. Hydrogen Energy*, **6**, 119 (1981).
73. R. N. IYER, I TAKEUCHI, M. ZAMANZADEH, and H. W. PICKERING, *Corrosion*, **46**, 360 (1989).
74. J. J. DELUCCIA, *in: Electrochemical Aspects of Hydrogen in Metals (ASTM STP 962), Edited by L. Raymong, American Society for Testing and Materials, Philadelphia, 1988, p. 17.*

75. D. E. HALL and V. R. SHEPARD, *Int. J. Hydrogen Energy*, **9**, 1005 (1984).
76. T. KITAMURE, C. IWAKURA, and H. TAMURA, *Electrochim. Acta*, **27**, 1723 (1982).
77. M. Y. C. WOO, *in: Industrial Application of Titanium and Zirconium, Edited by C. S. Young and J. C. Durham, (ASTM), Philadelphia, 1986, Vol. 4, p. 3.*
78. D. J. BLACKWOOD, L. M. PETER, H. E. BISHOP, P. R. CHALKER, and D. E. WILLIAMS, *Electrochim. Acta*, **34**, 1401 (1989).
79. V. N. KICHIGIN, N. I. KAVARDAKOV, and V. V. KUZNETSOV, *Elektrokhimiya*, **18**, 1059 (1982).
80. T. OKADA, *Electrochim. Acta*, **27**, 1273 (1982).
81. H. WENDT, H. HOFMANN, and V. PLZAK, *Mat. Chem. Phys.* **22**, 27 (1989).
82. M. NAGAMURA, H. UKIHASHI, and O. SHIRAGAMI, *in: Modern Chlor-Alkali Technology, Edited by C. Jackson, Ellis Horwood, Chichester, 1983, Vol. 2, p. 61.*
83. E. ENDOH, H. OTOUMA, T. MORIMOTO, and Y. ODA, *Int. J. Hydrogen Energy*, **12**, 473 (1987).
84. Y. CHOQUETTE, H. MENARD, and L. BROSSARD, *Int. J. Hydrogen Energy*, **14**, 6371 (1989).
85. P.-H. LO, W.-T. TSAI, J.-T. LEE, and M.-P. HUNG. *Surf. Coat. Technol.*, **67**, 27 (1994).
86. K. H. HUR, J. H. JEONG, and D. N. LEE, *J. Mater. Sci.*, **25**, 2573 (1990).
87. N. K. DIRJAL, K. A. HOLBROOK, and P. B. Wells, *Anal. Chim. Acta*, **290**, 287 (1994).
88. T. M. HARRIS and Q. D. DANG, *J. Electrochem. Soc.*, **140**, 81 (1993).
89. H. J. LEE, E. AKIYAMA, H. HABAZAKI, A. KAWASHIMA, K. ASAMI, and K. HASHIMOTO, *Corros. Sci.*, **37**, 321 (1995).
90. E. BREDAEL, J. P. CELIS, and J. R. ROOS, *Surf. Coat. Technol.* **58**, 63 (1993).
91. J. CROUSIER, Z. HANANE, and J.-P. CROUSIER, *Electrochim. Acta*, **38**, 261 (1993).

92. B.-P. ZHANG, H. HABAZAKI, A. KAWASHIMA, K. ASAMI, and K. HASHIMOTO, *Corros. Sci.*, **33**, 1519 (1992).
93. K. Lu, J.-T. WANG, and W. D. WEI, *J. Phys. D, Appl. Phys.*, **25**, 808 (1992).
94. R. L. ZELLER III and UZIEL LANDAU, *J. Electrochem. Soc.*, **137**, 1107 (1990).
95. A. KAWASHIMA, Y. P. LU, H. HABAZAKI, K. ASAMI, and K. HASHIMOTO, *Corrosion Engineering*, **38**, 643 (1989).
96. M. BREDAEL, B. BLANPAIN, J.-P. CELIS, and J. R. ROOS, *J. Electrochem. Soc.*, **141**, 294 (1994).
97. N. KRASTEVA, V. FOTTY, and S. ARMYANOV, *J. Electrochem. Soc.*, **141**, 2864 (1994).
98. R. L. ZELLER III and UZIEL LANDAU, *J. Electrochem. Soc.*, **139**, 3464 (1992).
99. R. B. DIEGLE and N. R. SORENSEN, *J. Electrochem. Soc.*, **133**, 1769 (1986).
100. H. WENDT, S. RAUSCH, and T. BORUCINSKI, *Adv. Catal.*, **40**, 87 (1994).
101. N. V. KRSTAJIĆ, M. D. SPASOJEVIĆ, and R. T. ATANASOSKI, *J. Appl. Electrochem.*, **14**, 131 (1984).
102. J. J. BORODZINSKI and A. LASIA, *J. Appl. Electrochem.*, **24**, 1267 (1994).
103. P. LOS and A. LASIA, *J. Electroanal. Chem.*, **333**, 115 (1992).
104. C. WELCH, G. N. HUGHES, R. A. CRAWFORD, and D. W. DUBOIS, *in: Advances in Chlor-Alkali and Chlorate Industry*, Edited by M. M. Silver and E. M. Spore, The Electrochemical society, Pennington, 1984, p. 192.
105. K. LOHRBERG and P. KOHL, *Electrochim. Acta*, **29**, 1557 (1984).
106. D. MIOUSSE, A. LASIA, and V. BORCK, *J. Appl. Electrochem.*, **25**, 603 (1995).
107. W. SCHNURNBERGER, R. HENNEN, and M. VON BRADKE, *in: Hydrogen Energy Progress*, Edited by T. N. VEZIROĞLU and J. B. TAYLOR, Pergamon Press, Oxford, 1984, Vol. 2, p. 933.
108. R. HENNE, M. V. BRADTKE, W. SCHNURNBERGER, and W. WEBER, *Proc. 11th International Thermal Spraying Conference*, Montreal, 8 - 12 Sept., p. 61, (1986).
109. D. E. HALL, *J. Appl. Electrochem.*, **14**, 107 (1984).

110. L. BROSSARD and J. Y. HUOT, *J. Appl. Electrochem.*, **21**, 508 (1991).
111. Y. HUOT and L. BROSSARD, *J. Appl. Electrochem.*, **20**, 281 (1990).
112. J. Y. HUOT and L. BROSSARD, *Int. J. Hydrogen Energy*, **14**, 229 (1989).
113. J. Y. HUOT and L. BROSSARD, *J. Appl. Electrochem.*, **18**, 815 (1988).
114. P.-H. LO, W.-T. TSAI, J.-T. LEE, and M.-P. HUNG, *J. Electrochem. Soc.*, **142**, 91 (1995).
115. G. L. GRAEF and G. W. CHANDLER, *J. Electrochem. Soc.*, **137**, 1506 (1990).
116. A. SZAAZ, D. J. FABIAN, Z. PAAL, and J. KOJNOK, *J. Non-Crystalline Solids*, **103**, 21 (1988).
117. L. M. ABRANTES and J. P. CORREIA, *J. Electrochem. Soc.*, **141**, 2356 (1994).
118. R. L. ZELLER III and L. J. SALVATI, *Corros.*, **50**, 457 (1994).
119. J. J. PODESTÁ, R. C. V. PIATTI, and A. J. ARVIA, *Int. J. Hydrogen Energy*, **20**, 111 (1995).
120. H. WENDT and G. IMARISIO, *J. Appl. Electrochem.*, **18**, 1 (1988).
121. L. CHEN and A. LASIA, *J. Electrochem. Soc.*, **140**, 2464 (1993).
122. L. CHEN and A. LASIA, *J. Electrochem. Soc.*, **139**, 3458 (1992).
123. L. CHEN and A. LASIA, *J. Electrochem. Soc.*, **139**, 3214 (1992).
124. Y. CHOQUETTE, H. MENARD, and L. BROSSARD, *Int. J. Hydrogen Energy*, **15**, 21 (1990).
125. Y. CHOQUETTE, L. BROSSARD, A. LASIA, and H. MENARD, *Electrochim. Acta*, **35**, 1251 (1990).
126. Y. CHOQUETTE, L. BROSSARD, A. LASIA, and H. MENARD, *J. Electrochem. Soc.*, **137**, 1723 (1990).
127. N. YOSHIDA, M. YOSHITAKE, E. ENDOH, and T. MORIMOTO, *Int. J. Hydrogen Energy*, **14**, 137 (1989).
128. A. NIDOLA and R. SCHIRA, *in: Hydrogen Energy Progress, Edited by T. N. Veziroğlu and J. B. Talor*, Pergamon Press, Oxford, 1984, Vol. **2**, p. 909.

129. K. MACHIDA, M. ENYO, K. KAI, and K. SUZUKI, *J. Less-Common Met.*, **100**, 377 (1984).
130. K. M. ENYO, I. TOYOSHIMA, K. KAI, and K. SUZUKI, *J. Less-Common Met.*, **96**, 305 (1984).
131. G. GORGE, R. FAURE, R. DURAND, and A. R. YAVARI, *Mat. Sci. Eng.*, **99**, 517 (1988).
132. M. NOEL and S. CHIDAMBARAM, *J. Electroanal. Chem.*, **396**, 25 (1994).
133. A. NIDOLA and R. SCHIRA, *J. Electrochem. Soc.*, **133**, 1653 (1986). C. BAILLEUX, A. DAMIEN, and A. MONTET, *Int. J. Hydrogen Energy*, **8**, 529 (1983). C. BAILLEUX, *Int. J. Hydrogen Energy*, **6**, 469 (1981).
134. E. PROTOPOPOFF and P. MARCUS, *J. Electrochem. Soc.*, **135**, 3073 (1988). P. MARCUS and E. PROTOPOPOFF, *Surf. Sci.*, **17**, 533 (1985). E. LAMY-PITARA, L. LGHOUZOUANI, Y. TAINON, and J. BARBIER, *J. Electroanal. Chem.*, **260**, 157 (1989).
135. J. H. BARBER and B. E. CONWAY, *J. Chem. Soc., Faraday Trans.*, **92**, 3709 (1996) and reference 19th therein.
136. E. LAMY-PITARA and J. BARBIER, *J. Electroanal. Chem.*, **416**, 47 (1996).
137. C. F. ZINOLA, A. M. CASTRO LUNA, and A. J. ARVIA, *J. Appl. Electrochem.*, **26**, 325 (1996). E. P. M. LEIVA, E. SANTOS, and T. IWASITA, *J. Electroanal. Chem.*, **215**, 357 (1986).
138. H. A. GASTEIGER, N. M. MARKOVIĆ., and P. N. ROSS Jr., *Catal. Lett.*, **36**, 1 (1996). B. BEDEN and C. LAMY, *Electrochim. Acta*, **35**, 691 (1990).
139. A. NIDOLA and R. SCHIRA *in: Advances in the Chlor-Alkali and Chlorate Industry*, Edited by M. M. Silver and E. M. Spore, The Electrochemical Society, Pennington, 1984, p. 206.
140. D. E. HALL, J. M. SARVER, and D. O. GOTHARD, *in: Advances in the Chlor-Alkali and Chlorate Industry*, Edited by F. Hine, R. E. White, W. B. Darlington, and R. D. Varjian, The Electrochemical Society, Pennington, 1988, p. 184.

141. J. E. BENNETT, *Int. J. Hydrogen*, **5**, 401 (1980).
142. L. BROSSARD and J. Y. HUOT, *J. Appl. Electrochem.*, **19**, 882 (1989).
143. J. Y. HUOT and L. BROSSARD, *Int. J. Hydrogen Energy*, **12**, 821 (1987).
144. H. E. G. ROMMAL and P. J. MORAN, *J. Electrochem. Soc.*, **132**, 325 (1985).
145. J. A. HARRISON and A. T. KUHN, *Surf. Technol.*, **19**, 249 (1983).
146. J. A. HARRISON and A. T. KUHN, *J. Electroanal. Chem.*, **184**, 347 (1985).
147. S. RAUSCH and H. WENDT, *J. Electrochem. Soc.*, **143**, 2852 (1996).
148. V. G. NEFEDOV, V. M. SEREBRITSKII, and O. S. KSENZHEK, *Elektrokhimiya*, **10**, 1382 (1987).
149. S. F. CHEN and T. J. O'KEEFE, *Electrochim. Acta*, **33**, 789 (1988).
150. L. J. J. JANSSEN and E. BARENDRECHT, *Electrochim. Acta*, **30**, 683 (1985).
151. D. W. DEES and C. W. TOBIAS, *in: Proceedings of 35th Meeting, International Society of Electrochemistry, Berkely, CA, 1984*, p. 717.
152. Y. FUKUNAKA, K. SUZUKI, A. UEDA and Y. KONDO, *J. Electrochem. Soc.*, **136**, 1002 (1989).
153. A. T. KUHN and M. STEVENSON, *Electrochim. Acta*, **27**, 329 (1982).
154. P. GALLONE, G. MODICA, and S. MAFFI, *J. Electroanal. Chem.*, **180**, 421 (1984).
155. B. E. BONGENAAR-SCHLENTER, L. J. J. JANSSEN, S. J. D. van STRALEN, and E. BARENDRECHT, *J. Appl. Electrochem.*, **15**, 537 (1985).
156. J. DUKOVIC and C. W. TOBIAS, *J. Electrochem. Soc.*, **134**, 331 (1987).
157. J. Y. HUOT, *J. Appl. Electrochem.*, **19**, 453 (1989).
158. B. E. CONWAY, D. F. TESSIER, and D. P. WILKINSON, *J. Electroanal. Chem.*, **199**, 249 (1986).
159. L. M. VRAČAR and D. M. DRAŽIĆ, *J. Electroanal. Chem.*, **265**, 171 (1989).
160. U. FREESE and STIMMING, *J. Electroanal. Chem.* **198**, 409 (1986).
161. B. E. CONWAY and D. J. MACKINNON, *J. Electrochem. Soc.*, **116**, 1665 (1969).
162. B. E. CONWAY and D. P. WILKINSON, *J. Electroanal. Chem.*, **214**, 633 (1986).
163. B. E. CONWAY and D. P. WILKINSON, *J. Electroanal. Chem.*, **210**, 167 (1986).

164. J. O'M. BOCKRIS and A. GOCHEV, *J. Electroanal. Chem.*, **214**, 655 (1986).
165. B. E. CONWAY, D. P. WILKINSON, D. F. TESSIER, and BER. BUNSENGES., *Phys. Chem.*, **91**, 484 (1987).
166. J. O'M. BOCKRIS and A. GOCHEV, *J. Phys. Chem.*, **90**, 5232 (1986).
167. M. J. WEAVER, *J. Phys. Chem.*, **80**, 2645 (1976).
168. W. SCHMICKLER, *J. Electroanal. Chem.*, **284**, 269 (1990).
169. E. GILEADI, *J. Electrochem. Soc.*, **134**, 117 (1987).
170. E. K. EISNER, M. SCHWARZ, and E. GILEADI, *Electrochim. Acta*, **34**, 1103 (1989).
171. L. B. KRIKSUNOV and V. M. TSIONSKI, *Elektrokhimiya*, **10**, 53 (1974).
172. A. C. FERREIRA, E. R. GONZÁLEZ, E. A. TICIANELLI, L. A. AVACA, and B. MATVIENKO, *J. Appl. Electrochem.*, **18**, 894 (1988).
173. I. P. IVANOV, M. P. VASILEVA-DIMOVA, and K. I. NONINSKI, *J. Elektrokhimiya*, **20**, 1522 (1984).
174. J. DE CARVALHO, G. TREMILIOSI-FILHO, L. A. AVACA, and E. R. GONZALEZ, *in: Electrode Material and Processes for Energy Conversion and Storage, Edited by S. Srinivasan, S. Wagner, and H. Wroblowa, The Electrochemical Society, Pennington, 1987, p. 356.*
175. V. M. TSIONSKII, L. I. KRISHTALIK, and L. B. KRIKSUNOV, *Electrochim. Acta*, **33**, 623 (1988).
176. E. K. EISNER, M. ROSENBLUM, M. SCHWARZ, and E. GILEADI, *J. Electroanal. Chem.*, **410**, 189 (1996), and references therein.
177. S. TRASATTI, *J. Electroanal. Chem.*, **39**, 163 (1972).
178. A. J. APPLEBY, *in: Comprehensive Treatise of Electrochemistry, Edited by B. E. Conway, J. O'M. Bockris, E. Yeager, S. U. M. Khan, and R. E. White, New York, Plenum Press, 1983, Vol. 7, p.173.*
179. E. YEAGER, *J. Electrochem. Soc.*, **128**, 160C (1981).

180. A. J. APPLEBY, H. KITA, M. CHEMLA, and G. BRONOËL, *in*: Encyclopedia of Electrochemistry of the Elements, *Edited by* A. J. Bard, Marcel Dekker, New York, Vol. IX, 1982, Part A, p. 383.
181. H. KITA, *J. Electrochem. Soc.*, **113**, 1095 (1966).
182. M. H. MILES, *J. Electroanal. Chem.*, **60**, 89 (1975).
183. M. M. JAKŠIĆ, *Electrochim. Acta*, **29**, 1539 (1984).
184. M. M. JAKŠIĆ, *Int. J. Hydrogen Energy*, **11**, 519 (1986).
185. L. BREWER, *in*: Electronic Structure and Alloy Chemistry of Transition Elements, *Edited by* P. A. BECK, Interscience, New York, 1963, P. 221.
186. M. M. JAKŠIĆ, *J. Mol. Catal.*, **38**, 161 (1986).
187. M. M. JAKŠIĆ and J. M. JAKŠIĆ, *Electrochim. Acta*, **39**, 1695 (1994).
188. H. EZAKI, M. MORINAGA, and S. WATANABE, *Electrochim. Acta*, **38**, 557 (1994).
189. H. EZAKI, M. MORINAGA, S. WATANABE, and J. SAITO, *Electrochim. Acta*, **39**, 1769 (1994).
190. H. WENDT, H. HOFMANN, and V. PLZAK, *Int. J. Hydrogen Energy*, **9**, 297 (1984).
191. L. ANGELY, G. BRONOËL, and G. PESLERBE, *J. Electroanal. Chem.*, **96**, 183, 191, and 203 (1979).
192. A. LASIA and A. RAMI, *J. Electroanal. Chem.*, **294**, 123 (1990).
193. J. P. DIARD, B. LEGORREC, and S. MAXIMOVITCH, *Electrochim. Acta*, **35**, 1099 (1990).
194. K. LIAN, S. J. THORPE, and D. W. KIRK, *Electrochim. Acta*, **37**, 2029 (1992).
195. N. V. KOROVIN, O. N. SAVELEVA, T. L. DOGONOVA, and E. Y. UDRIS, *Elekterokhimiya*, **23**, 707 (1987).
196. M. J. DE GIZ, S. A. S. MACHADO, L. A. AVACA, and E. R. GONZALEZ, *J. Appl. Electrochem.*, **22**, 973 (1992).
197. S. A. S. MACHADO, J. TIENGO, P. DE LIMA, and L. A. AVACA, *J. Appl. Electrochem.*, **26**, 431 (1996).
198. M. J. De GIZ, G. TREMILIOSI-FILHO, and E. R. GONZALEZ, **39**, 1775 (1994).

199. M. R. GENNERO DE CHIALVO and A. C. CHIALVO, *J. Electroanal. Chem.*, **372**, 209 (1994).
200. M. R. GENNERO DE CHIALVO and A. C. CHIALVO, *J. Electroanal. Chem.*, **388**, 215 (1995).
201. N. M. MARKOVIĆ, S. T. SARRAF, H. A. GASTEIGER, and PHILIP N. ROSS, JR., *J. Chem. Soc., Faraday Trans.*, **92**, 3720 (1996).
202. H. KITA, S. YE, and Y. GAO, *J. Electroanal. Chem.*, **334**, 351 (1992). S. TRASATTI, *Mat. Chem. Phys.*, **12**, 507 (1985).
203. I. M. NOVOSELSKII, *Elektrokhimiya*, **15**, 1285 (1979). A. M. MERETSKII, I. V. KUDRYASHOV, and Y. B. VASILIEV, *Elektrokhimiya*, **13**, 447 (1977).
204. V. L. KHEIFETS, B. S. KRASTSKOV, and A. L. ROTINYAN, *Elektrokhimiya*, **6**, 916 (1970).
205. B. V. TILAK, *Mat. Chem. Phys.*, **22**, 149 (1989).
206. S. TRASATTI, *in: Advances in Electrochemistry and Electrochemical Engineering, Edited by H. Gerischer and C. W. Tobias, Interscience, New York, 1977, Vol. 10, p. 213.*
207. H. GERISCHER, D. M. KOLB, and M. PRZASNYSKI, *Surf. Sci.*, **43**, 662 (1974).
208. S. TRASATTI, *Z. Phys. Chem.*, **98**, 75 (1975).
209. K. JÜTTNER, *Electrochim. Acta*, **31**, 917 (1986). R. R. ADŽIĆ, M. D. SPASOJEVIĆ, and A. R. DESPIĆ, *Electrochim. Acta*, **24**, 577 (1979).
210. A. M. ABD EI-HALIM, K. JÜTTNER, and W. J. LORENZ, *J. Electroanal. Chem.*, **106**, 193 (1980). N. FURUYA and S. MOTOO, *J. Electroanal. Chem.*, **102**, 155 (1979).
211. R. R. ADŽIĆ, M. D. SPASOJEVIĆ, and A. R. DESPIĆ, *Electrochim. Acta*, **24**, 569 (1979).
212. S. MOTOO and N. FURUYA, *Mat. Chem. Phys.*, **22**, 309 (1989).
213. N. V. KOROVIN, N. I. KOZLOVA, and O. N. SAVELEVA, *Elektrokhimiya*, **16**, 583 (1980).

214. N. V. KOROVIN, E. Y. UDRIS, and O. N. SAVELEVA, *Elektrokhimiya*, **22**, 360 (1986).
215. N. V. KOROVIN, N. I. KOZLOVA, and O. N. SAVELEVA, *Elektrokhimiya*, **10**, 1575 (1978).
216. R. W. MURRAY, *in: Techniques of Chemistry, Edited by W. H. Saunders, Jr., John Wiley and Sons Inc., New York, 1992, Vol. 22, p. 262.* G. KUMY, Y. YIE, and F. C. ANSON, *J. Electroanal. Chem.*, **413**, 165 (1996).
217. B. LINDHOL-SETHSON, T. TJÄRNHAGE, and M. SHARP, *Electrochim. Acta*, **40**, 1675 (1994).
218. R. M. KELLETT and T. G. SPIRO, *Inorg. Chem.*, **24**, 2373 (1985).
219. R. M. KELLETT and T. G. SPIRO, *Inorg. Chem.*, **24**, 2378 (1985).
220. B. KEITA and L. NADJO, *Mat. Chem. Phys.*, **22**, 2378 (1989).
221. B. KEITA and L. NADJO, *J. Electroanal. Chem.*, **191**, 441 (1985).
222. B. KEITA and L. NADJO, *J. Electroanal. Chem.*, **199**, 229 (1986).
223. B. KEITA and L. NADJO, *J. Electroanal. Chem.*, **243**, 87 (1988).
224. B. KEITA, L. NADJO, and J. M. SAVÉANT, *J. Electroanal. Chem.*, **243**, 105 (1988).
225. B. KEITA, L. NADJO, G. KREIR, and J. F. MULLER, *J. Electroanal. Chem.*, **223**, 287 (1988).
226. B. KEITA and L. NADJO, *J. Electroanal. Chem.*, **240**, 325 (1988).
227. B. KEITA, L. NADJO, and J. P. HAEUSSLER, *J. Electroanal. Chem.*, **243**, 105 (1988).
228. B. KEITA, T. LUCAS, and L. NADJO, *J. Electroanal. Chem.*, **208**, 343 (1986).
229. B. KEITA and L. NADJO, *J. Electroanal. Chem.*, **230**, 85 (1987).
230. B. KEITA and L. NADJO, *J. Electroanal. Chem.*, **287**, 149 (1986).
231. B. KEITA, T. LUCAS, and L. NADJO, *J. Electroanal. Chem.*, **269**, 447 (1989).
232. O. SAVADOGO and E. ENDZEBET, *J. Appl. Electrochem.*, **23**, 915 (1993).
233. O. SAVADOGO, *J. Electrochem. Soc.*, **139**, 1082 (1992).
234. O. SAVADOGO and S. LÉVESQUE, *J. Appl. Electrochem.*, **21**, 457 (1991).

235. O. SAVADOGO and K. AMUZGAR, and D. L. PIRON, *Int. J. Hydrogen Energy*, **15**, 783 (1990).
236. O. SAVADOGO and S. THIBAUT, *Int. J. Hydrogen Energy*, **14**, 865 (1989).
237. L. BROSSARD, *Int. J. Hydrogen Energy*, **13**, 315 (1988).
238. E. POTVIN, H. MENARD, J. M. LALANCETTE, and L. BROSSARD, *J. Appl. Electrochem.*, **20**, 252 (1990).
239. J. BALAJKA, *Int. J. Hydrogen Energy*, **8**, 755 (1983).
240. G. L. CAHEN, P. J. MORAN, L. L. SCRIBNER, and G. E. STONER, *J. Electrochem. Soc.*, **128**, 1877 (1981).
241. M. BONNER, T. BOTTS, J. McBREEN, A. MEZZINA, F. SALZANO, and C. YANG, *Int. J. Hydrogen Energy*, **9**, 269 (1984).
242. A. G. PSHENICHNIKOV, R. K. BURSHEIN, and V. D. KOVALEVSKAYA, *Elektrokhimiya*, **11**, 1465 (1975).
243. A. LASIA, *Int. J. Hydrogen Energy*, **18**, 557 (1993).
244. S. A. S. MACHADO, J. TIENGO, P. DE LIMA NETO, and L. A. AVACA, *Electrochim. Acta*, **39**, 1757 (1994).
245. M. J. DE GIZ, M. FERREREIRA, G. TREMILIOSI-FILHO, and E. R. GONZALEZ, *J. Appl. Electrochem.*, **23**, 641, (1993).
246. S. A. S. MACHADO, J. TIENGO, P. DE L. NETO, and L. A. AVACA, Abstract of the 44th ISE Meeting, Berlin (1993).
247. D. M. SOAREZ, O. TESCHKE, and I. TORRIANI, *J. Electrochem. Soc.*, **139**, 98 (1992).
248. J. Y. HUOT, *J. Electrochem. Soc.*, **136**, 1933 (1989).
249. G. P. POWER, *Electrochim. Acta*, **27**, 539 (1982).
250. S. MAXIMOVITCH and R. DURAND, *J. Electroanal. Chem.*, **149**, 273 (1983).
251. F. HAHN, B. BEDEN, M. J. CROISSANT, and C. LAMY, *Electrochim. Acta*, **31** 335 (1986).

252. B. BEDEN, D. FLONER, J. M. LÉGER, and C. LAMY, *Surface science*, **162**, 822 (1985).
253. A. VISINTIN, A. C. CHIALVO, W. E. TRIACA, and A. J. ARVIA, *J. Electroanal. Chem.*, **225**, 227 (1987).
254. M. R. GENENERO DE CHIALVO and A. C. CHIALVO, *Electrochim. Acta*, **33**, 825 (1988).
255. J. McBREEN *in: Modern Aspects of Electrochemistry*, Edited by R. E. White, J. O'M Bockris, and B. E. Conway, Plenum Press, New York, 1990, Vol. **21**, p. 29.
256. M. CAPADONIA, J. DIVISEK, T. V. DER HEYDEN, and U. STIMMING, *Electrochim. Acta*, **39**, 1559 (1994).
257. W. VISSCHER and E. BARENDRECHT, *J. Appl. Electrochem.*, **10**, 269 (1980).
258. T. C. LIU and B. E. CONWAY, *J. Appl. Electrochem.*, **17**, 983 (1987).
259. P. W. T. LU and S. SRINIVASAN, *J. Electrochem. Soc.*, **125**, 1416 (1978).
260. D. V. SOKOLSKII, B. Y. NOGERBEGOV, N. N. GUDELEVA, and R. G. MUSTAFINA, *Elektrokhimiya* **22**, 1185 (1986).
261. L. A. BURKALTSEVA and A. G. PSHENICHNIKOV, *Elektrokhimiya*, **12**, 42 (1976).
262. G. L. PADYUKOVA, G. A. PUSHKAREVA, and A. B. FASMAN, *Elektrokhimiya*, **20**, 963 (1984).
263. J. C. K. HO and D. L. PIRON, *J. Electrochem. Soc.*, **142**, 1144 (1995).
264. L. V. TAMM, Y. K. TAMM, and V. É. PAST, *Elektrokhimiya*, **11**, 1581 (1975).
265. H. DUMONT, P. LOS, L. BROSSARD, A. LASIA, and H. MENARD, *J. Electrochem. Soc.*, **139**, 2143 (1992).
266. H. DUMONT, P. W. WRONA, J. M. LALANCETTE, and H. MENARD, *J. Appl. Electrochem.*, **23**, 684 (1993).
267. H. DUMONT, P. LOS, A. LASIA, H. MENARD, and L. BROSSARD, *J. Appl. Electrochem.*, **23**, 684 (1993).
268. E. R. GONZALEZ, G. TREMILIOSI-FILHO, and M. G. de GIZ, *Current Topics in Electrochemistry*, **2**, 167 (1993).

269. A. G. PSHENICHNIKOV, *Mat. Chem. Phys.* **22**, 121 (1989).
270. E. JUSTI, W. SCHEIBE, and A. WINSEL, German Patent DPB 1 101 361 (1954).
271. A. G. PSHENICHNIKOV, S. F. CHERNYSHOV, Y. I. KRYUKOV, L. I. ALTENTALLER, E. I. TUMASOVA, and V. N. DUDIN, *Elektrokhimiya*, **18**, 1011 (1982).
272. J. DIVISEK, J. MERGEL, and H. SCHMITZ, *Int. J. Hydrogen Energy*, **7**, 695 (1982).
273. Th. BORUCINSKI, S. RAUCH, and H. WENDT, *J. Appl. Electrochem.*, **22**, 1031 (1992).
274. A. G. PSHENICHNIKOV, *Int. J. Hydrogen Energy*, **7**, 51 (1982).
275. G. L. PADYUKOVA, G. A. PUSHKAREVA, A. B. FASMAN, and B. K. ALMASHEV, *Elektrokhimiya*, **22**, 747 (1986).
276. V. G. SHALYUKHIN, G. L. PADYUKOVA, A. S. KUANYSHYEV, and A. B. FASMAN, *Elektrokhimiya*, **25**, 134 (1989).
277. I. A. RAJ and K. I. VASU, *J. Appl. Electrochem.*, **22**, 471 (1992).
278. R. KARIMI-SHERVEDANI and A. LASIA, *J. Electrochem. Soc.*, **144**, 2652 (1997).
279. S. A. S. MACHADO and L. A. AVACA, *Electrochim. Acta*, **39**, 1385 (1994).
280. R. PAUL, P. BUISSON and N. JOSEPH, *Ind. Eng. Chem.*, **44**, 1007 (1952).
281. D. MEARS and M. BOUDART, *AIChE J.*, **12**, 312 (1966).
282. C. BROWN, *J. Org. Chem.*, **35**, 1900, (1970).
283. H. VANDERBORRE, R. LEYSEN, and H. NACKAERTS, *Int. J. Hydrogen Energy*, **8**, 81 (1983).
284. R. SABELA and I. PASEKA, *J. Appl. Electrochem.*, **20**, 500 (1990).
285. H. VANDERBORRE, R. LEYSEN, H. NACKAERTS, and P. VAN ASBROECK, *Int. J. Hydrogen Energy*, **9**, 277 (1983).
286. I. PASEKA, *Electrochim. Acta*, **38**, 2449 (1993).
287. M. KISKINOVA and D. W. MAN, *Surf. Sci.*, **108**, 64 (1982).
288. S. JOHNSON and R. J. MADIX, *Surf. Sci.*, **108**, 77 (1982).
289. R. NARAGAN and M. N. MUNGOLE, *Surf. Technol.*, **24**, 233 (1985).

290. D. S. LASHMORE and J. F. WEINROTH, *Plat. and Surf. Finish.*, **68**, 72 (1982).
291. E. TOTH-KADAR, I. BAKONYI, A. SOLYON, J. HERING, and G. KONCZOS, *Surf. Finish. and Coat. Techno.*, **31**, 31 (1987).
292. M. RATZKER, D. S. LASHMORE, and K. W. PRATT, *Plat. and Surf. Finish.*, **74**, 74 (1986).
293. L. R. ZELLER III, *ibid*, **78**, 53 (1991).
294. A. A. WRONKOWSKA and A. WRONKOWSKI, *Mater. Sci.*, **27**, 1842 (1992).
295. U. HOFFMANN and K. G. WELL, *Corros. Sci.*, **34**, 423 (1993).
296. R. B. DIEGLE and N. R. SORENSEN, *J. Electrochem. Soc.*, **135**, 1085 (1988).
297. H. HABAZAKI, Y. P. LU, A. KAWASHIMA, K. ASAMI, and K. ASHIMOTO., *Corros. Sci.*, **32**, 1227 (1991).
298. J. L. CARBAGIAL and R. E. WHITE, *J. Electrochem. Soc.*, **135**, 2952 (1988).
299. A. KROLIKOWSKI and P. BUTKIEWICZ, *Electrochim. Acta*, **38**, 1979 (1993).
300. U. HOFFMANN and K. G. WELL, *Ber. Bunsenges. Phys. Chem.*, **95**, 1482 (1991).
301. P. K. NG, D. D. SNYDER, and J. LASALA, *J. Electrochem. Soc.*, **135**, 1376 (1988).
302. I. PASEKA and J. VELICKA, *Electrochim. Acta*, **42**, 237 (1997).
303. J. PODESTA, R. C. V. PIATTI, A. J. ARVIA, P. EKUNDGE, K. JÜTTNER, and G. KREYSA, *Int. j. Hydrogen Energy*, **17**, 9 (1992).
304. A. A. WRONKOWSKA, *J. Electrochem. Soc.*, **140**, 995 (1993).
305. G. KREYSA and B. HAKANSSON, *J. Electroanal. Chem.*, **201**, 61 (1986).
306. K. K. LIAN, D. W. KIRK, and S. J. THORPE, *J. Electrochem. Soc.*, **142**, 3704 (1995).
307. G. BARRAL, F. NJANJO-EYOKE, and S. MAXIMOVITCH, *Electrochim. Acta*, **40**, 709 (1995).
308. C. Q. CUI and J. Y. LEE, *Electrochim. Acta*, **40**, 1653 (1995).
309. M. C. BERNARD, P. BERNARD, M. KEDDAM, S. SENYARICH, and H. TAKENOUTI, *Electrochim. Acta*, **41**, 91 (1996).
310. BALEJ, *Int. J. Hydrogen Energy*, **10**, 89 (1985).

311. Y. J. KIM, S. SRIVIVASAN, and A. J. APPLEBY, *J. Appl. Electrochem.*, **20**, 377 (1990).
312. L. D. BURKE and T. A. M. TWOMEY, *J. Electroanal. Chem.*, **167**, 285 (1984).
313. W. VISSCHER and E BARENDRECHT, *J. Appl. Electrochem.*, **10**, 269 (1980).
314. G. BARRAL, S. MAXIMOVITCH, and F. NJANJO-EYOKE, *Electrochim. Acta*, **41**, 1305 (1996).
315. C. FAN, D. L. PIRON, A. SLEB, and P. PARADIS, *J. Electrochem. Soc.*, **141**, 382 (1994).
316. D. E. BROWN, M. N. MAHMOOD, A. K. TURNER, S. M. HALL, and P. O. FOGARTY, *Int. J. Hydrogen Energy*, **7**, 405 (1982).
317. M. V. ANANTH and N. V. PARTHASARADLY, *Int. J. Hydrogen Energy*, **15**, 193 (1990).
318. I. A. RAJ and K. I. VASU, *J. Appl. Electrochem.*, **20**, 32 (1990).
319. A. NIDOLA, *Int. J. Hydrogen Energy*, **9**, 367 (1984).
320. R. GONZALEZ, L. A. AVACA, A. CARUBELLI, A. A. TANAKA, and G. TREMILIOSI-FILHO, *Int. J. Hydrogen Energy*, **9**, 689 (1984).
321. M. M. JAKŠIĆ, *Mat. Chem. Phys.*, **22**, 1 (1989).
322. E. BROWN, M. N. MAHMOOD, M. C. M. MAN, and A. K. TURNER, *Electrochim. Acta*, **29**, 1551 (1984).
323. I. A. RAJ and V. K. VENKATESAN, *Int. J. Hydrogen Energy*, **13**, 215 (1988).
324. D. E. BROWN, S. M. HALL, M. N. MAHMOOD, M. C. M. MAN, A. K. TURNER, D. WOOD, and S. ANDERSON, *in: Electrocatalysis, Edited by W. E. O'Grady, P. N. Ross, and F. G. Will, The Electrochemical Society, 1982, p. 145.*
325. B. E. CONWAY, L. BAI, and M. A. SATTAR, *Int. J. Hydrogen Energy*, **13**, 215 (1988).
326. B. E. CONWAY and L. BAI, *Int. J. Hydrogen Energy*, **11**, 533 (1986).
327. B. E. CONWAY, H. ANGERSTEIN-KOZLOWSKA, and M. A. SATTAR, *J. Electrochem. Soc.*, **130**, 1825 (1983).

328. J. KUMAR and S. SAXENA, *Int. J. Hydrogen Energy*, **14**, 331 (1989). T. MATSUMOTO and A. MATSUSHITA, *J. Less-Common Met.*, **123**, 135 (1986).
329. E. HALL, J. M. SARVER, and D. O. GOTHARD, *Int. J. Hydrogen Energy*, **13**, 547 (1988).
330. O. A. PETRII, K. N. SEMENKO, I. I. KOROBOV, S. Y. VASINA, I. V. KOVRIGINA, and V. V. BURNASHEVA, *J. Less-Common Met.*, **136**, 121 (1987).
331. A. BÉLANGER and A. K. VIJH, *Int. J. Hydrogen Energy*, **12**, 227 (1987).
332. H. F. BITTNER and C. C. BADCOCK, *J. Electrochem. Soc.*, **130**, 193C (1983).
333. O. A. PETRII, I. V. KOVRIGINA, and S. Y. VASINA, *Mat. Chem. Phys.*, **22**, 51 (1989).
334. A. BAIKER, *Faraday Disc. Chem. Soc.*, **87**, 239 (1989).
335. D. L. COKE, *J. Metals*, **38**, 70 (1986).
336. C. YOON and D. L. COCKE, *J. Non-Cryst. Solids*, **79**, 217 (1986).
337. A. YOKOYAMA, K. KOMIYAMA, H. INOUE, T. MASUMOTO, and H. M. KIMURA, *J. Catal.*, **68**, 355 (1981).
338. M. SHIBATA and T. MASUMOTO, *in: Preparation of Catalysts, Edited by B. Delmon, P. Grange, P. A. Jacobs, and G. Poncelet, Elsevier, Amsterdam, 1987, Vol. IV*, p. 353.
339. W. BROWER, M. MATYJASZCZYK, T. PETTIT, and G. SMITH, *Nature*, **301**, 497 (1983).
340. B. E. CONWAY, H. A. KOZLOWSKA, M. A. SATTAR, and B. V. TILAK, *J. Electrochem. Soc.*, **130**, 1825 (1983).
341. L. VRAČAR and B. E. CONWAY, *Int. J. Hydrogen Energy*, **15**, 701 (1990).
342. L. VRAČAR and B. E. CONWAY, *J. Electroanal. Chem.*, **277**, 253 (1990).
343. B. V. TILAK and B. E. CONWAY, *Electrochim. Acta*, **21**, 745 (1976).
344. R. KARIMI-SHERVEDANI and A. LASIA, *J. Electrochem. Soc.*, **144**, 511 (1996).
345. M. D. ARCHER, C. C. COKE, and B. H. HARJI, *Electrochim. Acta*, **32**, 13 (1987).
346. K. MACHIDA, M. ENYO, I. TOYOSHIMA, K. MIYAHARA, K. KAI, and K. SUZUKI, *Bull. Chem. Soc. Japan*, **56**, 3393 (1983).

347. J. O'M. BOCKRIS and A. K. N. REDDY, *Modern Electrochemistry*, Plenum Press, N. Y., 1970, Vol. 2, p. 1231.
348. A. J. BARD and L. R. FAULKNER, *Electrochemical Methods, "Fundamental and Application"*, John Wiley and Sons, New York, 1980, p. 86.
349. B. A. N. FRUMKIN, *Disc. Faraday Soc.*, **1**, 57 (1947).
350. J. HORIUTI and M. POLANYI, *Acta Physicochim. URSS*, **2**, 505 (1935).
351. J. A. V. BUTLER, *Proc. R. Soc. London, Ser. A*, **157**, 423 (1936).
352. E. GILEADI, *Electrode Kinetics for Chemists, Chemical Engineering, and Material Scientist*, VCH, New York, 1993, p. 261.
353. P. DELAHAY, *Double layer and Electrode Kinetics*, Interscience, New York, 1965, Chap. 2.
354. D. M. MOHILNER, *Electroanal. Chem.*, **1**, 241 (1966).
355. R. PARSONS, *J. Electroanal. Chem.*, **7**, 136 (1964).
356. B. V. TILAK and B. E. CONWAY, *Electrochim. Acta*, **37**, 51 (1992).
357. B. E. CONWAY and L. BAI, *J. Electroanal. Chem.*, **198**, 149 (1986).
358. B. E. CONWAY and B. V. TILAK, *Adv. Catal.*, **38**, 1 (1992). B. E. CONWAY, *in: Modern Aspects of Electrochemistry*, *Edited by* R. E. White, J. O'M. Bockris, and B. E. Conway, Plenum Press, New York, 1985, Vol. **16**, p.103.
359. B. E. CONWAY and E. GILEADI, *Trans. Faraday Soc.*, **58**, 2493 (1962).
360. B. E. CONWAY and E. GILEADI, *in: Modern Aspects of Electrochemistry*, *Edited by* J. O'M. Bockris and B. E. Conway, Butterworths, London, 1964, Vol. **3**, p. 347.
361. J. TAFEL, *Z. Phys. Chem.*, **50**, 641 (1905).
362. B. E. CONWAY, *Prog. Surf. Sci.*, **16**, 1 (1984).
363. M. JAKŠIĆ, *Electrochim. Acta*, **29**, 1527 (1984).
364. G. KOKKINIDIS, *J. Electroanal. Chem.*, **201**, 217 (1986).
365. B. E. CONWAY and T. C. LIU, *J. Chem. Soc., Faraday Trans. 1*, **83**, 1063 (1987).

366. R. KARIMI-SHERVEDANI and A. LASIA, "Mechanism of the Hydrogen Evolution Reaction on Ni-Mo-P Electrodes in Alkaline solutions," 190th Electrochem. Soc. Meet., San Antonio, Texas, October 1996, Abstract No. 802.
367. S. SZPAK *in*: Techniques for Characterization of Electrodes and Electrochemical Processes, *Edited by* R. Varama and J. R. Seman, John Wiley and Sons, New York, 1991, p. 551 and 677.
368. A. LASIA, *J. Electroanal. Chem.*, **397**, 27 (1995).
369. L. GAO and B. E. CONWAY, *Electrochim. Acta*, **39**, 1681 (1994).
370. (a) H. GERISCHER and W. MEHL, *Z. Electrochem.*, **59**, 1049 (1955); (b) J. L. WEININGER AND M. W. BREITER, *J. Electrochem. Soc.*, **111**, 707 (1964).
371. R. D. ARMSTRONG and J. M. HENDERSON, *J. Electroanal. Chem.*, **39**, 81 (1972).
372. J. R. MACDONALD, *Impedance Spectroscopy*, Interscience, New York, 1987.
373. J. R. MACDONALD, *J. Electroanal. Chem.*, **223**, 25, (1987).
374. D. D. MACDONALD and M. C. H. McKURBE, *in*: Modern Aspects of Electrochemistry, *Edited by* R. E. White, J. O'M. Bockris, and B. E. Conway, Plenum Press, New York, 1984, Vol. 14, p.16.
375. A. LASIA, "Electrochemical Impedance Spectroscopy and its Applications," *in*: Modern Aspects of Electrochemistry, submitted, 1997.
376. T. PAJKOSSY, *J. Electroanal. Chem.*, **364**, 111, (1994). T. PAJKOSSY, T. WANDLOWSKI, and P. M. KOLB, *J. Electroanal. Chem.*, **414**, 209, (1996).
377. R. DE LEVIE, *in*: Advances in Electrochemistry and Electrochemical engineering, *Edited by* P. Delahay, Interscience, New York, 1967, Vol. 6 P. 329.
378. L. M. GASSA, J. R. VILCHE, M. EBERT, K. JUTTNER, and W. J. LORENZ, *J. Appl. Electrochem.*, **20** 677 (1990).
379. P. LOS and A. LASIA, and H. MENARD, *J. Electroanal. Chem.*, **360**, 101 (1993).
380. J. P. CANDY, P. FOUILLOUX, M. KEDDAM, and H. TAKENOUTI, *Electrochim. Acta*, **27** 1585 (1982).
381. EG&G M270, User's Guide, 222153-A-MNL-A, 1992, p. 74.

382. EG&G Model 273-81, Head Start Instruction Manual, 1986, p. 41.
383. H. DUMONT, P. LOS, L. BROSSARD, and H. MENARD, *J. Electrochem. Soc.*, **141**, 1225 (1994).
384. H. KEISER, K. D. BECCU, and M. A. GUTJAHR, *Electrochim. Acta.*, **21**, 539 (1976).
385. E. POTVIN, A. LASIA, and H. MENARD, *J. Electrochem. Soc.*, **138**, 900 (1991).
386. D. OHMS, V. PLZAK, S. TRASATTI, K. WIESENER, and H. WENDT, *in: Electrochemical Hydrogen Technology. Electrochemical Production and Combustion of Hydrogen*, Edited by H. Wendt, Elsevier, New York, 1990, p. 1.
387. K. SETO, J. NOEL, and J. LIPKOWSKI, *J. Electrochem. Soc.*, **136**, 1910 (1989).
388. G. O. MALLORY, *Plat. and Surf. Finish.*, **63**, 34 (1976).
389. G. O. MALLORY and T. R. HORHN, *ibid*, **66**, 40 (1979).
390. I. KOIWA, M. USUDA, K. YAMADA, and T. OSAKA, *J. Electrochem. Soc.*, **135**, 718 (1988).
391. S. L. LEE and H. H. LIANG, *Plat. and Surf. Finish.*, **79**, 56 (1992).
392. S. L. LEE, H. H. LIANG, M. W. LIANG, and T. H. CHUANG, *ibid*, **79**, 949 (1992).
393. O. MENDOZA, R. E. WHITE, D. L. COKE, and B. A. HORRELL, *ibid*, **79**, 51 (1992).
394. S. YAO, Y. ZENG, H. T. GUO, and M. KOWAKA, *Hgomen Gijutsu*, **45**, 77 (1994).
395. Y. L. LO, B. J. HWANG, and S. C. CHOU, Private communication (1994).
396. M. SCHWARTE, and G. O. MALLOR, *J. Electrochem. Soc.*, **123**, 606 (1976).
397. Y. ZENG, S. YAO, and H. GUA, *Plat. and Surf. Finish.*, **82**, 64 (1995).
398. R. DE LEVIE, *J. Electroanal. Chem.*, **281**, 1 (1990).
399. C. CACHET and R. WIRT, *J. Electroanal. Chem.*, **195**, 21 (1985).
400. C. CACHET, C. P. PAULI, and R. WIART, *Electrochim. Acta*, **30**, 719 (1985).
401. C. CACHET and R. WIART, *Electrochim. Acta*, **29**, 145 (1984).
402. J. P. CANDY, P. FOUILLOUX, M. KEDDAM, and H. TAKENOUTI, *Electrochim. Acta*, **26**, 1029 (1981).
403. I. D. RAIDSTRICK, *Electrochim. Acta*, **35**, 1579 (1990).

404. J. R. MACDONALD, J. SCHOOMAN, and A. P. LEHNER, *J. Electroanal. Chem.*, **131**, 77 (1982).
405. A. BUDNIOK and P. MATYJA, *Thin Film Solid*, **201**, 30 (1991).
406. J. BALEJ, J. DIVISEK, H. SCHMITZ, and J. MERGEL, *J. Appl. Electrochem.*, **22**, 711 (1992).
407. J. R. MCDONALD, *J. Electrochem. Soc.*, **124**, 1022 (1977).
408. G. INZELT and G. LANG, *J. Electroanal. Chem.*, **378** 39 (1994).
409. J. R. MCDONALD, *Electrochim. Acta*, **35** 1483 (1990).
410. (a) J. ZHANG, V. I. BIRSS, and P. VANÝSEK, *J. Electroanal. Chem.*, **378**, 63 (1994);
(b) S. C. THOMAS and V. I. BIRSS, *J. Electrochem. Soc.*, **144**, 566 (1996), references therein.
411. D. ZURAWSKI, M. WASBERG, and A. WIECKOWSKI, *J. Phys. Chem.*, **94**, 2076 (1990).
412. H. KITA, H. NAOHARA, T. NAKATO, S. TAGUCHI, and A. ARAMATA, *J. Electroanal. Chem.*, **386**, 197 (1995).
413. K. WANG, G. S. CHOTTINER, and D. A. SCHERSON, *J. Phys. Chem.*, **96**, 6742 (1992).
414. M. ZHAO, K. WANG, and D. A. SCHERSON, *J. Phys. Chem.*, **97**, 4488 (1993).
415. C. F. ZINOLA, E. J. VASINI, U. MÜLLER, H. BALTRUSCHAT, and A. J. ARVIA, *J. Electroanal. Chem.*, **415**, 165(1996).
416. A. CUESTA and C. GUTIÉRREZ, *J. Phys. Chem.*, **100**, 12600 (1996).
417. H. H. EWE, E. W. JUSTI, A. W. KALBERLAH, and A. F. SCHMITT, *Energy Conversion*, **12**, 1 (1972).